Studies on the solid acid catalysts containing Group VI Elements: Synthesis, Characterization and Screening for their catalytic activities.

THESIS

SUBMITTED FOR THE DEGREE OF

DOCTOR OF PHILOSOPHY

IN CHEMISTRY

TO THE

UNIVERSITY OF PUNE

BY

Tejas R. Gaydhankar

Research guide

Dr. K. J. Waghmare

Research co-guide

Dr. M.D. Nikalje

INORGANIC CHEMISTRY AND CATALYSIS DIVISION

NATIONAL CHEMICAL LABORATORY

PUNE - 411 008, INDIA

…..DEDICATED

TO

MY BELOVED

PARENTS,

WIFE & BROTHER

राष्ट्रीय रासायनिक प्रयोगशाला
(वैज्ञानिक तथा औद्योगिक अनुसंधान परिषद)
डॉ. होमी भाभा मार्ग पुणे - 411 008. भारत
NATIONAL CHEMICAL LABORATORY
(Council of Scientific & Industrial Research)
Dr. Homi Bhabha Road, Pune - 411 008. India.

CERTIFICATE

Certified that the work incorporated in the thesis entitled "**Studies on the solid acid catalysts containing Group VI Elements: Synthesis, Characterization and Screening for their catalytic activities**" submitted by Mr.Tejas R Gaydhankar, for the Degree of Doctor of Philosophy, in Chemistry was carried out by the candidate under my supervision in the Inorganic Chemistry and Catalysis Division, National Chemical Laboratory, Pune - 411008, India. Materials and characterization obtained from other sources have been duly acknowledged in the thesis.

(Research Guide)
Dr. K. J. Waghmare

(Research Co-Guide)
Dr. M.D. Nikalje

Communication Channels
NCL Level DID : 2590
NCL Board No. : +91-20-25902000
EPABX : +91-20-25893300
+91-20-25893400
FAX
Director's Office : +91-20-25893355
COA's Office : +91-20-25893619
COS&P's Office : +91-20-25893008
WEBSITE
www.ncl-india.org

Candidate's Declaration

I hereby declare that the thesis entitled **"Studies on the solid acid catalysts containing Group VI Elements: Synthesis, Characterization and Screening for their catalytic activities"** submitted by me for the degree of ***Doctor of Philosophy*** in ***Chemistry*** to the ***University of Pune*** is the record of work carried out by me during the period of September, 2008 to December, 2011 and has not been submitted by me for a degree to any other University or Institution. In addition, all information sources and literature used are indicated in the thesis. This work was carried out at Inorganic Chemistry and Catalysis Division, National Chemical Laboratory, Pune, India. Any inadvertent omissions that might have occurred due to oversight or error in judgment are regretted.

Tejas R Gaydhankar

August 2012
Inorganic Chemistry and Catalysis Division
National Chemical Laboratory
Pune 411008, Maharashtra
India

ACKNOWLEDGMENTS

First of all I would like to express my gratitude to my research guide Dr. K. J. Waghmare for his support, advice, valuable discussions constant encouragement, critical ideas, invaluable suggestions and unfailing guidance during the course of the whole research work presented in this thesis. I am always indebted to him. I have been able to learn a great deal from him and consider my association is a rewarding experience for me. I thank him for his patient guidance, open discussions, unbounded enthusiasm and interest. Words shall fail to fully acknowledge your contribution.

I find it very difficult to write something in short to acknowledge my research co-guide, Dr M. D. Nikalje. His constant inspiration, invaluable guidance and constructive criticism helped me a lot to focus my views in proper perspective. I take this opportunity to express my intense reverence towards him for guiding me in the right direction throughout the course of this work. My deepest personal regards are due for him forever.

I sincerely thank all my PG committee members, Prof. P. D. Lokhande and Dr. V. R. Chumbale for their constant encouragement and suggestions.

I express my deep gratitude to Dr. A.P. Singh and Dr. D. Srinivas, Chair, Catalysis Department and other faculty members of our department for the support and facilities provided in carrying out this thesis work. I owe my special thanks to Dr. R.A. Shaikh, Mr. Shelar, Mr. Jadhav, Dr. S. Awate, Dr. S.P. Mirajkar, Dr. S.B. Umbarkar, Dr. A.K, Kinage, Mr. Maulavi Akbar, Mr. Purshotom Dr. S.S. Deshpande and all other scientific and nonscientific staff in the Catalysis Division. I thank the staffs of Accounts, Administration, Engineering and Stores & Purchase sections for their help in a way or the other.

I owe my sincere gratitude to Dr. Koteswar Rao for XRF analysis, Dr. K. R. Patil for XPS analysis and discussion, Dr. Swati P & Dr. D Kamble for NMR analysis, Mr. Anup T and Savita for ICP analysis, Dr. A. B Gaikwad of CMC division and Mr. Ketan B for SEM/EDX analysis, Dr. R.K. Jha for N_2-sorption and TG-DTA analysis, Ms. V. Samuel for

XRD, Mr. K. M. Kalal and Dr. K. B. Sonavane for GC-MS analysis, Micro analysis laboratory staffs for elemental analysis, Dr. Anuya N for SAXS analysis and Mrs. Rupali V for Raman results. I am also grateful to Mr K. Sridhar for helping me for TEM microscopy and Dr. Trupti K for FT-IR & TPD measurements/analysis. I'm indebted to all of them for their help. I am also thankful to other research scholars in Catalysis division and other divisions for providing all joyful environments in the lab and helping me out in different ways.

I take this golden opportunity to convey my earnest gratitude to my friend Dr. Prashant. S. Niphadkar who always seems to go out of his way to drop whatever he is doing to help me with whatever I ask of him, scientific as well as personal.

The thesis could not have been completed without the endless love and blessings from my family, Mom: Mrs. Vimal R Gaydhankar, Dad: Mr. Ramchandra S Gaydhankar, my Brother: Mr. Ashish R Gaydhankar and his wife: Mrs Himani A Gaydhankar who encouraged me whenever needed. I should not belittle you by thanking; you taught me how to dream, gave me the skills to chase after those dreams, and encouraged me to reach for the unreachable star. I appreciate the supports and fun given by my nephew Ishan A Gaydhankar(Favda). I have received unfailing support and encouragement during many years of studies that they have shown to me in their own special way.

Of course, none of this would have been possible at all without the love and bottomless support of my wife, Priydarshani T Gaydhankar whose dedication, love, encouragement, and persistent confidence in me has taken the load off my shoulders.

I also take this golden opportunity to convey my earnest respect and gratitude to Dr. M. Laxikantam (IICT, Hyderabad) and Dr. A.A. Arbale for their steadfast faith in my capability has always spurred me to go ahead, especially in difficult times.

It gives me great pleasure to thank my old friends and relatives Milind Gaydhankar, Sunil Gaydhankar, Sunil Gaydhankar, Varsha Ohatkar, Megha Ingle, Papu Sadapule Abhijit Vhatkar, Narayan Sonawane, Pratap Zaveri, Rajesh Kadlak, Parimal Kadlak, Sarika

Kumbhare, Anuradha Joshi, Smita Jadahav, Sandeep Jadhav, Amita Shelar, Jeevan Gaikwad, Hemant Gaikwad, Yogesh Rati, Nadeem Tamboli, Rama, Sameer Gambhir, Nakto, Amit M, Kunal M, Hemant Kamble, Karuna Gaikwad, Mashila James, Anjali James, Pratibha K, Trupti Katke, Sarika Kawale, Arti M, Vishal Megrathi, Sunil Zope, Sarita Narayankar, Sony Kadam, Neha, Sudha, Teja, Naya,, Nikita M, Sameer M, Harshal M, Vaishali K, Shraddha, Jumana, Sangita, Roxy, Ritu, Reena K, Rajuu G, Harshal G, Sneha G, Kishore Borade and many others whose names I cannot recollect at this moment.

I also give my special thanks to my friends, Samadhan Lomate, Swati Pandhare, Vaibhav Acham, Rajesh Jadhav, Ashwini B, Atul K, Anuj Kumar, Nishita Lucas, Mohan Suryavanshi, Pavan More, Neelam Jagtap, Prakash, Vidya Ghantani, Sameer Mahajan, Arun Nikam, Sagar Jain, Atul Kulal, Prashant. Karndikar, Hari Jagtap, D. Bhange, Ganesh Kokate, S.R. Kadam, Neelam. Jagtap, V. Paike, Nagesh Kolhe, Kumar Paike, Pranjal Kalita, Prashant Lihitkar, Purshottam Desai, Matsagar Babasaheb, Pravin Shinde, Preeti Yadav, Prasenjit Bhaumik, Narasimharao Kanna, Ankush Biradar, Sunil Bhongale, Pravin Shinde, Dr. Mahendra Lokhande, Datta Bhangare, Manoj Chopade, Vivek T Humne, Deepali Pakhare, Nikita Parekh, Suryaprasad Ronaki, Harshali W many others, from whom I have received invaluable help and support.

Finally, I am thankful to Dr. S. Sivaram, (former Director) and present Director Dr. S. Pal, NCL, for permitting me to Ph.D degree course of University of Pune and allowing me to carry out the research at NCL and to submit the work in the form of thesis for the award of the Ph.D degree. I am thankful to National Chemical Laboratory where in I have carried out most of my research work and for providing the state-of-the-art facilities.

I take this opportunity to convey my hearty admiration to all my teachers from my school days to post graduation level. At last, I would like to thank everybody who was important to the successful realization of the thesis, as well as expressing my apology that I could not mention personally one by one.

Tejas R Gaydhankar

ABSTRACT

Zirconia has attracted considerable interest owing to its broad range of applications in various fields, ranging from catalysis to high performance transformation-toughened structural engineering ceramics, solid oxide fuel cells, gas sensors, electro-optical materials, fabrication, automotive exhaust treatment, etc., in addition to the classical application of catalyst support. But zirconia has poor thermal stability and is known to sinter at high temperatures, which leads to catalytic deactivation. Therefore, more efforts have been devoted in recent years to design a suitable porous zirconia having enhanced thermal stability, high surface area and catalytically active tetragonal phase. After, exhaustive literature survey, very few reports are found wherein tetragonal phase along with high surface area zirconia are stable at higher temperatures, however it is seen that the detailed comparative studies are not reported. As a result optimization of synthesis parameters for the preparation of high surface area tetragonal zirconia with good thermal stability using facile synthesis procedures was the primary objective of this work. The emphasis has been placed on the characterization of the structure at each stage of the route, leading to an understanding of the various possible mechanisms that play an important role in stabilizing the tetragonal zirconia. This study has also provided an opportunity to investigate broader issues concerning the solution based processing of zirconia. The redox and catalytic properties of porous zirconia and zirconia supported materials as composite oxides are dependent upon numerous factors, which include crystallite size, phase modification, acidity, oxidation state, dispersion, morphology etc. In addition, catalyst prepared with in nano-meter scale results in increasing the specific surface area, narrow pore size distribution, ordered channels, thus improving the catalytic performance. In order to enhance the thermal stability of tetragonal zirconia and its acidic nature, incorporation of the Group VI elements of the periodic table such as chromium, molybdenum and tungsten oxides which are thermally more stable than sulfated zirconia, is required. Especially, MoO_3 and WO_3 supported zirconia when calcined at high temperatures are found to be highly acidic and used as a powerful catalyst for vide variety of industrially important acid catalyzed reactions. Therefore, it is interesting to investigate the structural and catalytic properties of novel MoO_3 and WO_3 supported zirconia composite oxide materials. However the nature, number and strength of acid

sites, morphology, surface area, pore size, surface density, suitable phase for high selectivity toward the desired products etc and other physicochemical properties of solid acid catalyst strongly relies on the preparation methods, precipitating agent, starting precursors, calcination temperature, pre-treatment etc. Generally, two main methods are most commonly reported in the literature for the preparation of metal oxides; the conventional precipitation method and sol-gel method. However, most of the synthesis routes to prepare high surface area of t-ZrO_2 supported solid acid catalyst are complicated and require tedious procedures involving close control of synthesis parameters such as temperature, pressure, pH, and/or the use of relatively expensive zirconium alkoxides. In such context, simple and easy synthesis routes are highly desired especially for the practical applications of ZrO_2 based solid acid catalyst with high surface area. Therefore in the present investigations, MoO_3 and WO_3 supported zirconia solid acid catalyst, possessing high specific surface area and better thermal stability are synthesized. The thermal and structural stability of the solid acid catalyst prepared during these studies are strongly influenced by the synthetic methodology. All the samples are systematically characterized by using various analytical and spectroscopic techniques; the data obtained are co-related with synthesis parameters. This requires a wide range of complementary characterization techniques, including Powder XRD, N_2 adsorption-desorption, TG-DTA, TEM, SEM, UV-Vis, RAMAN, NH_3-TPD, XRF, AAS, ICP, SAXS, FT-IR and TPD. In conclusion, thermally stable high surface area, pure zirconia, molybdenum and tungsten oxide supported zirconia solid acid catalyst are successfully prepared after optimization of various synthesis parameters. Physico-chemical characterization of all these materials show that they are thermally stable up to 800 ^oC temperature; possessing high surface area, tetragonal phase and excellent textural properties. The results of this investigations contribute not only to the understanding of a particular route for processing zirconia based materials, but also to a broader understanding the effects of various other synthesis parameters on the physical and chemical properties of the catalyst. Molybdenum oxide supported zirconia solid acid catalyst is utilized for organic synthesis involving biologically important molecules.

KEYWORDS: Tetragonal Zirconia; MoO_3-ZrO_2, Claisen–Schmidt Condensation, Tungstated Zirconia, Solid Acid Catalyst, Chalcone.

LIST OF ABBREVIATIONS/TERMINOLOGY/SYMBOLS

%	Percentage
°C	Degree Celsius
Å	Angstrom
AAS	Atomic Absorption Spectroscopy
AHM	Ammonium Hepta-Molybdate, $[(NH_4)_6Mo_7O_{24}]$
AMT	Ammonium Meta-Tungstate, $[(NH_4)_6H_2W_{12}O_{40}]$
AP	Acetophenone
As synt.	As synthesized
Avg.	Average
A.U.	Arbitrary Units
BA	Benzaldehyde
BE	Binding Energy
BET	Brunauer, Emmett and Teller
BJH	Barrett-Joyner-Halenda
C.N.	Co-Ordination Number
c-ZrO_2	Cubic Zirconia
Cal.	Calcined
CMC	Critical Micelle Concentration
Conc.	Concentrated
Conv.	Conversion
CSC	Claisen - Schmidt Condensation
CTMABr	Cetyl Trimethyl Ammonium Bromide
CVD	Chemical Vapor Deposition
DR UV-Vis	Diffuse Reflectance Ultraviolet-Visible Spectroscopy
EDX	Energy Dispersive X-ray Analysis
ESR	Electron Spin Resonance
EtOH	Ethanol
eV	Electron Volt

EXAFS	Extended X-ray Absorption Fine Structure
Expt. No.	Experiment Number
FID	Flame Ionization Detector
FTIR	Fourier Transform Infrared
FWHM	Full Width Half Maximum
g	Gram
GC	Gas Chromatography
GC-MS	Gas Chromatography – Mass Spectroscopy
GFAAS	Graphite Furnace Atomic Absorption Spectroscopy
HPA	Heteropoly Acid
HR-TEM	High Resolution - Transmission Electron Microscopy
ICP	Inductively Coupled Plasma
ICP-MS	ICP-Mass Spectrometry
ICP-AES	Inductively Coupled Plasma-Atomic Emission Spectroscopy
IPA	Isopropyl Alcohol Or Iso-propanol
ISS	Ion Scattering Spectroscopy
IUPAC	International Union For Pure And Applied Chemistry
JCPDS	Joint Committee on Powder Diffraction Standards
K	Kelvin
KBr	Potassium Bromide
kg	Kilogram
kJ	Kilo Joule
LAT	Ligand Assisted Templating
LCT	Liquid Crystal Templating
LE-ISS	Low-Energy Ion Scattering Spectroscopy
MeOH	Methanol
min	Minute
ml	Milliliter
mmol	Milli Mole
Mol. Wt.	Molecular Weight

MoO_3	Molybdenum Oxide
MPA	Molybdophosphoric Acid
m-ZrO_2	Monoclinic Zirconia
N/A	Not Available
NH_4OH	Aqueous Ammonia Solution
nm	Nanometer
NMR	Nuclear Magnetic Resonance
P123	Pluronic 123 (A Nonionic Tri-Block Copolymer Surfactant); Ethylene Oxide (EO_{20}) – Propylene (PO_{70}) – Ethylene Oxide(EO_{20})
Pore Dia.	Pore Diameter
Pore Vol.	Pore Volume
ppm	Parts Per Million
rpm	Revolutions Per Minute
SAED	Selected Area Electron Diffraction
SAXS	Small Angle X-Ray Scattering
S_{BET}	Multipoint BET Surface Area
Sel.	Selectivity
SEM	Scanning Electron Microscopy
SIMS	Secondary Ion Mass Spectrometry
Soln.	Solution
STP	Standard Temperature and Pressure
Syn.	Synthesis
T	Temperature
TCD	Thermal Conductivity Detector
TG-DTA	Thermo-Gravimetric – Differential Thermal Analysis
TPA	Tungstophosphoric Acid
TPD	Temperature Programmed Desorption
t-ZrO_2	Tetragonal Zirconia
UV-Vis	Ultraviolet-Visible
Vol. %	Volume Percent

w/w	Weight per Weight
WO_3	Tungsten Oxide
Wt. %	Weight Percent
XANES	X-ray Absorption Near-Edge Spectroscopy
XPS	X-Ray Photoelectron Spectroscopy
XRD	X-Ray Diffraction
XRF	X-Ray Fluorescence
Y	Yield
Zr	Zirconium
ZrBt	Zirconium (IV) tert-butoxide, (80% in n-butanol) $\{Zr[OC(CH_3)_3]_4\}$
ZrBtCl	Mixture of Zirconium (IV) tert-butoxide and Zirconium Chloride
ZrCl	Zirconium Chloride, $ZrCl_4$
ZrNit	Zirconium Nitrate, $Zr(NO_3)_4 \cdot 3H_2O$
ZrO_2	Zirconia
ZrOCl	Zirconium Oxy-Chloride / Zirconyl Chloride, $ZrOCl_2 \cdot 8H_2O$
ZrONit	Zirconium Oxy-Nitrate / Zirconyl Nitrate, $ZrO(NO_3)_2 \cdot XH_2O$
$ZrSO_4$	Zirconium Sulfate, $Zr(SO_4)_2 \cdot XH_2O$

TABLE OF CONTENTS

CHAPTER 1

1. INTRODUCTION AND LITERATURE SURVEY

CHAPTER 2

2. SYNTHESIS AND CHARACTERIZATION TECHNIQUES

CHAPTER 3

3. SYNTHESIS AND CHARACTERIZATION OF t-ZrO_2

CHAPTER 4

4. MOLYBDENUM OXIDE SUPPORTED ZIRCONIA

CHAPTER 5

5. TUNGSTATED ZIRCONIA SOLID ACID CATALYST

CHAPTER 6

CHAPTER – 1

INTRODUCTION AND LITERATURE SURVEY

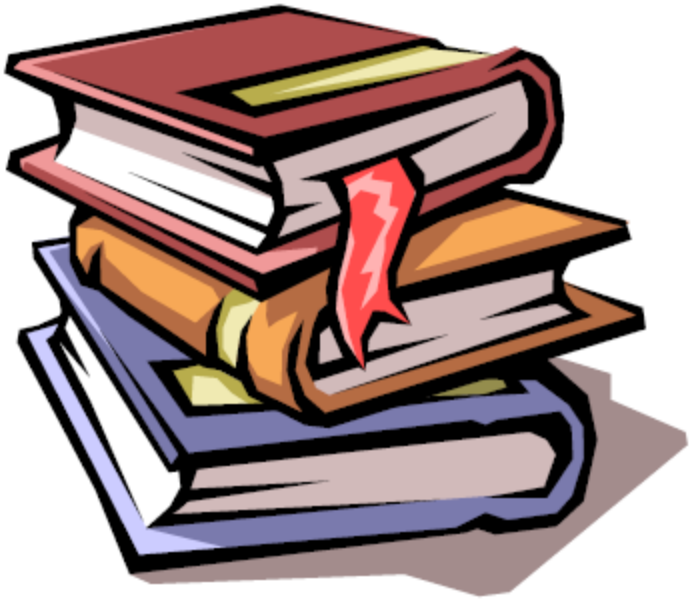

1.1. Catalyst and Catalysis

The terms catalyst and organic chemistry were both coined by the Swedish chemist Jöns Jakob Berzelius in 1835 and 1807 respectively [1]. Subsequently, catalysis and organic synthesis evolved along different paths. Berzelius defined a catalyst as a substance, which by its mere presence evokes chemical actions, which would not take place in its absence. The definition seems to get modified as the surface properties and the ideas of what constitute a catalyst and mechanism for catalytic activity have undergone continuous refinement, and Ostwald scientifically defined the term catalysis firstly in 1894. According to Ostwald, "Catalysis is the phenomenon in which a small quantity of substance (catalyst) increases the rate of reaction or the rate of approaching the equilibrium of a chemical reaction without itself being substantially consumed" [2]. In general catalysts are substances that facilitate a chemical reaction by lowering the energy barrier of the reaction pathway and thus increasing the reaction rate as shown in Fig. 1.1 [3].

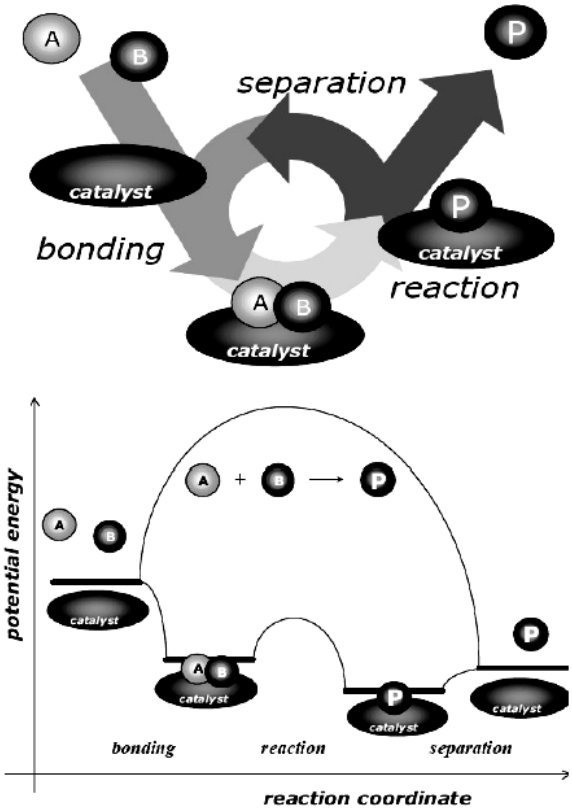

Fig. 1.1: Pictorial representation of a catalysis process

Catalysis is a process in which the chemical reactions are facilitated by mere presence of catalysts and plays a vital role in nature and society since almost every

reaction requires a catalytic material [4]. Catalysis is primarily a technology that draws on many fields such as organic chemistry, surface chemistry, chemical kinetics, thermodynamics, solid states, physics ceramics and physical metallurgy and so the term an interdisciplinary subject seems to be very aptful [4]. The branch of catalysis developed initially as a sub-discipline of physical chemistry. It was not until the start of 20^{th} century, the organo-metallic chemistry, material sciences, physical chemistry, chemical engineering and surface sciences enlarged the knowledge of catalysis and catalysts considerably. Catalysis is important academically and industrially. With the advent of petrochemical industry in 1920's, catalysis was widely applied in oil refining and to a large extent in bulk chemicals manufacture. Most of the early applications of catalysis in industry were confined to the manufacture of heavy chemicals, the major emphasis being on the petroleum and petrochemical industries. Manufacturing fine chemicals remained the domain of synthetic organic chemist who adhered to the stoichiometric reagents developed in the 19^{th} century. As the catalysis research expanded, its role in the manufacture of a wide range of products, from gasoline and plastics to fertilizers, pharmaceuticals and herbicides also grew, which would otherwise be unavailable or prohibitively expensive. Apart from manufacturing processes, catalysis is finding other important and ever increasing uses; for example, successful applications of catalysis in pollution control and its use in environmental control are certain to increase in the future. Catalysts are now seen as a preferred way to improve process efficiency, lower costs, increase output, use less energy, and meet both performance and environmental standards. Catalytic technologies play a key role in the economic development and growth of the chemicals industry and contribute to around 20% of world Gross National Product. More than 90% of today's chemical processes employ catalysts [5].

1.2. Homogeneous and Heterogeneous Catalysts

It is interesting to note that the first industrial catalytic process of soap making and alcoholic fermentation used homogeneous catalysts or enzymes without knowing anything of catalysis. If the catalyst is in the same state of matter as the reactants (i.e. reactants and catalyst are in liquid phase) then it is referred as homogeneous catalysis. If the catalyst is in another state of matter, then it is called heterogeneous catalysis. In

homogeneous catalysis, all the constituents of the reaction are present or brought into the same phase usually in liquid phase. Homogeneous catalysts, comprising of metal complexes or salts are usually soluble in the reaction medium. Homogeneous catalysts are usually known to their specific activity and eventually foster high selectivity generally at low temperatures and pressures. The performance of homogeneous catalysts depends on type of the metal, ligands, promoters and co-catalysts and in most cases the selectivity. The main disadvantages of the homogeneous catalysts are difficult separation of the catalyst from the product, degradation of the catalyst and high initial cost especially if noble metals are required. On the other hand, heterogeneous catalysis involves a reaction in which one or more of the constituents are in different phases. Thus, a heterogeneous catalyst is normally insoluble in the reaction medium. This is the reason why only 20 % of the industrial catalytic reactions involve homogenous catalysis whereas 80 % employing the classical heterogeneous catalysis involving supported metal catalysts. The catalyst may be pure, mixed with other catalysts or dispersed on an inert support e.g. metals and metal oxides. The advantages of using heterogeneous catalysts are their low cost, easy recovery and adaptability to either batch or continuous flow reactors. The disadvantages of these catalysts are their general lack of specificity and the energy requirements of high temperatures and pressures in many catalytic systems. The present day chemists, scientists, researchers in modern chemical industries, academic institutions, national laboratories and R&D centers all around the world are having the challenge of developing a catalyst which is economical, highly active and selective under lower temperatures and pressures. The stress is on a technology which will reduce the dispersion of harmful chemicals in the environment and impart regenerability and durability to the catalysts in such a way as to increase the industrial competitiveness [6,7,8,9]. Catalysis is predominantly known for its importance in process efficiency and product selectivity in reactions practiced starting from large scale industry to small-scale sector. It is evident that the key to cleaner process of fine chemicals and pharmaceuticals is the concept of selectivity. Although, various types of selectivity's have been categorized such as chemo-, regio-, stereo-selectivity involving shape, substrate and restricted transition state enantio- and diastereo-, selectivities etc., the major concern of an industrial environmental chemist relatively overlooked by an organic chemist is atom

economy and selectivity. The atom economy is obtained by dividing the molecular weight of the desired product by the sum of molecular weights of all the products formed in the process. But from the catalyst manufacturers' perspective, it is to note that these days economic and ecological environment directs their efforts towards cost/performance improvement rather than to implement more sophisticated manufacturing technologies, except the new technology results in a remarkable performance benefit of the catalyst at lower manufacturing cost and at higher environmental standard. New production technologies, usually, are associated with additional capital investment. The room for such an investment in catalyst manufacturing plants gets smaller and smaller primarily due to low catalyst prices caused by the increased buying power of catalyst users as a result of recent mega-mergers and also because the industry faces stricter safety and environmental regulations that make production equipment more expensive.

1.3. Environmental factors

In spite of the general advantages of being highly active and readily available the classical stoichiometric technologies such as reductions with metal hydrides and dissolving metals, oxidations with permanganate and hexavalent chromium compounds, halogenations, nitrations, Grignard reactions and a wide variety of reactions employing stoichiometric amounts of mineral (HF, HCl, H_2SO_4, etc.) or Lewis ($AlCl_3$, BF_3 etc.) acids, produce large amounts of inorganic salts as waste, which, till recently was not considered to be a serious problem. Acid-catalyzed reactions catalyzed by conventional homogenous acids exhibit significant disadvantages in handling, containment, separation and disposal because of their toxic and corrosive nature. On the contrary, solid heterogeneous acid catalysts have some additional advantages over these conventional homogenous acids, such as strong acid sites, ease of product separation, catalyst reuse, non-toxicity, non-corrosiveness, easy handling, low cost, easy to recover and process advantages through reactor operation in continuous flow versus batch configuration. Table 1.1 provides a comparison of conventional homogenous catalysts with solid heterogeneous catalysts. It is therefore of great interest throughout the world to find appropriate solid acid catalysts to substitute conventional homogenous acid catalysts due to the tightening legislation on the release of waste and toxic emissions causing

environmental pollution. However, to maintain economic viability, a suitable heterogeneous system must not only minimize the production of waste, but should also exhibit activities and selectivity's comparable or superior to the existing homogeneous systems.

Table 1.1: Comparison of homogenous and heterogeneous catalysis.

Sr.No.	Factors	Homogeneous catalysis	Heterogeneous catalysis
1	Reaction rate	Fast and high conversion	Moderate conversion
2	After treatment	Catalyst cannot be recovered, must be neutralized leading to waste chemical production	Can be recovered
3	Processing methodology	Limited use of continuous methodology	Continuous fix bed operation possible
4	Presence of water	Sensitive	Less Sensitive
5	Catalyst reuse	Not possible	Possible
6	Cost	Comparatively costly	Potentially cheaper

1.4. Solid Acid and Base Catalysts

Solid Acid and Base catalyzed processes are fundamentals in the oil refining and petrochemical industries as well as in the manufacture of a wide variety of specialty chemicals such as pharmaceuticals, agrochemicals and flavors and fragrances. Some of the solid Acid and Base catalysts that are employed in vide variety of organic reactions are listed in Table 1.2.

Table 1.2: Some typical solid acid and base catalysts employed for catalytic reactions.

Solid acid catalysts	Solid base catalysts
Nafion and Amberlyst -15 composites	Cs-exchanged sepiolite, faujasites etc
MCM family and type mesoporous materials	Oxides like MgO, CaO, La_2O_3, ZnO
Zeolites H-Y, H-Beta, H-ZSM-5 etc	Zinc aluminates
Sulphated zirconia/alumina, tin oxide	Metal salts of amino acids
Supported and pure Heteropoly acids	Li-promoted CaO, $CaCO_3$, $Ba(OH)_2$
Organo-sulphonic acid on mesoporous silica	Hydrotalcites (Mg-Al)

The number of solid acid, base, and acid-base bi-functional catalysts used in industry processes are 103, 10 and 14 respectively [10]. The number of solid acid catalysts is largest due to its great demand in the petroleum and petrochemical industry. There are only ten processes for solid base catalysis because the study of solid base catalysts started much later than that of solid acid catalysts. However, this study is now becoming more active. For acid-base bi-functional catalysts, the number is estimated to be fourteen, since

the solid acid-base bi-functional catalyst is strictly limited to those having evidence for the bi-functional catalysis. Among the above mentioned heterogeneous catalyst, acid catalysts play a substantial role in organic synthesis and transformations. Solid acid catalysts are the topics of everlasting interest due to numerous applications in many areas of the chemical industry. The present understanding of acid induced or catalyzed reactions cover an extremely broad field, ranging from large-scale industrial processes in hydrocarbon chemistry to enzyme-controlled reactions in the living cell. These are extremely useful catalysts in large volume applications, especially in the petroleum industry and in the production of fine and specialty chemicals. Solid acid catalyst used to catalyze a plenty of industrially important reactions, such as isomerization, esterification, Friedel-Crafts alkylation, oligomerization, etherification, dehydration, acylation, condensation, nitration, and cracking have garnered a great deal of research momentum because of its strong or super-acidic character. They have been also used in many new fields such as coal hydroliquefaction, decontaminating radioactive pollutants, and so on [11-23].

1.5. Acidity of Solid Acid Catalyst

Solid Acid Catalyst is a solid porous, rigid or non-rigid support, upon/into which active acid groups are incorporated. A solid acid may be generally defined as a solid which changes the color of a basic indicator or a solid on which a base is chemically adsorbed. According to Brønsted and Lewis definition solid acid catalyst is a solid material which has a tendency to donate a proton or to accept an electron pair from a molecule. Solid acids generally have both Brønsted and Lewis acid sites. Solid-acid catalysts are generally categorized by their Brønsted and/or Lewis acidity, the strength and number of these sites, and the morphology of the support (e.g., surface area, pore size etc). Considering the behaviors of the acid sites reaction, the acid sites on solid acid are distributed into two groups, Brønsted and Lewis acid sites. Brønsted acid site is known as protonic acid site usually exists in the form of acidic hydroxyl group and Lewis acid site usually appears in a metal which has coordinate unsaturated structure [24,25]. The material's used as a solid acid catalyst is governed by the number, type and strength of acid sites present. The acid strength of a solid is defined as the ability of the surface to

convert an adsorbed neutral base into its conjugate acid. The strength of an acid can vary and can be determined by using appropriate Hammett indicators; the Hammett acidity function, H_0 [26], which has been extensively used as a measure of acidity. The lower the value of the function, the stronger is the acid. The Hammett method is a feasible and simple method, which is widely used to measure the acid strength. Acid strengths of various liquid and solid acids materials as a Hammett acidity function is given in Fig. 1.2

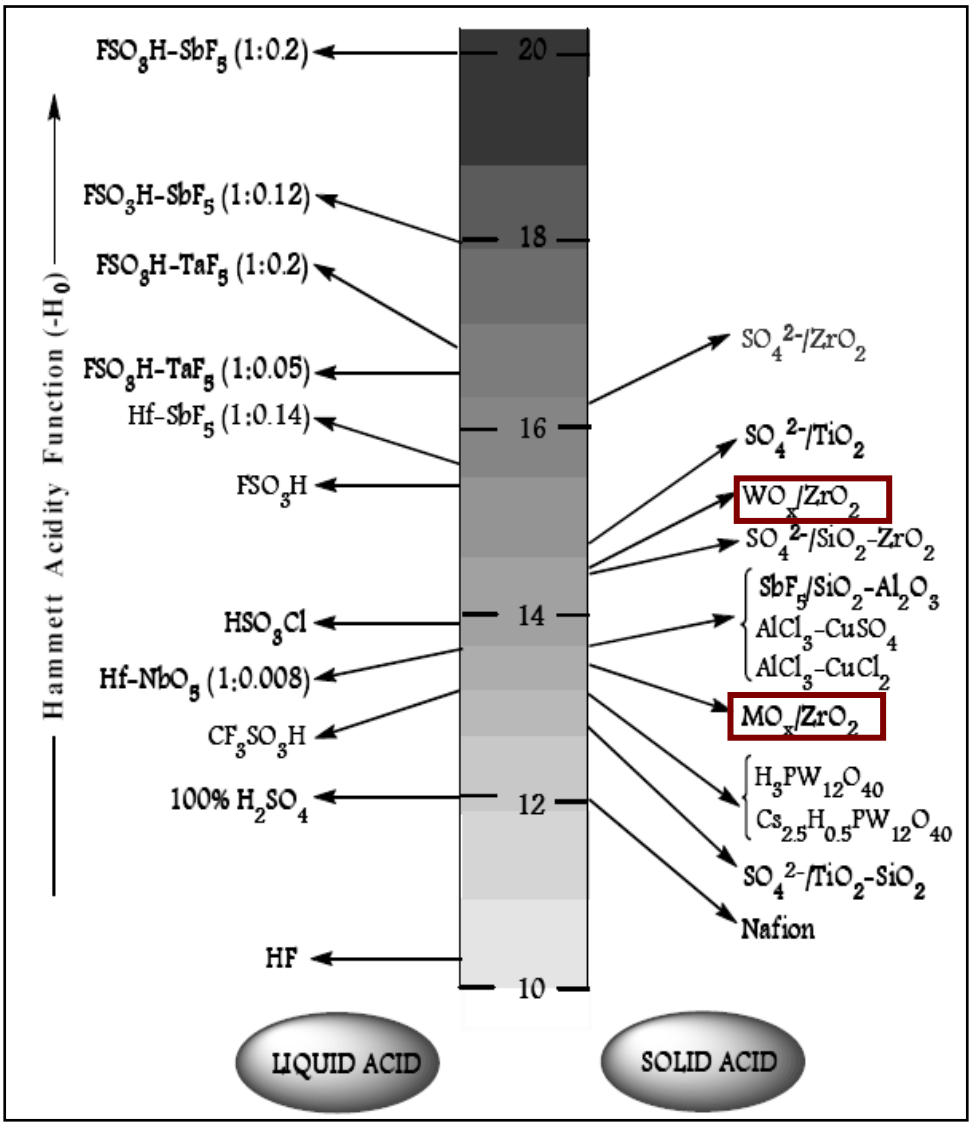

Fig. 1.2: Acid strengths of various liquid and solid acids materials.

Interpretation of acidic properties of solids is important for the investigation of solid acid catalysis. Two methods are mainly applied for the determination of acid strength and amount of solid acid, the amine titration method (n-butylamine titration) using Hammett

indicators and a gaseous base adsorption (ammonia or pyridine) [27]. In the titration method indicators are used, where the color of suitable indicators adsorbed on the solid surface gives the measure of its acid strength. If the color detected is that of the acid form of the indicator, then the value of the H_0 function of the solid is equal or lower than the pKa of the conjugate acid of the indicator applied. Temperature Programmed Desorption of Ammonia (TPD-NH_3) is a method to determine the amount and strength of acid site, but Brønsted and Lewis, cannot be differentiated by this method. The amount of acid on a solid is expressed as number or mmol of acid sites per unit weight or per unit surface area of the solid acid. IR spectroscopy using pyridine as a probe molecule can be used to ascertain the presence of Lewis or Brønsted acid sites at the surface of solid acid catalyst.

1.6. Super Acidity

The strength of super acid can be usually characterized by so-called Hammett acidity function, H_0. The Hammett acidity of 100% sulfuric acid is (H_0 – 11.93), and this is by convention the threshold of super acidity. Acids with acid strength higher than pure sulfuric acid are classified as super acids [28]. Micro-calorimetric measurement is usually used to measure the acidity of the super-acid because the method can be done at room temperature and would not destroy the structure of the super-acid However; micro-calorimetric measurement does not discriminate between Brønsted and Lewis acid sites. Gillespie's definition of super-acids relates to Brønsted acid systems [29]. While the Brønsted acid-base interaction always involves a proton transfer reaction that allows meaningful comparison, in the Lewis acid-base interaction there is no such common denominator [30]. The result is that the definition of acid strength has no real meaning with Lewis acids. The use of the H_0 function to determine the "superacidity" of heterogeneous solid acids has many obstacles. To test the acidity, the basic indicator has to be weak enough not to affect the original acidity of the solid acid sample. Over the surface of a solid sample, it is hard to achieve the equilibrium measurement using these indicators [31]. Moreover, the solid acid samples are often colored or dark and cause inaccuracy in visual observations of color changes. The acid sites on a solid surface are of different strengths and the indicators may be adsorbed only to part of the acid sites not distinguishing how they are absorbed. The surface area available for acidity

determinations may have widely different acidic properties from the bulk material. It is possible that only a small part of the detected acidic sites are strong enough. The generic term of acidity includes both acid strength and surface concentration of the acid sites. It is apparent that a single technique can not provide adequate accurate information on solid acids. The application of adsorption and desorption of base molecule provides other techniques to measure the acidity of a solid acid. Beside Hammett indicator method, there are many approaches to characterizing acid strength using some kind of adsorbed base as a probe molecule and a spectroscopic measurement of the acid-base interaction, such as TPD, FTIR, NMR etc. The adsorption heat and activation energy from temperature-programmed desorption tests have been correlated with acid strength in terms of the Hammett function [32,33]. However, this method can also lead to inaccurate conclusions. For example, the TPD of adsorbate molecules may involve decomposition species, especially on strong acids that can also be absorbed on both acid and base sites. The base molecules could be absorbed on acid sites that are not catalytically active. The desorbed molecules could diffuse and be reabsorbed on the acid sites [34]. Juskelis et al. have even shown that a non-acidic solid, such as CaO, can also retain a base, NH_3, at high temperatures [35], which points out the uncertainty of the correlation of acid strength with the results of desorption tests. Umansky et.al. [36] reported that a sulfated zirconia sample did not demonstrate strong superacidity and that its acidity was close to that of a mordenite or a Y-zeolite sample. They also found that the acid strength was more important than the acid concentration for the acidity of solids. Other researchers also found that the acidity of sulfated zirconia was not as high as expected [37-42]. Since there is a lack of satisfactory methods of determining the acidity of a solid, the superacidity of anion-modified zirconias is in doubt. Because of the complexity of a solid acid catalyst, all the experimental results should be interpreted with caution. In any case, it is important to note that the catalytic properties of solid acid catalysts strongly depend on the method of preparation, pre-treatment and storage. These differences add to the disagreement of acidity among various researchers. Even if the acidic properties of a solid acid could be accurately determined, it would still be difficult to relate acidity to catalytic reactivity because of the wide distribution of the type and strength of the surface acidic sites and the uncertainty about what sites are catalytically active.

1.7. Types of Solid Acid Catalyst

There are wide variety of solid acid catalyst available e.g. Clays, Zeolites, Mesoporous Materials, Ion-exchange resins, Heteropolyacids (HPAs), Metal promoted oxides, Sulfated oxides, Sulfonated polysiloxanes, etc. which are used in various industrial processes. Hundreds of solid acids have been developed to date. Some of the solid acids have been summarized here: (1) natural clay minerals (montmorillonite); (2) zeolites (H-ZSM-5, H-Beta, H-Y); (3) cation exchange resins (amberlyst-15, nafion); (4) heteropoly acids (MPA, TPA) (5) metal oxides (Al_2O_3, SnO_2, Nb_2O_5, WO_3); (6) mixed oxides (SiO_2-Al_2O_3, SiO_2-ZrO_2, TiO_2-MoO_3). Table 1.3 gives general classification and applications of various heterogeneous catalysts.

Table 1.3: General classification and applications of heterogeneous catalysts.

Class of catalysts	Examples	Applications
Metals (supported-mono, bi-, multi-metallic), alloys, etc.,	Pt, Pd, Rh, Ni, Fe, Co, Cu, Ag, etc., on SiO_2, Al_2O_3, activated carbon etc	Hydrogenation, dehydrogenation, aromatization, oxidation.
Metal oxides amorphous and crystalline and mixed metal oxides (acidic or redox)	CuO, SiO_2-Al_2O_3, zeolites, mesoporous metal oxides, AlPOs, SAPOs, Fe-Mo, Perovskites, spinels.	Alkylation, cracking, isomerization, amination. disproportionation, selective oxidation, dehydration,ammoxidation.
Metal sulfides (supported)	Co-Mo, Ni-Mo, Ni-W on Al_2O_3, SiO_2 or other supports	Hydrodesulfurisation, hydrotreating, hydrogenation
Ion-exchange resins	Nafion-H, amberlyst etc resins	Etherification, hydration, esterification, dehydration,
Heteropolyacids (supported)	$H_3PW_{12}O_{40}$, $H_3PMo_{12}O_{40}$, $H_4SiW_{12}O_{40}$	Acid catalyzed reactions, Oxidation, condensation
Clays and pillared clays,	Kaolinite,K-10 Montmorillonite.	Acid-catalyzed reactions, cracking, alkylation, nitration
Metal complexes (supported or encapsulated)	Metal porphyrins, salens and pthalocyanins)	Selective oxidation and epoxidation.

Zeolites are commonly grouped under ordered microporous molecular sieves, which are oxides of silicon and aluminum, typically structured around an organic template molecule in the form of a gel which later crystallizes. The template is then removed via calcination leaving an ordered porous material. Zeolites are widely used

within the petrochemical industry in acid catalyzed processes, and there are several reports concerning recent developments in their use in the synthesis of fine and specialty chemicals [43]. Clays were used for this purpose in early 1930's, till they were replaced firstly by ZSM-5, X and Y type etc zeolites in late 1960's. When compared with other solid acids, zeolites possess certain peculiarities which make them a unique type of material such as ability to control the number and strength of acid sites; crystalline well defined ordered porous structure enabling favorable high adsorption properties and the inclusion of active acid sites etc. The control of the molecular dimensions of the pores can result in shape selective effects and pre-activation of the molecules inside the pores by strong dielectric fields and molecular confinement [44]. Unfortunately, the use of zeolites under these conditions is restricted by their small pore sizes of (~ <1.2 nm), which makes them unsuitable for reactions involving bulky substrates. However, recent developments in materials chemistry have led to the discovery of the M41S family of mesoporous molecular sieves [45] offering pore sizes in the range 2–10 nm which opens up new possibilities for liquid-phase acid catalysis involving bulky molecules. Even if there is great potential for catalyzing reactions with zeolites and mesoporous molecular sieves, there are still many reactions which require stronger acid sites than those present on these materials. Therefore it is necessary to develop stronger solid acid sites which can be achieved using heteropolyacids or resins. Most of the work has been carried out on the Keggin-type HPAs because it is easy to prepare and reasonably stable. These materials exhibit very strong Bronsted acidity with stronger activity than some studied solid acid catalysts like SiO_2-Al_2O_3, zeolites HX, HY, etc. and there are many reviews discussing various aspects of catalysis using HPAs and summarizing all recent developments in this field [46]. Commercially available heteropoly acids such as $H_3PW_{12}O_{40}$, $H_4SiW_{12}O_{40}$, $H_3PMo_{12}O_{40}$ and $H_4SiMo_{12}O_{40}$ and their metal promoted species have low surface areas of 1–5 m^2/g, limiting their use in catalysis, which has led the researchers to investigate the use of HPAs immobilized on high surface area mesoporous materials such as MCM-41 (Mobil Composition of Matter No. 41), HMS (Hexagonal Mesoporous Silica), SBA (Santa Barbara), MSU (Michigan State University material) etc based supports in liquid-phase organic reactions. Supported HPAs can be prepared either by post-modification of the mesoporous support, or can be incorporated into the pore structure during the

synthesis by sol gel process. These materials exhibit high activity in a range of acid-catalyzed reactions, including the alkylation, esterification, hydrolysis etc. However, their fairly low thermal stability causes lost of acidity especially at temperatures ranging from 350 to 450 ^{o}C and also lead to difficulty of catalysts regeneration. Materials prepared using sol gel process is more resistant towards leaching of the HPA component but limits the accessibility and efficiency of the catalyst. Commercially available sulfonated resins Amberlyst-15 and Nafion-H based on sulfonated polystyrene and per-fluorinated sulfonic acid resins, respectively are sulfonic acids having strong Brønsted acid sites. Despite its low surface area, they have been used in a wide range of organic reactions [47] including alkylation, acylation, nitration, etherification, and esterification reactions. In an attempt to overcome the low surface area of these ion-exchange resins, a group of workers has developed Nafion-silica composites, in which Nafion particles are incorporated into silica structure during the sol gel process [48,49,50]. The main advantage of silica-supported solid sulfonic acid systems is its higher surface area (400–900 m^2/g compared to <1 m^2/g for resins). However, the complexity of the preparation of these materials is not really cost effective when compared other solid acid catalyst. The other issue associated with these catalysts is thermal stability and catalyst regeneration [51]. In view of these reasons there is an ongoing effort to develop stronger solid acid systems which are water tolerant, stable at high temperatures and suitable for both liquid and vapor phase conditions. Metal oxide based catalysts offer several advantages as they active over a wide range of temperatures and more resistant to thermal excursions. Aside from organic-inorganic supported solid acid catalysts, research has been carried out on alternative non porous supports. During the period some transition metal oxides were found to be highly acidic, containing both Lewis and Brønsted acid sites, and like Nafion today, were claimed to be "super-acidic". In the early eighties, it was found that when some transition metal oxides such as ZrO_2, TiO_2, SnO_2, Fe_2O_3, and HfO_2 modified by sulfate ion, such as SO_4^{2-}/ZrO_2, SO_4^{2-}/TiO_2, SO_4^{2-}/TiO_2-SiO_2, SO_4^{2-}/ZrO_2-SiO_2 and SO_4^{2-}/Fe_2O_3 etc by sulfuric acid or ammonium sulfate and were subsequently calcined, a remarkable increase in the surface acidity has been developed and used as a powerful catalyst for various acid catalyzed reactions [52]. Titanium dioxide has moderate acidic strength (H_0 = +1.5) and weak basic strength. The acidic and basic strengths of ZrO_2 are very weak. Ferric Oxide is an

almost neutral oxide. However, these oxides begin to show superacidity when they contain a small amount of sulfate ion or if a small amount (0.5-8 wt %) of ammonium sulfate or sulfuric acid is added [53]. Sulfated metal oxides were claimed to be super acidic on the basis of the following observations. Their acid strength measured by the Hammett indicators method goes up to H_0<-16.4. Adsorbed benzene, is a very weak base, desorbs at very high temperature in TPD experiments. These materials are able to isomerize n-butane at temperatures below 100 °C. On these bases, it was accepted that, indeed, a new type of solid super-acids were obtained. This opened new perspectives in the friendly use of solid catalysts for carrying out reactions involving very strong acid sites under mild conditions. It is not surprising that in this type of material the final catalytic properties can be strongly dependent on the preparation conditions. Several different methods are described for the preparation of these materials. The basic patent was assigned to Phillips Petroleum in 1962 [54]. This patent is related to sulfated zirconia doped with platinum for isomerization processes. Indeed, sulfated metal oxides were initially prepared by a two step process which involved the mixing of a zirconium hydroxide with sulfuric acid or ammonium sulfate and then calcining the mixture to temperatures of 500-650 ^{o}C. It has been shown that each one of the steps, that is, the formation of the zirconium hydroxide, sulfation and final calcination has to be optimized in order to produce an adequate catalyst [55,56]. Furthermore, this optimum can be different depending on the metal oxide to be sulfated. It appears that one of the key points in preparing active catalysts by a two step procedure is the amount of tetragonal-phase zirconia in the sulfated zirconia. The catalytic activity is higher when the amount of the tetragonal phase is larger. This tetragonal phase appears to be stabilized by the sulfate groups on the surface, and is responsible for the increase in surface area of the sulfated material. It is possible to control the amount of the tetragonal phase by an adequate control of the pH of precipitation of the zirconium hydroxide precursor. The reason for the above could be that the tetragonal phase has a higher content of non bridging surface hydroxyl groups than the monoclinic phase. This seems to be a crucial factor for producing active materials. From a practical point of view, sulfated metal oxides have some drawbacks. Besides possible problems in preparation, the maximum inconvenience lies in the fast deactivation of catalyst. The reasons for catalyst deactivation can be

sulfate loss during the process or catalyst regeneration, crystalline phase transformation from the tetragonal to the monoclinic and finally formation of coke during the process [57].

1.8. Advantages of supported materials

From some of the above mentioned solid acid catalysts, it is apparent that supported catalysts have advantages over unsupported materials. Supports serve various functions such as (a) acts as an inert substance onto which expensive catalyst components can be deposited uniformly to have maximum active sites for catalytic reactions (b) stabilizes the crystallites of the catalytically active component and prevent sintering (c) improves the mechanical strength, thermal stability and the lifetime of the catalyst [59].

1.9. Zirconia as a support

The most commonly used catalyst supports are Alumina, Silica, Titania and Activated Carbon etc [60]. High surface area alumina and silica both are commercially available. However, catalytic reactions requiring higher temperatures, these supports suffer from the loss in surface area, phase transformations, and chemical reactions with the active phase [61]. Among the non-silica mesoporous oxides, zirconia has received a particular interest in the past, due to the large field of applications ranging from catalysis to ceramics. There have been several reports on the usage of zirconia as a catalyst and/or catalytic support as compared to other transition metal oxides due to its high thermal stability, remarkable mechanical strength, high melting point, low thermal conductivity, high corrosion resistance, amphoteric behavior and unique properties of the surface due to the hydroxyl groups [62,63,64]. The application of zirconia as a catalyst support has been employed in many industrially important reactions as it is stable under oxidizing and reducing conditions and it possesses both acidic and basic properties. Also, unlike Al_2O_3, zirconia does not form solid solutions upon addition of a second metal oxide component. Commercially available zirconia has a relatively low surface area (40 m^2/g or less), which is rather lower than the conventional supports such as alumina and silica. The use of zirconia, from both scientific and industrial application point of view requires high specific surface area and suitable pore structure for catalysis applications. One way of increasing the surface area is using amphoteric, anionic, or neutral templates.

Depending on the synthesis pathway, zirconyl salt or zirconium alkoxide as zirconium precursors, hexagonal, cubic or disordered high surface area mesoporous zirconia can be successfully obtained [65,66,67]. However, as it is the case for most of other mesoporous transition metallic oxides, it is very difficult to preserve the structure after the surfactant removal at high calcination temperature, as the structure generally collapses after the pores are freed from the surfactant causing loss of surface area and thereby its catalytic activity.

1.10. Molybdenum and Tungsten oxide modified Zirconia

It is well known that zirconia has three stable crystalline phases: tetragonal, monoclinic and cubic [68,69]. It is seen earlier that SO_4^{2-}/ZrO_2 catalyst containing tetragonal phase is more active as compared to other crystalline phases. Tetragonal phase (t-ZrO_2) has both acidic and basic properties [62] and gives the most active catalyst for some catalytic reactions [63]. However, the thermal stability of t-ZrO_2 is crucial since the transition from the tetragonal to the monoclinic phase results in sintering and deactivation of the catalyst. The concentration and transformation among tetragonal, monoclinic and cubic phases depend on synthesis procedure and doping zirconia with foreign ions and/or thermal treatment conditions. Doping zirconia with a variety of oxo-anions such as sulfate, phosphate and heteropolyanions results in stabilization of the tetragonal phase by interacting with the surface, inhibiting the crystallite growth, and consequently, hindering its transition into the monoclinic phase [70,71,72,73]. The acidic nature and crystalline structure of zirconia can also be modified by group VI elements from the periodic table like chromium molybdenum or tungsten oxides which are more thermally stable then sulfated zirconia [23,53,74]. The acidic and basic strengths of ZrO_2 are very weak, while modifying zirconia with CrO_3, MoO_3 and WO_3 between 2-20 wt% were estimated to have H_0 = -14.5, indicating the formation of new acid sites, considerably stronger than those of the ZrO_2. The higher the content of metal oxide content, the higher the phase transition temperature of ZrO_2 from amorphous to tetragonal. The formation of a solid super acid was attributed to stabilization of the tetragonal ZrO_2 phase and the double bond nature of the group six elements with ZrO_2 during the crystallization of tetragonal ZrO_2 [75,76]. Applying this method, several authors found that the tungstated zirconia

support can accede highly acidic properties with a $H_0 = -14.5$. However, all the methods described the preparation of powder catalyst, whereas formed catalysts are needed for most of the applications in industry, e.g. for the isomerization of C_5/C_6 mixtures in refineries to enhance the octane number. In 1996, UOP, commercialized the first solid acid catalyst based on zirconia (shaped as extrusions) [77] but the preparation method of this catalyst was never published. Probably, the preparation procedure is based on the patent of the Research Association for Utilization of Light Oil [78]. Even though these catalyst are comparatively less active than sulfated zirconia at lower temperatures (<100 ^oC) in alkane isomerization reactions, they are more stable at higher temperatures [79] and in reducing atmosphere [69].

Although supported chromium oxide catalysts have be used for reactions such as polymerization, hydrogenation and oxidation-reduction, etc [53], the divalent, trivalent chromium compounds and metallic chromium are toxic, whereas chromium (VI) compounds are very toxic and carcinogenic [80]. Care must be taken when handling chromium (VI) reagents in finely powdered form, because such compounds have extremely high toxicity from inhalation and oral exposure. If chromium compounds are used in excess, typically for the oxidation of alcohols to carbonyl compounds and carboxylic acids, any remaining chromium (VI) species can be quenched by the addition of 2-propanol. A color change from a typical orange to deep green indicates the complete quenching.

Seaborgium is a synthetic 106^{th} Element and the heaviest member of Group VI in the Periodic Table, whose most stable isotope ^{271}Sg has a half-life of 1.9 minutes. This element is projected to be the third member of the 6d series of transition metals, below chromium, molybdenum and tungsten. All the members of the group readily portray their group oxidation state of +6 and the state becomes more stable as the group is descended. Therefore Chromium and Seaborgium have not been considered in the scope of our studies. Tungsten is rare and its compounds are generally inert, the effects of tungsten on the environment are limited. Direct inhalation or ingestion of molybdenum and its oxides should be avoided. Acute toxicity due to molybdenum and its oxides has not been seen in humans. The MoO_3 and WO_3 supported on zirconia when calcined at high temperatures were found to be highly acidic and used as a powerful catalyst for various acid catalyzed

reactions [22,23,53,74]. The formation of a solid super acid was attributed to stabilization of the tetragonal ZrO_2 phase and the double bond nature of the Group VI elements with ZrO_2 during the crystallization of tetragonal ZrO_2 [76,79]. Even though, it is possible to generate super solid acid catalyst without sulfation, it is not yet routinely possible to obtain uniform pore architecture as well as the stability of the solid in the system. As a general conclusion, it can be said that a large variety of solid acid catalysts are now available and their acidic properties, their catalysis, and the structure of acid site have been elucidated and these results have been reviewed by several workers. The nature, number and strength of acid sites, morphology, surface area, pore size, surface density, suitable phase for high selectivity toward the desired products etc and other physicochemical properties of solid acid catalyst strongly relies on the preparation methods, precipitating agent, starting precursors, calcination temperature, pre-treatment etc [59,81,82,83,84]. Considering the drawbacks in the conventional synthesis of these materials it is proposed to synthesize high surface area zirconia catalyst with/without surfactant so that some of the above mentioned problems can be avoided. There is also need to develop and optimize the synthesis procedure to obtain a solid acid catalyst with strong acidity, high surface area, and high thermal stability and to relate its physical and chemical properties, synthesis procedures and its catalytic activity. Further studies are required to characterize solid acid catalysts in order to relate physical and chemical properties to acidity and catalytic activity in liquid phase reactions. However, so far it is not reported with any given catalysts to possess simultaneously very strong acidity, very high surface area, high mechanical resistance, high thermal and hydrothermal stability, and inexpensive catalyst production.

1.11. Objectives of the Research

Since the last decades there has been a search for a catalyst that can meet the new requirements from both the legislation and the market. One class of catalysts that has received a lot of attention is anion modified metal oxides, which show good acidic properties. The focus has been on anion modified zirconia in particular. Therefore, the main aim of the present study is to design and develop, anion modified zirconia based solid acid catalysts with high surface areas and thermal stabilities and their utility in organic synthesis.

- Zirconia requires a high specific surface area, suitable pore structure and tetragonal crystalline phase for catalytic applications from both, scientific and industrial application point of view. The present work deals with optimization of synthesis parameters for the preparation of high surface area tetragonal zirconia with/without surfactant having good thermal stability.

- Although the synthesis, characterization and catalytic evaluation of solid acid catalyst containing Group VI elements such as Mo, W, etc on zirconia have been reported earlier, no systematic studies have been carried out and reported so far for these materials. Therefore there is a need to develop facile procedures for the synthesis of Solid acid catalyst containing Group VI elements having strong acidity, high surface area, high thermal stability and economical catalyst production.

- Physico-chemical characterization of the above mentioned catalysts by Powder XRD, N_2 adsorption-desorption, TG/DTG, TEM, SEM, UV-Vis, RAMAN, XPS, Ammonia-TPD, XRF, AAS, ICP and EDAX to carry out the systematic studies for exploring the cause and effective relationship of several synthesis variables (viz. pH, starting precursor, gel composition, calcination temperature etc.) on the physicochemical and morphological properties including its stability and catalytic activity.

1.12. Outline of the Research

On the whole, pure zirconia and zirconia-based solid acid catalysts were successfully synthesized by various facile routes. Physicochemical characterization of all these catalysts revealed that the incorporated group VI elements show a significant influence on the surface and bulk properties of the ZrO_2 and stabilize the metastable zirconia tetragonal phase at ambient conditions and enhance the total number and strength of acid sites. Structural and surface properties strongly depend upon synthesis parameters.

Chapter 1 comprised of a thorough literature survey on the significance of solid acid catalysts in various domains of chemical industry and importance of anion promoted zirconia catalysts. Classification of solid catalyst and their applications are given in short. Various type solid acid catalyst, their brief advantages and disadvantages from industrial and academic point of view. Importance of zirconia modified by group VI elements is also outlined. The aims and objectives of the present investigation are also given at the end of this chapter.

Chapter 2 deals with the experimental procedures and techniques employed in this investigation. Scientific aspects of the precipitation, impregnation and sol-gel methods were outlined. The experimental details of surface area measurements by BET method, application of XRD studies for crystalline phase and size determination, TPD of ammonia analysis for acid strength distribution, Raman, ICP, AAS, XRF and XPS techniques to determine bulk and surface properties of the prepared catalysts have been described. Theoretical background of various techniques is also provided with schematic drawings and relevant literature references.

Chapter 3 deals with the optimization, preparation and intensive characterization of pure zirconia support, in terms of obtaining maximum possible surface area with tetragonal phase. The bulk and surface properties of the catalyst have been examined by TG-DTA, X-ray powder diffraction, BET surface area and IR spectroscopy techniques. All the characterization results revealed that the incorporated ions showed a significant influence on the phase formation and thermal stability ZrO_2 materials. In this investigation, various

zirconium precursors are used for preparing zirconia materials and its thermal stability was assessed. The role of the principal preparation variables controlling the phase composition and thermal stability, such as pH, concentration of the solution, the nature of parent zirconium salt as well as aging/digestion of the precipitate was studied.

Chapter 4 deals with the preparation and intensive characterization of molybdate promoted zirconia solid acid catalysts and their application in organic synthesis and transformation reactions. To investigate the structural and textural properties, the synthesized catalysts are characterized by TG-DTA, X-ray powder diffraction, BET surface area, temperature programmed desorption of ammonia, scanning electron microscopy, Raman spectroscopy, and FT-infrared spectroscopy etc techniques. In this study, molybdate promoted zirconia catalysts are evaluated for the synthesis of chalcones under solvent free conditions. Optimization of reaction conditions were also carried out. Molybdate promoted zirconia is found to be excellent catalyst for Claisen-Schmidt condensation reaction.

Chapter 5 deals with synthesis and characterization of WO_3-/ZrO_2 solid acid catalyst. More emphasis is being given on how the properties may affect by altering the various synthesis variables. A vast variety of characterization techniques have been used to evaluate surface and bulk properties of the catalyst by means of X-ray powder diffraction, ammonia-temperature programmed desorption, IR spectroscopy, TG-DTA, X-ray photo electron spectroscopy and BET surface area measurements methods. Elemental characterization for the determination of W in the catalyst has been carried out using ICP, EDX, XRF and XPS and their results are compared. Effect of various synthesis parameters and starting precursors are also studied in detail with respect to formation of acid sites, thermal stability, surface area and surface density of W. All these aspects are discussed in this chapter.

Chapter 6 summarizes the conclusion obtained from the above studies and scope of future work.

1.13. References:

[1] G. Ertl, T. Gloyna, Z. Phys. Chem. 2003, 217, 1207−1219.

[2] Ian. M. Campbell, Catalysis at Surfaces, Chappman and Hall, New York, 1988.

[3] J.M. Thomas, Principles and Practice of Heterogeneous Catalysis, VCH, Weinheim, 1997.

[4] G. Ertl, H. Knozinger, J. Weitkamp, Handbook of Heterogeneous Catalysis, Willey-VCH, Weinheim, 1997

[5] M.S. Simmons, P.T. Anastas, T.C. Williamson (Eds.), Green Chemistry: Designing Chemistry for the Environment, American Chemical Society, Washington, DC, 1996, 10, 116.

[6] B. Lindstr, L.J. Pettersson, Cat. Tech., 2003, 7, 130.

[7] C. Christ, Ed. Production-Integrated Environmental Protection and Waste Management in the Chemical Industry, Wiley-VCH, Weinheim, 1999.

[8] P.T. Anastas, J.C. Warner, Eds., Green Chemistry: Theory and Practice, Oxford Univ. Press, Oxford, 1998.

[9] P.T. Anastas, T.C. Williamson, Eds., Green Chemistry: Frontiers in Chemical Synthesis and processes, Oxford Univ.Press, Oxford, 1998.

[10] K. Tanabe, W. F. HÖlderich, *Appl. Catal., A*, **1999**, *181*, 399.

[11] S.Y. Kim, G. James, Jr. Goodwin , D. Farcasiu, Appl Catal A, 2001, 207, 281–286.

[12] J.Z. David , S. Lerasool, P.K. Doolin, Catal. Today, 1999, 53, 419–432.

[13] S. K. Samantaray, K.J. Parida, Mater Sci, 2004, 39, 3549–3562.

[14] P. Salas, J.G. Hernandez, J.A. Montoya, J. Mol Catal A:Chem, 1997, 123, 149–154.

[15] J.R. Sohn, S.H. Lee, J.S. Lim, Catal. Today, 2006, 116, 143–150.

[16] G.D. Yadav, G.S. Pathre, Micro. Meso.Mater, 2006, 89, 16–24.

[17] G.D. Yadav, G. George, Micro. Meso. Mater, 2006, 96, 36–43.

[18] J.R. Sohn, C. Dong, Shin, Appl. Catal. B, 2008, 77, 86–394.

[19] D.Q. Zhou, J.H.Yang, G.M. Dong, M.Y. Huang, Y.Y.Jiang, J. Mol. Catal. A: Chem, 2000, 159, 85–87.

[20] H. Matsuhashi, M. Tanaka, H. Nakamura, K. Arata, Appl. Catal. A-General, 2001, 208, 1–5.

[21] W.U. Yanni , L.I.A.O. Shijun, Front. Chem. Eng. China 2009, 3, 330–343.

[22] M. J. Climent, A. Corma, and S. Iborra, Chem. Rev.2010, In Press.

[23] B. M. Reddy and M. K. Patil, Chem. Rev., 2009, 109, 6.

[24] J.T. Richarrdson, Principles of Catalyst Development. New York: Plenum Press, 1989, 240-241.

[25] K. Tanabe, Misono, M., Ono, Y., and Hattori, H. Studies in surface and Catalysis. 1989, 51, 1-4.

[26] L. P. Hammett and A. J. Deyrup, J. Am. Chem. Soc.,1932, 54, 2721 .

[27] M.Yurdakoç, M. Akçay, Y. Tonbul, and K. Yurdkoç Turk. J. Chem., 1999, 23, 319–327.

[28] J. R. Sohn and M. Y. Park Langmuir, 1998, 14, 6140–6145.

[29] R.J. Gillespie, T.E. Peel, J. Am. Chem. Soc., 1973, 95, 5173.

[30] G.A. Olah, G.K.S. Prakash, J. Sommer, Superacids, Wiley, New York, 1985.

[31] (a)T.K. Cheung, B.C. Gates, Chemtech 27 (1997) 28; (b) B.S. Umansky, W.K. Hall, J.Catal., 1990, 124, 97.

[32] N. Katada, J. Endo, K. Notsu, N. Yasunomu, N. Naito, M. Niwa, J. Phys. Chem. B, 2000, 104, 10321.

[33] H. Matsuhashi, K. Arata, Chem. Commun, 2000, 387.

[34] S.B. Sharma, B.L. Meyers, D.T. Chen, J. Miller, J.A. Dumesic, Appl. Catal. A: Gen., 1993, 102, 253.

[35] M.V. Juskelis, J.P. Slanga, T.G. Roberie, A.W. Peters, J. Catal.1992, 138, 391.

[36] B. Umansky; J. Engelhardt, W.K.J. Hall, Catal. 1991, 127, 128.

[37] K. Ebitani, J. Tsuji, H. Hattori, H.J. Kita, Catal. 1992, 135, 609.

[38] T.K. Cheung, F.C. Lange, B.C.J. Gates, Catal.1996, 159, 99.

[39] R.S. Grago, N.J. Kob, Phys. Chem. B 1997, 101, 3360.

[40] F. Arena, R. Dario, A. Parmaliana, Appl. Catal., A 1998, 170, 127.

[41] J.C. Vartuli, J.G. Santiesteban, P. Traverso, N.Cardona-Martinez, C.D. Chang, S.A.J. Stevenson, J. Catal. 1999, 187, 131.

[42] K. Arata, H. Matsuhashi, M. Hino, H. Nakamura, Catal. Today 2003, 81, 17.

[43] A. Corma. Chem. Rev. 95, 1995, 559.

[44] A. Corma, Current Opinion in Solid State & Materiels Science 1997, 2, 63-75.

[45] J.S. Beck, J.C. Vartuli, W.J. Roth, M.E. Leonowicz, C.T. Kresge, K.D. Schmitt, T.W. Chu, D.H. Olsen, E. W. Sheppard, S.B. McCullen, J.B. Higgins, J. L. Schlenker. J. Am. Chem. Soc. 114, 1992, 10834.

[46] I.V. Kozhevnikov. Chem. Rev. 98,1998, 171.

[47] G.A. Olah, P. S. Iyer, G.K.S. Prakash. Synthesis, 1986, 513.

[48] M.A. Harmer, W.E. Farmeth, Q. Sun. J. Am. Chem. Soc., 1996, 118, 7708.

[49] Q. Sun, M. A. Harmer, W.E. Farneth. Chem. Comm., 1996, 1201.

[50] M.A. Harmer, W.E. Farmeth, Q. Sun. Adv. Materials , 1998, 10, 1255.

[51] Z. Helwani, M.R. Othman, N. Aziz, J. Kim, W.J.N. Fernando, Appl. Catal. A: General., 2009, 363, 1–10.

[52] X. Song, A. Sayari . Cata/Rev-Sci Eng 1996, 38, 329-412 .

[53] J. R. Sohn, Ind. Eng. Chem., 2004, 10, 1-15.

[54] V.C.F. Holm, G.C. Bailey, US Patent 3,032,599 (1962), assigned to Phillips Petroleum.

[55] M.A. Coelho, D.E.Resasco, E.C.Sikabwe, R.L.White, Catal Lett 1995, 32, 253-262.

[56] A.V. Corma, MI. Juan Rajadell, J.M. Lopez Nieto: App. Catal. A - Gen 1994, 116, 151-163.

[57] Y.Y. Yori, J.C. Luy, J.M. Parera, Catal. Today 1989, 5, 493.

[58] F.T.T. Ng, N. Horr´at, Appl. Catal. A 1995, 123, 195.

[59] A.B. Stiles (Ed.), Catalyst Supports and Supported Catalysts: Theoretical and Applied Concepts, Butterworths, Boston, 1987.

[60] C.N. Sattereld, Heterogeneous Catalysis in Practice, McGraw-Hill, New York, 1980.

[61] K. Maeda, F. Mizukami, M. Watanabe, N. Arai, S. Niwa, M.Toba and K. Shimizu, J. Mater. Sci. Letts., 1990, 9, 522.

[62] T. Yamaguchi, Catal. Today, 1994, 20, 199.

[63] G. Centini, G. Cerrrato, S.D. Angelo, U. Finardi, E. Giamello, C. Morterra and S. Perathoner, Catal. Today,1996, 27, 265.

[64] Y. Zhu, S. Liu, S. Jaenicke and G. Chuah, Catal. Today, 2004, 97, 249–255.

[65] G. Pacheco, E. Zhao, A. Garcia, A. Sklyarov, JJ. Fripiat , Chem Commun 1997, 491.

[66] P. Yang, E. Zhao, DI. Margolese, BF. Chmelka, GD. Stucky . Chem. Mater, 999, 11, 2813.

[67] J.A. Knowles, M.J. Hudson, J. Chem. Soc., Chem. Commun., 1995, 2083.

[68] P.T. Tanev and T.J. Pinnavaia, Science, 1995, 267, 865-868.

[69] U. Ciesla, S. Schacht, G.D. Stucky, K.K. Unger and F. Schueth, Angew. Chem.Int. Edn Engl., 1996, 35, 541-543.

[70] G. Pacheco, E. Zhao, A. Garcia, A. Sklyarov, J. J. Fripiat ,. J. Mater. Chem., 1998, 8, 219.

[71] Y.Y. Huang, T.J. McCarthy, W.M.H. Sachtler . Appl. Catal. A 1996, 148, 135.

[72] M.S. Wong, J. Ying . Chem. Mater.,1998, 10, 2067.

[73] U. Ciesla, M. Froba, G. D. Stucky, F. Schuth. Chem. Mater, 1996, 11, 227.

[74] K. Arata, Appl. Catal. A: General, 1996, 146, 3-32.

[75] M. Hino, K. Arata, J. Chem. Soc., Chem. Commun, 1988, 1259.

[76] B. Li and R. D. Gonzalez Ind. Eng. Chem. Res., 1996, 35, 3141–3148.

[77] C. Gosling, R. Rosin, P. Bullen, T. Shimizu, T. Imai, World refining, in: Proceedings of Vehicle Technology & Fuel Quality Conference, Brussels, May.1997, 21–23.

[78] S. Baba, Y. Shibata, T. Kawamura, H. Takaoka, T. Kimura, K. Kousaka, Y. Minato, N. Yokoyama, K. Iida, T. Imai, US Patent 5,036,035 (1991), assigned to Research Association for Utilization of Light OiL.

[79] S.A. Bagshaw, & T.J. Pinnavaia, Angew. Chem. Int. Edn Engl.1996, 35, 1102-1105.

[80] M. Costa, Toxicity and carcinogenicity of Cr (VI) in animal models and humans. Crit. Rev. Toxicol, 1997, 27, 5, 431-42.

[81] M.A. Cortes-Jacomea, C. Angeles-Chaveza, X. Bokhimib, J.A. Toledo-Antonio, Journal of Solid State Chem., 2006, 179, 2663–2673.

[82] D.E. Lopez, K. Suwannakarn, D.A. Bruce, J.G. Goodwin Jr., J. Catal., 2007, 247, 43–50

[83] J.G. Santiesteban, J.C. Vartuli, S. Han, R.D. Bastian, and C. D. Chang, J. Catal., 1997, 168, 431–441.

[84] A. Martinez, G, Prieto, M.A. Arribas, P. Concepcion, J.F. Sanchez-Royo, J. Catal., 2007, 248, 288–302.

CHAPTER – 2

SYNTHESIS AND CHARACTERIZATION TECHNIQUES

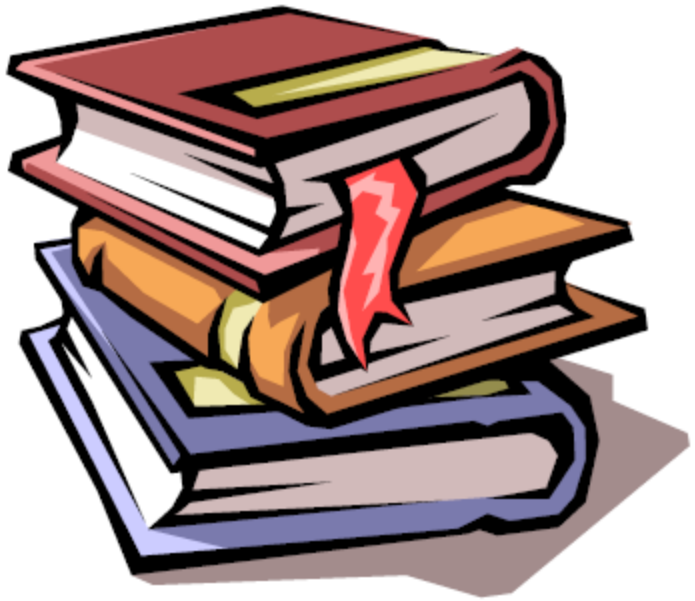

2.1. INTRODUCTION

Since last many years, the development and preparation of heterogeneous catalysts were considered more as alchemy than science, with the predominance of trial and error experiments. However, this approach is expensive, time-consuming and does not offer assurances on the final results. But, now-a-days the approach is changed to scientific and involves a wide number of specific competencies of solid state chemistry, analytical chemistry, physical chemistry and spectroscopy. A wide range of techniques has been employed for the incorporation of a catalytically active species onto a support material. A summary of the most widely used techniques is given below as an introduction to later sections in this Chapter, which describe the more important chemical and physical factors involved in the dispersion of metal salts onto supports and their influence on the activity, selectivity, and durability of the catalyst system. All the techniques of catalyst preparation can be reduce to two simple steps, First, rendering a metal-salt component into a finely divided form on a support and secondly; conversion of the supported metal salt to a metallic or oxide state. The first stage is known as dispersion and is achieved by impregnation, adsorption from solution, co-precipitation, or deposition, while the second stage is variously called calcination or reduction. The art of catalyst preparation is, has been, and probably always will be the art of preparing a material or suitable combination of materials in a highly dispersed form, and in maintaining that dispersion and combination against every natural thermodynamic tendency towards agglomeration. The primary aim of applying a catalytically active component to a support is to obtain the catalyst in a highly dispersed form and hence in a highly active form when expressed as a function of the weight of the active component. Preparation of good catalyst involves a sequence of several complex processes; many of them are very complicated. As a result, subtle changes in the preparative details may result in dramatic alteration in the properties of the final catalyst. The properties of a good catalyst may be divided, at least for the purpose of easy classification, into two categories: (1) properties which determine directly catalytic activity and selectivity, here such factors as bulk and surface chemical composition, local microstructure, and phase composition are important; and (2) properties which ensure their successful implementation in the catalytic process, here thermal and mechanical stability, porosity,

shape, and dimension of catalyst particles enter. The requirements which are fundamental for catalyst performance generally require a compromise in order to produce a material which meets the contradictory demands imposed by industrial processes. Catalysis is a complex surface phenomenon occurring on the surface of a catalyst. The adsorption of the reactant molecules and their interaction to give the product on the active phase of the catalyst depend not only on the reaction variables, but also on the nature of sites on the catalyst surface, which in turn determines the 'quality' of the catalyst system, In the production of catalysts, even a minute change in the conditions of preparation changes the quality of the catalyst. Hence utmost care should be taken during the preparation of the systems. The performance of a catalyst can be better appreciated if one knows as many of its physicochemical properties as possible. Measuring the same parameters after use often helps in understanding the cause of catalyst deactivation. Supported Mo and W catalysts form a complex class of catalysts, which are used in various reactions of industrial importance. The nature of the active sites in these catalysts is expected to vary over a wide range with % loading and with the nature of the support. To understand the phenomenon of adsorption and catalysis on a molecular basis, the nature of the molecular structure of the active oxide species on these catalysts should be thoroughly investigated and it is essential that the adsorption and active sites are to be extremely probed. The fundamental aspects in the preparation and characterization of solid acid catalysts are discussed elaborately in this chapter. The materials used and the methodologies are described in the following sections. In the preceding Chapter, the various synthesis methods and characterization techniques have been reviewed. This chapter will present the actual experimental procedures regarding (i) Synthesis of ZrO_2 (ii) Modified ZrO_2 with Group VI elements such as Mo and W through various precipitation, impregnation and sol-gel methods. (iii) Catalytic activity studies for the synthesis of chalcones.

2.2. MATERIALS

All chemicals and solvents used in this study were commercially available and used without further purification. Few chemicals which have been used for standardization such as AAS/ICP standard solutions, XRD-Silicon, UV-Barium Sulphate, NMR solvent etc are mentioned in the below list.

Acetone [CH_3COCH_3, 99.5%, S.D. Fine, India]
Acetophenone [$CH_3COC_6H_5$, 99%, Aldrich, USA]
Ammonium Hepta-Molybdate, [$(NH_4)_6Mo_7O_{24}$, 99.8%, Loba Chemie, India]
Ammonium Meta-Tungstate [$(NH_4)_6H_2W_{12}O_{40}$, 99.9 %, Aldrich, USA]
Benzaldehyde [C_6H_5CHO, 99%, Aldrich, USA]
Benzonitrile [C_6H_5CN, 99%, Merck, India]
Di-methyl Sulfoxide [$(CH_3)_2SO$, 99.5%, Merck, India]
Ethanol [CH_3CH_2OH, 99.9 %, Changshu Yangyuan, China]
Hydrochloric acid [HCl, 35%, Analytical Grade, Thomas Baker, India]
Hydrofluoric acid [HF, 48%, Electronic Grade, Thomas Baker, India]
Isopropyl Alcohol [$(CH_3)_2CHOH$, 99.9%, Thomas Baker, India]
Nitric acid [HNO_3, 70%, Analytical Grade, Thomas Baker, India]
o-Methoxy-acetophenone [$CH_3OC_6H_4COCH_3$, 98%, Fluka]
o-Methoxy-benzaldehyde [$CH_3OC_6H_4CHO$ 98%, Aldrich, USA]
p-Chloro-acetophenone [$ClC_6H_4COCH_3$, 97%, Aldrich, USA]
p-Chloro-benzaldehyde [ClC_6H_4CHO, 97%, Aldrich, USA]
Pluronic 123 [(A Nonionic Tri-Block Copolymer Surfactant); Ethylene Oxide (EO_{20}) – Propylene (PO_{70}) – Ethylene Oxide(EO_{20}), FW-5800, Aldrich, USA]
Zirconium (IV) butoxide [$\{Zr[OC(CH_3)_3]_4\}$, 80% in n-butanol, Aldrich, USA]
Zirconium Chloride [$ZrCl_4$, 98%, Merck, India]
Zirconium Oxy-Chloride [$ZrOCl_2 \bullet 8H_2O$, 98%, Loba Chemie, India]
Zirconium Oxy-Nitrate [$ZrO(NO_3)_2 \bullet XH_2O$, 98%, Loba Chemie, India]

2.3. SYNTHESIS

The nature, number and strength of acid sites, morphology, surface area, pore size, metal oxide surface density, metal dispersion on support, suitable phase for high selectivity toward the desired products etc and other physicochemical properties of solid acid catalyst strongly relies on the preparation methods eg hydrothermal, sol-gel, wet impregnation, co-precipitation, mix-precipitation/impregnation, neutral templating method, double hydrolysis, reflux, dry gel etc methods and subsequent calcination treatments and temperature. Catalyst should have the essential attributes of activity,

stability, selectivity, and regenerability. These can be related to the physical and chemical properties of the catalyst, which in turn can be related to the variable parameters inherent in the method used for the preparation of the catalyst. A wide range of methods has been employed for the preparation of the catalyst some which has been listed below.

Preparation methods for supported catalysts

- Impregnation
- Ion exchange / equilibrium adsorption
- Gelation / Sol-Gel
- Grafting
- Anchoring / heterogenization of homogeneous catalysts
- Deposition-precipitation / Co-precipitation
- Spreading and Wetting
- Immobilization of metal particles and clusters
- Chemical vapor deposition (CVD)

Keeping in sight the advantages and disadvantages of the synthesis methods 3 techniques have been employed (impregnation, precipitation and sol-gel) in this studies whose detailed description has been explained.

There are only two main routes for the preparation of almost all catalysts. These can be divided into the two categories: methods in which the catalytically active phase is generated as a new solid phase by either precipitation or a decomposition reaction, and methods in which the active phase is introduced and fixed onto a preexisting solid by a process which is intrinsically dependent on the surface of the support. The method of precipitation is the best known and most widely used procedure for synthesis of both mono-metallic and multi-metallic oxides. Precipitation results in a new solid phase (precipitate) that is formed discontinuously (i.e., with phase separation) from a homogeneous liquid solution. A variety of procedures, such as addition of bases or acids, addition of complex-forming agents, and changes of temperature and solvents, might be used to form a precipitate. The term coprecipitation is usually reserved for preparation of multi-component precipitates, which often are the precursors of binary or multi-metallic oxide catalysts. The same term is sometimes improperly used for precipitation processes which are conducted in the presence of suspended solids. Depending on the particular

application, the newly formed solid phase may be further subjected to various treatments, such as aging and hydrothermal transformation, washing, filtration, drying, grinding, tableting, impregnation, mixing, and calcination. During all these preparative steps, physicochemical transformations occur which can profoundly affect the structure and composition of the catalyst surface and even its bulk composition. If the adage the catalyst "remembers" how it was prepared, even after being subjected to various heat treatments at elevated temperatures is valid, then any cause-and effect correlations that can eventually be made between the precipitation procedures and the final characteristics of the catalyst becomes significant. A scientific approach to the preparation of catalysts by precipitation routes was introduced by [1-4]. The formation of the precipitate from a homogeneous liquid phase may occur as a result of physical transformations (change of temperature or of solvent, solvent evaporation) but most often is determined by chemical processes (addition of bases or acids, use of complex forming agents). In almost all cases, the formation of a new solid phase in a liquid medium results from two elementary processes which occur simultaneously or sequentially: (1) nucleation, i.e., formation of the smallest elementary particles of the new phase which are stable under the precipitation conditions; and (2) growth or agglomeration of the particles. The process involves dissolving a salt precursor, usually a chloride, oxy-chloride or nitrate. The corresponding metal hydroxides usually form and precipitate in water by adding a base solution such as sodium hydroxide or ammonium hydroxide to the solution. The resulting chloride salts, i.e. NaCl or NH_4Cl, are then washed away and the hydroxide is calcined after filtration and washing to obtain the final oxide powder. In the synthesis of multi-component systems, the problems are even more complex. Coprecipitation rarely allows one to obtain good macroscopic homogeneity. In a system with two or more metallic compounds, the composition of the precipitate depends on the differences in solubility between the components and the chemistry occurring during precipitation. Generally, under the conditions of either a slow precipitation rate or poor mixing within the reaction medium, coprecipitation is selective and the co-precipitate is heterogeneous in composition. This method is useful in preparing composites of different oxides by co-precipitation of the corresponding hydroxides in the same solution. One of the disadvantages of this method is the difficulty to control the particle size and size

distribution. Very often, (uncontrolled) precipitation takes place resulting in large particles. Co-precipitation is achieved by treatment of a solution containing both the support precursor and the catalytic precursor with a suitable precipitating agent. The resulting precipitate contains both the active component and the support material. One disadvantage of this method is that a large portion of the active species is buried in the support hence unavailable for reactions. Another method for preparing supported oxide catalysts involves the dispersion of the active species or its precursor onto the surface of a support oxide. This can be achieved by equilibrium adsorption, wet impregnation and incipient wetness impregnation. Impregnation is the procedure whereby a certain volume of solution containing the precursor of the active phase is contacted with the solid support, which, in a subsequent step, is dried to remove the imbibed solvent. Two methods of contacting may be distinguished, depending on the volume of solution. Those are wet impregnation and incipient wetness impregnation. In wet impregnation an excess of solution is used. After a certain time the solid is separated and the excess solvent is removed by drying. In incipient wetness impregnation the volume of the solution of appropriate concentration is equal or slightly less than the pore volume of the support. The maximum loading is limited by the solubility of the precursor in the solution. For both methods the operating variable is the temperature, which influences both the precursor solubility and the solution viscosity and as a consequence the wetting time. The concentration profile of the impregnated compound depends on the mass transfer conditions within the pores during impregnation and drying. The incipient wetness method involves the wetting of the support with just enough of a solution of the active species to fill the pores of the support material. This is normally achieved by adding the solution slowly to the solid material with continuous stirring. If the volume of the liquid needed to reach this point is known, the concentration of the solution can be adjusted to give the desired catalytic loading. Once the incipient wetness point has been reached, the solvent is evaporated and the modified support is calcined to give the catalyst. With this method of preparation it is essential to have an understanding of both chemical and physical properties of the support and the chemistry of the impregnating solution in order to control the physical properties of the finished catalyst. Incipient wetness can be used with aqueous or organic solutions depending on the solubility of the catalytic precursor.

Evaporation of high surface tension solvents such as water can result in pore disruption in the support resulting in a decrease of the surface area of the catalyst. The average size of the catalytic precursor particles depends on the concentration of the solution used. High catalytic loadings tend to give larger particles than low loadings.

In recent years, a wide variety of porous materials have been obtained using sol-gel method. This technique has long been known for the preparation of metal oxides and has been reported in several journals, books and reviews [5-9].The process is typically used to prepare metal oxides via the hydrolysis of metal reactive precursors, usually alkoxides in an alcoholic solution, resulting in the corresponding hydroxide. Condensation of the hydroxide molecules by giving off water leads to the formation of a network of metal hydroxide. When hydroxide species undergo polymerization by condensation of the hydroxy network, gelation is achieved and a dense porous gel is obtained. The gel is a polymer of three-dimensional skeleton surrounding interconnected pores. Removal of the solvents and appropriate drying of the gel is an important step which results in an ultra-fine powder of the metal hydroxide. Heat treatment of the hydroxide is a final step that leads to the corresponding ultra-fine powder of the metal oxide. Depending upon the heat treatment procedure the final product may end up in the form of a nanometer scale powder, bulk material or oxygen deficient metal oxides. The precursor in a sol–gel preparation can either be a metal salt or metal alkoxide or a stable colloidal suspension of preformed sols. The important variables are the relative rates of hydrolysis and condensation. The high purity obtained by sol–gel technology starting from alkoxides can also be obtained in case of conventional precipitation if high purity raw materials are used. Conventional precipitation usually results in a homogeneous distribution on an atomic level but is mostly restricted to stoichiometric compositions, whereas in case of sol–gel technology, molecular distribution can only be obtained under ideal hydrolysis–condensation conditions. However, sol–gel methods are superior to precipitation in the ability to vary compositional homogeneity on a molecular level. Another advantage of the sol–gel preparation lies in the possibility to better control grain size or porosity of the formed catalyst precursor as compared to conventional precipitation where these parameters are very difficult to control. However, since many catalysts regardless of the technology used for the precursor preparation need further thermal treatment, some of the

advantages of the sol–gel technology will disappear. The removal of the solvent must be done very carefully in order to preserve the desired physical properties of the grains, which is either time consuming and therefore expensive or needs expensive special production equipment. These weaknesses of the sol–gel method are the reason why this method has not found wide application in commercial catalyst production, except in case of some carriers such as alumina, silica–alumina and hydrotalcites from alkoxides and hydrothermal synthesis of zeolites. The experimental procedure used to synthesize pure and supported catalysts are given in this chapter.

2.3.1. Synthesis of t-ZrO_2 materials

Under identical and judiciously pre-optimized synthesis conditions, the influence of different combinations of zirconium sources and/or post treatment conditions on structural properties, thermal stability, phase composition and morphology of zirconia has been investigated.

2.3.1.1. Preparation of ZrO_2 via precipitation method.

In a typical synthesis, 23.12g of zirconium oxy-nitrate was dissolved in 200 ml of distilled water whose initial pH was less then 2. To this a separately prepared dilute aqueous ammonia solution (12wt%,~100ml) was added drop wise under vigorous stirring followed by aqueous ammonia solution (25 wt.%, ~200ml) or until the pH of the solution reached to 11. The pH was continuously monitored with a pH meter for next 2 h and adjusted by addition of aqueous ammonia solution in such way as to maintain the pH as follows: $10 < pH \leq 11$. After 2h no further pH adjustment was done and the slurry was aged overnight (~12 h) in the mother liquor with constant stirring. After aging the pH of the precipitated solution was less then 10. This procedure also led to a precipitate that could be easily filtered and washed free of the nitrates. After checking the supernatant liquid for complete precipitation the precipitate obtained was filtered using Whatman No. 1 filter paper and vacuum suction. This precipitate was washed 3 times with 250 ml deionized-distilled water and firstly dried overnight at room temperature then at 100 °C for 6 h, powdered and dried for another 6 hrs. If large amounts of water are used peptization of the gel occurs therefore the volume of water used for washing is also important. Since residual nitrate ions are thermally decomposed, thorough washing of the

precipitates is not needed; a few times is enough. The hydroxide precipitate was divided into equal proportions and calcined in air using pre-optimized calcination procedure at 400, 500, 600 and 700 ^{o}C for 3 h at each temperature. In order to investigate the influence of different zirconium source materials on the quality of ZrO_2 materials another batch of ZrO_2 was prepared by precipitation technique using zirconium tert-butoxide (31.2g in 200 ml of ethanol) instead of zirconium oxy-nitrate aqueous solution under identical set of synthesis conditions. The procedures for synthesis of this zirconia sample is similar to procedure given above expect the starting precursor. Another set of ZrO_2 samples from ZrONit via precipitation was prepared to evaluate the effect of digestion on the thermal and structural properties. Here in the wet un-dried washed hydroxide precipitate obtained by using the above synthesis procedure was transferred to Teflon conical flask and suspended in 100ml of basic ammonia solution (25 wt.%) and refluxed at 80°C under continuous stirring using magnetic needle for 12 or 24 h as shown in Fig. 2.1.

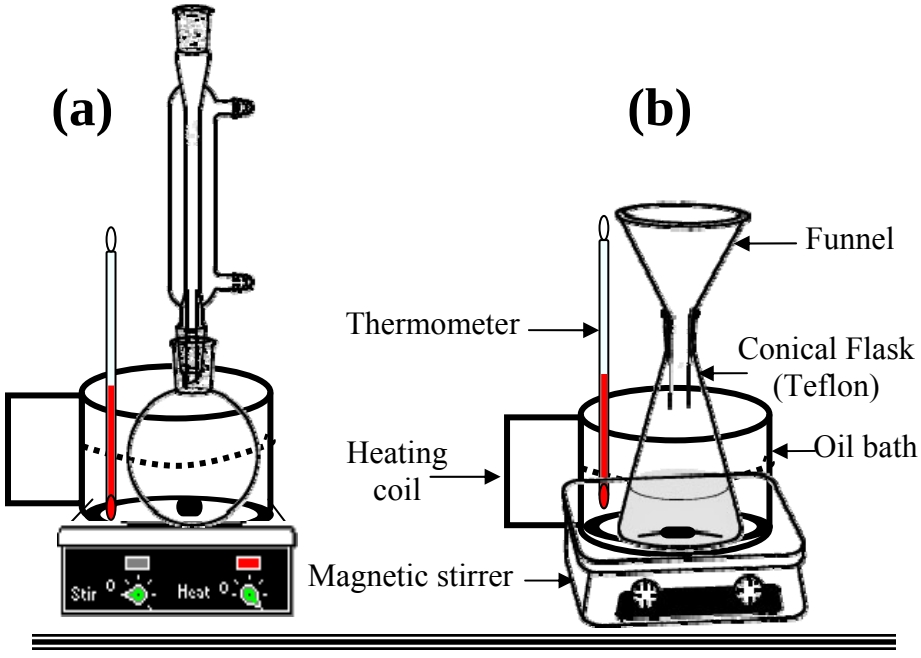

Fig. 2.1: (a) Typical schematic diagram of the experimental setup usually seen and used for synthesis and digestion with ammonia, **(b)** Simple and facile experimental setup used for synthesis and digestion of the catalysts prepared in this studies.

The pH was monitored periodically and adjusted as $11 < pH \leq 12$, by adding aqueous ammonia solution to cover up the losses during reflux digestion. After digestion procedure the resulting hydroxide precipitate was filtered and divided into equal

proportions and firstly dried overnight at room temperature and then at 100 ^{o}C for 6 h, powdered and dried for another 6 h. These samples were calcined in air using pre-optimized calcination procedure at 400, 500, 600, 700 and 800 ^{o}C for 3 h at each temperature.

2.3.1.2. Preparation of ZrO_2 by modified sol-gel method

First, 22 g of Pluronic P123 was dissolved in 100 g of ethanol with continuous stirring till clear solution is obtained. Then 7.2 g of zirconium chloride powder was added slowly to the above solution using a spatula. At one point it is not possible to transfer the powder using the spatula, then about 25 g of ethanol was used to transfer the remaining powder instantly. After completion of this addition about immediately 31.2 g of zirconium tert-butoxide mixed in 50 g of ethanol was added insuring minimum loss of the alkoxide precursor due to its highly sensitive nature towards moisture. Zirconia to surfactant molar ratio is 0.03. This mixture was stirred for another 1 h which is transparent until further addition of 25 g water in 25 g of ethanol, wherein a white precipitate starts to from. The pH of the gel was less then 2 at this point. After prolong stirring (~12 h) the precipitate formed initially re-dissolves forming a transparent gel. Then the formed transparent gel was divided into equal proportions and transferred to about 300 mm petri-dishes for solvent evaporation at room temperature. The materials in the dishes were some what sticky and gelatinous even after 24 h of ambient temperature drying. Further drying was carried out slowly in a step wise programmed manner to avoid instant shock to the structure. Initially the dishes were heated in an oven at 60 ^{o}C for 6 h, washed with water followed by drying at 80 ^{o}C for 6 h and finally at 100 ^{o}C for 12 h. These samples were calcined in air using pre-optimized calcination procedure at 400, 500, 600, 700 and 800 ^{o}C for 3 h at each temperature.

2.3.2. Synthesis of MoO_3-ZrO_2 Solid Acid Catalyst

A series of MoO_3-ZrO_2 catalysts with different MoO_3 loadings were prepared by modified co-precipitation method. Although we studied samples containing MoO_3 up to 40 wt.%, we focused attention on catalysts with loading in the range 15-30 wt%, because they are reported to show highest activity, surface area and better physicochemical

properties. The co-precipitation from mononuclear molybdate and zirconium oxy-hydroxide was first investigated, prior to preparation of MoO_3/ZrO_2 catalysts by impregnation method. The physico-chemical features of the MoO_3-ZrO_2 materials generated via impregnation and co-precipitation procedure are strongly dependent on the synthesis conditions such as pH, Mo loading, temperature of calcination etc. In particular pH plays an important role which will discussed in detail in the next chapter under the heading influence of pH. At present we shall only discuss how pH may effect dispersion and/or % loading of Mo or W on zirconia support. In the diluted aqueous solutions, AHM exhibits pH close to 5.5. In the pH region between 2 to 6, $(MoO_4)^{2-}$ ions coexist with $(Mo_7O_{24})^{6-}$ ions, while at higher pH only $(MoO_4)^{2-}$ ions exist [10,11]. This dependence of monomeric and polymeric ions upon solution pH is also agreed for AMT solutions, that at alkaline pH >10, monomeric $(WO_4)^{2-}$ is the only species in solution. It has also been reported that at concentration values < 5 $x10^{-5}$M, no polyanions are formed [12,13]. At higher pH, the use of low nuclearity anionic precursors does not allow to obtain samples with the desired loadings because in neutral or basic solutions, the zirconia surface is negatively charged [14,15] causing repulsion of the $(MoO_4)^{2-}/(WO_4)^{2-}$ anions and therefore limiting their interaction with zirconia surface. This is mainly the consequence of electrostatic repulsions between zirconia surface and ions originating from AHM/AMT solutions, which occur in equilibrium at the given pH [16]. However at lower pH, zirconia surface is positively charged, but the anions are present in the form of large nuclear polyanion species, leading to poor dispersion and formation of clusters with a high degree of aggregation. These clusters may partially transform into bulk WO_3/MoO_3 or $Zr(WO_4)_2/Zr(MoO_4)_2$, depending on the calcination temperature (< 700°C) and on % loading (<10 wt. %). As seen in previous section fine dispersion of catalytically active species on the support is prime importance in order to obtain a good catalyst. Also at higher pH allows obtaining zirconia with a high specific surface area with tetragonal phase and better thermal stability. Sighting above reasons all MoO_3-ZrO_2 catalysts were prepared in basic medium whose detailed procedure are given below.

2.3.2.1. Preparation of MoO_3-ZrO_2 (10-30 wt %) catalyst via co-precipitation

MoO_3-ZrO_2 catalysts with varying amounts of MoO_3 loading (10-30 wt%), were synthesized by co-precipitation method using zirconium oxy-nitrate, ammonium heptamolybdate and aqueous ammonia solution as starting materials. In a typical synthesis of 15 wt.% MoO_3 on zirconia, 2.48 g of ammonium heptamolybdate (AHM) dissolved in 25 ml deionized-distilled water + 25 ml of dilute NH_4OH. This AHM solution was added drop wise to zirconium oxy-nitrate solution containing 21.5 gm of zirconium oxy-nitrate dissolved in 200 ml of deionized-distilled water. To this a separately prepared dilute aqueous ammonia solution (12wt%,~100ml) was added drop wise under vigorous stirring followed by aqueous ammonia solution (25 wt.%, ~200ml) or until the pH of the solution reached to 11. The pH was continuously monitored with a pH meter for next 2 h and adjusted by addition of aqueous ammonia solution in such way as to maintain the pH as follows: $10 < pH \leq 11$. After 2h no further pH adjustment was done and the slurry was aged overnight (~12 h) in the mother liquor with constant stirring. After aging 100ml basic ammonia solution (25 wt.%) was added and the slurry was refluxed at 80°C under continuous stirring using magnetic needle for 12h. The pH was monitored periodically and adjusted to a value of 12 by addition of aqueous ammonia solution to cover up the losses during reflux digestion. Subsequent to digestion the slurry was stirred for another 4 h without pH adjustment and uncovered to allow greater interaction between Mo and Zr species. The resulting precipitate was filtered and washed with 500 ml deionized-distilled water and dried overnight at room temperature and then at 100^{o}C for 6 h. The dried sample was calcined in air using pre-optimized calcination procedure at 400, 500, 600,700 and 800^{o}C for 3 h at each temperature. Using similar method, the MoO_3-ZrO_2 catalyst with different MoO_3 loading (10, 20 and 30) were synthesized and calcined at 700 ^{o}C and 800 ^{o}C for 3 hrs.

2.3.2.2. Preparation of MoO_3/ZrO_2 (15 wt %) catalyst via wet impregnation

In a typical synthesis of 15 wt.% MoO_3 on zirconia catalyst prepared using impregnation method, 21.5 g of zirconium oxy-nitrate was dissolved in 200 ml of distilled water whose initial pH was less then 2. To this a separately prepared dilute aqueous ammonia solution (12wt%,~100ml) was added drop wise under vigorous stirring

followed by aqueous ammonia solution (25 wt.%, ~200ml) or until the pH of the solution reached to 11. The pH was continuously monitored with a pH meter for next 2 h and adjusted by addition of aqueous ammonia solution in such way as to maintain the pH as follows: $10 < pH \leq 11$. After 2 h no further pH adjustment was done and the slurry was aged overnight (~12 h) in the mother liquor with constant stirring. After aging the precipitate obtained was filtered using Whatman No. 1 filter paper and washed with 500 ml deionized-distilled water. This hydroxide precipitate was transferred to Teflon conical flask and suspended in 100ml of basic ammonia solution (25 wt.%) and refluxed at 80°C under continuous stirring using magnetic needle for 12 or 24 h. The pH was monitored periodically and adjusted as $11 < pH \leq 12$, by adding aqueous ammonia solution to cover up the losses during reflux digestion. The digested was filtered and suspended in 100 ml deionized-distilled water. Under vigorous AHM (2.48 g) solution prepared in 25 ml deionized-distilled water + 25 ml of dilute NH_4OH was added drop wise. After complete addition temperature of the mixture was slowly increased to 100 ^oC and maintained till thick paste was obtained, which was further dried in oven. The dried sample was calcined in air using pre-optimized calcination procedure at 400, 500, 600,700 and 800^oC for 3 h at each temperature.

2.3.2. Synthesis of WO_3-ZrO_2 Solid Acid Catalyst

In the previous section we have learnt the effect of basic and acidic media on dispersion and loading of active species. In the synthesis of WO3-ZrO2 catalyst we have also tried to optimize and study the active species (W) precursor effect on the properties of the materials formed, but their details have not been mentioned as they could not be prepared under identical set of synthesis conditions due to reactive nature and sensitivity towards moisture of some precursors. In our earlier publication we have successfully determined the precursor effect on the properties and activity of the materials formed [17]. Tungsten (VI) ethoxide ($W(C_2H_5O)_6$, , 5% w/v in ethanol 99.8%, Alfa Aesar), tungsten hexa-chloride (WCl_6, 99.9 %, Aldrich), and ammonium metatungstate were initially screened for the preparation of the catalyst. Considering the advantages and disadvantages of these precursors and taking into account the structure characterization results, we have selected the best precursor (ammonium meta-tungstate) for all further

studies. Bulk monoclinic WO_3 sample was also prepared by calcining ammonium meta-tungstate in a muffle oven at 600^oC for 6 h. This sample is used as reference when discussing some of the characterization results reported in this work. In this work we have prepared WO_3-ZrO_2 catalyst using co-precipitation, impregnation and modified sol-gel method whose detail synthesis procedures are given below.

2.3.2.1. Preparation of WO_3-ZrO_2 (20 wt %) catalyst via wet impregnation

The procedure for synthesis of 20 wt.% WO_3 on zirconia via impregnation is similar to procedure for the synthesis of 15 wt.% MoO_3 on zirconia as given in section 2.3.2.2., besides the desired loading here AMT (3.03 g) solution is used instead of AHM, rest all the parameters including the weights are same. In case were in Pluronic P-123 block copolymer surfactant has been used for the synthesis of WO_3-ZrO_2 catalyst it was added to zirconium oxy-nitrate dissolved in 200 ml and stirred till complete dissolution. The molar ratio of zirconia to surfactant was 0.03. In addition one sample was prepared using zirconium hydroxide precipitate which was not digested. In order to investigate the influence of zirconium precursor on various physico-chemical properties another batch was prepared by using zirconium oxy-chloride (29.9 g in 200 ml of water) instead of zirconium oxy-nitrate under identical set of synthesis conditions. Thorough washing was essential when zirconium oxy-chloride is used as a starting precursor, because from application point of view ions as chlorides or sulfates act as poisons in many catalytic reactions. Therefore after hydrolysis, the hydroxide precipitate was exhaustively washed with distilled water until the absence of chlorides. After each wash, a couple of drops of a 3M $AgNO_3$ solution were added to the filtrate liquid until it showed no visible signs of AgCl formation. This procedure was followed were ever zirconium oxy-chloride is used.

2.3.2.2. Preparation of WO_3/ZrO_2 (20 wt %) catalyst via co-precipitation

In the typical synthesis of 20 wt.% WO_3-ZrO_2, zirconium oxy-nitrate/oxy-chloride, ammonium meta-tungstate and aqueous ammonia solution are used as starting materials. The procedure used for the synthesis is same as mentioned in section 2.3.2.1., besides the desired loading here in AMT (3.03 g) solution is used instead of AHM, rest all the parameters including the weights are same. In case were in Pluronic P-123 block

copolymer surfactant has been used it was added to initial salt solution and stirred till complete dissolution. The molar ratio of zirconia to surfactant was 0.03.

2.3.2.3. Preparation of WO_3/ZrO_2 (20 wt %) catalyst via modified sol-gel

First, 22 g of Pluronic P123 was dissolved in 100 g of ethanol with continuous stirring till clear solution is obtained. Then 7.2 g of zirconium chloride powder was added slowly to the above solution using a spatula. At one point it is not possible to transfer the powder using the spatula, then about 25 g of ethanol was used to transfer the remaining powder instantly. After completion of this addition about immediately 31.2 g of zirconium tert-butoxide mixed in 50 g of ethanol was added insuring minimum loss of the alkoxide precursor due to its highly sensitive nature towards moisture. This mixture was stirred for another 1 h to which 3.18 g of AMT dissolved in 25 g water + 25 g of ethanol, was added very slowly. Stirring was continued overnight (~12 h) after which a transparent gel is obtained. Then the transparent gel was transferred to a big shallow tub for solvent evaporation at room temperature. The material was some what sticky and gelatinous even after 24 h of ambient temperature drying. Initially the dishes were heated in an oven at 60 ^oC for 6 h, washed with water followed by drying at 80 ^oC for 6 h and finally at 100 ^oC for 12 h. These dried samples were immediately calcined in air using pre-optimized calcination procedure at 400, 500, 600, 700 and 800 ^oC for 3 h at each temperature.

2.3.4. Optimization of Calcination Temperature

Calcination involves the medium to high temperature treatment of the catalyst with an aim to eliminate the extraneous materials such as organics, surfactants etc as well as the volatile and unstable cations/anions that may have been previously introduced but are not desired in the final catalyst. Calcination is generally carried out in an oxidizing/inert atmosphere and the selection of calcination temperature is of critical importance in catalysis. In the case of mixed metal oxides, substantially elevated temperature may be required to cause mixing by diffusion of individual species to form a desired compound or crystal phase. In the case of sulphated metal oxides, calcination introduces strongly bonded sulphate moieties on the surface and immediately underneath thereby imparting a combination of acidity and one electron oxidizing ability to the

catalyst. The calcination temperature significantly affects the physico-chemical properties and the catalytic performance of zirconia systems [18,19]. Calcination at an appropriate temperature is also essential for the formation of the species with a proper configuration that generates strong acidity [20,21,22]. The optimization of calcination conditions used in the mixed oxide process, however, has not received detailed attention, and the effects of applied dwell time and heating/cooling rates have not yet been studied extensively. Therefore effect of calcination temperature, dwell time and heating/cooling rates on phase formation of the powders were examined. Since the samples are prepared using various synthesis methods and with a variety of precursors including surfactants, it was difficult task to optimize and select calcination program which would be applicable to all of them. Using different procedure of calcinations for different samples would render then incomparable as their properties will change, therefore prior optimization of calcination temperature, dwell time, heating rate was carried out. Out of several programs, 4 have been demonstrated in Fig. 2.2.

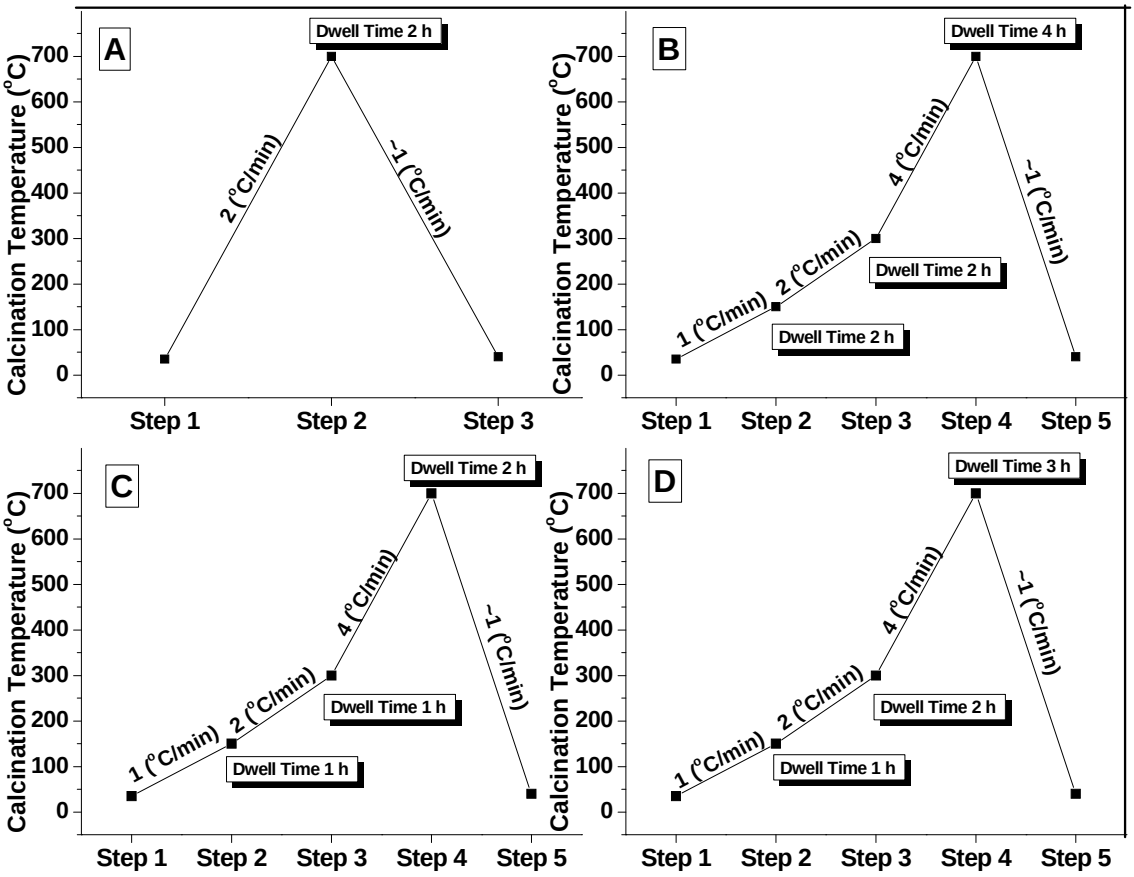

Fig. 2.2: Calcination programs used for optimization of calcination temperature, dwell time and heating rate.

As a illustrative example effect of different calcination program on the properties of 15 wt.% WO_3 on zirconia prepared via impregnation method (20WZim-II) is discussed in Chapter-5. Similar studies were carried out for pure zirconia and MoO_3 on zirconia catalysts. As seen from Fig. 2.2 calcination program "A" does not include any steps which poses a problem with sample prepared with surfactant leading to pore collapse and incomplete decomposition of surfactant, while program "B" is too slow and excessive heating leads to lower surface area and formation of monoclinic phase. Therefore program "C" was developed by reducing the time by half of program "B", but when using this program at final calcination temperature 500 ^oC for samples prepared using surfactants and/or alkoxide precursors complete removal of carbon was not insured. Calcination program "D" was therefore found to be suitable on the basis of data obtained by XRD, surface area and IR analysis for calcination of samples prepared by various techniques. Thus it can be seen how fine tuning of calcination program such as dwell time, heating rate etc is required to obtain materials with best possible properties

2.3.5. Designation of samples

The samples are in general designated as follows, the letters M, W and Z denotes to MoO_3, WO_3 and ZrO_2 respectively. The numbers 10, 15, 20 and 30 represents metal oxide (MoO_3 or WO_3) loading in Weight % while the numbers 4C, 5C, 6C, 7C and 8C are referred to the calcination temperatures, (C = Calcination). The non-appearance of the denotation like 4C, 5C etc indicates the samples are not calcined and are in as-synthesized form. The short forms of the synthesis preparation method such as "cp" for Co-precipitation, "im" for Impregenation and "sg" for Modified Sol-Gel are indicated before the calcination temperature. For eg. 15MZcp7C-1 indicates the sample containing 15 wt. % MoO_3 on ZrO_2, prepared by co-precipitation method, having serial number 1 and calcined at 700°C. Two digestion methods have been used for the preparation of various catalysts. Depending upon the time of digestion they have been labeled as d1 and d2, where d1 conditions are as: pH=12, time = 12 h, temperature = 80 ^oC and d2 conditions are as: pH=12, time = 24 h, temperature = 80 ^oC. (The first number from the time **1**2 h and **2**4 h is used for designation)

2.4. PHYSICO-CHEMICAL CHARACTERIZATION

Most of the catalysts used in the chemical industry are prepared by dispersing an active component in the form of very small particles on support. These moieties have dimensions of 1 to 20 nm and are often referred to as nano-particles. Given that most supports surfaces are structurally non-uniform and because supported particles are extremely small and irregular in both size and shape, an understanding of catalyst structure and texture is of vital importance for optimizing catalysts with respect to performance and lifetime. For a given catalytic reaction, activity and selectivity are two important parameters that indicate how good a catalyst is. However, these parameters stem from measurements carried out at macroscopic scale, which is considerably greater than the atomic scale of the molecular events taking place on the catalyst surface. From a scientific point of view, research into catalyst composition, the structure of the framework of the solid and the nature of its porosity are essential parameters to correlate with catalyst performance. In most cases, this provides a way of understanding the role that surface atoms play in the catalytic reaction. This basic information on the structure-property relationship for existing catalysts is valuable in the design of more efficient ones. The objective of understanding catalyst structure and texture has been pursued for nearly thirty years with the advent of many new physical tools developed through surface science and often reiterated. Thus, this chapter offers the non-specialist reader an account of the most relevant methods employed to characterize the size, shape, structure, and composition of the catalyst, as well an assessment of the specific area and pore size of the catalysts. A short review of the instrumental methods employed, its physical basis and relevant information gained from it is given in Table 2.1. Various types of spectroscopy, diffraction and imaging techniques can therefore be used to achieve the ultimate goal of determining and understanding quantitative structure/composition-activity/selectivity relationships. The techniques such as XRD, XPS, TG, TEM, FTIR, DR UV-VIS, AAS, ICP, and RAMAN are expected to be powerful tools to study the changes of the local environment and nature of surface Mo and W species along with the support. Several spectrometric methods were investigated prior to beginning of this study and considering the advantages and disadvantages of each method were weighed in relation to each other before a specific method or instrument technique was chosen to perform the analysis.

Each technique is unique by itself and provides important information for the understanding of different structural and compositional features. Among all, the most commonly used characterization techniques in the field on catalysis are given in Fig. 2.3. A brief description is provided for each technique used in this thesis of its physical basis and relevant information.

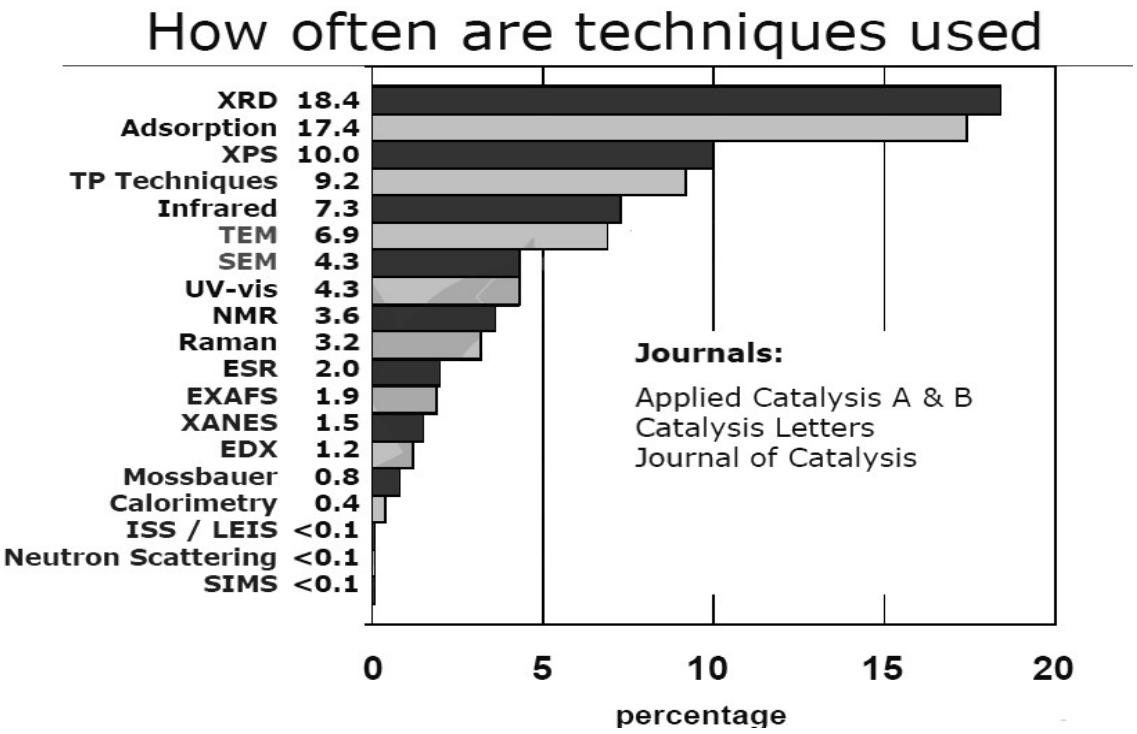

Fig. 2.3: Shows various characterization techniques frequently utilized to determine the structure and composition of catalysts

Table 2.1: A short review of information that can be by gained by different analytical methods and its basis.

Analytical method	Physical basis	Information/Uses
(TG-DTA)	Change in weight of a system as the temperature is increased at a linear rate/Measuring of thermal effects associated with physical and chemical changes by a differential method	Determination of compositions of complex mixture, purity and thermal stability associated with physical/ chemical changes with respect to temperature.
(XRD)	Monochromatic beam of X-rays incident on a sample made of small crystallites will be diffracted by sets of planes of high atomic concentrations.	% Crystallinity, Crystallite size, Phase analysis, Unit cell parameter, Rietveld refinement, composition etc
(N2 – Sorption)	Adsorptions of gaseous molecules or liquids at lower temperature and high pressure and desorption of the same at decreased pressure.	Surface area, pore size distribution and pore volume, micro-porosity of solid materials.
(FTIR)	Vibrational excitation of surface atoms by adsorption of infrared radiation	Phase composition, surface functional groups, adsorption sites, structure and bonding of adsorbates.
(DR-UV)	Molecules containing π-electrons or non-bonding electrons (n-electrons) can absorb the energy in the form of ultraviolet or visible light to excite these electrons to higher anti-bonding molecular orbitals.	Oxidation state and coordination environment of transition metal ions and its existence in the framework or extra-framework position of solids.
(TPD)	Measurement of base adsorbed over the acid sites and desorption of the same at elevated temperatures.	Amount and nature of acid sites and acid strength
(XPS)	Energy distribution of electrons that are emitted from the catalyst due to photoelectric effect.	Composition at the surface, chemical or electronic state of each element in the surface.
(TEM)	Interaction of the electrons transmitted through the specimen.	Nature and dispersion of catalytic active component, morphology, particle size distribution, d spacing and compositions, phase analysis, pore size and shape etc.
(SEM)	Secondary electrons and backscattered electrons emitted are used for producing images.	Morphology, Topography, particle size, defects and compositions

(EDX)	EDX makes use of the X-ray spectrum emitted by a solid sample bombarded with a focused beam of electrons to obtain a localized chemical analysis	Non-destructive determination of wide range of metals and metalloids (Qualitative and quantitative, semi-quantitative)
(XRF)	Identification and measurement of "secondary" (or fluorescent) X-rays emitted from a material that has been excited by bombarding with high energy x-rays or gamma rays	Fast, accurate, non-destructive determination of wide range of metals and metalloids (Qualitative and quantitative, semi-quantitative)
(AAS)	The technique is based on the fact that atoms of various metals at ground state absorb light at specific wavelengths, the amount of light absorbed can be measured against a standard curve for estimation of unknown	Destructive type Qualitative and quantitative estimation of metals and metalloids
(ICP)	Emission spectroscopy that uses plasma to produce excited atoms that emit electromagnetic radiation at wavelengths characteristic of a particular element. The intensity of this emission is indicative of the concentration of the element.	Destructive type Qualitative and quantitative estimation of metals, metalloids and some non-metals.
(RAMAN)	Frequency of the light scattered by molecules as they undergo rotations and vibrations.	Determining the organic/inorganic functional molecules/groups/atom.
(NMR)	Change in the direction of nuclear spin quantum number in the presence of strong magnetic field	Structural determination by means of coupling, decoupling, coordination position of an atom/element
(SAXS)	A scattering pattern is detected when a monochromatic beam of X-rays is directed onto the sample. The scattering pattern contains the information on the structure of the sample.	Sizes and shapes of particles, internal structure of disordered and partially ordered systems.

Note: 1] The curves, graphs and fittings were performed by Origin software (Origin-Pro 8, OriginLab Corporation) from the raw data obtained from various analytical techniques. 2] The term amorphous in this thesis will be used in the broad sense to describe a material with no long range order, such as that which leads to diffraction. Amorphous materials may still have considerable short-range order.

2.4.1. Thermo Gravimetric - Differential Thermal Analysis (TG-DTA)

When a substance is subjected to a programmed heating or cooling it normally undergoes changes, which may be physical, chemical, mechanical or magnetic in nature. The analysis of these changes recorded as a function of temperature permits the study of composition, structure, physical, and chemical behavior On the basis of the changes involved, techniques that fall under thermal analysis can broadly be classified into the following: (i) TG- (Thermo Gravimetric − Relates to mass changes) (ii) DTA − (Differential Thermal Analysis − Relates to energy changes). Thermo gravimetric analysis is a technique measuring and recording the loss of weight of a sample over a period of time under controlled heating rate. Changes in weight are due to the rupture and/or formation of various physical and chemical bonds at elevated temperatures which lead to the evolution of volatile products. Thermal analysis is widely used to study the structural stability of molecular sieves and related porous materials. It also provides information about temperature required for the removal of adsorbed water, decomposition of the occluded organic cations in the pores and channels of porous materials and de-hydroxylation at higher temperatures to produce Lewis acid sites. Data obtained from DTA and DTG helps in evaluating the thermal properties of porous materials. The shape and splitting of the low temperature endotherms helps to identify the location of water molecules and also helps in studying the kinetics of dehydration. The temperature at which an exotherm appears in the DTA after the loss of water molecules, gives helpful information about the temperature required to remove the template molecules from the pores of the materials under study during calcinations. Phase transformations if any can also be understood from the exotherms obtained at higher temperatures. The amount lost in the given temperature range also gives the estimate of the concentration of that species.

Thermal analysis of all the as-synthesized samples (~15 mg) was carried out by Perkin-Elmer Diamond TG-DTA thermal analyzer equipped with platinum pan under air atmosphere (flowing 60ml/min) from ambient to 1000 °C with the heating rate of 10°C/min. The base line correction was made using inert α-alumina as the reference sample.

2.4.2. Powder X-Ray Diffraction (XRD)

X-rays are defined as short-wavelength electromagnetic radiation produced by the deceleration of high-energy electrons or by electronic transitions involving electrons in the inner orbitals of atoms. The wavelength range of X-rays is from perhaps 10^{-4} nm to about 10 nm. For analytical purposes, X-rays are obtained in three ways, (1) by bombardment of a metal target with a beam of high-energy electrons, (2) by exposure of a substance to a primary beam of X-rays in order to generate a secondary beam of X-ray fluorescence, and (3) by employment of radioactive source whose decay process results in X-ray emission. X-ray tube and synchrotron are the well-known equipments for the generation of X-rays. X-ray tubes are basically used for the measurements of scattering and diffraction of X-rays and quite usual in the common X-ray labs due to their relatively simple structures and much lower cost than synchrotron. In X-ray diffractometry, X-rays are generated within a sealed X-ray tube under vacuum. In an X-ray tube, electrons produced at a heated cathode are accelerated toward a metal anode (the target, commonly made of copper, cobalt, iron or molybdenum) by a potential as great as 100 kV; upon collision, part of the energy of the electron beam is converted to X-rays. These X-rays are collimated and directed onto the sample, consisting of many crystallites and each crystallite in turn is made up of a regular, ordered array of atoms. An ordered arrangement of atoms (the crystal lattice) contains planes of high atomic density which in turn means planes of high electron density. When a monochromatic beam of X-ray photons hits a sample they will be scattered by these atomic electrons and if the scattered photons interfere with each other, diffraction maxima occurs. In general, one diffracted line will occur for each unique set of planes in the lattice. The distances between the planes of the atoms of the sample can be obtained by applying Bragg's Law ($n\lambda = 2d\sin\theta$) Where n is the order of diffracted beam and it is an integer (1, 2, 3…); λ is the wavelength of the incident X-ray beam; d is the distance between adjacent planes of atoms; θ is the angle of incidence of the X-ray beam and the atomic plane. Since we know λ and we can measure θ, we can calculate the d spacing. The characteristic set of d spacings generated in a typical X-ray scan provides an unique "fingerprint" of the material comprising the sample, which is then processed either by a microprocessor or electronically, converting the signal to a count rate. Because the wavelengths of X-rays

are on the nanometer scale, they are especially suitable for investigating the substances in nanometer or atomic scales, which are invisible by using electromagnetic radiations with longer wavelengths, such as visible light or ultraviolet. Furthermore, in contrast to neutrons, which are sensitive to the difference of nucleus of the matters, X-rays are sensitive to the changes of electron densities. Therefore, they are mainly utilized to study materials having non-uniform electron densities. X-ray diffraction is one of the non-destructive techniques and does not require elaborative work for the sample preparation. For characterization of oxides powder X-ray diffraction is the most important and commonly used tool to monitor structure, phase purity, degree of crystallinity and unit cell parameters of crystallite materials. Mixed oxide solids generally show characteristic peaks in the 2 theta range of 10-80º. The results of this analysis are described graphically as a set of peaks with intensity on the y-axis and the diffraction angle on the x-axis. Identification of phase is generally based on the comparison of the set of reflections of the specimen with that of pure reference phases, or with a database provided by the International Centre for Diffraction Data (ICDD) (formerly ASTM then JCPDS). ICDD is a non-for-profit organization located in Newtown Square, Pennsylvania. This group is made up of a staff of permanent officers along with a number of academic and industrial scientists who are active in the field of XRD. Besides the material identification the XRD method can be used also for quantitative analysis, i.e., to determine average crystallite size (D) of a material by using Debye-Scherrer equation ($D = k\lambda/\beta\cos\theta$) where D is the averaged dimension of the crystallite (nm), k is constant (shape factor) =0.90, λ is the radiation wavelength (0.15406 nm for CuKα), β is the full-width at half maximum height (FWHM) of the X-ray line (radians), θ and is the diffraction peak angle. The X-ray diffractometer can also be used to determine the crystal lattice parameters, changes in phase or lattice parameters before and after thermal treatment, strain, composition and the amount of each phase present in a sample.

About 1 g of dried sample was ground to fine powder, and then lightly pressed as thin layers on glass/aluminum slides, prior to scanning. The powder X-ray diffractograms of as-synthesized and calcined samples were recorded on Rigaku Miniflex diffractometer using a Ni-filtered monochromatic Cu *K*α radiation (λ = 1.5406 Å, hv = 8048.0eV). Radiation was produced by the X-ray tube operated at a voltage of 30 kV and

a current of 15 mA. Following parameters were used for various slits, Divergence slit - Variable, Scattering slit - 4.2 deg, Receiving slit - 0.3mm. The scanning range was 10-80° (2θ) with a scanning rate of 2 °/min. Alignment of the instrument was verified on daily basis using polycrystalline silicon reference standard supplied by Rigaku. Low angle powder XRD patterns were collected on the Philips X'Pert Pro 3040/60 diffractometer in the 2 theta range of 0.5 to 5 with a scan rate of 1 deg/min.

2.4.3. Nitrogen Adsorption-Desorption Measurements (N_2 Sorption)

Surface area of a solid sample is generally determined by gas adsorption or mercury penetration methods. The total surface is calculated from the amount of physically adsorbed nitrogen at -196 °C. The other techniques that are not in extensive use include electron microscopy, X-ray diffraction, and chromatography. During the 1930's, Brunauer, Emmett and Teller presented a theory dealing with the multilayer adsorption of gas on solids. The BET (Brunner, Emmet and Teller) method is the most acceptable technique in determining the specific surface area of solid samples by physisorption of gases. The significance of the BET theory lies in its ability to determine the number of molecules required to form a monolayer of adsorbed gas on a solid despite the fact that a mono molecular layer is never actually formed. The BET theory was applied to multilayer adsorption with the following hypotheses. First, the first layer of gas molecules is adsorbed more strongly than the subsequent layers, and the heat of adsorption of all subsequent layers is constant. Second, lateral interaction between adsorbed molecules is absent. Third, the Langmuir theory of monolayer adsorption can be applied to each layer. From the adsorption isotherm, a value corresponding to the volume of an adsorbed monolayer is calculated. With physical adsorption, the amount of gas adsorbed is usually plotted as a function of the relative pressure P/P_0, where the relative pressure is the actual pressure divided by the saturation pressure at the same temperature. The basic equation for finding out surface area by BET method is given by:

$$\frac{P}{V_a(P_0-P)} = \frac{1}{V_mC} + \frac{C-1}{V_mC} \times \frac{P}{P_o}$$

Where, P = Desorption equilibrium pressure, P_0 = Saturation vapour pressure of absorbate (liquefied gas) at the adsorbing temperature, V_a = Volume (at standard

temperature and pressure, STP) of absorbate adsorbed at pressure P, V_m = Volume of absorbate (at STP) required for a monolayer coverage, C is a constant relating to the energy of adsorption.

From the surface area of one molecule absorbed in the monolayer, the total surface area can be calculated. Nitrogen is usually used as the adsorbate, although argon and xenon can also be used. According to the BET method, a plot of P/V_a (P_0-P) against P/P_0 yields a straight line when $P/P_0 < 0.03$. From the slope and intercept of the straight line, V_m can be calculated which in turn is used in calculating specific surface area of the catalyst by the following equation:

$$\text{Surface Area } (m^2/g) = \frac{V_m \times N}{22414 \times W} \times A_m$$

Where, V_m = Monolayer volume in ml at STP, N = Avogadro number, W = Weight of the catalyst sample (g), A_m = Cross sectional area of adsorbate molecule (0.162 nm^2 for N_2) BET surface area was calculated using the conventional BET equation as shown above. Pore size distribution and pore volume was calculated using Barrett-Joyner-Halenda (BJH) model and t-plot analysis were used to determine the micropore surface area and pore volume. According to the IUPAC definition of porosity, it is the ratio of pore volume to apparent volume of particle or granule. The pores are classified as follows: (a) Micropore Pore of width less than 2 nm, (b) Mesopore Pore of width between 2 and 50 nm, (c) Macropore Pore of width greater than 50 nm. The understanding of the surface area and porosity of an adsorbent can be achieved by the construction of an adsorption isotherm. The adsorption isotherm is the relationship between the amount adsorbed and the equilibrium pressure (or relative pressure) at a known temperature. Similarly the desorption isotherm is the relationship between the amount of gas desorbed and the equilibrium pressure at a known temperature. Generally, there are many different shapes of isotherms depending on the type of adsorbent/absorbate and intermolecular interactions between the gas and the surface. In 1945, Brunauer proposed the classification of the different kinds of adsorption isotherms into five general forms while the type VI is of recent origin [23]. The Brunauer, Deming, Deming and Teller (BDDT) classification has also become the basis of the modern IUPAC classification of adsorption

isotherms [23] (Fig. 2.3). There are six broad categories of adsorption isotherms shown in Fig. 2.3 [24].

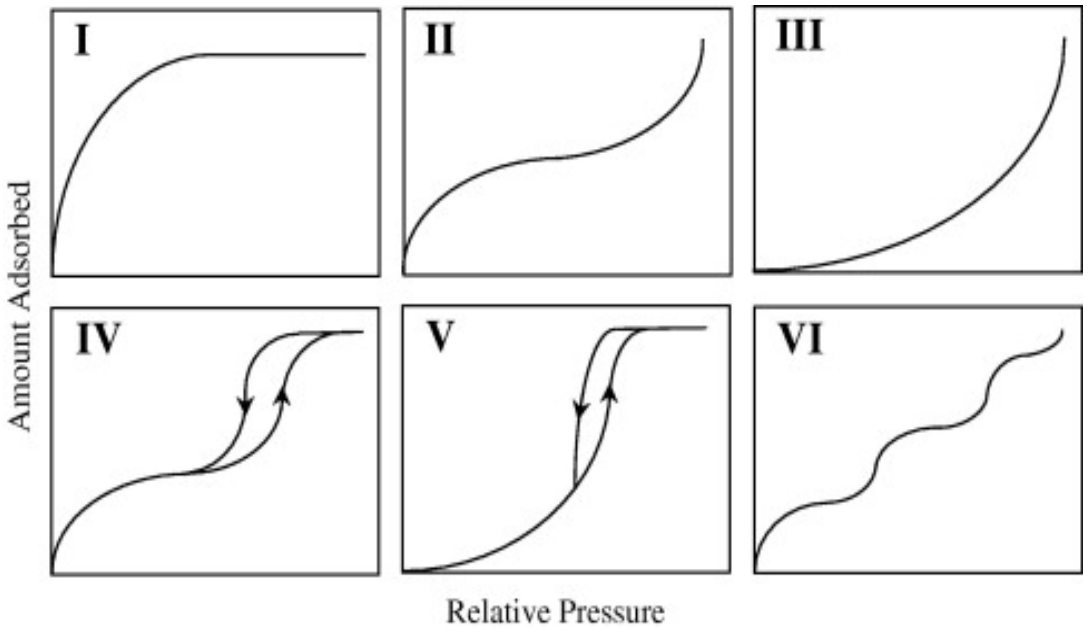

Fig. 2.3: IUPAC classification for adsorption isotherms (Types I–VI) with the x-axis representing the relative pressure of the fluid and the y-axis denoting amount of gas adsorbed.

Type I - these are typical of adsorbents with a predominantly microporous structure, as the majority of micropore filling will occur at relative pressures below 0.1. The adsorption process is usually complete at a partial pressure of ~0.5. **Type II** - physical adsorption of gases by non-porous solids is typified by this class of isotherm. Monolayer coverage is followed by multi-layering at high relative pressures. Carbons with mixed micro and meso-porosity produce Type II isotherms. **Type III** - the plot obtained is convex to the relative pressure axis. This class of isotherm is characteristic of weak adsorbate-adsorbent interactions and is most commonly associated with both non-porous and microporous adsorbents. The weak interactions between the adsorbate and the adsorbent lead to low uptakes at low relative pressures. However, once a molecule has become adsorbed at a primary adsorption site, the adsorbate-adsorbate interaction, which is much stronger, becomes the driving force of the adsorption process, resulting in accelerated uptakes at higher relative pressure. This co-operative type of adsorption at high partial pressures is known as cluster theory and examples include the adsorption of water molecules on carbon where the primary adsorption sites are oxygen based. **Type**

IV - A hysteresis loop, which is commonly associated with the presence of mesoporosity, is a common feature of Type IV isotherms, the shape of which is unique to each adsorption system. Capillary condensation gives rise to a hysteresis loop and these isotherms also exhibit a limited uptake at high relative pressures. **Type V** - these isotherms are convex to the relative pressure axis and are characteristic of weak adsorbate-adsorbent interactions. These isotherms are indicative of microporous or mesoporous solids. The reasons behind the shape of this class of isotherm are the same as those for Type III and again water adsorption on carbon may exhibit a Type V isotherm. **Type VI** - introduced primarily as a hypothetical isotherm, the shape is due to the complete formation of monomolecular layers before progression to a subsequent layer. It has been proposed, by Halsey [25] that the isotherms arise from adsorption on extremely homogeneous, non-porous surfaces where the monolayer capacity corresponds to the step height. Type VI shows the gradual formation of individual adsorbate layers, which stem from a multimodal pore distribution.

Like for physisorption isotherms, the IUPAC classifies hysteresis loops in four types (Fig. 2.4) and relates them with pore structures [26].

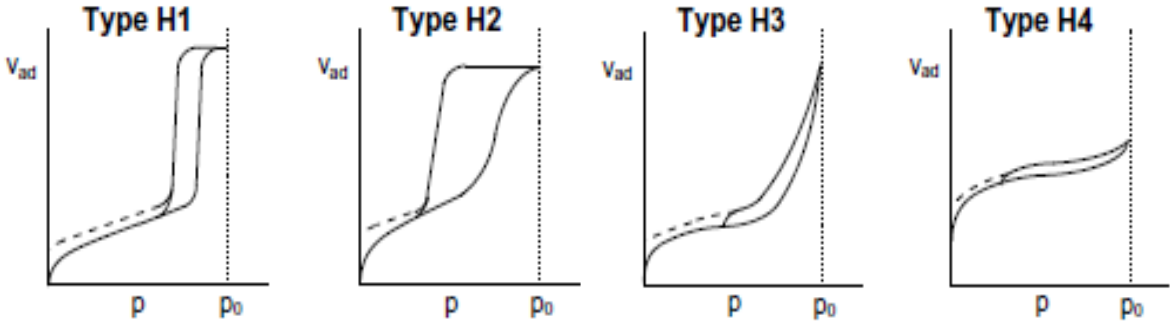

Fig. 2.4: Possible hysteresis loops for mesoporous materials.

According to the IUPAC classification of physisorption hysteresis loops, Type-H1 is representative of an adsorbent with a narrow distribution of relatively uniform mesopores, whereas Type-H2 is associated with a more complex pore structure in which network effects are important. Type-H2 loops are given by adsorbents containing narrow slits-shaped pores such as activated carbons. Type-H3 and H4 do not exhibit any limiting adsorption at high relative pressure. This is clear indication that the adsorbents do not possess well-defined mesopore structures and therefore it is not possible to attempt to

derive either the pore size distribution or the total pore volume from these isotherms. Type-H3 loops are often obtained with plate like materials such as clays. A particular feature of many hysteresis loops (Types-H2, H3, and H4) is the very steep region of the desorption branch which leads to a lower closure point of the loop at a constant P/P_0 for a given adsorbate and temperature (e.g. P/Po = 0.42 for nitrogen at -196^{o}C). This feature is thus dependent on the nature of the adsorbate rather than the distribution of pore size.

J. De Boer [27] in 1958 has identified five types of hysteresis loops and correlated them with various pore shapes as shown in Fig. 2.5.

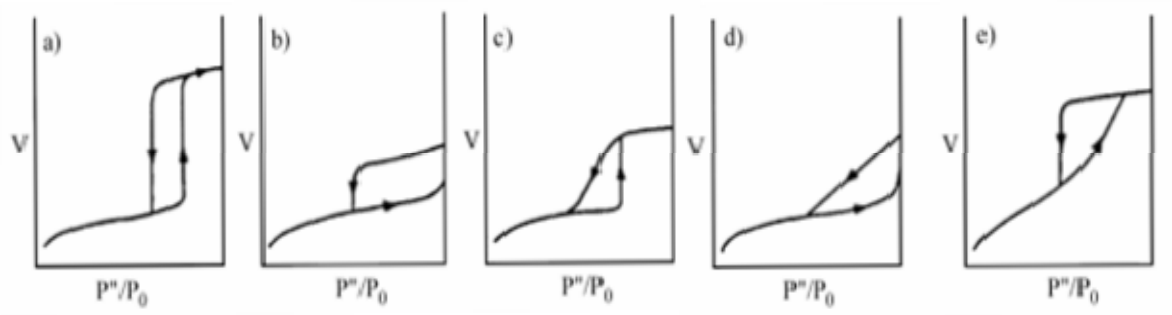

Fig. 2.5: De Boer's five types of hysteresis

Type A hysteresis is attributed to cylindrical pores; Type B is associated with slit shaped pores; Type C hysteresis is produced by wedge-shaped with open necks at one or both open ends. Type D loops result from wedge-shaped pores with narrow necks at one or both ends. The type E hysteresis loop has been attributed to "ink-bottle" pores. Characteristically, the hysteresis loops in all isotherms close before reaching a relative pressure of 0.3 in the desorption process except when microporosity is present. The distribution of pore volume with respect to pore size is called a pore size distribution. It is generally accepted that the desorption isotherm is more appropriate than the adsorption isotherm for evaluating the pore size distribution of an adsorbent due to the attainment of thermodynamic equilibrium.

The nitrogen adsorption–desorption isotherms for the solid samples were measured using a (Micromeritics ASAP 2010 system/ NOVA-1200[Quanta chrome, USA]). Prior to measurements, the samples were degassed for 12 h under a flow of nitrogen at temperatures 200°C – 300°C in order to remove any adsorbed moisture and organic impurities. 100 – 200 mg of sample was usually measured in the special quartz

sample tube with a bulb end and then cooled to –196^{o}C using liquid nitrogen and the sorption of nitrogen was carried out at different equilibrium pressures. Analysis of the shape of the adsorption/desorption isotherms yields information about the surface, porous structure and internal pore characteristics of the material. The instrument accuracy is approximately ±5% of measured value, with the instrument calibration verified by a SiO_2/Al_2O_3 reference standard. The specific surface area of the sample was calculated using BET method. The calculation of the particle size or BET surface area was also attempted from by the equation "d = 6000/(ρ X S_{BET})", where d is the average particle size (nm), S_{BET} is the specific surface area expressed in m^2/g^{-1} and ρ = specific density of zirconia or WO_3 modified zirconia sample expressed in g/cm^3. Theoretical density of WO_3 = 7.16 g/cm^3 and ZrO_2 = 5.68 g/cm^3 while the actual measured density of our catalyst samples is between 1.4 to 1.6 , which far less the individual theoretical calculated components. Therefore it was nearly impossible to get values any close to calculated from XRD, N_2 sorption and TEM measurements.

2.4.4. Fourier-Transform Infrared Spectroscopy (FTIR)

Infrared spectroscopy has been highly successfully applied in both organic and inorganic chemistry. In heterogeneous catalysis, infrared spectroscopy can be used for study of solid catalysts. Such characterization can be very useful in determining the nature of the support, and surface groups such as hydroxyls on the surface of oxides. Bands arising from the bulk structure of catalysts or supports can readily be observed. Infrared bands are produced if the vibration causes a change in the dipole moment (or induced dipole moment). From the infrared spectra of supported metals oxides, the information of the bonding modes of metal atoms with oxygen atoms can be determined, and hence the coordination structures of the supported and bulk metal oxides are determined. It is basically a bulk technique that takes advantage of the surface aspects of the catalyst and provides information about the structure of surface sites those are either directly observable or made observable by pre-adsorption of probe molecules. The frequencies and intensities of the IR bands can give abundant evidence on the state of supported metal dispersion, structure, metal-support interaction, metal-metal interaction, etc. It can also be used to measure the surface acidity of catalysts. FTIR offers higher

sensitivity and higher resolution than conventional IR. Fundamentally, the FT Infrared Spectroscopy testing system transmits an IR (infrared) beam of light through an area that is to be analyzed then captures this beam after passing through the area and finally generates a full infrared spectrum of the light, resulting in the identification of the materials present and allows for the concentration to be identified. The infrared light emitted from a source (e.g. a SiC Globar) is first directed into an interferometer, which modulates the light after which the light passes through the sample compartment and is then focused into the detector. FT-IR (Transmission) Testing is the most fundamental of the infrared spectroscopic sampling procedures. In many cases, sample preparation requires production of potassium bromide (KBr) discs.

The technique use for FTIR analysis of the samples is potassium bromide (KBr) pressed pellet technique. For each pellet the sample to KBr ratio was maintained as 1:100 respectively, and the mixture of the sample and the KBr was grounded in an agate mortar for 5 min and then this mixture was placed between two 13 mm evacuable die under 10 tons of pressure for 2 minutes to form transparent pellet. These KBR pellets were made using Techno-search KBr press model # M-15. FT-IR spectra of the samples were recorded on a Thermo Nicolet IR instrument as KBr pellets with resolution of 4 cm-1 and averaged over 100 scans.

2.4.5. Diffuse Reflectance UV-Vis Spectroscopy (DR-UVis)

The diffuse reflectance UV-Vis spectroscopy is known to be a very sensitive and useful technique for the identification and characterization of the metal ion coordination and its existence in the framework or extra-framework position of solids samples or molecules embedded on the solid surface. Diffuse reflectance UV-visible spectroscopy allows the study of electronic transitions between orbital's or bands in the case of atoms, ions and molecules in gaseous, liquid or solid state. In catalysis, DR-UVis is used for studying the speciation of supported transition metal ions because it measures both their d-d transitions and charge transfer bands. This technique can therefore be used from detecting the presence of a certain oxidation state to a detailed distribution of different oxidation states and coordination environments of the catalyst under study. However DRS (Diffuse reflectance spectrum) are usually broad and overlap with each other,

leading to a biased spectral analysis. In addition, the origin of the specific electronic transition is sometimes difficult to isolate due to its dependence on the local coordination environment, the polymerization degree and the specific oxidation state. Diffuse Reflectance UV-Vis (DR-UVis) spectroscopy is a spectroscopic technique based on the reflection of light in the ultraviolet (UV), visible (VIS) and near-infrared (NIR) region by a powdered sample. In a Diffuse Reflectance spectrum (DRS), the ratio of the light scattered from an "infinitely thick" closely packed catalyst layer and the scattered light from an infinitely thick layer of an ideal non-absorbing (white) reference sample is measured as a function of the wavelength λ. The scattered radiation, emanating from the sample and the reference material is collected by an integration sphere and the detector of the double beam spectrometer. The most popular continuum theory describing diffuse reflectance effect is Schuster-Kubelka-Munk (SKM) theory. If the sample is infinitely thick, the diffuse reflection of the sample (R_∞) is related to an apparent absorption (K) and apparent scattering coefficient (S) by the SKM equation [28,29]: $F(R_\infty) = (1-R_\infty)2 / 2R_\infty = K/S$. At low concentrations of supported transition metal ions (TMI), this equation is a good representation of the absorbing spectrum and allows a quantitative determination of the TMI. $F(R_\infty) = (1- R_\infty)2 / 2R_\infty = K/S = \alpha C_{TMI} / S = k\, C_{TMI}$. At a given wavelength λ, S is constant, the above equation gives a linear relation between $F(R_\infty)$ and the TMI concentration, C_{TMI}. The coefficients α and k are proportionality constants.

Diffuse reflectance UV-visible spectra of fine powder samples were recorded on a Perkin-Elmer Lambda-650 UV-vis spectrometer equipped with a diffuse reflectance attachment. $BaSO_4$ was used as an external standard to correct the baseline in the spectra. Few g of sample is pressed in the sample holder and the spectrum was measured in the range of 200-800 nm in air at room temperature. The reflectance spectra were converted into the Kubelka-Munk function, *F(R)*, which is proportional to the absorption coefficient for low values of *F(R)* and plotted vs. wavelength. Though only charge transfer transitions in the UV region (200-400 nm) are of interest, no absorptions were found in the visible region.

2.4.6. Temperature Programmed Desorption of Ammonia (TPD-NH_3)

The strength, the type and the amount of acidity can be determined using probe molecules by temperature programmed desorption (TPD). In TPD of NH_3 technique, NH_3 is initially allowed to adsorb on an activated solid catalyst at a defined temperature. The adsorbed molecules are then allowed to desorb in a flow of He or Ar by heating the catalyst material in a programmed manner. The amount of ammonia desorbed from the catalyst is estimated by a TCD close to the reactor outlet. Based on the amount of base molecules desorbed, the total acidity and the relative strength of the acid sites can be determined. Ammonia, n-butylamine, and pyridine are gaseous bases commonly used for the determination of strength and amount of a solid acid. The advantages of the gaseous base adsorption and desorption method are: (1) It can be used to determine the amount of acid sites for a solid at high temperature or under its actual working conditions. (2) It can also be applied even to colored samples. However, the disadvantage is the Brønsted and Lewis acid sites can not be differentiated by this method. This technique can be used to characterize the acid sites present in solids such as zeolites, mesoporous materials and oxides Gaseous bases adsorbed on acid sites give information about the acidity of the solid surface. A base adsorbed on strong acid site is more stable and more difficult to desorb than one adsorbed on a weak acid site. As temperature is increased, evacuation of the adsorbed bases from acid sites occurs. Bases adsorbed at weaker acid sites will be evacuated at lower temperature than those at stronger acid sites. Thus, the evacuation temperatures indicate the strength of various acid sites. Based upon above desorption of gases at different temperatures a TPD spectrum may have one or more peaks, the ones at low temperatures corresponding to NH_3 desorbing from the weaker acidic sites and the ones at higher temperatures corresponding to the stronger acidic sites. The areas under these peaks give information about the amount of acidic sites of different acidity, whereas the peak (–maximum–) temperatures give information about the relative acid strengths. The TPD curves can be de-convoluted into individual peaks and the areas under the peaks are converted into mmol of NH_3 per g catalyst based on injection of known volumes of NH_3 at similar conditions. The acid sites per unit area are calculated as follows: The acid sites per unit area are calculated as follows: Acid site ($\mu mol/m^2$) = Acidity ($\mu mol/g$) $\times$ S_{BET} (m^2/g), where S_{BET} is the surface area of the catalysts.

The overall acidity and acid strength associated with sites were measured by Ammonia Temperature Programmed Desorption (NH_3-TPD) using a Micromeritics AutoChem (2910, USA) equipped with thermal conductivity detector. Prior to the measurements, sample was heated to 600 ^oC with heating rate 20 ^oC/min in He flow (30 ml/min) for 1 h. The temperature was then decreased to 60 ^oC with He flow (50 ml/min), after the temperature was stable NH_3 was allowed to adsorb by exposing sample to a gas stream containing 10% NH_3 in He (30 ml/min) for 1/2 h or till no further adsorption was observed. Temperature was then increased to 100 ^oC and flushed with He (30 ml/min) for another 1 h to remove physisorbed NH_3. The NH_3 desorption was carried out in He flow (30 ml/min) by increasing the temperature up to 550 ^oC with a heating rate of 10^o C/min.

2.4.7. X-Ray Photoelectron Spectroscopy (XPS)

X-ray photoelectron spectroscopy (XPS) is widely used for probing the electronic structure of atoms, molecules and condensed matter. It gives information on the elemental composition, the oxidation state of the elements and in some cases on the dispersion of one phase over another. XPS is based on the photoelectric effect. When an X-ray photon of energy hν is incident on a solid matter, the kinetic energy (E_k) and the binding energy (E_b) of the ejected photoelectrons can be related as follows: $E_k = h\nu + E_b$. This kinetic energy distribution of the photoelectrons is fabricated by a series of discrete bands, which symbolizes for the electronic structure of the sample. The core level binding energies of all the elements (other than H and He) in all different oxidation states are unique, which provides instant detection of the chemical composition of the sample after a full range scan. However, to account for the multiplet splitting and satellites accompanying the photoemission peaks, the photoelectron spectra should be interpreted in terms of many-electron states of the final ionized state of the sample, rather than the occupied one-electron states of the neutral species [30,31]. Photoelectron peaks are labeled according to the quantum numbers of the level from which the electron originates. An electron coming from an orbital with main quantum number n, orbital quantum number l (0, 1, 2, 3…. indicated as s, p, d, f ...) and spin quantum numbers (+1/2

or -1/2) is indicated as nl_{l+s}. Almost all photoelectrons used in the laboratory XPS have kinetic energy in the range of 0.2 to 1.5 keV, and probe the outer layer of the catalyst.

X-ray photoelectron spectra were obtained using X-ray Photoelectron spectrometer [V. G. Scientific (UK) ESCA-3000). All the measurements are made on as received powder samples using X-ray source Mg Kα (hv = 1253.6eV) at room temperature. The spectrometer was operated at 12 mA and 12.5 kV with analyzer at a constant pass energy mode (50 eV) for wide scan spectra. High resolution spectra (pass energy 20 eV, step size 0.1-0.2 eV) of the W4f, Zr3d, C1s and O1s regions were measured with the largest possible aperture in order to obtain maximum signal intensity. The residual gas pressure in the spectrometer chamber during the data acquisition was less than $1.3X10^{-7}$ Pa. Multi-channel detection system with nine channels is employed to collect the data. The overall energy resolution of the instrument is better than 0.7 eV, determined from the full width at half maximum of $4f_{7/2}$ core level of clean gold surface. Before the experiments the spectrometer was calibrated against (Au $4f_{7/2}$) - 84.0 eV and (Cu $2p_{3/2}$)-932.6 eV. The $Zr3d_{5/2}$ and/or C1s lines were taken as internal references with a binding energy of 182.0 and 285.0 eV, respectively [32,33]. An estimated error of ±0.1 eV in all BE (binding energy) values can be assumed for the measurements. A drop of thick paste made from acetone and finely grounded oven dried samples were mounted on the standard sample holder. The sample holder was then fixed on a rod attached to the pretreatment chamber. Before transferring them to the main chamber the samples were degassed in the pretreatment chamber at room temperature. The degassed samples were then transferred into the main chamber and the XPS analysis was done at room temperature. A minimum of 3 spots for each sample were simultaneously analyzed to test sample heterogeneity; the results reported here are averages of these multiple spots.

2.4.8. Transmission Electron Microscopy (TEM)

The TEM working principle can be described as follows: the electron beam is generated in an electron gun (heated tungsten filament). The electrons are accelerated towards the anode by applying a high voltage between the anode and the cathode (gun). The accelerated beam is focused by a condenser lens and travels through the specimen, where the objective lens produces the primary magnified image of the specimen. A series

of projector lenses further enlarges this image, which is displayed on a fluorescent screen, or recorded photographically or digitally. As SEM, the TEM can be connected to an energy dispersive X-ray analyzer. TEM offers the unique advantage of allowing the direct information about the micro texture of the catalyst and structural information by lattice imaging. The technique of high-resolution electron microscopy (HRTEM) is performed with axial illumination using an objective aperture, which allows several diffracted beams to be combined with the axial transmitted beam to form the image. From images it is possible to obtain accurate information on the shape and size of particles belonging to active phases, structural information such as symmetry and unit cell parameters of crystallites, crystal orientations and lattice defects can be obtained by electron diffraction and lattice imaging techniques. The topographic information obtained by TEM is in the vicinity of atomic resolution which can be utilized for structural and compositional characterization and identification of various phases. In addition it can also be used to detect the location and dispersion of metal clusters on the support material. The critical step in electron microscopy is specimen preparation, because the quality of the image and the significance of the analyses are highly dependent on how the different solid phases are dispersed on the microscope grid and how thin they are. The thickness should be less than 50-100 nm to allow transmittance through the sample. The thinner the specimen, the better will be the resolution and contrast of the image. Specimens should be deposited on 2/3 mm diameter copper grids (100−400 mesh) covered with a thin amorphous carbon film. The easiest way is to ultrasonically disperse a very few milligram of the powder in a few milliliter of ethanol, take a drop of the suspension deposit it on a carbon coated grid and let the liquid evaporate. Electron diffraction and transmission electron microscopy are combined to study crystalline or periodic materials. The results gained from both techniques are complementary, since the formation of an image and diffraction are intimately related. The image of a specimen obtained on a screen or a photographic film by TEM is formed by scattered or diffracted electrons. By varying the focus mode of the projection system of the electron microscope, one can obtain either an image or a diffraction pattern on the screen or film. In imaging mode, one generates either a bright field image or a dark field image depending on the position of the microscope objective aperture (contrast aperture). In the dark field image, only the

beams corresponding to a selective reflection hkl contribute to the image formation. The dark field imaging allows working in diffraction mode with the formation of an electron diffraction pattern, when a selected area aperture is used instead of an objective aperture. The aperture is used to define the area from which a diffraction pattern is formed in a TEM specimen. The resulting pattern contains information about the phases present (lattice spacing) and sample orientation. The electron diffraction pattern can be described as a plane section of the diffracted lattice in the reciprocal space, and Bragg's fringes can be indexed. In this study, the electron microscopic investigations were carried on a Tecnai G^2 F20 U-TWIN from FEI (USA), transmission electron microscope with Energy Dispersive Spectroscopy detector for micro-analysis and at an accelerating voltage of 200 kV. The samples for TEM analysis were prepared by dispersing tiny amount of finely grounded powder as slurry in iso-propanol and ultra-sonicated for minimum 45 min. A drop of the sol was then placed onto a carbon-coated copper grid and left for evaporation, after evaporation it was mounted on a sample holder

2.4.9. Scanning Electron Microscopy (SEM)

The Scanning Electron Microscopy is one of the most versatile and widely used tools of modern science, which provides information about the morphology (shape, size, arrangement of the particles), the topography (determination of the surface features of an object, its texture), the compositional differences, the crystal orientation and the presence of defects. SEM requires that the specimen have some composition or topographical variation on the specimen surface in order to produce a sharp image of sufficient contrast. Therefore, a very smooth surface of uniform composition will produce a featureless image on SEM. The basic working principle of the scanning electron microscopy is based on the bombardment of the sample with a scanning beam of electrons to collect the slow moving secondary electrons generated by the sample. These electrons are collected, amplified, and displayed on a cathode ray tube. The electron beam and the cathode ray tube scan synchronously, so that, an image of the surface of the sample is formed. The main difference between SEM and TEM is that SEM sees contrast due to the topology of a surface, whereas TEM projects all information in a two dimensional image, which is of nanometer resolution. The path of the electron beam within the scanning electron

microscope differs from that of the TEM. The technology used in SEM is based on television techniques.

Table 2.2: Detailed comparison of TEM and SEM is given in below.

Feature	TEM	SEM
Uses	SAED-crystal type and lattice distances, Dark field imaging - crystal orientation, EELS-spatial distribution of all chemical elements etc.	Surface morphology, Fractures, wear or corrosion surfaces, IC chips, chemical segregation etc.
Source Of Illumination	High speed electrons	High speed electrons
Best Resolution	0.2nm	3-6 nm
Magnification Range	500-1000000x	2-2000x
Depth Of Field	0.004-0.006nm	0.003-1 nm
Lens Type	Electromagnetic	Electromagnetic
Image ray-formation spot	On phosphorescent screen by lens	On CRT by Scanning device
Limiting Factors	Lens quality	Brightness, Signal/noise ratio, Emission volume

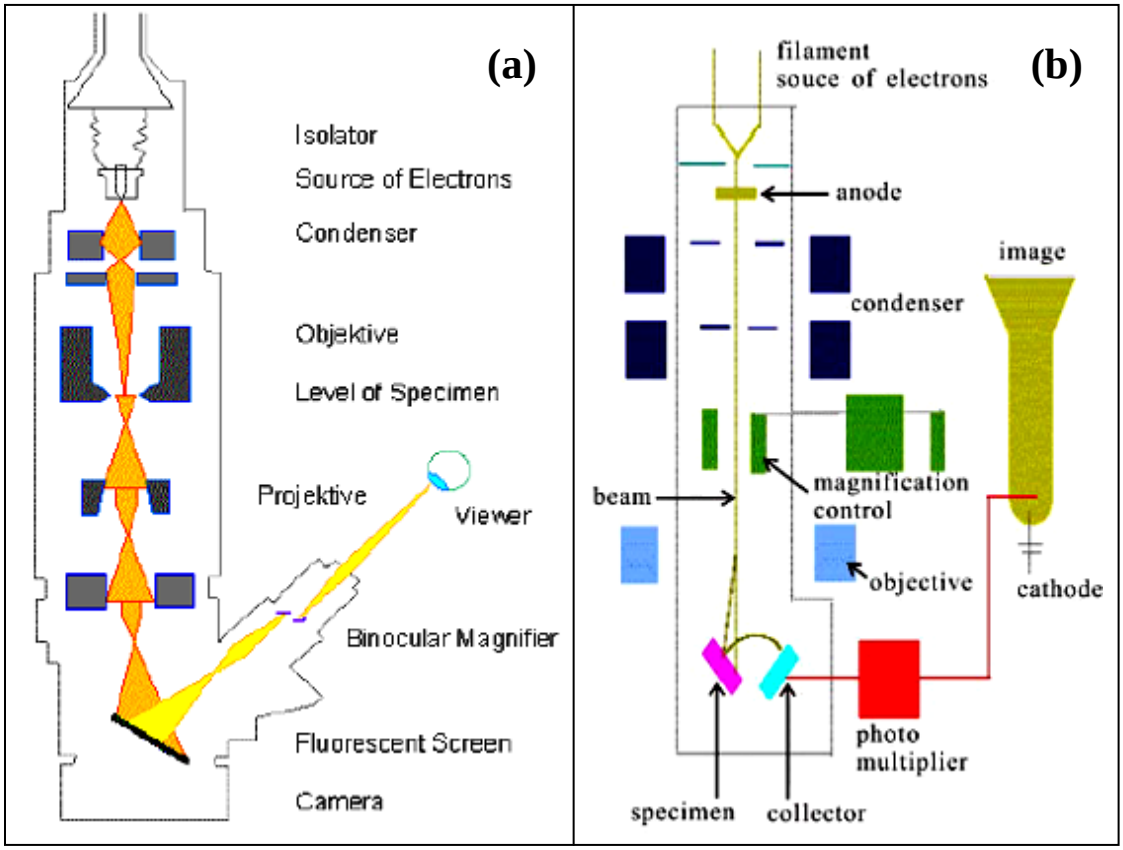

Fig. 2.6: Schematic diagrams of the setups of TEM **(a)** and SEM **(b)**.

The size and shape of the particles was examined using scanning electron microscope JEOL JSM-5200-Model/ FEI Quanta 2003D Dual Beam-ESEM. Small amount of finely grinded powder was spread on double-sided carbon tape stuck on a stub, which was then fixed to the sample holder and placed into the testing chamber which is protected with nitrogen gas. During the observation and photo sessions the SEM was operated between 10-20 kV in low vacuum with a resolution of 6nm. In addition to the SEM, energy dispersive x-ray analysis (EDX) analysis was used with the same setup to identify the major element distribution of any spot over the sample. Using EDX, we can identify the composition of particles of interest on a SEM image. Usually to prevent charge build up on the specimen surface it is coated with a conductive material. For coating, vacuum evaporation method and sputtering method are been used. Various substances are used for coating such as C (for general analysis), AU, AU-Pd, and Pt depending on the purpose, type of sample and magnification. Coating is usually necessary for higher magnification

2.4.10. Energy Dispersive X-Ray Spectroscopy (EDX)

Information about the chemical composition of the samples can be obtained using an Energy Dispersive X-ray spectrometer with the SEM. In the SEM-EDX, electrons interacting with samples cause x-rays to be generated from the atoms present. These x-rays have varying energy depending on the element it came from. In this technique the X-rays emitted from a sample, under electron bombardment, are collected with a liquid nitrogen cooled solid-state detector and analyzed via a computer according to their energy. The computer programs used in EDX display a histogram of the number of X-rays detected versus the energy. The energy of the detected X-rays relates to the elements present in the sample and the intensity of the peaks is proportional to the amount of the element present in the compound. In this way qualitative analysis (identification of elements) as well as quantitative analysis (amount of each element in the sample) can be performed. Once these x-rays are seen on the detector they are amplified and passed through a multi-chemical analyzer, the elements can be identified and semi-quantified. The elements are essentially identified based on the energies of the x-rays which are emitted from the sample. This is a powerful analytical tool as it can detect most of the

elements in the periodic table above an atomic number of 4. Detection limits are in the low percentage range. The method is a surface analytical procedure.

Chemical composition of the samples was obtained using FEI Quanta 2003D Dual Beam-ESEM with EDX (Genesis) attachment. This system was equipped with a standard Si(Li) large field detector and Tungsten Filament (Thermionic emission) as electron source. The EDX was calibrated with the pure elements Cu and A1. During the EDX measurements the system was operated at 30 keV in low vacuum. The collection time for the EDX spectra was 30-60 s and the working distance was set to 15 mm. ZAF Correction - Specific factors related to sample composition (called matrix effects) can affect the x-ray spectrum developed in an electron microprobe analysis and may have to be corrected for if a precise analysis needs to be performed. These matrix corrections are known as ZAF corrections, referring to the three parts of matrix effects - the atomic number (Z), absorption (A), and fluorescence (F). EDX was employed for the elemental mapping of the W, Mo, Zr and O applying ZAF corrections.

2.4.11. X-Ray Fluorescence Spectrometry (XRF)

X-ray fluorescence (XRF) spectrometry is a powerful multi-elemental and nondestructive analytical technique, which provides accurate analysis of the bulk chemical composition of a solid/liquid sample. In this method a suitable sample is radiated by high energy X-rays by which electrons can be expelled from the different atoms, leaving empty space (holes) in low lying orbitals. The main mechanism for relaxation then is that an upper electron falls into this vacancy. The energy released may result either in the generation of radiation, which is called X-ray fluorescence (Fig. 2.7), or in the ejection of another electron, the secondary electron of the so-called Auger effect. Both X-ray fluorescence radiation and the Auger electrons are characteristic for the emitting atoms and can be used for quantitative elemental analysis. X-ray fluorescence makes use of the ability of high energy X-rays (10^{-6} nm to 10 nm) to excite electrons in an atom to a higher energy state. In most cases, but not all X-rays are produced by accelerating electrons through a vacuum tube from a heated tungsten cathode towards a metal anode, often molybdenum, chromium, rhodium, scandium, cobalt, tungsten etc with a potential difference of up to 100kV. When these electrons strike the large anode

plate, made of copper with the anode material embedded in it, an X-ray continuum or line spectrum is produced. The apparatus must be cooled to avoid melting the anode. These X-ray radiations when strikes the sample are electronically excited. When the sample returns to its ground state it fluoresces, emitting a photon which is lower in energy then the initial excitation photon. These emitted X-rays are first collimated and then selectively separated on an analyzing crystal often lithium fluoride or sodium chloride by diffraction applying Bragg's law. The number of emerging X-ray photons is detected by a transducer such as Geiger counter, ionization chamber or scintillation counter.

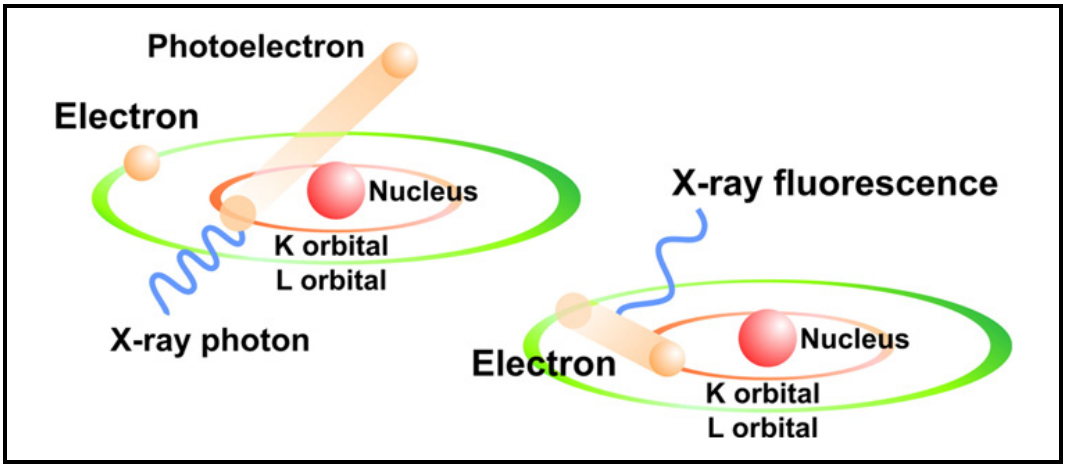

Fig. 2.7: Production of X-ray fluorescence

The energy (or wavelength or "color") of the fluorescent photons is an indication about the elemental composition of the sample. The intensity of the fluorescent beam (number of photons per sec) is an indication of the element's concentration in the sample. The goal of the spectrometer is to analyze the fluorescent beam and measure its characteristics in energy (or wavelength) and in intensity. Software coupled to the spectrometer converts this information into concentration's values. Corrected intensities from inter-element effects are linearly correlated with certified concentrations of reference materials.

The composition of catalyst was measured using a PANalytical MiniPal 4 EDXRF (Energy Dispersive XRF) spectrometer, equipped with a 30 kV, rhodium anode 9 Watt tube with a helium purge facility having five filters and a silicon drift detector which can analyze elements in the range from Na to Bi, in concentrations from 100% down to ppm levels. Following EDXRF conditions were used for the determination of W, Mo and Zr concentration from the catalyst in air atmosphere. Voltage of 30 kV was set

and automatically adjustment of the current was done. Approximately 5 g of finely grounded sample was taken in a 30mm sample cup having nylon-6 foils at the bottom. The sample cups were allowed to spin twice for 30 sec to obtain maximum homogeneity in sample powders. 3 measurements were carried out for with 100 s acquisition time without any filter and the average of the 3 readings was considered.

2.4.12. Atomic Absorption Spectrometry (AAS)

Atomic absorption is the process that occurs when a ground state atom absorbs energy in the form of light of a specific wavelength and is elevated to an excited state. The amount of light energy absorbed at this wavelength will increase as the number of atoms of the selected element in the light path increases. The relationship between the amount of light absorbed and the concentration of analyte present in known standards can be used to determine unknown concentrations by measuring the amount of light they absorb. Instrument readouts can be calibrated to display concentrations directly. The principle of atomic absorption is based on energy absorbed during transitions between electronic energy levels of an atom. When some sort of energy is provided to an atom in ground state by a source such as a flame, most commonly in the form of an air-acetylene or nitrous oxide-acetylene flame (temperature ranging from 2100–2800 °C), outer-shell electrons are promoted to a higher energy excited state. The radiation absorbed as a result of this transition between electronic levels can be used for quantitative analysis of metals and metalloids present in solid matrices, which have to be dissolved by appropriate solvents before analysis. The basis of quantitative analysis depends on measurement of radiation intensity and the assumption that radiation absorbed is proportional to atomic concentration. Analogy of relative intensity values for reference standards is used to determine unknown elemental concentrations.

Although AAS it is a destructive technique, the sample size needed is very small (typically about 10-100 milligrams). Small amount of solid sample approximately 100mg was weighed out accurately using the microbalance and dissolved in mixture containing few drops of 48% Hydrofluoric acid (HF) and 5ml 70% Nitric acid (HNO_3). Dissolution times are generally in the region of 1-6 hours for the samples to completely dissolve depending upon the type of sample. After complete dissolution of the sample the

solutions are then diluted with ultra-pure water to decrease their element concentrations to within the linear range for the particular element under study. Neutralization of the HF was then done by adding boric acid (~2g) in excess. All standards were also spiked with same amount of acid added for sample preparation to reduce matrix effects. The resulting solution is introduced as an aerosol into the flame of the instrument and atomized. Light of a suitable wavelength for a particular element is shone through the flame, and some of this light is absorbed by the atoms of the sample. The amount of light absorbed is proportional to the concentration of the element in the solution, and hence in the original object.

Concentrations of Mo, W and Zr in the dissolved samples were determined using Varian SpectrAA-220FS-**F**ast **S**equential atomic absorption spectrometer. Calibration was carried out using standard solutions, and the wavelength was adjusted to 313.3 nm, 255.1 or 455 nm, and 360.1 nm for estimation of Mo, W and Zr respectively using single element hollow-cathode lamps. The instrument has 4 fixed sockets in which the respective hollow-cathode lamps can be fixed and these elements can be analyzed in a sequential mode. Atomic absorption measurements were carried out in (N_2O) nitrous oxide-acetylene flame without background correction. The measurement time and pre-ready delay was set to 10 s. Some important operating parameters are given below in the Table 2.3 while other parameters were set as recommended by the manufacturer's manual.

Table 2.3: AAS operating parameters optimized for the estimation of Zr, Mo and W

Parameter	**Zr**	**Mo**	**W**
Slit Width:	0.2 nm	0.5 nm	0.2 nm
EHT:	59 volts	34 volts	52 volts
Lamp Current:	10.0 mA	12.0 mA	20.0 mA
Lamp Position:	4	3	2
N_2O Flow:	9.98 L/min	10.50 L/min	10.60 L/min
Acetylene Flow:	7.49 L/min	7.71 L/min	7.05 L/min

2.4.13. Inductively Coupled Plasma (ICP)

Inductively coupled plasma atomic emission spectrometry (ICP-AES), despite the necessity to decompose the sample, is sensitive enough for the determination of broad type of samples with high accuracy and precision. Another great advantage of the technique is that it allows the simultaneous determination of major, minor and trace elements. Inductively Coupled Plasma (ICP) is a high energy source that permits the excitation of most elements, both metals and non-metals. The coupling of ICP with atomic emission spectroscopy (ICP-AES), a reproducible and very accurate analysis technique, is for all types of liquid and some solid samples. Atomic emission spectroscopy is an analytical method whereby the radiation emitted by excited atoms and ions are measured. The emission occurs when sufficient thermal or electrical energy is available to excite a free atom or ion to an unstable energy state. Light is emitted when the atom or ion returns to a more stable configuration or the ground state. The wavelengths of light emitted are specific to the element which are present in the sample. The basic instrument used for atomic emission is very similar to that used for atomic absorption with the difference that no primary light source is used for atomic emission. One of the more critical components for atomic emission instruments is the atomization source, because it must also provide sufficient energy to excite the atoms as well as atomize them. Due to the limitations of the early sources, atomic emission initially did not enjoy the universal popularity of atomic absorption. This changed dramatically with the development of the Inductively Coupled Plasma (ICP) as a source for atomic emission. The ICP eliminates many of the problems associated with past emission sources and has caused a dramatic increase in the utility and use of emission spectroscopy. The ICP is argon plasma maintained by the interaction of Radio frequency (RF) field and ionized argon gas. The ICP is reported to reach temperatures as high as 10,000 °C, with the sample experiencing useful temperatures between 5,500 °C and 8,000 °C. These temperatures allow complete atomization of elements, minimizing chemical interference effects. When a RF power is applied through the coil, an oscillating magnetic field is formed. When argon gas is passed through a micro wave RF coil an excitation is initiated with a high voltage spark which creates seed electrons and ions, these charged particles (electrons and ions) are forced through a closed annular path,

where additional heating and ionization occurs, this ionizes the argon and produces a plasma state which is at a temperature of 6000°C to 10,000°C. The process occurs almost instantaneously, and the plasma expands to its full dimensions. The cont. plasma is formed by a tangential stream of argon gas flowing between two quartz tubes. As viewed from the top, the plasma has a circular, "doughnut" shape. The fluid sample is pumped into a nebuliser via a peristaltic pump. The nebuliser generates an aerosol mist and injects humified Ar gas into a chamber along with the sample. The fine aerosol mist containing Ar gas and sample is interjected vertically up the length of the torch assembly into the plasma. When this fine aerosol of aqueous or organic solutions or suspension of metals /non metals is injected to the argon plasma, excitation of the elements will occur resulting in emission of specific wave lengths of electromagnetic radiation. Light emitted from the plasma is focused through a lens and passed through and entrance slit into the spectrometer. Emission spectroscopy requires identification and selection of suitable analysis lines (wavelengths). Often, analysis lines of reasonable intensity and those with the least spectral interferences with the other elements present are chosen. The intensity of radiation is proportional to the concentration of the element in the solution. Each element emits at multiple wavelengths. These wavelengths are separated by a diffraction grating and sent to photo multiplier tubes. With appropriate amplifiers, A to D converters, computers and software a powerful analytical instrument is then at the disposal of experienced analytical chemists. The main advantage of ICP Atomic Emission Spectrometry is the linear dynamic concentration of the analysis from ppb levels to high ppm levels and the ability to analyze for multiple elements simultaneously. The reason for this advantage is because the sample is injected as an aerosol through the center of the doughnut which confines the sample to a narrow region and provides an optically thin emission source and a chemically inert atmosphere, resulting in a wide dynamic range and minimal chemical interactions in an analysis. ICP-AES usually gives linear calibration curves, thus making it possible to determine both high and very low concentrations. The accuracy of the analysis can be optimized by using blank solutions with a similar matrix as the samples to be determined. The background correction will then produce good results. ICP-AES provides the lowest detection limits for a number of high melting elements such as B, W, Zr, Al and Ti.

ICP-AES analysis was performed to determine the bulk composition of the catalysts. The total W and Zr concentration was determined by means of ICP-AES SPECTRO ARCOS-Advanced Rowland Circle Optical System, instrument. The spectrometer optical system is optimized paschen-runge assembly and aluminum half shell technology having a resolution of 8.5 picometer. The wavelength range is 130-770 nm with 32 Linear CCD detectors. The monochromator is equipped with an 1800 grooves/mm holographic grating. Sample was introduced using 4 channel peristaltic pump with auto diluter. The general ICP-AES operating conditions were:

Parameter	**Value**
Injector ceramic tube internal diameter (mm)	2
Spray chamber type	Cyclonic
Nebulizer type	Lichte model
Plasma power (kW), 27.12 MHz	1.4
Auxiliary argon flow rate (liters/min)	1
Nebulizer argon flow rate (liters/min)	0.777
Coolant gas flow (liters/min)	13
Plasma viewing mode	Radial
Background correction	2 points per peak

The axially viewing observation mode is usually recommended for the improvement of the detection limits; however matrix effects are larger in axial mode as compared to radial view mode [34] Therefore radial view was chosen because accuracy and precision was vital then detection limit. The most sensitive W (239.709/400.87 nm) and Zr (339.198 nm) wavelengths were used for their determinations. Ultra spec single element standards from Aldrich were used for preparation of calibration solutions and standardization. Deionised water (resistivity of 18.2 MΩ cm), purified by a Milli-Q system (from Millipore) was employed for preparing calibration solutions and samples. All glassware and polyethylene bottles were kept overnight by soaking in 10% HNO_3, and cleaned by rinsing five times with distilled deionised water. All standard solutions were prepared in 5% (v/v) HNO_3 with few drops of HF. Blank digestion was also carried out by

completion of full analytical procedure without sample. All determinations were made in triplicate and average value was reported. All results were obtained as ppm (parts per million) which was converted to atomic weight % since the weight of the sample is known. The atomic weight % was converted to oxide weight % and normalized to 100. Sample preparation was similar to the procedure given in previous AAS section 2.4.12. For estimation using ICP the sample solutions were further diluted in order to bring them within the instrument calibration range of 10-20 ppm.

With the availability of a variety of atomic spectroscopy techniques such as flame atomic absorption, graphite furnace atomic absorption, inductively coupled plasma emission, and ICP mass spectrometry, we must decide which technique is best suited for our samples. Important selection criteria for atomic spectroscopy techniques include detection limits, analytical working range, sample throughput, cost, interferences, ease of use, and the availability of proven methodology all these are summarized in Fig. 2.8 and tabulated in Table 2.4.

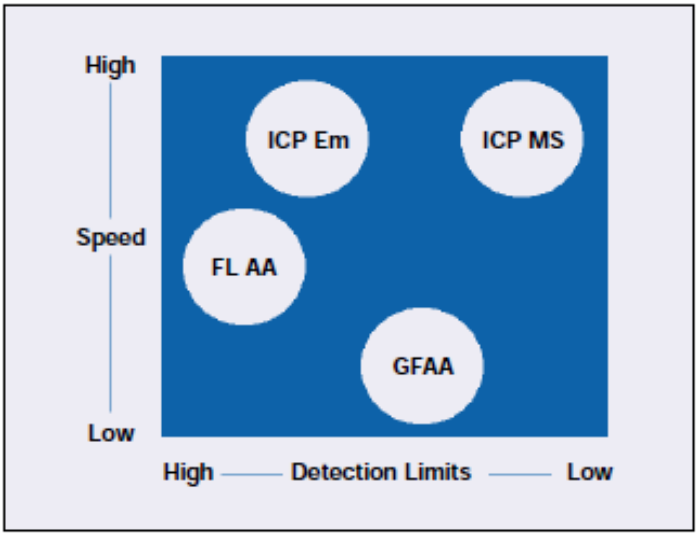

Fig. 2.8: A general selection guide for atomic spectroscopy instrumentation based on sample throughput and concentration range.
(ICP Em - Inductively Coupled Plasma-Emission spectroscopy, ICP MS - Inductively Coupled Plasma-Mass Spectroscopy FL AA- Flame-Atomic Absorption spectroscopy, GF AA - Graphite Furnace-Atomic Absorption spectroscopy).

Table 2.4: AAS Vs ICP quick selection guide.

Factor	AAS	ICP
Detection Limits	Best for group I metals, volatile elements, rare earth. For AAS the detection limits are in the range of ppm whereas these may go down to ppb level for GFAAS	Best for Refractory metals, metalloids, Non-metals. Detection limits are generally very low: 0.1 to 1 ppb
Sample through put	Best if less then 6 elements per sample	Best if more then 6 elements per sample
Precision	0.1-1%	0.3-2%
Spectral Interferences	Virtually None	Many
Chemical Interferences	Some	Virtually None
Ionization	Some	Minimal
Operational Cost	Low	High
Combustible gases	Yes	No
Advantages	Fast, accurate, well documented, lower operational cost	Fast, accurate, extensive dynamic range, multi-element detection.
Dis-Advantages	Must have element specific lamp, Short dynamic range. Not suitable for the elements like, B, Ce, La, Nb, Pr, Ti etc	Spectral Interferences. The elements that are difficult to be determined by AAS, can be measured by AES.
Dynamic Range	The dynamic range is spread over three orders of magnitude for FAAS and two orders for GFAAS.	The dynamic range is large and extends over a range of 4 to 6 orders of magnitude. It is suitable for analytes from parts per billion to 99.9 per cent.
Back ground Interference	The flame constituents contribute to the spectral, background and chemical Interferences.	Plasma is an optically thin emission source and is relatively free from chemical interferences.
Operation	Flame AAS is easy to set up and to use, and requires minimal operator skills, the GFAAS on the other hand is considerably more difficult.	It falls between these two AAS techniques; however, it is a bit easier to master than GFAAS.
Automation	FAS procedure cannot be automated whereas it is possible to automate GFAAS.	ICP-AES measurements can be automated.
Versatility	The AAS determinations using flame are rapid and precise and are applicable to about 67 elements.	It can be used for the determination of most elements except Ar. In practice, approximately 70 elements can be determined.

Bases upon above table and diagram one can select the best suited atomic spectroscopy technique.

2.4.14. Raman Spectroscopy (RAMAN)

Raman spectroscopy is an invaluable technique, which offers non-destructive qualitative (identification) and quantitative (particle size determination) microanalysis of materials. This technique relies on inelastic scattering of monochromatic light, usually from a laser in the visible, near infrared, or near ultraviolet range. The laser light interacts with phonons or other excitations in the system, resulting in the energy of the emitted photons being shifted up or down. The Raman Effect arises when the incident light excites molecules in the sample, scattering subsequently the light. While most of this scattered light is at the same wavelength as the incident light (Raleigh scattering), some part is scattered at different wavelengths. This inelastically scattered light at different wavelengths is called Raman scatter (Raman scattering). It results from the molecule changing its molecular motions. The energy difference between the incident light (Ei) and the Raman scattered light (Es) is equal to the energy involved in changing the molecule's vibrational state (i.e., getting the molecule to vibrate, Ev). This energy difference is called the Raman shift and is given as follows: Ev = Ei – Es. Several different Raman shifted signals will often be observed, each signal being associated with different vibrational or rotational motions of molecules in the sample. The particular molecule and its environment will determine which Raman signals will be observed. A plot of Raman intensity versus Raman shift represents a Raman spectrum. The Raman spectroscopy technique is used to investigate the vibrational, rotational and other low frequency modes in a system.

Raman measurements were performed on Horiba Jobin Yvon HR 800 instrument having mirror based reflective optics equipped with a confocal microscope (Olympus BX41). The excitation source used was He Ne Laser system which provides a wavelength of 632.81nm resolution 0.3cm^{-1}/pixel. For conventional Raman spectroscopy, the laser power of the He Ne laser attached to the LabRam spectrometer was limited to ~ 1mW in order to prevent heating of the samples by neutral density filters. The slit width was usually set to 200 μm resulting together with the grating in a spectral resolution of 2 cm^{-1}. The achromatic flat field monochromator is equipped with an 1800 grooves/mm grating. Light from the illuminated spot is collected with a lens and sent through a monochromator. Wavelengths close to the laser line, due to elastic Rayleigh scattering,

are filtered out (Rayleigh frequency rejection upto 10 cm^{-1}) while the rest of the collected light is dispersed onto a detector. The scattered light was removed effectively by two notch filters. The spectra were recorded in the back-scatter mode using a thermoelectric cooling Synapse CCD camera and the identifications of the various peaks were carried out by taking references to the various literature values. About 500 mg of finely grounded sample is pressed in the sample holder and the spectrum was measured in the range of 100-1200 cm^{-1}. The Raman shift was corrected before taking measurements using a silicon reference sample and spectrum. Even though it is a complementary technique to classical IR spectroscopy, it is the only spectroscopy able to detect adsorbent vibrations in a wave number range where the support itself is not transparent to IR radiation.

2.4.15. Small Angle X-Ray Scattering (SAXS)

SAXS is an analytical technique that is based on the interaction of monochromatic X-rays with matter. It differs from XRD in that it is used to examine substances with large d-spacings (1 to 100 nm). According to Bragg's law, when the wavelength of the X-ray is constant, smaller angles lead to the detection of large d-spacing. In SAXS, the angle of incidence is usually smaller than 5 degrees, which means that it detects the d-spacing in the domain of nanometers. Therefore, SAXS is a technique for studying structural features in the nanometer range. It is performed by focusing a low divergence X-ray beam onto a sample and observing a coherent scattering pattern that arises from electron density inhomogeneities within the sample. Due to its considerable ability to probe the materials in nanometer scales, SAXS plays an important role in polymer research, nanoscience, medical-biological studies, liquid crystals, microemulsions, catalyst development, nanoporous materials and so on. Due to their quasi-crystalline nature, surfactant meso-phases respond well to SAXS analysis. At low concentrations, information can be collected (gained) describing the size and shape of the molecules and at higher concentrations (from above about 5%) the different mesophases give rise to different SAXS "fingerprints".

Small-angle X-ray scattering data were obtained with a Bruker Nanostar equipped with a rotating anode X-ray generator with a pinhole camera (Nanostar, Bruker AXS) with CuKα radiation monochromatized and collimated from crossed Goebel mirrors and

detected by a 2D position sensitive detector (HiSTAR). The machine was operated at voltage of 45kV and a current of 100mA. Data was collected over a q range of 0.01 - 0.2A. All SAXS patterns were radially averaged and corrected for background scattering to obtain the scattering intensities in dependence on the scattering vector $Q= 4\pi \sin\theta / \lambda$, being 2θ the scattering angle and k = 0.1542 nm the X-ray wavelength.

2.5. CATALYTIC ACTIVITIES

Anhydrous AR grade chemicals and solvents used in this study are commercially available and used without further purification. All the reactions were carried out in liquid phase batch mode. These reactions were carried out by taking the mixture of reactants, catalyst and a suitable solvent in a round bottom flask provided with a condenser and stirred / refluxed for appropriate time. Completion of the reaction was monitored by GC. After completion of the reaction, catalyst was recovered by simple filtration and reused. The product were recovered from the filtrate, concentrated on a rotatory evaporator and re-crystallized in ethanol. The products were also confirmed using FT-IR, GC-MS (Shimadzu 2000 A) by injecting authentic samples and ^{1}H-NMR and ^{13}C-NMR (Bruker AC200). Detail experimental setup, reaction conditions and product analysis techniques are described.

NMR (Nuclear Magnetic Resonance) spectroscopy is the procedure that takes advantage of the magnetic properties of nuclei. NMR spectra arise from the spinning of nucleus. In its most straightforward form, NMR Spectroscopy allows for the identification of each atom in a pure molecule. Similar to using IR spectroscopy in the identification of functional groups, examination of a ^{1}H proton NMR spectrum shows how many atoms of each type and what atom environments exist within the specimen (sample). Since it is based in quantum mechanical nuclei properties, NMR spectroscopy is reproducible, predictable, and very reliable. Mass Spectrometer when coupled with GC the detection system is often referred to as the mass selective detector or more simply GC-MS. The power of this technique lies in the production and identification of mass of each analyte detected, instead of merely an electronic signal that varies with the amount of analyte. This data can be used to determine the identity as well as the quantity of unknown components after comparing with reported standard database.

2.5.1. Experimental setup

MoO_3-ZrO_2 catalysts were found to be a good catalyst for various types of reactions such as oxidation, condensation etc. The applications of these MoO_3-ZrO_2 catalysts in preparation of biologically important species have not been explored yet, hence Claisen–Schmidt condensation (CSC) which is an important C-C bond forming reaction for the synthesis of chalcones was carried out over MoO_3-ZrO_2 catalysts. In the present work we report the use of for CSC under solvent-free conditions to give Chalcone. The liquid phase Claisen–Schmidt condensation (CSC) of benzaldehyde (BA) with acetophenone (AP) was carried out in a magnetically stirred two necked round bottom flask (capacity 50 mL) attached to a condenser and a septum, immersed in a thermostat bath with a magnetic stirrer as show in Fig.2.9. The reaction was done under N_2 atmosphere and solvent-free conditions to give Chalcone. The temperature of the reaction vessel was maintained using an oil bath. The reaction mixture was magnetically stirred and heated to the required temperature at atmospheric pressure. In a typical experiment, benzaldehyde (2.12 g), acetophenone (2.40 g), {Benzonitrile (5 g) for the reaction in the presence of solvent} and dried catalyst (0.06 g) were added to the reactor, and then heated to 150 °C for 16 h.

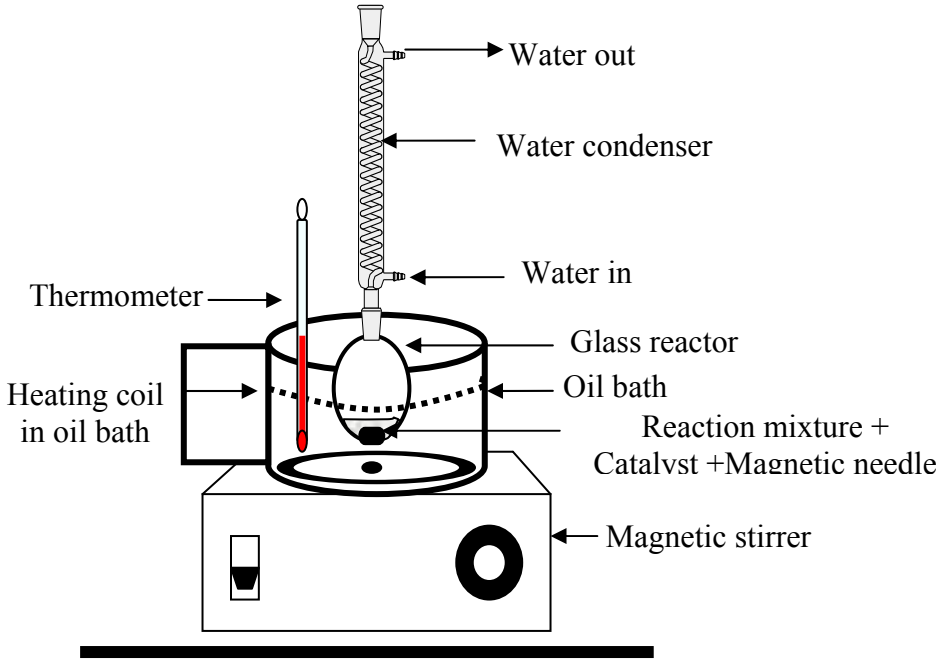

Fig. 2.9: A typical schematic diagram of the experimental reaction setup.

2.5.2. Analysis of reaction products

The product samples were withdrawn at regular intervals of time and analyzed on a gas-chromatograph (HP 6890) equipped with a flame ionization detector and a capillary column (HP-5 capillary column, 30 m length X 0.32 mm internal diameter).

The following GC-FID program set up was used for identifying product distribution.

GC parameters: FID: 300 ^{o}C, Injector: 280 ^{o}C, 0.2 µl sample.

Rate	**Oven Temp.**	**Hold Time**
Initial Set	100 ºC	1 min
15 ºC/min	180 ºC	2 min
30 ºC/min	280 ºC	12 min
15 ºC/min	300 ºC	1 min

2.6. REFERENCES:

[1] C.Marcilly, Pet. Tech. 1986, 328, 12.

[2] C.Marcilly, Rev. Inst. Fr. Pet. 1984, 39, 189.

[3] Ph. Courty, Ch. Marcilly, In. Preparation of Catalysts III; G. Poncelet, P. Grange, J.A. Jacobs, Eds. Stud. Surf. Sci. Catal. 1983, 16. 485.

[4] P. Courty, C. Marcilly, In Preparation of Catalysts I. B. Delmon, P.A. Jacobs, G. Poncelet, Eds. Stud. Surf. Sci. Catal. 1976, 1,119.

[5] R. M. Richards. Metal oxide nanoparticles. In J. A. Schwarz, C. Contescu, and K. Putyera, editors, Encyclopedia of Nanoscience and Nanotechnology. Marcel Dekker, New York, 2004.

[6] H. Itoh, S. Utamapanya, J. V. Stark, K. J. Klabunde, and J. R. Schlup. Chem. Mater., 1993, 5, 71.

[7] V. R. Palkar. Nanostruct. Mater., 1999, 11(3), 369.

[8] L. V. Interrante and M. J. Hampden-Smith, editors. Chemistry of Advanced Materials: An Overview. Wiley-VCH, New York, 1998.

[9] H. D. Gesser and P. C. Gosswami. Chem. Rev., 89:765, 1989.

[10] A. Bielan´ski, Fundamental Inorganic Chemistry. PWN, Warsaw16, 1987.

[11] D.S. Kim, M. Ostromecki, I. E Wachs, S.D. Kohler, J.G. Ekerdt. Catal. Lett., 1995 , 33, 209.

[12] J-P. Jolivet, Metal oxide chemistry and synthesis from solution to solid state. John Wiley & Sons; 1994

[13] A. Ogundipe, J. Pavlov, W. Braida, A. Koutsospyros, G. Sen, C. Christodoulatos. G. O'connor, Global NEST Journal, 2009, 11, 3, 308-317.

[14] GA Parks, Chem Rev, 1965, 65, 177.

[15] J.Ryczkowski , Appl Surf Sci., 2005, 252, 813.

[16] O.Collart , Van Der Voort P, EF Vansant , E Gustin , A. Bouwen , D. Schoemaker , Ramachandra Rao R, BM. Weckhuysen , RA. Schoonheydt RA , PCCP, 1999, 1, 409915.

[17] T. R. Gaydhankar, P.N. Joshi, P.Kalita and R. Kumar, Journal of Molecular Catalysis A : Chemical, 2007, 265, 306-315.

[18] D. E. López, K. Suwannakarn, D. A. Bruce, J G. Goodwin Jr, Journal of Catalysis, 2007, 247, 43–50 .

[19] B.M. Devassy, S.B. Halligudi, Journal of Molecular Catalysis A: Chemical, 2006, 253, 8–15.

[20] S.R. Vaudagna, S.A. Canavese, R.A. Comelli, N.S. Figoli, Appl. Catal. A, 1998, 168, 93.

[21] J.R. Sohn, M.Y. Park, Langmuir, 1998, 14, 6140.

[22] J.G. Santiesteban, J.C. Vartuli, S. Han, R.D. Bastian, C.D. Chang, J. Catal.1997, 168, 431.

[23] S. Brunauer, L. Deming, W. Deming, E. Teller, Journal of American Chemical Society , 1940, 62,1723.

[24] IUPAC, Pure Applied Chemistry, 1994, 66, 1739.

[25] G.D. Halsey, J. Chem. Phys. 1948, 16, 931.

[26] International Union of Pure and Applied Chemistry., 1986, 57, 603–19.

[27] Dullien, F.A.L. Porous Media Fluid Transport and Pore Structure. 2 ed. Academic Press, 1991.

[28] B. M. Weckhuysen, R. A. Schoonheydt, Catal. Today,1999, 49, 441.

[29] R. A. Schoonheydt, Diffuse Reflectance Spectroscopy, Chapter 4, in: Characterization of Heterogeneous Catalysts, F. Delannay (Ed.), Marcel Dekker, New York, 1984.

[30] C.S. Fadley, Electron Spectroscopy: Theory, Techniques and Applications, Vol. 2, Eds: C.R. Brundle, A. D. Baker, Academic Press, New York, 1978.

[31] W.N. Delgass, T.R. Hughes, C.S. Fadley, Catal. Rev., 1970, 4, 179.

[32] P. Ratnasamy, J. Catal., 1975, 40, 137.

[33] D. Briggs, M.P. Seah (Eds.), Practical Surface Analysis, Auger and X-ray Photoelectron Spectroscopy, 2nd Edition, Vol. 1, Wiley, New York, 1990.

[34] I.B Brenner, A.T Zander, Spectrochimica Acta Part B: Atomic Spectroscopy, Volume 55, Issue 8, 1 August 2000, Pages 1195-1240.

CHAPTER – 3

SYNTHESIS AND CHARACTERIZATION OF $t\text{-}ZrO_2$

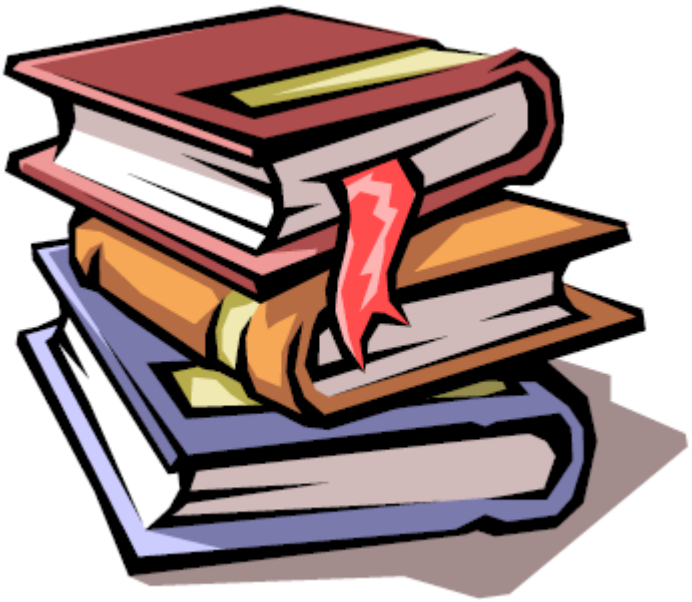

3.1. INTRODUCTION

Among the non-silica mesoporous oxides zirconia has received a particular interest, due to the large field of applications ranging from catalysis to ceramics because of its high thermal stability, remarkable mechanical strength, easy availability, high melting point, low thermal conductivity, high corrosion resistance, amphoteric behavior and unique properties of the surface. Zirconia exhibits several crystalline modifications: (a) monoclinic, that is thermally stable at the temperature below 1172 °C, (b) tetragonal, that is stable at the temperature range 1172- 2347 °C, (c) cubic, stable above 2347 °C and (d) rhombic, which is stable at a high pressure. However, tetragonal and cubic zirconia can be prepared at low temperatures (500-700 °C) in the form of highly dispersed metastable phase. The crystalline structure, concentration, transformation between each other and catalytic properties of zirconia are generally depends upon its synthesis method and thermal treatment. The common reported methods for preparation of zirconia are by precipitation and sol-gel. The source may be zirconium oxy- chloride/nitrate, zirconium n-butoxide, zirconium propoxide, zirconium nitrate/chloride etc. The hydrolysis of these materials results the formation of zirconium hydroxide and the calcination leads to the zirconium oxide. The traditional precipitation technique may give rise to microcrystalline zirconia; but the sol-gel method produces nanocrystalline zirconia, which is very attractive for novel applications. Commercially available zirconia has a relatively low surface area 40 m^2/g or less, which is rather lower than the surface area of conventional supports such as alumina and silica. The use of zirconia, from both scientific and industrial application point of view requires high surface area, crystalline tetragonal phase and suitable pore structure for catalysis applications; eg. High surface area zirconia is widely used as a catalytic support or oxygen censor electrolytes in automobile exhaust emission control system. However, loss of surface area and transition from the tetragonal to the monoclinic phase results in sintering and deactivation of the catalyst after thermal treatment thereby the stability of tetragonal phase is crucial. The concentration and transformation among tetragonal, monoclinic and cubic phases depend on synthesis procedure and doping zirconia with foreign ions and/or thermal treatment conditions. Molybdenum and Tungsten oxide species form strong acid sites on zirconia supports and inhibit ZrO_2 crystallite sintering and tetragonal to monoclinic structural transformation.

These catalysts are active for vide variety of catalytic reactions. Zirconia and its mixed oxides can be used as an acid-base bifunctional catalyst. In this case where an acid site acts as an active site in one step of a reaction and a basic site acts as an active site in another step. It is therefore called acid-base concerted bifunctional catalysis. This is due to its pronounced catalytic behavior in spite of its almost neutral surface property. The co-operation of weakly acid sites and weakly basic sites of which acid-base pair sites are suitably oriented on zirconia surface is surprisingly powerful for particular reactions and causes highly selective reactions and long catalytic life. Apart from addition of foreign ions the retention of tetragonal phase is possible if the particle size is below some critical value primarily due to high surface energy.

3.2. IMPORTANCE OF ZIRCONIA

The two main source of zirconia are baddeleyite (impure monoclinic zirconia) and Zircon, ($ZrSiO_4$) which occurs as secondary deposits in Kerala, Florida and South Africa. It is frequently mixed in sand with other minerals like rutile and monazite. Baddeleyite is found in smaller deposits and usually contain contaminants such as silica and iron oxide.

Zirconia is a remarkable material, which has attracted a great deal of attention from scientists, technologists and researchers. It is one of the most widely studied materials in the aspects of mechanical, structural and electrical properties. It is well known for good wear resistance, hardness, low coefficient of friction, chemical inertness, elastic modulus ionic conductivity, low thermal conductivity and high melting temperature which make it attractive as an engineering material. Due to these properties zirconia is used in extrusion dies, machinery wear parts and piston caps. Zirconia (monoclinic and partially stabilized) powder is used for the production of refractory composites with enhanced thermal shock resistance and abrasion resistance. These materials find applications as sliding gate plates for pouring steel, and in steel immersion applications such as stopper rods and as components in submerged entry nozzles for oxygen lances and sensors. In addition, they are used in electrochemical cells (fuel cells, oxygen pumps, etc.) due to their high oxygen-ion conductivity at elevated temperature. Its low thermal conductivity allows its use for thermal barrier coatings for aerospace engine components. It is also used in resistive heating elements which can be operated in

air beyond the temperature range of conventional elements [1]. While refractory applications represent the tonnage usage of stabilized zirconia it is also used as a glower for incandescent lighting. Industrial application of zirconia has been increased after the discovery of the concept of transformation toughening. In addition to that amorphous zirconia is used as a catalyst in various reactions and it is an important high-K dielectric material that is being investigated for potential applications as an insulator in transistors in future nano-electronic devices. Other applications are in cathodes for plasma torches and as a nucleating agent for glass ceramics. Zirconia ceramics are used as orthopaedic implants, notably as a femoral head component in hip implants. Zirconia also finds applications in dental prosthetics, where the high strength and good biocompatibility of the material makes single-piece implants with excellent aesthetic appearance. Zirconia is a suitable material for applications as seals and impeller blades because of its chemical resistance, hardness, good surface finish and high toughness to prevent damage during assembly or by impact in operation [2]. Further, zirconia based mixed oxides are of great importance due to their multiple applications, including catalysis and solid-oxide fuel cells [3]. It is known that the catalytic efficiency of metal oxides can be improved by doping the metal oxide with a metal [4] and functionalizing the acidic organo-species over support materials [5].

3.3. DIFFERENT POLYMORPHS OF ZIRCONIA

ZrO_2 is a high temperature ceramic oxide. Its physical properties include high melting point (2710 ^oC) and is resistant to chemical attack by strong acids. Zirconia is also stable in oxidizing environments, allows oxygen diffusion through its bulk, exhibits good thermal conductivity, and is electrically insulating. Zirconia exists in three phases [6,7,8]. However, tetragonal and cubic zirconia can be prepared at low temperatures (500-700 °C) and are known as metastable phases. At atmospheric pressure, pure zirconia may exist as one of three phases: cubic, tetragonal and monoclinic. The monoclinic and tetragonal phases can be thought of as distortions of the 'parent' cubic fluorite structure. At pressures above 3.5 GPa (Giga-pascals), several orthorhombic phases may be formed, but these phases will not be discussed.

Cubic Phase of Zirconia (c-ZrO_2)

The cubic phase, c-ZrO_2, is the simplest structure formed by pure zirconia, and is stable from the melting point temperature at 2710 to 2380 °C. The structure is based on the fluorite (CaF_2) structure, in which each zirconium atom is coordinated by 8 equidistant oxygen atoms. This can be visualized by cations occupying FCC positions in a cubic lattice, with eight interstitial oxygen atoms and a large vacancy in the centre, as shown in Fig. 3.1. The space group of this structure is Fm3m.

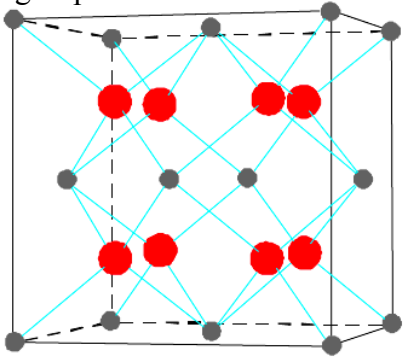

Fig. 3.1: Unit cell of the cubic zirconia phase. (Zirconium atoms: small grey dots, Oxygen atoms: big red dots).

Tetragonal Phase of Zirconia (t-ZrO_2)

The tetragonal phase, t-ZrO_2, is thermodynamically stable in bulk zirconia from the temperature 2380 °C to ~ 1100 °C. It is closely related to the cubic structure, as shown in Fig. 3.2, but differs in two respects.

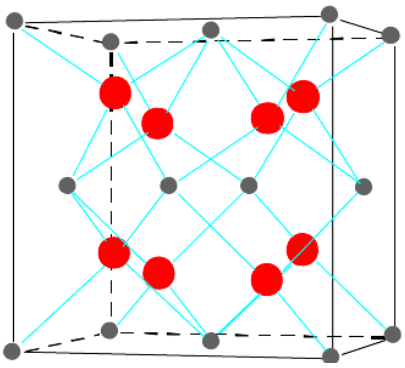

Fig. 3.2: Unit cell of the tetragonal zirconia phase, using the P4m2 'supercell'. (Zirconium atoms: small grey dots, Oxygen atoms: big red dots).

Firstly, there is a distortion in the lattice, corresponding to a slight elongation along the c axis. Secondly, there is a displacement of columns of oxygen atoms alternately up or down the c axis. The effect is to move four oxygen neighbours closer to the zirconium

atom, and the other four oxygen neighbours away from it. These interdependent distortions are required to prevent O–O contact. Each zirconium atom maintains its eight-fold co-ordination of oxygen: four oxygen atoms at a distance of ~ 2.1 Å, and four at a distance of ~ 2.3 Å. Note that the 'outer' oxygen neighbours for one zirconium atom, are also the 'inner' neighbours for neighbouring zirconium atoms. The space group of the body-centered, primitive unit cell is $P4_2/nmc$. The tetragonal phase can also be indexed to a higher symmetry, face-centred 'supercell', P4m2. This 'supercell' has a parallel c axis. The near-cubic 'supercell' is useful when examining phase transformations and comparing the structure to the other phases, as its axes are parallel to those of the cubic FCC fluorite cell, and near-parallel to those of the monoclinic cell. It is unfortunate that in the literature the distinction between the primitive cell and 'supercell' is rarely made clear. The diffraction pattern of the tetragonal phase is almost identical to that of the cubic phase, except for the 'splitting' of a number of peaks to form doublets, caused by the slight elongation of the c axis. When the peaks are broad, for instance due to small crystal size, it may be difficult to distinguish the diffraction patterns of the two phases unless the high-angle peaks are examined or vibrational spectroscopy is used [9,10,11].

Monoclinic Phase of Zirconia (m-ZrO_2)

The monoclinic zirconia phase m-ZrO_2 is thermodynamically stable in bulk zirconia at temperatures below ~ 1100 °C.

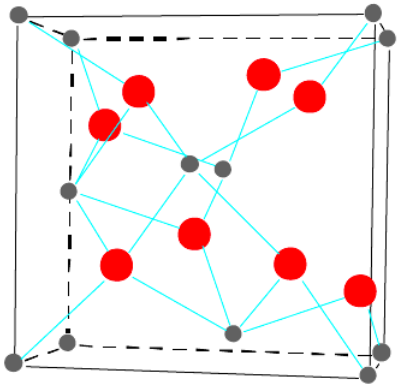

Fig. 3.3: Unit cell of the monoclinic zirconia phase. (Zirconium atoms: small grey dots, Oxygen atoms: big red dots).

The unit cell can be described as a distorted cubic cell, although the structure is significantly more complex than that of the cubic and tetragonal phases. Unlike the

simpler phases, each zirconium atom in the monoclinic structure is coordinated by 7 oxygen atoms, with bond lengths varying from 2.04 - 2.26 Å, and with a range of O-Zr-O bond angles. The oxygen atoms are arranged in two parallel (100) planes, separated by layers of zirconium atoms. The structure is indexed with the space group P_21/c. The unit cell parameters at room temperature vary somewhat during studies.

3.4. META-STABLE ZIRCONIA AND ITS TRANSFORMATIONS

The crystallisation of metastable phases from amorphous materials is not unusual in transition metal oxides, although the mechanisms vary. Well known examples include the crystallization of amorphous titania into the anatase phase, alumina into the γ-Al_2O_3 phase, and yttria into a monoclinic phase [12].

Ruff and Elbert first reported in 1929 that nominally-pure zirconia could exist in the tetragonal phase at room temperature [13] and in the following decades a few other papers were published on the phenomenon [14,15].These papers attributed the appearance of this phase to trapped anions in the crystal lattice. The low-temperature tetragonal phase is generally referred to as 'metastable' (i.e. stabilised by kinetic factors). In 1965, Garvie suggested that differences in the surface energy between the tetragonal and monoclinic phases could cause the tetragonal phase to be thermodynamically stable in very small crystals, [16] and since then many other theories have been suggested, based on various thermodynamic and kinetic arguments. It has been established that the stabilization of the metastable tetragonal phase in nano-crystalline zirconia is the result of the minimization of surface energy [17]. There has been a wide range of suggested mechanisms for the nucleation and stabilization of the tetragonal phase at low temperature, such as lattice defects, non-stoichiometry, structural similarity with the amorphous precursor, retention of various anions or water, strain, surface energy, etc. Over the past 30 years there have been many theories proposed to explain the crystallization and meta-stability of the tetragonal phase, and its eventual transformation to the monoclinic phase. However, none have achieved universal acceptance.

When tetragonal to monoclinic transformation (t$\rightarrow$m) occurs, it is called a Martensitic transformation, and is accompanied by a 3-5 vol% expansion which may result in material fracture [18]. Thus, the need to stabilize higher temperature forms of

zirconia at room temperature arises. It is note worthy that when carbon-free amorphous zirconia-precursors are crystallized in air by heating; the tetragonal phase always forms, regardless of preparation route. However, the chemical conditions under which the precursor material is prepared may affect the crystallization temperature considerably, and this is attributed to primary particle size in the precursor. The metastable tetragonal phase can be held for some hours at any temperature while remaining stable. Some studies have found that transformation occurs slowly during holding at temperatures below 800 °C [19,20] while others reported no transformation over several hours at temperatures above 900 °C [21,22] These different observations are most probably due to differences in preparation and structure of the precursor. The extent and conditions of heat treatment also strongly affect the t→m transformation. A greater maximum heating temperature, and a longer holding time, increased the fraction of material transformed to monoclinic phase. Increasing the rate of cooling delayed the onset temperature of the formation of monoclinic zirconia. By reducing the heat treatment, the onset temperature could be delayed so that the transformation did not go to completion, resulting in mixed phases after cooling [21,22]. The metastable tetragonal phase will partly, or fully, transform to the equilibrium monoclinic phase after heat treatment at 500 – 600 °C or greater. Until relatively recently, all studies of the tetragonal-to-monoclinic (t→m) transformation were carried out after the material had been cooled from heat treatment [23,24,25]. These studies showed that samples contained a small fraction of monoclinic zirconia after heating in air to ~ 500°C, and that the fraction transformed increased with increasing temperature or heating time, up to ~ 900°C, by which point the transformation to monoclinic was complete. Naturally, this data was interpreted assuming that the transformation occurred during heating. Recent in-situ studies have shown that the tetragonal phase is largely stable at high temperature, and that the t→m transformation mainly occurs during cooling from high temperature [21,26]. The temperature at which transformation occurs may be as low as 400°C or less. Much of the previously-gathered data now needs to be reinterpreted in the light of these recent discoveries.

Zirconia is very useful in its 'stabilized' state. If sufficient quantities of the metastable tetragonal phase is present, then an applied stress, magnified by the stress concentration at a crack tip, can cause the tetragonal phase to convert to monoclinic, with

the associated volume expansion. This phase transformation can then put the crack into compression, retarding its growth, and enhancing the fracture toughness. This mechanism is known as transformation toughening, and significantly extends the reliability and lifetime of the products made with stabilized ZrO_2.

3.5. SYNTHESIS METHODS OF ZIRCONIA

Number of methods have been explored to get ZrO_2 powders with high surface area and suitable pore size distribution viz glycol-thermal process, alcohol-thermal-SCFD (supercritical fluid drying) process, CO_2 supercritical drying , sol–gel method , solid-state reaction method etc [19,27,28,29,30,31,32].The most common methods described include the precipitation from soluble inorganic zirconium salts (e.g., zirconium oxy-chloride and zirconium oxy-nitrate) [33-44]. While the synthesis of undoped nanocrystalline t-ZrO_2 has been achieved by using zirconium alkoxides as precursors via sol-gel, solvothermal, and spray pyrolysis methods [45-53]. Recently, much attention was paid to the synthesis of the nano-structured mesoporous oxides with high surface area and uniform pore size distribution using a surfactant-assisted route which is discussed in detail in next section [54,55,56]. Very few papers have dealt with the synthesis of zirconia by using a stronger reducing agent such as sodium boro-hydride [57].

However, most of these synthesis routes to prepare stable high surface area t-ZrO_2 are complicated and require tedious procedures, close control of reaction parameters such as temperature, pressure, pH and the use of relatively expensive raw materials. In this context, simple, easy synthesis routes are highly desired, especially for the practical applications of ZrO_2. Having said that we have selected the most facile synthesis procedures: Precipitation and Sol-Gel, these are discussed below in detail.

Precipitation

Precipitation is one of the most widely employed and easiest methods to obtain single component catalyst or supports. It is obtained by precipitating the hydrous oxide from the aqueous solution of a precursor salt by addition of a base, with subsequent washing, drying and calcination. However, the relative ease of the experimental technique is in strong contrast with the complexity of the involved processes of polymerization, nucleation and growth. Small changes in the conditions (pH, ionic

strength, presence of complexing ions) may strongly affect the rates of growth, the aggregation and re-organization of oxide particles, thus leading to severe changes in the texture and phase composition of the resulting solid. Factors that affect the properties of precipitated catalyst are schematically mentioned in Fig. 3.4.

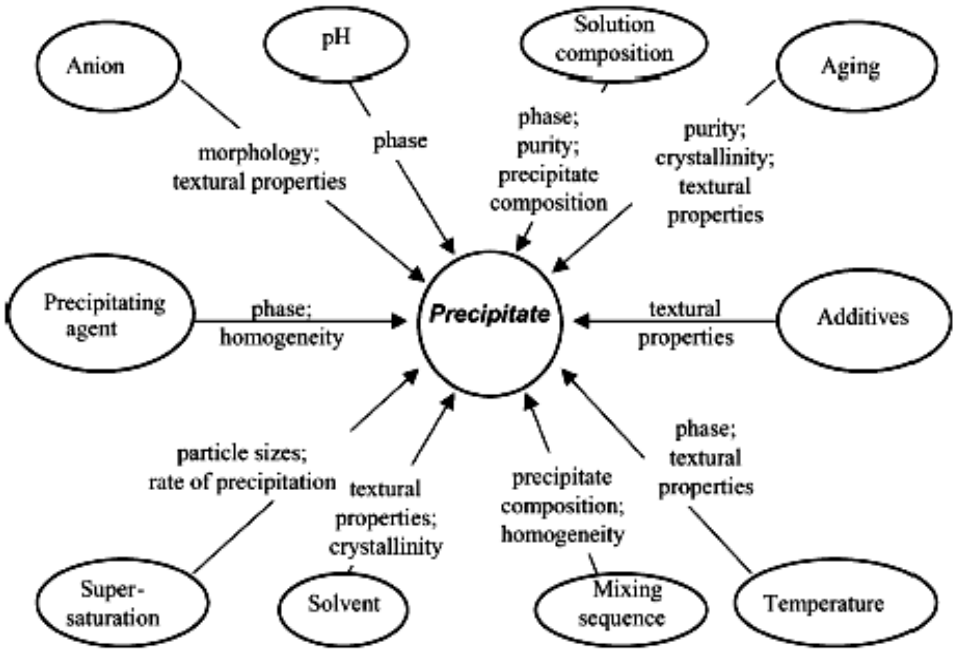

Fig. 3.4: Factors affecting the properties of catalyst or supports prepared by precipitating method.

Thus it can be seen from the above diagram that there are numerous factors that can affect the properties of the precipitate, thus optimizing each parameter is important for preparation of good quality materials.

Sol-Gel

Sol-gel is a chemical synthesis technique for preparing glasses, gels and ceramic powders. A process that has, in the past years, gained much notoriety in the glass and ceramic fields is the sol-gel reaction. This chemistry produces a variety of inorganic networks from silicon or metal alkoxide monomer precursors. Although first discovered in the late 1800s and extensively studied since the early 1930s, a renewed interest surfaced in the early 1970s when monolithic inorganic gels were formed at low temperatures and converted to glasses without a high temperature melting process.

[58,59,60]. Through this process, homogeneous inorganic oxide materials with desirable properties of hardness, optical transparency, chemical durability, tailored porosity, and thermal resistance, can be produced at room temperatures. The specific uses of these sol-gel produced glasses and ceramics are derived from the various material shapes generated in the gel state, i.e., monoliths, films, fibers, and mono-sized powders. Many specific applications include optics, protective and porous films, optical coatings, window insulators, dielectric and electronic coatings, high temperature superconductors, reinforcement fibers, fillers, and catalysts. In the sol-gel process a system of colloidal particles in a solution (sol) becomes a macroscopic material (gel) after gelation of the sol to form a network in a continuous liquid phase. Once the liquid evaporates, a strong glass-like material remains. The basic sol-gel reaction of Zr alkoxide consisting of hydrolysis and condensation steps is illustrated below. The hydrolysis reaction produces the sol, and then, in the condensation reaction, a macroscopic gel is formed.

Hydrolysis: $Zr(OR)_3OR + H_2O \rightarrow Zr(OR)_3OH + ROH$.

Condensation:

$$Zr(OR)_3OH + Zr(OR)_3OR \rightarrow (OR)_3Zr\text{-}O\text{-}Zr(OR)_3 + ROH$$

and

$$Zr(OR)_3OH + Zr(OR)_3OH \rightarrow (OR)_3Zr\text{-}O\text{-}Zr(OR)_3 + H_2O$$

The precursors for synthesizing these colloids consist of a metal or metalloid element surrounded by various reactive ligands. Metal alkoxides are most popular because they react readily with water. However, the characteristics and properties of a particular sol-gel inorganic network are related to a number of factors that affect the rate of hydrolysis and condensation reactions, such as, pH, temperature and time of reaction, reagent concentrations, catalyst nature and concentration, water/alkoxide ratio, aging temperature and time, and drying. All these parameters are interrelated to each other and usually one step affects the next step. Thus, by controlling these factors, it is possible to vary the structure and properties of the sol-gel-derived inorganic network over wide ranges. Though important, the sol-gel synthesis parameters were not thoroughly optimized in this work because of wide variety of fine tunable number of factors affecting the properties of the product, however one sample is prepared via modified sol-gel for comparison.

3.6. MESOPOROUS ZIRCONIA

Many heterogeneous catalysts are less active for fast reactions than the corresponding homogeneous catalysts because the reaction rates are limited by the transport of reactant to the active sites on the particle surface. The rate of a reaction that is limited only by mass transfer is directly proportional to the particle surface area [61]. The best approach to get highly active heterogeneous catalysts is to use porous supports such as mesoporous silica or mesoporous metal oxides. Transition metal oxides are widely used as industrial catalysts and as catalysts supports. Unfortunately they usually have poorly defined pore structures. The synthesis of mesoporous silica partially substituted by zirconium has been attempted to circumvent the difficulty of preparing stable mesoporous zirconia. Zirconium oxide is of particular interest because it is stable under oxidizing and reducing atmosphere and possesses both acid and base properties. The acid site (Zr^{4+}) and base site (O^{2-}) present in ZrO_2 are very weak [62]. In solution, acidic and basic sites are neutralized immediately; however, they may exist independently at the surface. Thus acidic and basic sites on the surface of oxides work both independently and cooperatively and hence ZrO_2 act as an acid-base bifunctional oxide and hence show acid-base bi-functional catalysis. The existence of both acidic and basic properties is evidenced by the adsorption of CO_2 and NH_3 [63]. These are critical for some reactions that need bifunctional catalysts. The search for zirconium oxide as supports for various catalysts has received keen interest in the past decade. Porous zirconia is attracting increasing interest on account of its use as a catalyst support or membrane partially because it is chemically more stable. Therefore zirconium is chosen as the metal species and also for the reason that it has only one stable oxidation state and exhibit pronounced polyoxo ion chemistry in aqueous solutions [64]. Usually mesoporous metal oxides are prepared through a template-assisted mechanism. After the formation of pore structure, the template will be removed by extraction or calcination at 550 °C. If the calcination temperature is above 600 °C the porous structure collapses and zirconia starts to transform from the metastable tetragonal phase to the stable monoclinic phase with increasing temperature. This phase transformation is accompanied by a dramatic change in pore structure of zirconia. Great efforts have been made to prepare

mesoporous zirconium oxide with high surface area via a surfactant templating route due its complexity in achieving high surface area porous structure with suitable stability.

The discovery of silica-based mesoporous materials raised an enormous interest in catalysis because of the possibility to extent the concept of shape selectivity to large molecules [65,66]. Soon after the discovery of the MCM materials, various researchers put forward an idea of non-silica-based mesoporous oxides. Titanium [67,68], zirconium [69-82], niobium [83], tantalum [84], aluminum [85], hafnium [86], tin [87], and manganese [88] have been synthesized using ionic or neutral templates as structure directing agents, although most of them were comprised of mainly non-porous framework walls, which would limit their thermal and hydrothermal stability and greatly compromise their usefulness in catalytic application. Stucky et al. then synthesized mesoporous metal oxides with a semi crystalline framework by block copolymer templating materials [89]. Hudson and Knowels [69], first achieved the synthesis of zirconium-based mesoporous materials by cationic surfactant adopting the scaffolding mechanism, where the preparation of mesoporous zirconium (IV) oxide samples was obtained by surfactant exchanged hydrous zirconium oxide. The proposed scaffolding mechanism by the authors is given in Scheme 3.1.

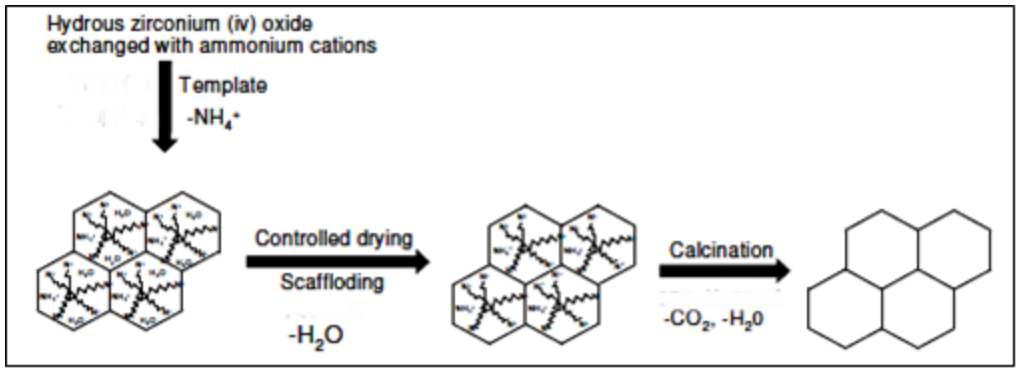

Scheme 3.1: Synthesis of mesoporous zirconia using zirconium (IV) oxide with cationic surfactant via scaffolding mechanism [69].

Ciesla et al. [71,72] studied the formation of porous zirconium oxo-phosphate by a surfactant assisted synthesis, where they used two different syntheses leading to zirconia compounds with high surface areas and regular pore systems, in which either zirconium sulfate or zirconium propoxide is used as zirconia source with cationic surfactant to obtain sulfate containing material. Blin et al. [72] synthesized the mesoporous zirconia

using cationic surfactant with zirconyl chloride as zirconia source and studied the kinetics of synthesis mechanism. They postulated a scaffolding mechanism with zirconia, where only a few detergent molecules formed a loose scaffold that kept the pores from collapse. This mechanism differs from the micelle templating mechanism that is prevalent in the silica system. Unlike the well-ordered templated material, the scaffolded material is disordered and porous with no relationship between the d-spacing and the chain length of alkyl trimethyl ammonium bromide surfactants. Ordering in the scaffolded material only develops during calcination. Further heating to 700–800 ^{o}C resulted in a collapse of the porous structure and the material converted to dense zirconia in the tetragonal form. The scaffolding mechanism was also postulated for mesoporous zirconia formed by slow hydrolysis of zirconium propoxide in the presence of anionic surfactants-doceyl phosphate, [90]. The question how ZrO_2/surfactant mesophase nucleate was addressed by Ne´ et al. [91]. They used in-situ time resolved small angle scattering of X-rays and neutrons with CTMABr as template. Ulagappan et al. [73] reported the preparation of lamellar and hexagonal forms of mesoporous zirconia by the neutral amine route. They further reported that the lamellar form of mesoporous zirconia turned in to hexagonal form upon removal of template. Antonelli [92] reported the synthesis and mechanistic studies of sulfated mesoporous zirconia with chelating carboxylate surfactants where he used long chain acid as surfactant (Scheme 3.2).

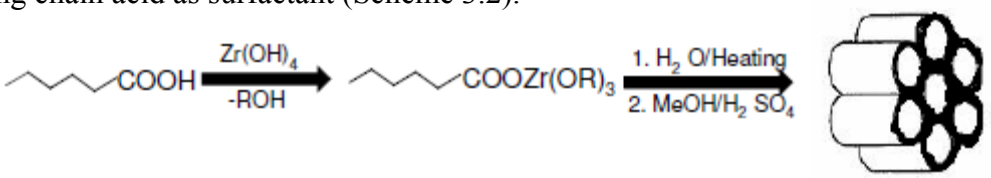

Scheme 3.2: Synthetic strategy for mesoporous ZrO_2. In the first step the metal alkoxide is combined with the carboxylic acid prior to addition of water. After addition of water and aging from ambient to 150 °C over several days the meso-structure is obtained. [92].

Reddy and Sayari [75] studied the formation of nanoporous zirconium oxide using cationic template at acidic pH via supramolecular templating approach. Zhao et al. [76] reported metal doped mesoporous zirconia using anionic surfactants with various Al/Zr ratios. Pacheco et al. [77] studied the formation of mesoporous zirconia from anionic and neutral surfactants. Wong and Ying [78] reported the extensive study of mesostructured zirconium oxide via amphiphilic templating mechanism with a variety of headgroups

(anionic and nonionic) and tail group chain lengths (1-18 carbons). They further proposed two types of interaction between the surfactants and zirconium source (Scheme 3.3).

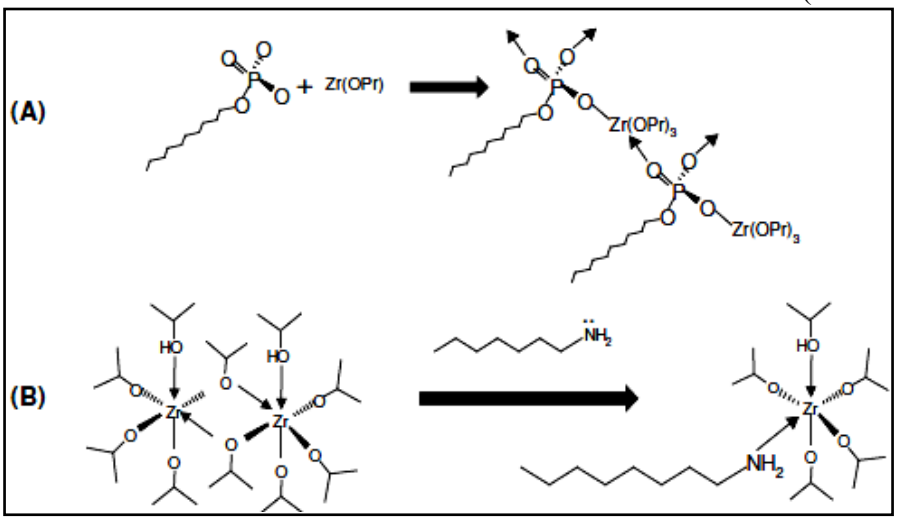

Scheme 3.3: Representative schematic drawings of **(A)** the anionic amphiphile zirconium n-propoxide interaction, and **(B)** the nonionic amphiphile-zirconium isopropoxide interaction [78].

Parvulescu et al. studied extensively the synthesis of mesoporous zirconium oxide using cationic surfactant and claimed that the synthesis occurred via a scaffolding mechanism [94]. The possibility of obtaining such material with a mesoporous texture has made this oxide even more interesting.

3.7. STABILIZATION OF ZIRCONIA

3.7.1. Influence of the starting precursor

The name zirconium comes from the Persian word *zargun*, which means gold-like metal. Zirconium is able to form compounds with 1, 2, 3 or 4 valences. Oxidation states lower than 4 are difficult to find. Zirconium compounds commonly exhibit coordination numbers of 4, 6, 7 and 8, with tetrahedral, octahedral, pentagonal bi-pyramidal and dodecahedral forms respectively. Aqueous solution chemistry is dominated by hydrolysis and the presence of polymeric species. These species are sensitive to their environment and their equilibrium is established slowly, making study results difficult to obtain. The practical effect of this is that it is difficult to control the production of zirconium chemicals with consistent properties. It was noted earlier that the influence of the precursor is so strong that a precursor obtained from the same supplier at different times

may produce significantly different tetragonal over monoclinic (t/m) ratios [95]. The reason is seemingly the presence of polymeric zirconium cations in the crystalline salts, which persist in the solutions. The degree of polymerization can vary widely, with the composition of the salt, especially for the commercial oxy-nitrate. The properties of the precipitate are also strongly affected by the nature of the anions present in the solution because the equilibria of complexation and hydrolysis determine the rates of polymerization of zirconium species [96]. Zirconium oxy-nitrate obtained from Aldrich gave a turbid aqueous solution at its own pH, probably because of the presence of large polymeric species. The nitrate anion presents no complexing properties to Zr(IV) polycations at any reasonable pH [97]. Therefore rapid nucleation and growth occurred, leading to a dense microporous precipitate. Zirconium oxy-chloride solutions at gradually increasing pH undergo complex transformations of polymeric species, beginning from the tetramer initially present in the crystalline $ZrOCl_2.8H_2O$ [98], to octamers [99] and finally tridimensional agglomerates [100]. It has be stated that the anion of the precursor salt should not be too complexing (*sulfate anion has strong complexing properties in a wide range of pH, so that upon pH increase, the precipitation of different basic sulfates might occur*) that it then remains in the precipitate, neither too weakly complexing that rapid uncontrollable hydrolysis of Zr(IV) species occurs just upon dissolution in water. Chloride ion seems to provide an optimum of the complexing properties [101]. Lastly preparation of pure ZrO_2 under identical synthesis conditions using zirconium oxy-nitrate and zirconium nitrate precursors didn't have a much effect on the specific surface area and other physiochemical properties [102].

3.7.2. Concentration of initial salt solution

The concentration of the zirconyl salt solution was found to affect the surface area. Smaller crystallites were formed from the more dilute solutions, resulting in material with higher surface area even after calcination [6,103].

3.7.3. Effect of addition of anionic, cationic or neutral surfactants

The addition of anionic, cationic or neutral surfactants in the suspensions of aqueous zirconium hydroxides have been successfully used to control its agglomeration [104]. Mesoporous zirconia was obtained recently [54,69,105,106] using tetra-alky-

ammonium templates, by analogy with the silica "MCM" syntheses. It was claimed that the scaffolding and decreasing surface tension by large organic ions is crucial for the texture improvement. The first unambiguous synthesis of a MCM-41 type zirconia analogue was presented by Ciesla et al. in 1999 [71]. XRD and electron micrographs confirmed the hexagonal MCM-41 structure. These authors used quarternary ammonium surfactants with different chain length. V.I. Parvulescu et. al. have done vast amount of studies on mesoporous zirconia using tetra-alky-ammonium templates [108]. Recently non-siliceous ordered zirconium mesoporous materials having high surface area ~150 m^2/g were obtained after calcination at 400 ^oC using zirconium alkoxide and/or zirconium tetrachloride in non-aqueous medium with the help of Pluronic P123, with relatively thick amorphous walls via sol-gel technique [89,109]. Nonionic alkyl poly(oxyethylene) surfactants and poly(oxyalkylene) block copolymers are important families of surfactants that are widely used in emulsifying, defoaming/antifoaming, coating, thickening, solubilizing, cleaning, lubricating, wetting, pharmaceutical, coal and petrochemical industries, and household applications [110,111,112]. They display excellent interfacial stabilization properties and are low-cost, nontoxic, and biodegradable. In composite materials synthesis, nonionic block copolymers are an interesting class of structure-directing agents whose self assembly characteristics lead to kinetically quenched structures. Block copolymers have the advantage that their ordering properties can be continuously tuned by adjusting solvent composition, molecular weight, or copolymer architecture. Moreover, they permit solution organization of larger structural features than is possible with low-molecular-weight surfactants. Several authors have therefore preferred and successfully prepared high surface area mesoporous metal oxides using of nonionic block copolymers [89,109]. It is worth mentioning that the preparations used in the some of the cited works include reflux of the precipitates in supernatant solutions having high values of pH for extended times for attaining high surface area and thermal stability. However, after calcining at high temperatures, the ordered structures collapsed, resulting in the dense material containing wormhole-like pores with reduced surface area and tetragonal phase. Structural collapse on removing of the pore-filling micelle formers from the precursor material was also reported by Ciesla et al. [70].

3.7.4. Influence of the precipitation pH

The pH of the solution of the precursor has a marked influence on the phase formed as well as on the crystallite growth in ZrO2 precipitates [113]. The control of the pH of the liquid in contact with hydrous zirconia precipitate was used to prepare either tetragonal or monoclinic phases of zirconia [20]. Differences in the solubility of hydrous zirconia at different pH was put forth to explain the formation of different crystallite phases. At low pH, the solubility is high and the amorphous hydrous zirconia undergoes dissolution-precipitation to form the monoclinic phase. At intermediate pH of 4–6 where the hydrous zirconia has low solubility, the phase changes from amorphous to tetragonal to monoclinic with extended refluxing or hydrothermal treatment. With increase of pH from 6 to 14, the solubility of hydrous zirconia increases but in situ crystallization of hydrous zirconia to the tetragonal form predominates over production of the monoclinic form, so that at the highest pH of 14, only the tetragonal phase is formed. The textural properties of the hydrated zirconias prepared at pH values 3, 6, 10 and 12 are significantly different but no stabilisation of any pure phases was there. The solids prepared at a strongly basic pH i.e. in a large excess of ammonia showed better properties. A thorough washing of precipitates with NH_4NO_3 solution followed by treatment with boiling distilled water in a Soxhlet apparatus decreased the difference between the samples prepared at low and high pH, and therefore substantially decreases the "influence of precipitation pH" on the properties of the oxide.

The crystallization of zirconia from hydrous zirconia involves three stages [114]: (a) loss of loosely bound water and terminal hydroxo groups (b) oxolation of hydroxyl bridges to from embroyonic oxide nuclei and lastly (c) the growth of the nuclei to crystallites. Mamott et al. [115] used dynamic diffraction technique to show that the pH of the liquid in contact with the hydrous oxide affects the temperature and rate at which the amorphous precursor transforms to crystalline zirconia. A higher pH of preparation also lowered the transformation temperature for the metastable tetragonal to monoclinic phase. The authors proposed that at a higher pH, the polymerization rate of the tetrameric units increases, and although the resulting material is amorphous, numerous units of two- or three-dimensional ordered assemblages are present. These can act as nuclei for crystallization of zirconia.

3.7.5. Rate and sequence of addition of precipitation agent

Srinivasan et al. [35] reported that in addition to the pH, the time taken to reach the final pH of the mother liquor containing the precipitate determines the crystal structure of the zirconia. Rapid precipitation in the pH range of 7–11 results in the monoclinic zirconia while the tetragonal phase was observed for precipitates formed under slow conditions. At high pH of 13, only the tetragonal phase was formed, irrespective of the rate of precipitation. A mechanism involving the incorporation of hydroxyl ions into polyzirconium species was proposed to explain the difference in crystal structure. With rapid precipitation, the penetration of hydroxyl ions into the polyzirconium species is slow while a slow rise in pH allows hydrolysis reaction to occur so that the polyzirconium species have a lower valency. These different species in turn determine the zirconia crystal structure. The X-ray powder patterns showed that hydrous zirconia with monoclinic or tetragonal structure had almost similar d-spacings as the calcined oxides, thus suggesting that the bulk of the solid is zirconia and only the surface layers contain hydroxyl groups and water [116]. However, some authors stated [35,117] that instantaneous mixing of solutions always gave somewhat superior textural properties compared to slow drop wise addition. Data on the influence of the mixing rate are not given since it seems to be a less reproducible.

3.7.6. Aging of the precipitate in the mother liquor

Aging of the precipitate in the mother liquor or ethanol produced further precipitation of fine particles and a corresponding higher surface area was noted as compared to the un-aged sample. Aging in the suspension may also lead to various modifications of the resultant precipitate such as change in particle size and morphology or even cause the crystallization of amorphous particles [118]. Rinsing with ammonium hydroxide instead of water was also helpful in attaining a higher surface area [119]. An additional stabilization of the nano-structured t-ZrO_2 can be achieved by preferential erosion of the high energy facets, upon prolonged digestion of the precipitate. Digestion in a strongly basic medium by preferential erosion of high energy planes should, therefore, lead to restructuring of the morphology of zirconia particles. In addition, a sequence of crystallization-dissolution processes, occurring during aging, gives rise to

reticulation of the hydrous zirconia precipitate via deoxolation, constituting an apposite proto-structure for direct crystallization into the t-ZrO_2 polymorph. Another beneficial effect of aging is the stiffening of the hydrated gel, which inhibits the extent of shrinkage that takes place during drying and subsequent calcination.

3.7.7. Influence of digestion

Freshly precipitated or aged (at room temperature) hydrous zirconia consists of a loose agglomeration of primary particles. In alkaline solution, these particles are negatively charged and repel each other. During digestion, the higher temperature leads to increased thermal agitation. Collisions between the charged particles occur at a higher rate than at room temperature. This enhances the formation of surface bonds between particles by condensation of surface hydroxyl groups. Thereby, a network of particles with higher porosity than in the undigested sample forms. In addition to the network formation by coalescence of primary particles, another effect of the higher temperature is the dissolution and re-precipitation of material which helps in strengthening the network of particles. It is then possible to remove the water from the pores without collapse of the network structure. Undigested samples do not form a stabilized network because of electrostatic repulsion between the charged particles. Hence, it can be envisaged that during drying, the coagulated particles collapse and form a dense structure. Previous results indicate that the dissolution/redeposition is enhanced at pH ~14 as compared to pH 9. This is in agreement with the thermodynamic calculations of Denkewicz et al. [120]. who showed that the solubility of zirconium hydroxide at pH 9 is smaller than at pH 14 by a factor of 10^4. However, the trend is that the longer-digested samples are better able to withstand higher temperatures. It is assumed that, this may be the result of greater crystalline perfection in these samples. The most frequently occurring type of defects in zirconia is Schottky defects consisting of pairs of cation and anion vacancies [121]. A more defect-free structure is expected as digestion progresses. Diffusional mass transport got reduced in the longer-digested samples so that nucleation and grain growth are hindered. The influence of digestion is interpreted in terms of the enhanced agglomeration of primary particles during digestion and the strengthening of the network structure which is then better able to withstand thermal treatment. While it is impossible

to achieve a surface area (100 m^2/g for pure zirconia without silica doping, digestion still has a beneficial effect in enhancing the surface area). Aguila et al. [122] observed that refluxing of hydrous zirconia in ammonium hydroxide led to an increase in the surface area of the zirconia obtained after subsequent calcination at 700 ^oC for 3 h. The reflux times of 3 to 9 h, the Si concentration in the samples is below detection limits. The effect of digestion on hydrous zirconia has been postulated to be as follows [40]. The initially precipitated hydrous zirconia undergoes dissolution and re-precipitation during digestion so that the network of primary particles is strengthened. This allows a porous network to be formed which can withstand collapse during drying and calcination. Greater crystalline perfection also occurs from Ostwald ripening and annealing in the samples so that mass transport leading to nucleation and grain growth is hindered during the transformation to zirconia.

3.7.8. Effect of crystallite size

Besides the attribution to dopants or impurities in the formation of the metastable tetragonal zirconia, a crystallite size effect has also been put forth by Garvie [16]. Garvie developed the following equation for critical grain size in pure unconstrained ZrO_2 based on surface free energy considerations as given below. On the basis of the lower value of the surface energy t-phase (γt) in relation to m-phase (γm), Garvie considers that in order to stabilize t-phase at low temperature the following equation must be satisfied: $(G_t - G_m) + S_{t\gamma t} - S_{m\gamma m} \leq 0$, Where G is the molar free energy and S is the surface area in the single crystal particle. It was determined that particle size for stabilizing t-phase must be $\leq$ 30 nm. The surface energy theory proposed by Garvie is that crystal surface area determines the relative stability of the tetragonal and monoclinic phases. This is generally expressed as a 'critical crystal/particle size', and there has been considerable interest in the measurement of 'crystal size' in order to evaluate the theory. However, most studies have used diffraction to measure the average diffracting crystal size, which is not necessarily a reliable measure of crystal surface area, and the evidence remains inconclusive. It is suggested that domain boundaries inhibit t→m transition; existence of an active nucleation site and mobility of grain boundaries can be strongly reduced by pores, dopants and particles of a second phase. The most stable polymorphic phase is the one

that has the lowest free energy under given conditions (composition, temperature and pressure). Other researchers have investigated strain in the crystals. One study has shown that stress is relieved during the transformation, and may be a driving force [25]. Another study shows that the t→m transformation appears to take place when strain generated by realignment of crystals during heating exceeds ~ 2 % [24]. These studies are important, as it is well known that stress can influence martensitic transformations.

3.7.9. Effect of calcination temperature and time

Calcination of zirconium hydroxide precipitate to form ZrO_2 can be described by the equation: $ZrO(OH)_2 \cdot H_2O \rightarrow ZrO_2 + 2H_2O$ or $Zr(OH)_4 \cdot H_2O \rightarrow ZrO_2 + 3H_2O$. Carter et al. [123] has shown that the hydrous zirconia produced at acidic pH~3 is best formulated as $Zr[OH]_4$, whereas at basic pH~12 the product is more consistent with $ZrO(OH)_2$. The different observed transformation behaviors may be due to the differences in the structures. Murase and Garacia suggest that the presence of water/moisture during drying, calcination and other processing steps [23,124,125] reduces the amount of tetragonal zirconia present. Duchet et al. [126] reported that surface area of 126 m^2/g for zirconia formed after calcination of the hydrous zirconia for 2 h at 500 ^oC. This decreased to 60 m^2/g after a further treatment at 700 ^oC. It can therefore be concluded that a calcination time of 10-12 h and absence of water during calcination process is necessary to obtain a stable surface area with more % of tetragonal zirconia. Where shorter calcination times had been employed, the reported surface area is probably an upper limit, and may not be stable under reaction conditions.

3.7.10. Effect of synthesis method (Sol-Gel)

Research has also been carried out with the use of sol–gel synthesis methods to obtain high surface area zirconia [58,117,127]. The hydrolysis of zirconium alkoxides differs from silicon, aluminum or titanium alkoxides as oxo and aqua groups are formed rather than true hydroxides [128]. The sol–gel process is usually chosen to obtain a gel privileging with maximum association of Zr-O-Zr. The overall hydrolysis and condensation reactions are already shown in previous section of sol-gel / synthesis methods. The relative rates of hydrolysis and condensation depend on pH, temperature, nature of the alkoxide and the water/alkoxide ratio. In water, zirconium alkoxides

undergo rapid hydrolysis and condensation, so that in the absence of acid a precipitate forms readily. The resulting gel is weakly cross-linked, and a low surface area oxide forms on calcination. At lower pH, the protonated species $(RO)_3Zr–OH_2^+$ predominates. The electrostatic repulsion reduces the rate of condensation relative to that of hydrolysis. This allows branching to occur, producing a strongly cross-linked gel, which during calcination transforms to zirconia with high surface area and a large pore volume. However, with high acid concentration, condensation is so severely hindered that only a weakly branched network can form. This gel shows poor stability and collapses to a low surface area material upon calcination. Yoldas [129] found that the particle size and morphology of the resultant zirconia was also affected by these parameters. In addition, use of a longer alkyl group in the alkoxide led to a coarser texture of the final zirconia. Although the nature of the acid used, e.g., acetic or nitric acid, appears to have very little effect on the morphology of the resulting zirconia [130], the acid concentration does affect the transparency and bounce of the gel [131,132]. At low acid concentration, an opaque precipitate is formed but with increasing acid concentration, the gel formed is translucent containing precipitates within the gel network and, finally, a transparent polymeric gel with good bounce is obtained. It is postulated that the transparent gel has a rigid porous framework so that after calcination at 500 ^oC for 2 h, the resulting zirconia had a surface area of 100 m^2/g. The acid concentration also affects the average pore size: at high acid concentration, a lower degree of cross-linking is present in the gel, and consequently, smaller pores are formed. Aging the gels led to a narrower distribution without affecting the pore volume. Additionally, aged samples had higher surface areas than un-aged ones [29]. For example, aerogels aged for 2 and 47 days at room temperature formed zirconia with surface areas of 114 and 136 m^2/g respectively after calcination. Aging at elevated temperatures led to similar results as those obtained at room temperature. The nature of the solvent can influence the molecular structure of the zirconium alkoxide and in turn affect the rate of hydrolysis and condensation. Highest surface area was obtained when ethanol was used as the solvent while propanol, butanol and tert-amyl-alcohol resulted in lower surface area. Aerogels are typically dried by supercritical drying to retain its pore structure and high surface area since calcination at

higher temperature leads to loss in surface area which can be largely attributed to pore collapse as a result of the high surface tension of pore water.

3.8. RESULT AND DISCUSSION

3.8.1. Synthesis of Catalysts

3.8.1.1. Literature review

An exhaustive literature search on zirconia based materials was carried out to collect all the relevant information on synthesis method, characterization technique and catalytic applications. More emphasis was given on synthesis methodologies for the preparation of high surface area pure tetragonal zirconia and zirconia based materials containing group VI elements like W and Mo. A brief review of the various strategies which have been employed to prepare high surface area zirconia has been given.

1. A. Shrivastava et. al. [133] prepared zirconium citrate using zirconium oxy-chloride and citric acid. **The XRD studies showed that powder prepared by this method is tetragonal up to the temperature 600 °C after which it progressively transforms to monoclinic.** Beyond the temperature 800 °C the phase is completely monoclinic.

2. R. Ramamoorthy et. al. [134] **observed that tetragonal phase stabilization and the associated phase transformations processes seem to depend on the grain size to a certain extent and more dependent on the chemical composition of the powders**. The nano crystalline ZrO_2 powder was prepared by the method of hydrolysis of zirconium oxy-chloride and neutralizing it with ammonia solution.

3. G.K. Chuah et. al. [40,135] prepared high-surface-area zirconia by digestion of hydrous oxide precipitated with ammonia and sodium hydroxide. **Zirconia formed using sodium hydroxide has the highest surface area after 24 h of digestion; a longer digestion time leads to a decrease in surface area**. **In contrast, the surface area of zirconia formed by precipitation with ammonia increases with digestion time**. **The acid strength of the digested samples was higher than that of undigested samples. This is attributed to the smaller crystallite size, which results in a larger number of highly uncoordinated zirconium ions**. **The use of sodium hydroxide as a precipitant results in the adsorption of sodium ions at the surface regions of zirconia, which reduces the acidity**. Hydrous oxides digested at pH 9 are less thermally stable than those digested at pH 14.

4. J.A Wang et. al. [30] made a **comparative study of zirconia powders synthesized by sol-gel and precipitation technique**. For the powder prepared by **precipitation technique the crystallization temperature is 470 °C shown by**

DTA. An additional phase also exists with zirconia at that temperature. Based on the XRD analysis, they ascribed this phase to a quasi-amorphous tetragonal produced in the decomposition process of zirconium hydroxide **whereas in sol gel method ZrO_2 crystallization occurs around the temperature 650 °C**.

5. B. Ksapabutr et. al. [136] prepared **zirconia powders by sol gel method using sodium glycol-zirconate complex**. The resulting zirconia was characterized using XRD, based on which it is reported that the first crystalline structure developed from the amorphous phase was the tetragonal, which was formed between the temperatures 500 °C and 800 °C.

6. B. Tyagi et. al. [137] prepared zirconia having predominantly tetragonal crystalline phase by sol-gel method as well as conventional precipitation techniques from zirconium hydroxide obtained by the hydrolysis of both zirconium propoxide and zirconium oxy-chloride precursors. Both the techniques result in nano-crystalline zirconia; however, **the sol-gel technique is advantageous particularly to prepare stabilized nano-crystalline tetragonal zirconia**. **Thermal drying of zirconium hydroxide gel in an oven (Temp. - 110 °C, Time - 12 h) results in lower crystallite size (11-13 nm) as compared to drying under vacuum (50 mbar, Temp. - 70 °C), which results in higher crystallite size (20-21 nm) in both sol-gel and conventional precipitation synthesis**.

7. M Rezaei et. al. [103] produced nano crystalline zirconia powder with high surface area, pure tetragonal phase and mesoporous structure by a surfactant-assisted route in which the precursor solution was zirconium oxy-nitrate to which ammonia solution was added drop wise. The zirconium to surfactant molar ratio, pH of precipitation, aging time and zirconium molarity were optimized. **The sample prepared under optimized conditions (surfactant to zirconium molar ratio 0.03, pH 11, aging time 24 h and Zr molarity 0.001460) showed a high surface area of 129 m^2/g, pure tetragonal crystallite phase and a mesoporous structure after calcination at temperature 700 °C for 5 hrs**. **The obtained results also indicated that the surface area was decreased by increasing the molar ratio of surfactant to zirconium more than 0.03**. The XRD results of the samples calcined at temperature 600 °C for 5 hrs showed a pure tetragonal crystallite phase, except for the sample prepared without the addition of surfactant.

8. S.G. Liu et. al. [54] synthesized mesoporous zirconia with ultra high thermal stability via a controllable and facile sol–gel approach using Pluronic P-123 and zirconium propoxide as starting materials. It is found that the strong alkaline solution of NaOH or KOH, post-treatment exerted a critical influence on improving the thermal stability of the product. **Even after calcination at the temperature 700 °C for 4 h, the mesopore system was fairly preserved in the post-treated product and the sample exhibited a high specific area.** Whereas for samples without any post-treatment, its pore walls totally collapsed during

calcinations above the temperature 400 °C, and the specific area decreased drastically. Therefore, NaOH or KOH post-treatment seemed to be more effective than ammonia post-treatment in promoting the thermal stability of mesoporous zirconia in this process.

9. M. Tahmasebpour et. al. [138] produced pure monoclinic zirconia via a simple, fast and low cost method: poly acryl amide gel method. Also, the effect of initial salt precursor on thermal behavior of gel network and structure of the synthesized nano particles was studied TG-DTA, XRD and TEM analysis. The XRD pattern of the products calcined at the temperature 400 °C contains only tetragonal phase. As the calcination temperature increases to 600 °C, both monoclinic and tetragonal phases are detected. Further increasing of the temperature, causes an increase in the proportion of monoclinic phase and at temperature 800 °C the transformation to monoclinic phase is completed. **The XRD results showed that the presence of nitrate ions not only retarded the crystallization, but also delayed the tetragonal to monoclinic phase transformation of zirconia nano particles which resulted in smaller particle sizes in comparison with the chloride samples**. However, TG-DTA analysis confirmed accelerator role of nitrate ions on degradation of polymeric network. Therefore, the presence of nitrate ions affects the synthesized nano particle size via two different mechanisms: the retarded crystallization and polymeric network degradation. But, TEM images revealed that the controlling mechanism is the former.

10. M.M. Rashad et. al. [139] prepared ZrO_2 nano powders via three processing routes: precipitation, citrate gel combustion and micro emulsion refined precipitation. The change in processing routes at different thermally treated temperatures led to the change of crystalline phases and properties of the produced ZrO_2 nano powders. Precursors derived from these three processing routes exhibited very different formation temperature for ZrO_2 phases. **Directly precipitated precursor and the citrate ZrO_2 precursor gave tetragonal ZrO_2 phases at the temperature 700 °**C which inverted to monoclinic ZrO_2 phase at higher temperatures. On the other hand, micro emulsion refined precipitation technique gave tetragonal ZrO_2 phase at the temperature 500–700 °C and cubic ZrO_2 phase at 1000–1200 °C. Amorphous ZrO_2 was converted to tetragonal phase at low temperatures for all synthesis techniques and the tetragonal phase is transformed to cubic or monoclinic phase by increasing the temperature, depending on the particular kinetic conditions and chemical environments. It is reported that the **morphology of zirconia particles was affected by synthesis routes and thermally treated temperature.**

11. B.B. Nayak et. al. [140] synthesized ZrO_2 nano-particles by chemical reduction of zirconium salt in an aqueous medium with sodium boro-hydride ($NaBH_4$) as a reducing agent, at two different pH of 3.0 and 8.7. **Pure t-ZrO_2 nano-particles with crystallite size as small as 7 to 8 nm resulted on heating the amorphous as-prepared precursor powders at the temperature 600 °C.** The tetragonal to monoclinic phase transformation occurred at the temperature 800°C as the

crystallite size increases to 30 nm. **This is a novel technique for stabilizing the t-phase of ZrO_2 at moderate temperature for different applications**.

12. Ciesla et. al. / J. Hudson et. al. and G. Stucky et. al. [69,71,105] have obtained high surface area zirconia from a large number of preparation routes**. The use of surfactants-anionic, cationic, non-ionic and zwitter ionic in acidic as well as basic medium has resulted in well-ordered porous materials with a narrow pore size distribution**. However, it is reported that after calcination at higher temperatures above 500 ^oC the ordered structures collapsed.

13. P. Yang et. al. / B. Tian et. al. [89,109] have prepared non-siliceous ordered zirconium mesoporous materials having high **surface area ~150 m^2/g using zirconium alkoxide and/or zirconium tetrachloride in non-aqueous medium with the help of Pluronic P123 surfactant**, with relatively thick amorphous walls via sol-gel technique.

14. Cao et. al. [141] **synthesized ZrO_2 having a surface area of 462 m^2/g as prepared, 270 m^2/g surface area at 400 ^oC temperature and 206 m^2/g surface area after calcination at the temperature 500 ^oC**. They used a combined alcothermal and super-critical fluid drying technique to prepare the zirconia sample. It was reported that the sample was a grey in color instead of white, most probably due to the presence of carbon.

15. Cassiers et. al. [142] **used dodecylamine and N, N-dimethyl dodecylamine as a templating agent and zirconium propoxide as a zirconium source**. They used an evaporation induced self-assembly technique followed by digestion in an ammonia solution and obtained a maximum surface area of 438 m^2/g and 153 m^2/g after calcination at 300 ^oC and 700 ^oC temperature respectively.

16. N.L. Wu et. al. [143] synthesized tetragonal ZrO_2 nano-crystallites with or without yttria via a precipitation process in which the hydrous oxide precipitate reacts with hexamythyl disilazane vapour before calcinations. **The nano-crystallites are formed and retain a tetragonal structure after calcinations at high temperatures. The enhanced structural stability has been attributed to the combined effect of suppressed grain growth and reduced surface energy.**

17. J. Liang et. al. [144] **synthesized pure ZrO_2 via sonochemical method, which is a simple and energy efficient way to synthesize inorganic materials**.

18. H. Zhu et. al. [145] **worked on the synthesis of tetragonal zirconia with diameter of 5nm by hydrothermal process of hydrazine hydrate**. Structural characterization of the ZrO_2 products using X-ray diffraction and Raman spectroscopy revealed that the predominant crystal phase was the tetragonal phase. High resolution transmission electron microscopy images further showed that the diameter of the majority of the tetragonal ZrO_2 was < 5nm. **The**

mechanism of hydrothermal process and the critical roles of hydrazine hydrate in the hydrothermal formation of the small-sized ZrO_2 have been discussed.

19. R. Srinivasan et. al. [146] studies was undertaken to examine the crystallite size effect on the low-temperature transformation of tetragonal zirconia. Zirconia was prepared by precipitation from a solution of zirconium tetrachloride by adding ammonium hydroxide. Portions of the sample, after drying, were calcined at 500 ^{o}C for various time intervals. Phase transformation was followed by X-ray diffraction, the data shows that the tetragonal phase was initially formed and it was transformed to the monoclinic phase at longer periods of calcinations. **TEM and XRD results showed that the transformation does not appear to be due to a critical particle size effect**.

20. F.J. Berry et. al. [147] studied the influence of the pH of the reaction mixture on the nature of zirconia formed from zirconium (IV) acetate solution processed either by boiling under reflux or by hydrothermal methods. The resulting gels and powders were calcined in air at various temperatures and characterized by XRD and **Raman Spectroscopy. The latter technique was found to be superior in differentiating tetragonal and cubic zirconia. Zirconia formed from solutions at high pH was found to contain a greater quantity of the tetragonal polymorph, suggesting that the addition of alkali to the solution tends to stabilize the tetragonal form against the conversion to the monoclinic form**. The high pressure associated with the hydrothermal treatment is important for the direct formation of monoclinic zirconia under acidic condition.

21. R. D. Carter et. al. [123] studied the effect of pH of precipitation, starting solution concentration, and agitation levels on the particle size of hydrous zirconia precipitates. It was found that all three variables affect the particle size of the hydrous zirconia. **The smallest particle size is produced by a 0.81 M starting solution, precipitated at pH 12 with a high agitation level**. The pH of precipitation was also found to have a significant impact on the type of hydrous zirconia produced. TG-DTA, micro-combustion and TEM-EDX were used to investigate the difference in the powders produced at pH 3 and 12. This study suggests that powders produced at pH 3 will have a structure similar to $Zr[OH]_4$ whilst those prepared at pH 12 are more likely $ZrO[OH]_2$. **XRD and micro-combustion results suggest that the powders produced at pH 3 retained ammonium chloride whilst those produced at pH 12 did not**. The filtration rates for the pH 3 products were significantly faster than that of the powders made at pH 12 which are significant in the industrial production of these materials.

3.8.1.2. Summary of literature review

There are several more reports which have contradicting results and have been omitted to avoid confusion. From the above literature survey it is observed that high

surface area tetragonal zirconia can be obtained from a large number of preparation routes. A summary of common conclusions are as follows.

- High-surface-area and thermally stable tetragonal zirconia can be obtained by digestion of hydrous oxide precipitated with ammonia hydroxide and sodium hydroxide for 24 hrs at elevated temperatures. Sodium hydroxide post-treatment seemed to be more effective than ammonia hydroxide post-treatment in promoting the thermal stability of high-surface-area zirconia. But the use of sodium hydroxide as a precipitant results in the adsorption of sodium ions at the surface regions of zirconia, which reduces the acidity. Hydrous oxides digested at pH 9 are less thermally stable than those digested at pH 14.

- Garvie was the first to study and propose the critical size of the crystallite for tetragonal to monoclinic transformation. It was determined that particle size for stabilizing t-phase must be $\leq$ 30 nm [16]. The tetragonal phase stabilization and the associated phase transformations processes seem to depend on the crystallite size and chemical composition. Stabilization of t-phase is most likely due to low surface energy of the t-phase relative to m-phase.

- It was reported that the tetragonal phase could be obtained either at a low pH (3-5) range or at a high pH range (13-14), and that the monoclinic phase could be obtained in the medium pH (8-11) range. High percentage of monoclinic form was obtained by precipitation at pH 10 only when the initial zirconium species is well dispersed.

- The addition of anionic, cationic or neutral surfactants in the suspensions of aqueous zirconium hydroxides have been successfully used to control its agglomeration and increase in surface area and pore volume.

- Precipitation from zirconium salts offers the most economical route, as compared to use of zirconium alkoxides or surfactants to form high surface area zirconia.

- Thermal drying of zirconium hydroxide gel in an oven results in lower crystallite size as compared to drying under vacuum which results in higher crystallite size in both sol-gel and conventional precipitation synthesis. Flowing air/nitrogen during calcination gives ZrO_2 having higher tetragonal content.

- As the calcination temperature increases to 600°C, both monoclinic and tetragonal phases are detected. Further increasing of the temperature, causes an increase in the proportion of monoclinic phase and at temperature 800°C the transformation to monoclinic phase is completed. Heating to higher temperatures led inevitably to a loss in surface area and increase in the crystallite size.

- The use of surfactants - anionic, cationic, non-ionic and zwitter ionic in acidic as well as basic medium has resulted in well-ordered porous materials with a narrow pore size distribution. However, after calcining at temperature above 500 ^{o}C the ordered structures collapsed, resulting in the material containing wormhole-like pores having reduced surface area and mesoporosity.

- Sol-gel technique is advantageous particularly to prepare stabilized nano-crystalline tetragonal zirconia. The relative rates of hydrolysis and condensation depend on pH, temperature, nature of the alkoxide and the water/alkoxide ratio. The sol-gel process also depends upon: gel formation, aging, drying, and heat treatment each of which consists of a large number of tunable parameters. Aerogels are typically dried by supercritical drying to retain its pore structure and high surface area since calcination at higher temperature leads to loss in surface area which can be largely attributed to pore collapse as a result of the high surface tension of pore water.

3.8.1.3. Optimization of synthesis parameters

From the above exhaustive literature survey it is seen that very few reports are there wherein tetragonal phase and surface area are stable at higher temperatures. Further it is observed that they have either used less economical zirconium alkoxides or surfactants, tedious post digestion methods or complex preparation method using

additional chemicals. Therefore optimization of synthesis parameters for the preparation of high surface area tetragonal zirconia with/without surfactant having good thermal stability was attempted. The primary objective of this study is to synthesize high surface area tetragonal zirconia with good thermal stability using facile synthesis procedures. As seen from the above literature survey the formation and transformation of crystalline phases and thereby the catalytic properties of zirconia depend on synthesis parameters such as type of precursor, pH during hydrolysis, doping with ions and the post-thermal treatments.

In order to investigate the influence of various synthesis parameters on the formation and quality of the ZrO_2 materials, numerous synthesis trials were conducted using ZrONit as a source of Zr by varying one parameter at a time. The results obtained from these runs indicated that, t-ZrO_2 (400 ^oC-calcination temperature) could be synthesized with high yield and in cost-effective manner from 1M solution of ZrONit at pH-11 using aqueous ammonia solution as a precipitant. Therefore, it was thought to undertake further synthesis trials using these pre-optimized conditions for further enhancing the quality of ZrO_2 materials. Further optimization was aimed at screening various synthesis variables such as effect of rate of addition of precipitant, influence of calcination temperature and time, effect of digestion time and temperature, aging of precipitate in mother liquor, influence of addition of surfactant, modification of synthesis method etc.

- From the viewpoint of the t-ZrO_2 content in the final oxide, the nature of the precursor plays also an important role. This can be inferred from the studies where both $ZrOCl_2$ and $ZrO(NO_3)_2$ salts were used as precursors [91]. Chlorides appear to be superior as a parent compound for preparation of the tetragonal zirconia in comparison to nitrates used in the same concentration and subjected to the same preparation method. The content of t-ZrO_2 in the latter case was not higher than 60%. The importance of the starting zirconium salt has been ignored repeatedly by workers in the preparation of crystalline zirconia ceramics by precipitation, and it is felt that this is a likely source for the diversity of results that have been reported. Jada and Peletis [113] suggested that the solution

chemistry of zirconia precursor materials plays a key role in controlling the formation of the crystal structure, polymorphic transformation, and crystalline growth. Oxy-chlorides are well studied and are known for their complexing abilities while nitrates are not. But from practical and industrial point of view nitrates are more suitable for the large scale synthesis and down stream processing as nitrates may be easier to remove than chloride in the calcination stage [148]. Bearing in mind the above benefits and large scale synthesis of t-ZrO_2, it is challenging study to prepare tetragonal zirconia from $ZrO(NO_3)_2$ salts by optimizing synthesis parameters. Sulfate solutions, although used in industry, will not be covered, as the chemistry of these solutions is more complex and less well understood, also sulfate anion is difficult to remove consequently it will not be used in the experimental part of this thesis. Also from further application point of view ions as chlorides or sulfates act as poisons in many catalytic reactions. Such ions should therefore be avoided in the precipitation.

- A concentration of 1 M, zirconyl salt solution was selected on the basis of practical application for all our catalyst synthesis, even though dilute solution could have given better results, the reason been that very dilute solutions produce voluminous gels which are difficult to handle, filter and reproduce.

- Hydroxides and carbonates are the preferred precipitates because of their low solubility, minimal toxicity and easy decomposition during thermal treatment. Precipitation of zirconium hydroxide from aqueous solution of zirconyl salt by using aqueous ammonia solution is widely used in the literature to synthesize stable zirconia while the use of carbonates decreases the surface area [149], therefore we have preferred the use aqueous ammonia solution.

- The temperature of precipitation and the thermal conditions of subsequent aging were also found to be important factors governing the phase composition of the final ZrO_2. Only for the samples precipitated at room temperature a single phase t-ZrO_2 was obtained upon aging. When the precipitation temperature was increased above 80°C, the content of t-ZrO_2 dropped down to just few percents, and at

100°C almost pure m-ZrO_2 was produced. Seeing the results the precipitation is carried out at room temperature.

- pH – 11 is selected for precipitating hydrous zirconia from the salt solution, pH values higher than 11 is difficult to maintain for longer times using aqueous ammonia solution. While digestion of the precipitate could be done at pH~12 which could be maintained due to closed system. During precipitation and digestion, the desired pH level is adjusted and kept constant.

- Due to contrast results available in the literature regarding rate of addition of precipitant, very slow or fast additions are avoided. Rate of addition is maintained such that the pH of the mother liquor would remain in the desired pH range for maximum time.

- When the sequence of mixing of both components is reversed i.e. (the zirconium salt solution is added directly to the concentrated ammonia solution), the content of t-ZrO_2 did not exceed 70%, for both the aged and non-aged samples which matches with previous reported results [150]. Hence both the solutions were added simultaneously.

- Aging in the mother liquor led to both: enhancement of the t-ZrO_2 content in the final solid and to a more uniform particle size distribution. In the case of aged samples a narrow size distribution with a maximum at 15 nm, distinctly below the critical value of 30−40 nm, was observed [151]. Aging of the precipitate in the mother liquor over night (10-12 h) for further precipitation of fine particles was done. Effect of aging time in mother liquor for 6 h and 24 h was also done, it was found that 24 h to be optimum, but only comparable enhancement was observed hence to save catalyst synthesis time we have utilized 12 h aging time for all our experimental runs. It is worth noting here that the precursor effect cannot be leveled off by subsequent aging.

- Influence of digestion time had the greatest effect on the thermal stability, surface area, pore volume etc keeping other synthesis conditions same. A low temperature

of digestion (< 40 °C) and using zirconyl salt, monoclinic zirconia is obtained whereas higher digestion temperatures resulted in increasing amounts of tetragonal phase [152]. The pure tetragonal phase was formed from zirconium oxy-nitrate after digestion at 80 °C temperature or higher. Digestion time from our studies indicated for 48 h to be ideal based upon XRD and surface area data, collected after calcination of samples at temperature 500 ^{o}C. However when the samples were calcined at higher temperatures (700 ^{o}C) surface area dropped down to 92 m^2/g, 90 m^2/g and 73 m^2/g for 48, 24 and 12 h of digestion time respectively. From the above experimental data it is observed that the increase in digestion time to above 48 h is essential for generating high surface area sample when calcined at lower temperature, but when calcined at 700 ^{o}C temperature it is observed that the surface area is not more then 90 ± 5 m^2/g. This judgment is done on the basis of previous literature and data obtained during our experiments. Therefore the digestion time adopted is either 12 and/or 24 h at digestion temperature 80 ^{o}C keeping other synthesis parameters constant for preparation of the catalysts.

- Sodium hydroxide post-treatment seemed to be more effective than ammonium hydroxide solution post-treatment in promoting the thermal stability of high-surface-area zirconia. But the use of sodium hydroxide as a precipitant results in the adsorption of sodium ions at the surface regions of zirconia, which reduces the acidity. Therefore digestion is carried out using ammonium hydroxide solution at maximum sustainable pH of value 12.

- Thermal drying of zirconium hydroxide gel in an oven results in lower crystallite size as compared to drying under vacuum in both sol-gel and conventional precipitation synthesis. The surface area is also high when as-synthesized samples are calcined in flowing air/nitrogen rather then static air [149]. Hence for all the samples, drying and calcination is carried out in static air instead of flowing inert gas/air to evaluate their practical thermal stability [153]. For comparative purpose all calcinations are carried out for 3 h at their respective temperatures.

- The small size of the crystallites causes broadness of the X-ray diffraction peaks which leads to some ambiguity in attributing the phases using powder X-ray diffraction. Therefore in addition to XRD measurements, the phase composition of the samples is verified by Raman spectroscopy and FTIR, which is much more sensitive to small differences in the position of oxygen ions, characteristic of different zirconia polymorphs. This latter spectroscopy technique allows for facile distinction between the cubic and tetragonal zirconia, which, by using XRD technique alone, is much more demanding. With Raman spectroscopy, the cubic phase sample has a distinguishing single band at 490 cm^{-1} which is not present in a tetragonal sample [35]. Five additional characteristic Raman bands can be observed for tetragonal zirconia which is not seen in cubic zirconia.

- Sol-gel technique is advantageous particularly to prepare stabilized nano-crystalline tetragonal zirconia. The relative rates of hydrolysis and condensation depend on pH, temperature, nature of the alkoxide and the water/alkoxide ratio. The sol-gel process also depends upon the following stages such as: gel formation, aging, drying and heat treatment, each consists of a large number of tunable parameters. All these parameters are interrelated to each other and usually one step affects the other step. Therefore more systematic studies are necessary to identify the key parameters in each sol-gel step and to understand the underlying physical and chemical processes affecting the properties of the material formed. Though important, the sol-gel synthesis parameters are not thoroughly optimized in this work because of wide variety of fine tunable factors, however one sample is prepared via modified sol-gel using zirconium alkoxide and zirconium chloride in the presence of surfactant for comparison. A new approach for preparing high surface area ZrO_2 with zirconium (IV) tert-butoxide [$Zr(OC_3H_7)_4$] used as the main zirconium source, and zirconium tetrachloride [$ZrCl_4$] serving as the pH 'adjustor' and hydrolysis–condensation 'controller', in the presence of Pluronic P123 is attempted. The earlier problems such as long synthesis period can be conquered since the pH value of the mother solution is significantly and controllably reduced. (highly ordered mesostructure is formed when the pH value

is 1-2) [54,89,109]. Compared to single $ZrCl_4$, the Zr–O–Zr bridges may partially result from the condensation between Zr–Cl and Zr–OR formations as shown in Scheme 3.4.

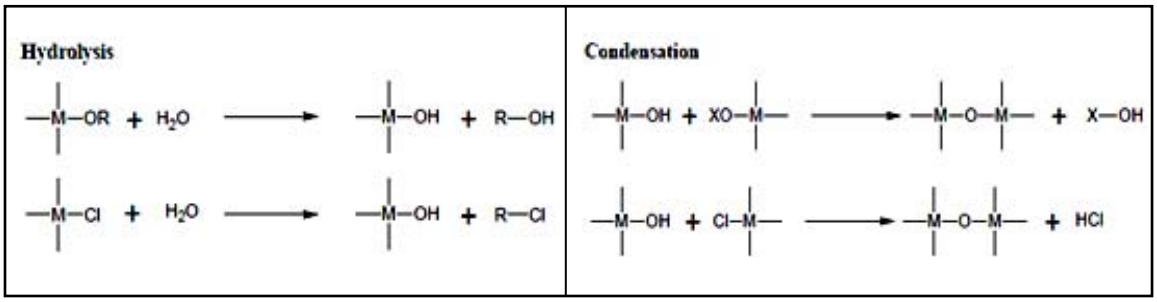

Scheme 3.4: Possible condensation reaction of mixed inorganic precursors under aqueous condition. (M – Metal, X=H or R).

The reaction mechanism of non-aqueous sol-gel chemistry is more complex than aqueous sol-gel chemistry, and a lot of studies on it are still going on [154]. Therefore, the general reaction schemes of non-aqueous sol-gel process are not presented here.

Following above optimized conditions ZrO_2 was synthesized by different methods including standard precipitation, followed by digestion and modified sol-gel using various starting precursors with and without surfactant. Here five samples of zirconia are prepared using different methods and precursors for the study which are as follows: precipitation from zirconyl salt (Z1), precipitation from zirconium alkoxide (ZII), precipitation followed by digestion-d2 from zirconyl salt (ZIII), precipitation followed by digestion-d1 from zirconyl salt (ZIV) and modified sol-gel using zirconium alkoxide and zirconium chloride in the presence of surfactant (ZV). The details of the samples prepared are given in Table 3.1.

Table 3.1: Details of the zirconia samples prepared by various synthesis methods.

Sr. No	Sample Name	Synthesis Method	Zr Source	Surfactant Used	Syn pH*	Digestion pH/Time/Temp	% Weight Loss (TG)
1	ZI	Precipitation	ZrONit	Nil	11	Nil	26.93
2	ZII	Precipitation	ZrBt	Nil	11	Nil	22.09
3	ZIII	Precipitation	ZrONit	Nil	11	12/24 h/80 ^oC	26.13
4	ZIV	Precipitation	ZrONit	Nil	11	12/12 h/80 ^oC	30.95
5	ZV	Sol-Gel	ZrBtCl	P123	2	Nil	51.26

* = precipitating pH

The samples are designated as follows, the letter Z denotes ZrO_2. The numbers 5C, 6C, 7C and 8C are referred to the calcination temperatures (C – Calcination). The non-

appearance of the denotation like 4C, 5C etc indicates the samples are not calcined and are in as-synthesized form. Two digestion methods have been used for the preparation of zirconia materials. Depending upon the time of digestion they have been labeled as d1 and d2, where d1 the conditions are: pH=12, time = 12 h, temperature = 80 ^{o}C and for d2 the conditions are: pH=12, time = 24 h, temperature = 80 ^{o}C. (The first number from the time **1**2 h and **2**4 h is the time used for digestion). The term sol-gel process should only be applied to those procedures which yield gel materials after formation of a true sol. However, in practice the term sol-gel is often loosely used for a much wider range of processes, such as solution-based preparations of materials involving hydrolysis reactions from alkoxide precursors to form colloidal particles and/or a gel. Therefore in this study the sample ZII even though prepared using zirconium alkoxide, is designated as prepared by precipitation method, while sample ZV as sol-gel. Characterization of these zirconia samples was made using several techniques such as: TG-DTA, N_2-adsorption–desorption, XRD, SAXS, FTIR and SEM.

3.8.2. TG-DTA Studies

Fig. 3.5 shows the TG-DTA profiles of as-prepared zirconia powders prepared by different synthesis procedure and starting precursors. The weight loss according to TG curves for zirconia samples prepared using precipitation technique are between 22 to 31 wt%, while that of sample prepared using sol-gel method had a weight loss 51.2 %, due to the presence of surfactant. The values are given in Table 3.1. In DTA curves the positive peaks indicate exothermic processes whereas negative peaks represent endothermic processes. The DTA figures of all samples show an endothermic peak accompanied by weight loss in the temperature region between 50-200 °C, this peak is due to loss of water of crystallization or physically absorbed water decomposition of the organic groups. It is usually found that there are two separate endothermic mass losses that occur during heating: the first loss is of free water at approximately 100 °C, and the second loss is of bound water between 150-200 °C [155]. The second step (200-400 °C) is probably the decomposition of organics residues, trace amounts of ammonium nitrate and nitrate containing zirconium hydroxy compounds through high temperature hydrolysis [105].

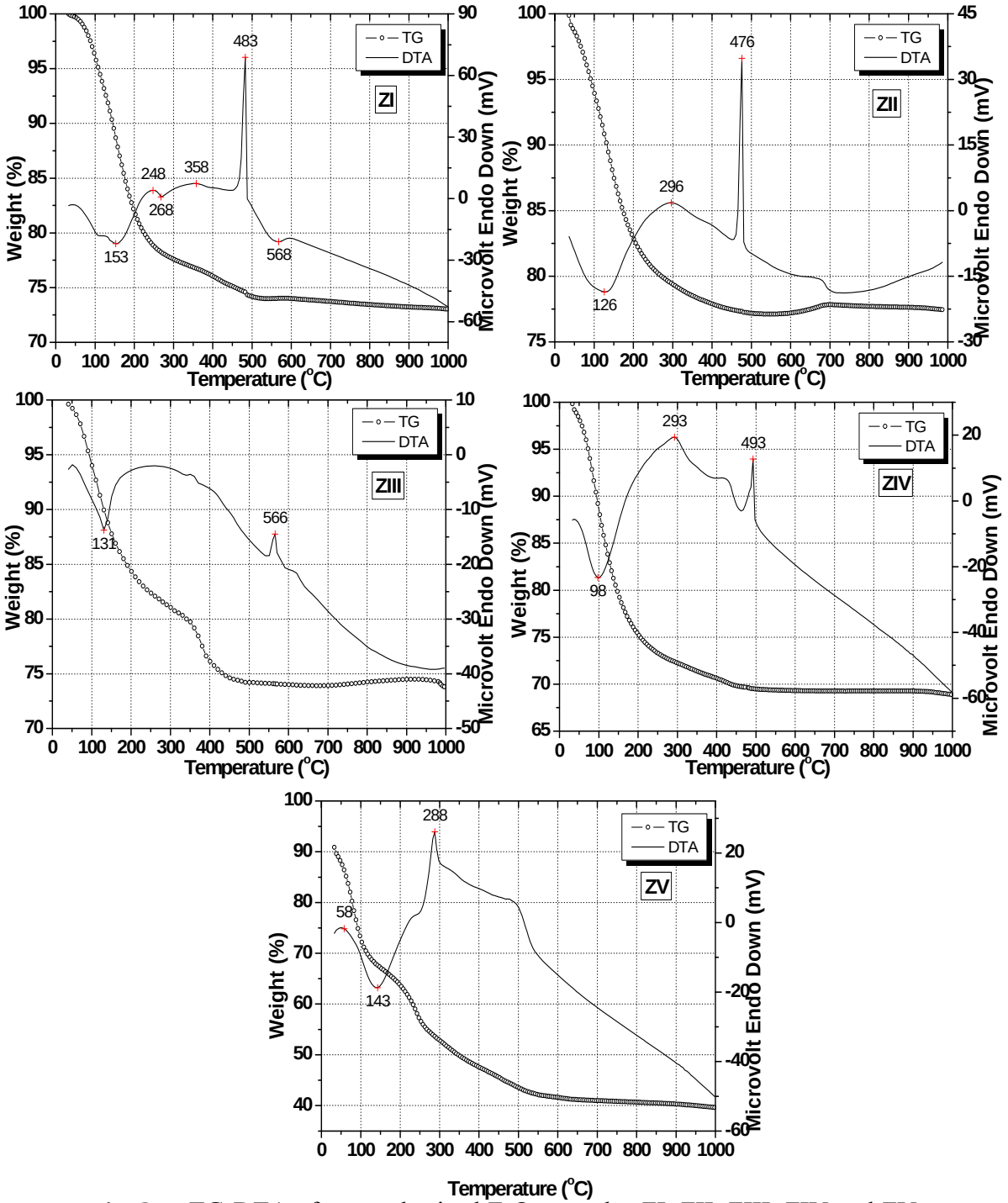

Fig. 3.5: TG-DTA of as-synthesised ZrO_2 samples ZI, ZII, ZIII, ZIV and ZV.

The third decomposition step, with the highest rate between 400-500 °C, is the complete removal of nitrates through pyrolysis as seen in DTA profile of samples ZIV and ZV. This peak might have got masked in other sample due to presence of nearby peaks or the decomposition of the nitrate containing zirconium compounds is accompanied by appreciable heat absorption related to crystallization process. The pyrolytic character of

the high temperature nitrate decomposition step is supported by the DTA curves in this temperature range. It can be seen that the exothermic zirconia crystallization process occurs concurrently with this decomposition process. As a result, the net heat effect of the process is insignificant in magnitude [156].

When the temperature of the amorphous material is raised so does the vibrational energy and mobility of the atoms until a point is reached in some regions where they may rearrange into energetically-favorable crystalline structures. Crystallization occurs when nuclei of a crystalline phase form in the amorphous material, and grow to convert it to a polycrystalline material. Crystallization of zirconia precursors is frequently studied by heating the precursor at a constant rate, usually 5-20 °C/min, through the crystallization reaction by *in-situ* diffraction or TG/DTA. During the transformation to the oxide, a sharp exothermic peak is normally observed in the differential thermal scan of the hydrous zirconia in the temperature range from 400 to 450 ^{o}C [35,36] Since optimized synthesis conditions are used in this study, this sharp exothermic peak is found shifted in the temperature zone from 470 ºC to 570 ºC. This exothermic peak, not accompanied by any weight loss is due to conversion of the amorphous zirconia phase to the tetragonal zirconia [155]. The glow phenomenon is essentially a surface process, corresponding to the destruction of a thermodynamically meta-stable surface condition. Also it is noticed that this crystallization peak is occurred at higher temperature (566 ^{o}C) for sample ZIII due to digestion-d2 process whereas for the sample ZIV wherein the digestion process is reduced to half time, the crystallization peak is at 493 ^{o}C, both the values are higher, when they are compared with samples prepared without digestion. This shows that on increasing the digestion time, the crystallization peak can be shifted and retain the tetragonal phase up to higher temperature. Another noteworthy feature observed in present TG-DTA analysis concerning sample ZV prepared by sol-gel method which exhibited a broad exothermic peak rather a sharp peak pertaining to conversion of the amorphous to the tetragonal zirconia. There is no specific peak to indicate the tetragonal to monoclinic phase transformation although in the present studies all zirconia samples show a mixture of tetragonal and monoclinic phases. The likely reason for non-appearance of the peak and presence of mixed phases could be that the transformation of tetragonal to monoclinic phase happens during cooling instead of heating. It is suggested

that the elimination of organic surfactants through combustion generates an exothermic reaction. As it can be seen, a separate exothermic peak corresponding to the removal of surfactant has not appeared in this DTA profile of sample ZV, this may be due to the coincidence between the strong endothermic peaks related to the water removal and exothermic peak corresponding oxidative decomposition of trace amounts of HCl, organic residues and various zirconium hydroxy compounds incorporated into the hydrous oxide. Block copolymer surfactant species are decomposed and desorbed from the mesoporous silica materials channels between the temperature 145-190 °C, these temperatures are much lower than the decomposition temperature of pure surfactant itself (250°C). It is also much lower than the temperature required (360 °C) to remove lower-molecular-weight cationic surfactant (CTMABr) [157]. Thermo-gravimetric experiments indicate that the block copolymers are completely removed from the as-synthesized zirconium composites upon calcination at 400 °C. A single exothermic peak assumed to be corresponding to the removal of surfactant appeared at 280 ^{o}C temperature. A large peak in the DTA profile of sample ZV at 288 °C, can be due to the loss of surfactant which is a close match with reported peak value of 280 ^{o}C temperature [158]. The trivial difference in the exothermic peaks may be due to variation of synthesis procedure and staring precursor. No further weight loss is observed on the TG curve after 500 °C, indicating that the samples has been completely crystallized and all the organics have been removed. This is also confirmed by FTIR results. It is learned from the results of a detailed thermal analysis [150], the process of ZrO_2 formation is quite complex and involves several mutually related steps such as dehydration of hydrous zirconia, nucleation of ZrO_2 proto-structures and coalescence of primary particles [159]. The glow exotherm is usually accompanied by a steep decrease in the surface area. To substantiate the above results, the as-prepared powders are calcined at various temperatures ranging from 500 to 800 °C and their XRD patterns are analyzed which will be discussed in detail in the forth coming sections.

3.8.3. Nitrogen Adsorption-Desorption Studies

From N_2 gas sorption studies of calcined zirconia samples showed not well-defined type of isotherm as per IUPAC; however, the shape of isotherms shows the

presence of micropores, mesopores and in some cases macropores. The presence of both H3 and H2 hysteresis indicates the combined presence of ink-bottle, wedge and slit-shaped pores in these samples [160]. Even though the shapes of isotherms did not fit clearly with defined isotherms as per IUPAC, the closest possible isotherm and hysteresis have been used for describing the type of materials and porosity. Type II, III and IV isotherms with obvious hysteresis loops were observed for samples calcined at 500 ^{o}C indicating the presence of mesopores. As an illustrative example the N_2 physisorption isotherms of the ZIII sample calcined at 500 and 700 ^{o}C is given in Fig. 3.6.

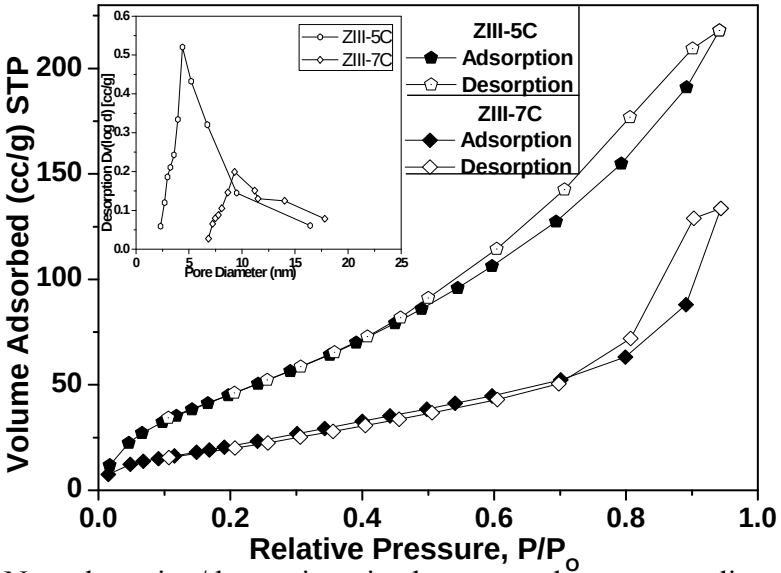

Fig. 3.6: N_2 adsorption/desorption isotherms and corresponding BJH pore size distribution (Inset) of sample ZIII calcined at 500 and 700 ^{o}C.

N_2 physisorption isotherms of the ZIV were identical to ZIII with lower surface area values. The nitrogen sorption isotherms of ZIII-5C and ZIII-7C exhibit a type-III isotherm with a H3-type hysteretic loop at $P/P_0 \sim 0.6–0.9$ and $P/P_0 \sim 0.8–0.9$ respectively. H3 type hysteresis indicates that the samples exhibit an inter-particular porosity which can be ascertained by the uptake at high pressure associated with the void spaces between the particles. Type H3 is usually found on solids consisting of aggregates or agglomerates of particles forming slit shaped pores (plates or edged particles like cubes), with non-uniform size and/or shape. Conversely presence of regular pores is depicted in Fig. 3.6 (Inset) which shows pore size distribution (PSD) with a peak maximum around 5 and 9.8 nm for samples ZIII-5C and ZIII-7C respectively. The shift of the hysteresis loop to higher relative pressure with increasing calcination temperature suggests an increase in

the pore size, which is confirmed from PSD. The adsorption-desorption curves of N_2 and the BJH pore size distribution determined from desorption isotherms of sample ZI and ZII calcined at 500 ^oC are presented in Fig. 3.7.

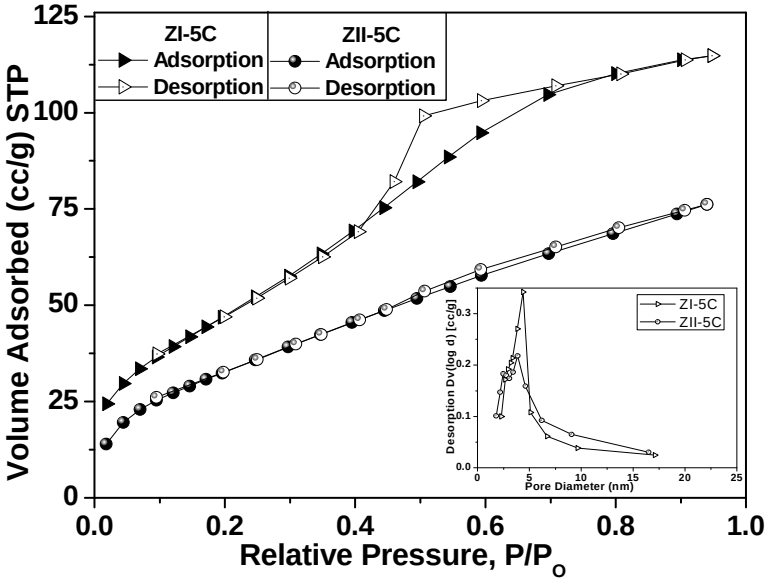

Fig. 3.7: N_2 adsorption/desorption isotherms and corresponding BJH pore size distribution (Inset) of sample ZI and ZII calcined at 500 ^oC.

Adsorption–desorption isotherm of zirconia sample prepared using zirconium oxy-nitrate as a starting precursor calcined at 500^oC is not well defined since it exhibits a linear region from P/P_0 0.1 to 0.4 before reaching a plateau. This kind of isotherm is situated between the type I, related to microporous materials, and the type IV, characteristic of mesoporous materials. In agreement with M.M. Dubinin [161], such types of materials are known to possess super-micro-pores, i.e. pores with sizes ranging from 1.5 to 2.0 nm [56]. However the sample posses PSD with a peak maximum at 4.9 nm demonstrating that it may be more of mesoporous type then of microporous one. Adsorption–desorption isotherm of ZII-5C is also not well defined with a H3-type hysteretic loop at $P/P_0 \sim 0.5$–0.8. This kind of isotherm is situated between the type I, related to microporous materials, and the type II, characteristic of non-porous solids. The PSD shows bimodal pores with a peak maximum at 4.4 nm. The effect of calcination temperature on the surface area and crystallite size of the zirconia materials are studied using nitrogen adsorption/desorption and XRD respectively. The resulting specific surface areas are calculated using the BET method, while crystallite size was determined from the line broadening of the (111) reflex

at 28.1° for the monoclinic and (101) at 30.2° for the tetragonal phase, using the Scherrer formula. Linear decrease in surface area and increase in crystallite size with increasing calcination temperature was found in the temperature range studied as shown in Fig. 3.8.

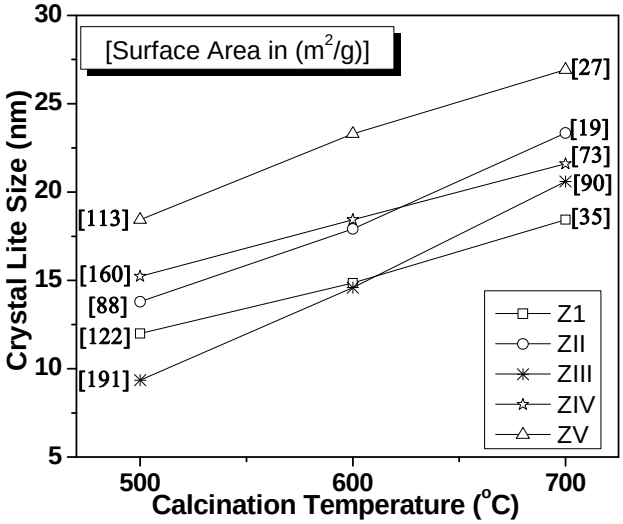

Fig. 3.8: Crystallite size of tetragonal phase of the zirconia samples as a function of calcination temperature. The crystallite size of the tetragonal phase was calculated from its characteristic peak at 30.2° (101) 2θ angle using Scherrer formula. Surface area values of the corresponding calcination temperature are in given brackets.

The crystallite size of the digested samples of both series d1 and d2 have smaller crystallite sizes, with expected digestion-d2 having smaller size as compared to digestion-d1. Stabilization of small crystallites is an effect of digestion and results in the high surface area of digested samples. An unusual lower crystallite size was shown by undigested samples calcined at 500 ^{o}C having lesser value then sample ZIV prepared using digestion-d1. Sample ZI and ZII has tetragonal phase when calcined at 400 ^{o}C, when the temperature is increased to 500 ^{o}C this phase collapsed giving birth to monoclinic phase. Due to mixed phase content of tetragonal and monoclinic and poor peak intensity, as seen in subsequent section of XRD (Fig. 3.13) of these phases, may have resulted in the deviated values. Further in our system the relationship between the crystallite size and the surface area is not observed due to diverse factors. Ideally smaller crystallites should give higher surface areas, while at higher calcination temperature larger crystallites should have corresponding lower surface areas. Even though there is linear decrease in surface area and crystallite size for each sample, no co-relation between the surface area and crystallite size is observed. This was specially true for samples ZI

and ZII. Though there is no satisfied interpretation for this, it is suggested related to preparation method that results in different phase compositions and crystalline size distributions. For example, if a batch of powder is composed of equal amounts of very large and very small crystallites the result of FWHM measurement may only stand for the larger crystallites [162]. Also if powders contain strong agglomerates which are difficult to separate, the results may be affected [152]. In agreement with the literature [152,162,163], an almost linear decrease of surface area with increasing calcination temperature is found, although the linearity is not similar for all the samples studied. Increasing the calcination temperature leads to a continuous decrease in the BET surface area as the initial zirconia sinters, crystallizes and undergoes significant pore collapse. The surface area of the undigested samples ZI and ZII prepared by precipitation method and calcined at 500 ^{o}C was less, 122 and 88 m^2/g respectively while digested samples calcined at same temperature have higher surface areas in excess of 160 m^2/g. It is also observed that digested samples calcined at 700 ^{o}C possess surface area values similar to undigested samples calcined at 500 ^{o}C e.g. sample ZIII-7C has surface area of 90 m^2/g, while sample ZI-5C, ZII-5C and ZIII-5C posses surface area about an average of 100 m^2/g. It is worth-noting that the BET specific area of the zirconia samples remained 90 m^2/g for digestion-d2 and 73 m^2/g for digestion-d1 even after 700 ^{o}C annealing, whereas those samples without any digestion irrespective of preparation method exhibited specific area as low as 20 m^2/g at same calcination temperature. It is surprising, that sample prepared with modified sol–gel using surfactant, has less surface area, against the sample prepared using standard precipitation technique without surfactant. One possible reason could be that synthesis conditions used for sample ZI are finely tuned after an exhaustive literature survey, while the modified sol-gel synthesis parameters are not fine tuned or optimized. Further optimization of the sol-gel synthesis can lead to higher surface area sample, but it is not within the scope of this thesis due to large number tuneable parameters, which affect the properties of the sol-gel derived materials. From Fig 3.8 it can also be noted that ZIII sample has higher surface area as compared to other samples of the same calcination temperatures. This finding is valuable because it shows that by the optimized precipitation conditions thermal-resistant tetragonal zirconia can be produced at a low cost. From above results it is possible to draw a linearity equation of

decrease in surface area vs synthesis conditions, as ZIII > ZIV > ZI ≥ ZV > ZII. This equations states that sample ZIII sinters less with a smaller amount loss of surface area with increasing calcination temperature as compared to sample ZIV and so on. This behavior of samples suggests that the final materials produced are quite dependent upon the mechanism in which they are formed. The mechanism of formation of hydrous zirconia from zirconyl salt precursors is strongly connected with its aquatic chemistry. The aquatic chemistry of zirconium is featured by its tendency to form inorganic polymers via oxolation and olation processes [164]. The resultant oligomeric species, depending on their particular molecular structure and the extent of a framework development, gives rise to different zirconia polymorphs [165]. When zirconyl salt is dissolved in water, cyclic tetramer complexes $[Zr(OH)_2 \cdot 4H_2O]_4^{8+}$ are formed as dominant entities [166]. The four zirconium atoms in each tetramer complex are arranged in a square, and each zirconium atom is coordinated by four bridging OH groups and four H_2O molecules. This structure is illustrated in Fig. 3.9.

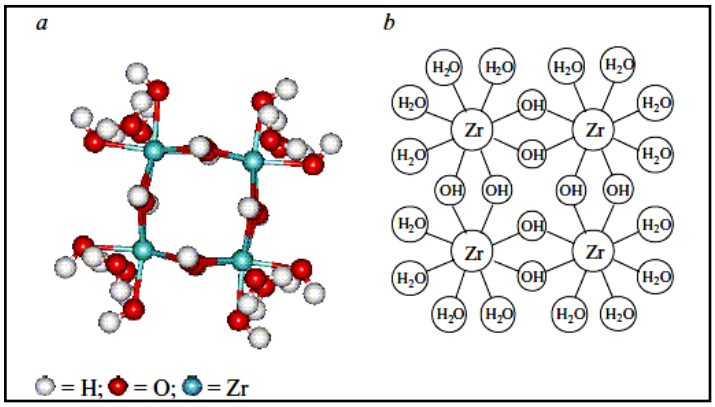

Fig. 3.9: Illustrations of the cyclic-tetramer cation, using a) a ball and stick model and b) a schematic model [167].

The tetramer is the dominant species in concentrated chloride solutions at pH below 1.5, coexisting with minority species such as the trimers. The cyclic-tetramer has been sometimes assumed to be the predominant zirconyl species in nitrate solutions with little direct evidence. When enough base is added, the polycondensation of zirconyl species, consuming all or most of the original species takes place. The rate of condensation between species is particularly sensitive to the pH of solution. Although gradual polycondensation occurs under most of the conditions, the rate of reaction is greatly enhanced at higher pH, and can be inhibited by addition of an acid, decreasing the pH.

The polycondensation takes place by olation (Zr-OH + H_2O-Zr → Zr-OH-Zr + H_2O) and oxolation (Zr-OH + HO-Zr → Zr-O-Zr + H_2O) processes leading to the formation of hydroxyl- and oxo-bridges between tetramer units, respectively. When the concentration of the polymeric species reaches a critical super saturation level, crystal nuclei of hydrous zirconia are generated, and primary particles of hydrous zirconia are formed by growth of the crystal nucleus firstly, by hydrolysis which forms reactive terminal-hydroxy groups required for the condensation reaction. Secondly, hydrolysis reduces the positive charge on the zirconyl species, diminishing the electrostatic repulsion and increasing the chance of interacting and reacting. In short the formation mechanism for hydrous zirconia particles produced by hydrolysis can be given as in Scheme 3.5.

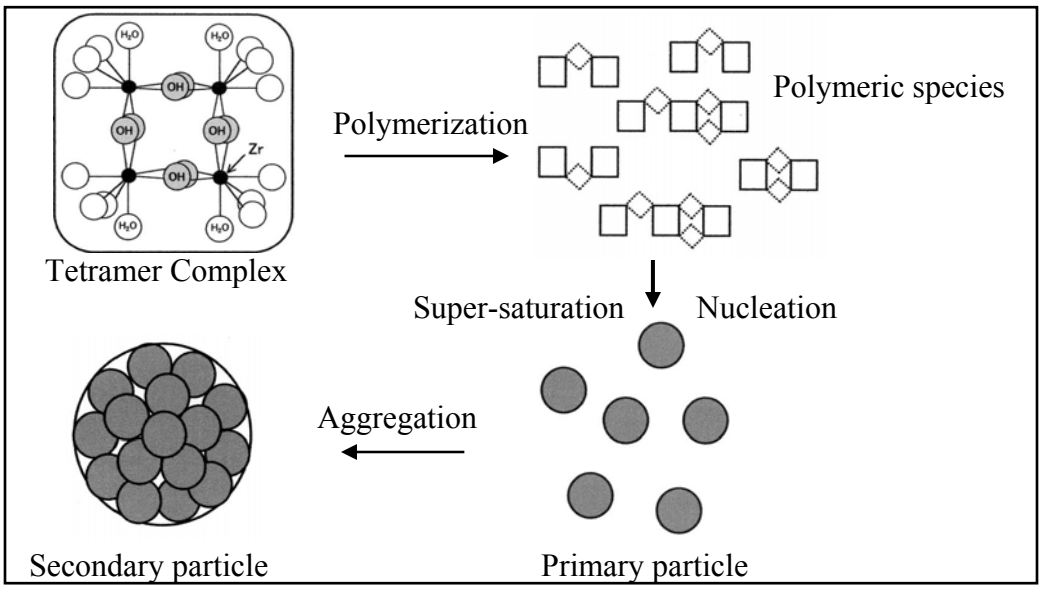

Scheme 3.5: Scheme of formation mechanism for hydrous zirconia particles produced by hydrolysis of Zr salt solutions. (□) indicates tetramer complex. $[Zr(OH)_2{\cdot}4H_2O]_4^{8+}$ Bent dash line connected to two squares represents —ol bridge.[168].

The transformation of an amorphous hydrous zirconia to a metastable tetragonal zirconia is attributed to the loss of the hydration water, and the water produced during the olation process. While the hydrolysis and condensation steps of Zr alkoxide in the presence of $ZrCl_4$ the Zr–O–Zr bridges may partially result from the condensation between Zr–Cl and Zr–OR formations as shown in Scheme 3.6. The metal alkoxide or metal chloride is hydrolyzed and M-OH species are generated during the first step, while in the second step, the hydroxy groups react with each other and/or other metal alkoxide/chloride and a

M-O-M network is formed upon the propagation of the condensation reaction resulting the elimination of ROH, water and/or HCl.

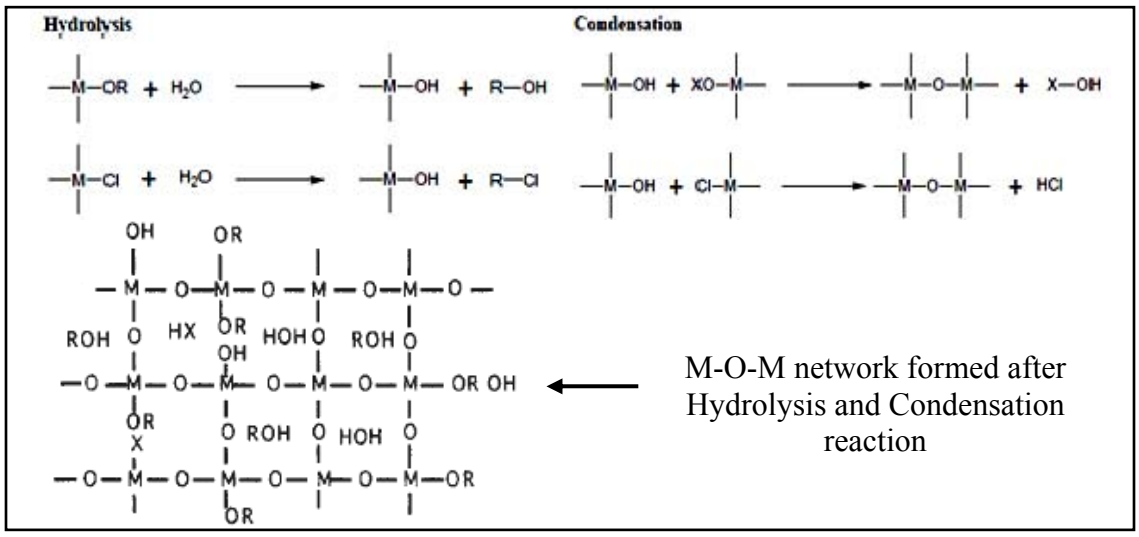

Scheme 3.6: Possible condensation reaction of mixed inorganic precursors under aqueous condition. (M – metal, X = H or R).

The presence of surfactant during controlled hydrolysis and condensation of zirconium alkoxide and zirconium chloride can lead to formation of ordered metal oxides generally suggesting inorganic-oxide/block-copolymer assembly mechanisms as shown in Fig. 3.10.

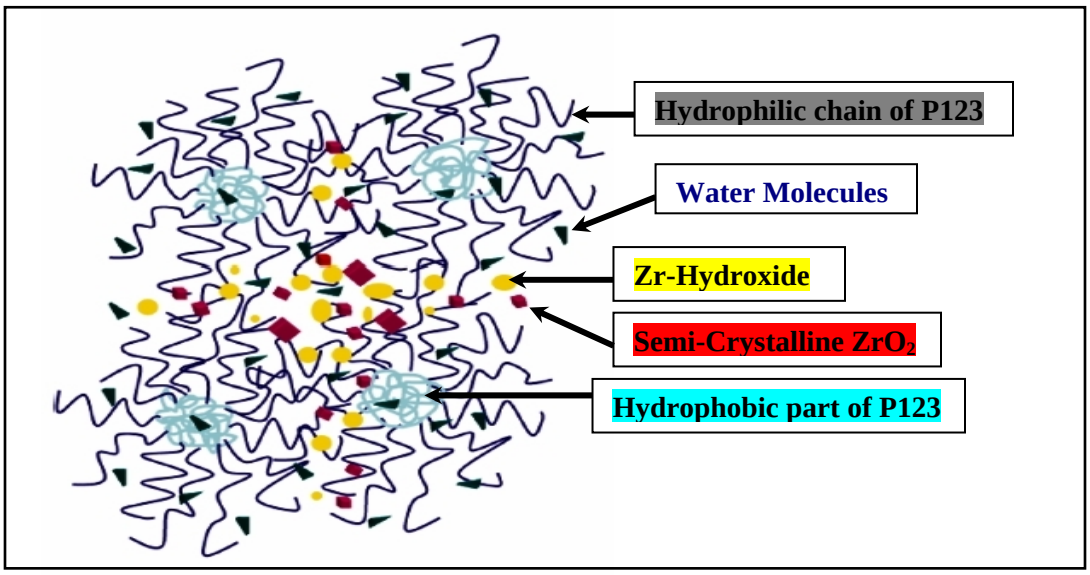

Fig. 3.10: Model of the self-assembly processes of hydrous zirconium (IV) oxide incorporated in 4 molecules of Pluronic 123, A Nonionic Tri-Block Copolymer Surfactant; Ethylene Oxide (EO_{20}) – Propylene (PO_{70}) – Ethylene Oxide(EO_{20}). Note: E and P units are shown in schematic form. [169].

After hydrolysis, the multivalent metal species can associate preferentially with the hydrophilic poly(ethylene oxide) (PEO) moieties mediated by HCl released by ZrCl4. Zirconium tetrachloride reacts rapidly with water, vapour or liquid to exchange two chlorines for oxygen. In powder form, it reacts in water to form zirconium hydroxychloride and free hydrochloric acid. The proposed assembly mechanism for these diverse mesoporous metal oxides uses PEO-metal complexation interactions, in conjunction with electrostatic, hydrogen bonding, and van der Waals forces to direct mesostructure formation. Controlled hydrolysis and condensation of the inorganic-organic species appears to be important for forming mesophases of most of the non-silica oxides, because of their strong tendency to precipitate and crystallize into bulk oxide phases directly in aqueous media. Thus it can be seen from the above mechanisms the diversity of the properties the materials can exhibit due to different path and chemistry involved in their formation.

3.8.4. Powder XRD and SAXS Studies

Mixture of m-ZrO_2 and t-ZrO_2 shows intense and well defined diffraction peaks at 2θ values of 28.2° and 31.5° corresponding to the reflections from the 111 and (-111) planes of monoclinic zirconia phase (JCPDS file no. 37-1484) and at 30.2° corresponding to the reflections from the (101) plane of tetragonal phase (JCPDS file no. 79-1770). The volume fractions of monoclinic (V_m) and tetragonal (V_t) phases were calculated in the way reported previously on the basis of the integrated intensities of (111) and (-111) peaks of m-ZrO_2 and the (101) peak of t-ZrO_2 [170]. Im = Intensity of corresponding XRD monoclinic peaks mentioned in the brackets and It = Intensity of tetragonal (101) peak.

$$V_m = \frac{1.311x}{1+0.311x}, \qquad V_t = 1-V_m, \qquad x = \frac{Im(111)+Im(-111)}{Im(111)+Im(-111)+It(101)}$$

This calculation cannot account for amorphous zirconia fractions, because they are not detectable by XRD. 2θ values and intensities of different phases of ZrO_2 are tabulated in Table 3.2. The values are collected from the respective JCPDS cards, by selecting variable silt and wavelength as 1.54184. For monoclinic phase, intensity values smaller

than 10% are not given. Fig. 3.11 gives presentation of JCPDS cards as a visual aid of monoclinic, tetragonal and cubic zirconia

Table 3.2: 2θ position and intensity of standard peaks of different phases of ZrO_2.

(37-1484) m-ZrO_2		**(79-1770) t-ZrO_2**		**(49-1642) c-ZrO_2**	
2θ	Intensity	2θ	Intensity	2θ	Intensity
24.068	12	30.267	100	30.145	100
24.461	9	34.624	9	34.989	20
28.198	100	35.322	15	50.236	52
31.494	76	43.042	2	59.793	31
34.188	25	50.296	54	63.736	4
34.412	13	50.815	29	74.010	2
35.338	16	59.370	22	81-840	5
40.759	17	60.296	43	84.483	8
49.309	31	62.952	11		
50.159	38	73.046	4		
50.603	23	74.713	10		
54.151	21	81.876	20		
55.449	21	82.684	10		
59.828	16	83.828	8		

It is well known that most XRD peaks of cubic ZrO_2 overlap with those of tetragonal ZrO_2, resulting in the difficulty to unequivocally proof the presence or absence of cubic ZrO_2 from the XRD patterns. According to JCPDS cards 79-1770 and 49-1642 (Fig. 3.11 and Table 3.2), the diffraction peaks of tetragonal zirconia appear at same 2θ as that of cubic zirconia with similar relative intensities.

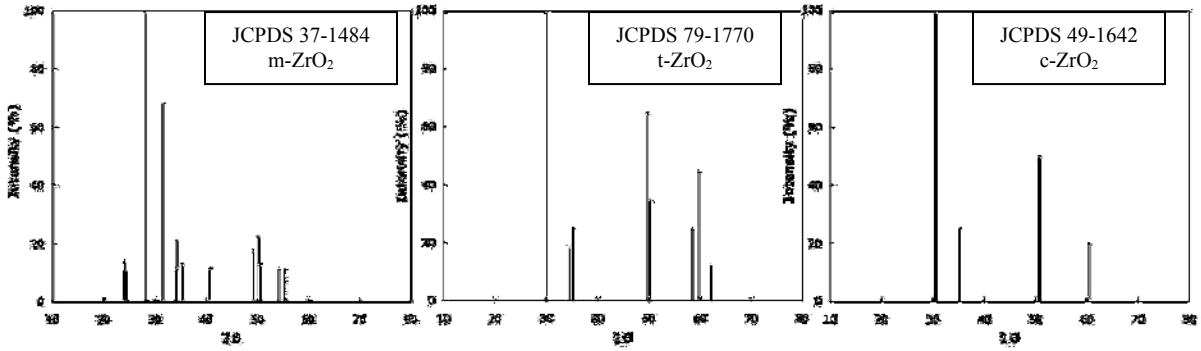

Fig. 3.11: Standard peaks of m-ZrO_2, t-ZrO_2 and c-ZrO_2.

However tetragonal phase can occasionally be distinguished from the cubic phase by the characteristic 'peak splitting' in the 2θ range 34-36°. But this splitting is often not resolved well in the XRD figures due to small particle size, stress, poor resolution and many other factors. In such a case additional spectroscopy and microscopy techniques may be employed for verifying the meta-stable tetragonal phase. XRD patterns were used

to identify the various phases and the crystallite sizes of the samples. Figure 3.12 shows the XRD patterns of zirconia sample ZIII calcined at different temperatures.

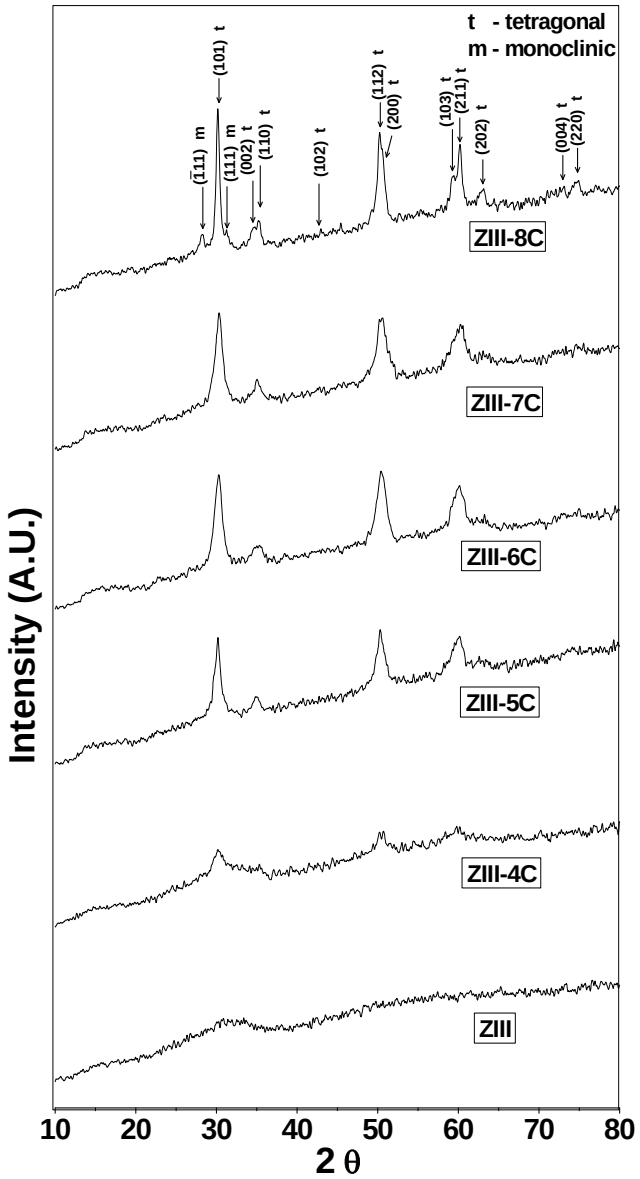

Fig. 3.12: XRD patterns of as-synthesized zirconia sample ZIII and calcined at 400 ^{o}C, 500 ^{o}C, 600 ^{o}C, 700 ^{o}C and 800 ^{o}C.

It is seen that, the as-synthesized zirconia powder has amorphous structure as they are not heated above 100 ^{o}C during drying process. When the sample was calcined at 400 ^{o}C, a semi-crystalline structure with major part still amorphous can be detected from XRD pattern. By rising the calcination temperature to 500 ^{o}C pure tetragonal phase is formed. The crystallization DTA peak of t-ZrO_2 from zirconium hydroxide for sample ZIII was observed at 566 °C from TG-DTA studies whilst the XRD pattern of ZIII-5C should have

been more of amorphous type rather then crystalline. The possible reason for this behavior could be that in TG-DTA analysis the sample is heated at a rate of 10 ^{o}C/min, while during calcination, sample is heated at a maximum rate of 4 ^{o}C/min with a dwell time of 3 h, which is also absent in TG analysis, due to which hydroxide must have converted to crystalline form relatively earlier as compared to temperature reported in TG/DTA. Garcia et al. [23] crystallized zirconium hydroxide precipitate after 12 hours of heating at 375°C which usually crystallites between the temperature 400-450 °C, thus supporting our possible reason of crystallization of zirconia at lower temperature as compared to TG-DTA study. Further increasing the temperature up till 700 ^{o}C only tetragonal phase is seen, however both monoclinic (25%) and tetragonal (75%) phases are detected at temperature 800 ^{o}C. Thus it can be concluded that high surface area tetragonal zirconia with thermal stability up to 700 ^{o}C can prepared via precipitation followed by digestion-d2 under optimal synthesis condition. Reduction in the digestion time also reduces the amount of tetragonal zirconia present at 700 ^{o}C. During digestion, the higher temperature leads to increased thermal agitation of negatively charged particles which repel each other in alkaline solution. Collisions between the charged particles occur at a higher rate than at room temperature. This enhances the formation of surface bonds between particles by condensation of surface hydroxyl groups. Thereby, a network of particles with higher porosity than in the undigested sample forms. In addition to the network formation by coalescence of primary particles, another effect of the higher temperature is the dissolution and re-precipitation of material which helps in strengthening the network of particles. It is then possible to remove the water from the pores without collapse of the network structure. Previous results indicate that the dissolution/re-deposition is enhanced at pH ~14 as compared to pH 9, also longer the digestion time higher will the interaction between the primary charged particles thus enhancing the network. The influence of digestion is thus interpreted in terms of the enhanced agglomeration of primary particles, strengthening the network structure which is then better able to withstand thermal treatment. All the zirconia samples when calcined at 400 °C, only tetragonal phases were obtained but due to presence of carbon residual impurities detected by IR in the samples prepared using ZrBt, studies of all the samples calcined only above 400 ^{o}C have been considered in these studies. This is in agreement

with the TG-DTA data, which showed that the onset of the conversion of the amorphous to tetragonal phase started in the temperature range 450-500 ^{o}C. Although at 400 ^{o}C the main phase is tetragonal, but when the temperature increased, the tetragonal phase concentration decreased with an increase in concentration of monoclinic phase. Fig. 3.13 shows the XRD patterns of zirconia powders prepared by altering various synthesis parameters/precursors and calcined at 500 °C and 600 °C.

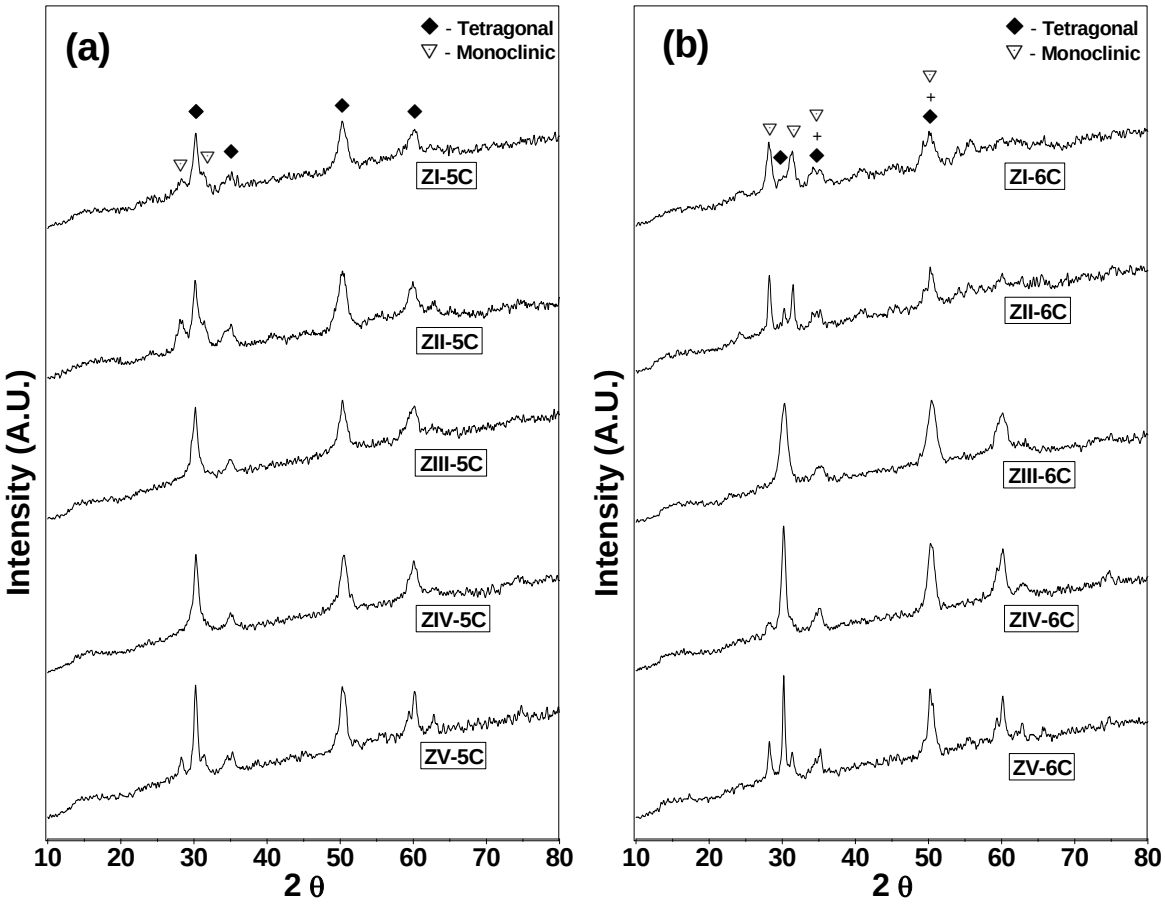

Fig. 3.13: XRD patterns of zirconia samples prepared by different synthesis parameters and precursors (a) calcined at 500^{o}C, (b) calcined at 600^{o}C.

The XRD patterns of zirconia samples ZI and ZII calcined at 500 °C synthesized using different precursors, ZrONit and ZrBt respectively under identical synthesis conditions consists of tetragonal and monoclinic phases. As it can be seen, the digested samples ZIII and ZIV retain majority of the tetragonal phase up to 600 ^{o}C. The sample ZIV digested with lesser amount of time as compared to ZIII contain small amount of monoclinic phase with dominant tetragonal phase when calcined at 600 ^{o}C, indicating digestion time

plays an important role in stabilizing t-ZrO_2. Sample ZV calcined at 500°C and 600°C prepared using sol-gel technique in acidic pH consists mixture of tetragonal and monoclinic phases which converts to monoclinic at higher temperature. It is observed that, the samples prepared without digestion irrespective of the preparation method, in an acidic or basic media contained both tetragonal and monoclinic without cubic phase when calcined at 600°C. Fig. 3.14 shows XRD patterns of samples calcined at 700°C.

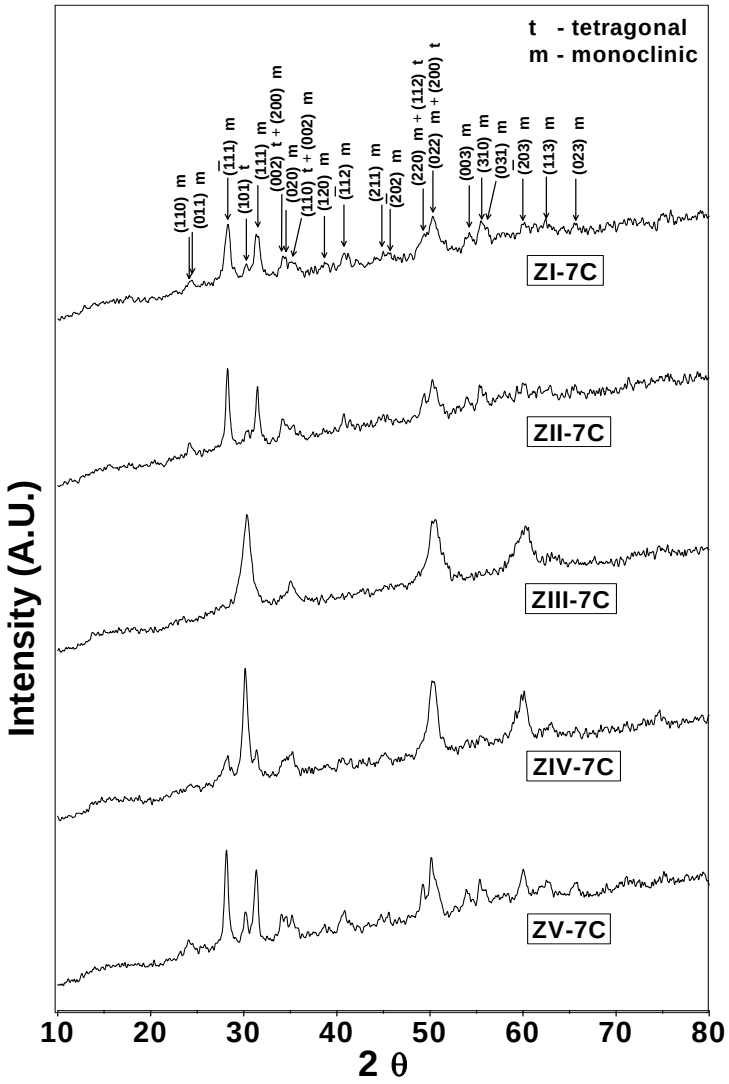

Fig. 3.14: XRD patterns of zirconia samples calcined at 700°C prepared by different synthesis parameters and precursors.

The annealing of the samples at higher temperatures (700°C) increased the crystallite size and caused irreversible transformation of the tetragonal phase into the monoclinic one. In case of samples ZI and ZII prepared using precipitation process using ZrONit and ZrBt

shows complete monoclinic phases. Also in case of zirconia powder obtained from sol-gel method in acidic pH using ZrBtCl shows only monoclinic phase with some traces of tetragonal (12%) zirconia. Sample ZIV prepared with digestion time 12 h contains a mixture of monoclinic and tetragonal phase (60%), increasing the digestion time up to 24 h for sample ZIII led to complete stabilization of t-ZrO_2 containing only tetragonal phase. Fig. 3.15 illustrates the variation of the tetragonal phase content as a function of calcination temperature for zirconia samples prepared using various staring precursor and synthesis parameters. As mentioned earlier, increasing of calcination temperature leads to increase of monoclinic phase content radically with the decrease in tetragonal phase content. Samples ZI and ZII prepared using different staring precursors ZrONit and ZrBt respectively under identical synthesis conditions shows small variation in tetragonal phase content when calcined at 500^oC indicating the sample prepared with ZrONit is more stable as compared to sample ZII prepared from ZrBt. Before comparing the results some possible mechanisms regarding stabilization of tetragonal zirconia must be understood.

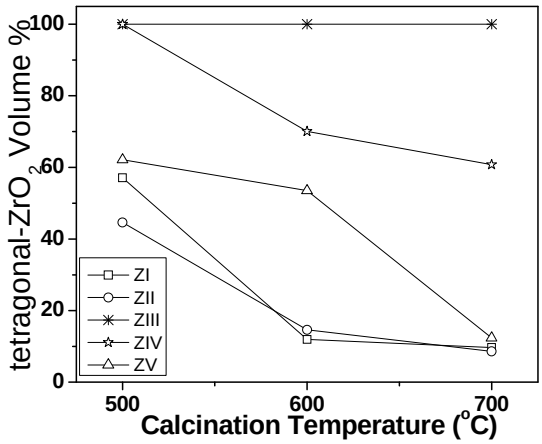

Fig. 3.15: Volume % of tetragonal zirconia of samples ZI-ZV as a function of calcination temperature.

As stated earlier, the high temperature stabilization of tetragonal zirconia was its crystallite size [16]. All the samples prepared during this study, calcined at various temperatures have crystallite size less then 30 nm (Fig. 3.8) and yet few of them have transformed to monoclinic phase. The studies on the t→m transformation with heating found a weak correlation between crystal size and the point at which the transformation takes place; however, it is known that that other factors, such as chemical preparation conditions, are more important [42,117,171,172]. Other studies have found no significant

correlation thus supporting the idea of stabilization of tetragonal phase is not only related to crystallite size [19,26,146,173]. Thus another mechanism involving the incorporation of hydroxyl ions into poly-zirconium species is adopted to explain the difference in crystal structure and thermal stability. The freshly derived zirconium gels of the precipitation samples are amorphous and have a solid skeleton that contains many hydroxyls. During annealing, surface hydroxyls condensation causes the nucleation of new oxide crystals for the growth of the existing ones. The phase transformation from zirconium hydroxide to ZrO_2 involves several possible steps: the loss of the loose water and terminal hydroxyl groups, oxolation of hydroxyl bridges to form embryonic oxide nuclei and growth of the nuclei to form observable crystallites. With rapid precipitation, the penetration of hydroxyl ions into the poly-zirconium species is slow while a slow rise in pH allows hydrolysis reaction to occur so that the poly-zirconium species have a lower valency. These different species in turn determine the zirconia crystal structure. In water under basic conditions, zirconium alkoxides undergo rapid hydrolysis and condensation, so that in the absence of acid a precipitate forms readily, resulting in a gel is which is weakly cross-linked containing less amount of hydroxyl ions as compared gels prepared from zirconyl salt solutions. Possibility of ions other then OH^- has also been considered. During sample preparation, H_2O, OH^- ions, H^+ ions, nitrate and chloride ions vacancies occur. When samples are annealed to 300 ^oC, the H_2O present left them. Therefore, water did not stabilize the tetragonal structure. It is known that zirconia prepared from strongly acidic solutions (pH<1) gives rise to the monoclinic phase [174] which also eliminated H^+ ions from stabilizing the tetragonal structure. These results suggest that a mixture of OH^- ions and Zr vacancies in the crystalline structure could cause the observed tetragonal structure stabilization under basic conditions. However when the sulphuric acid is used as hydrolysis catalyst, the SO_4^{2-} ions present in the Zr–O framework would replace for OH^- ions. Because the thermal stability of the sulphate to zirconium linkages is much higher than that of the hydroxyl bridges across two Zr atoms, the removal of SO_4^{2-} ions needs a higher temperature, i.e., 600^oC, which delays the formation of some oxo bonds and thus stabilizes the low-temperature tetragonal structure. Similar results are obtained by Bokhimi et al. [175] who prepared zirconia powders using sol–gel process with zirconium n-butoxide under different hydrolysis conditions and pH. When the calcination

temperature increased, the unit cell of monoclinic showed a distortion because it expanded in c dimension with a contraction in a direction. The lattice cell distortion is usually caused by the guest ions like OH^- inserting in the crystalline structure and the calcination temperature. The foreign ions with different radius or charges produce charge unbalance in the local structure and the calcination temperature may affect the behavior of lattice sites vibration, these factors, in turn, lead to the lattice cell modification in comparison with the ideal crystalline structure. The presence of nitrate and chloride ions also affects the crystallization temperatures and delay tetragonal to monoclinic phase transformation of zirconia. Negatively charged ions such as sulphates, nitrates and/or chlorides are found to be important in forming the tetragonal and cubic phases of zirconia [171,176,177]. One report found that the presence of NH_4Cl inhibited the t→m transformation [171] while others found that the presence of Cl^- anions had no effect [35]. The dehydroxylization behavior and presence of stabilizing ions in the zirconia structure depend upon the synthesis procedure and starting precursors thus affecting the quantity of tetragonal phase in zirconia at a particular temperature. At the same calcination temperature the structural distortion caused by the insertion of OH^- in the structure is more important. The sample precipitated from ZrBt retained less hydroxyl in its structure as compared ZrONit to due to its highly reactive nature. When these samples were calcined at 500 ^oC, their dehydroxylation behavior and phase transformation thus crystal grain varied from one to another. Therefore the sample precipitated from ZrONit gave slightly higher % of tetragonal zirconia at 500 ^oC since it retains a more of hydroxyls in its crystals producing many cationic defects. Another possible reason could be due to presence of nitrates ions in the structure which could not be confirmed using available analytical techniques used in these studies. Accordingly when samples are annealed at temperatures higher then 500 ^oC, there was drastic decrease in hydroxyl ions thus destabilizing the tetragonal structure and transforming it into the monoclinic one. This transformation, however, is not reversible since the O^{2-} ions associated to the OH^- ions left the sample. Thus samples ZI and ZII showed less then 15% of tetragonal phase when calcined at 600 ^oC, with a further decrease in tetragonal phase when calcined at 700 ^oC. In each sample, tetragonal and monoclinic crystals coexisted. Their concentrations changed with the annealing temperature. The obtained results showed that the type of

zirconium precursor affected the quantity of tetragonal phase at temperature lower then 700 ^oC. The acidic pH chemically controlled condensation of zirconium alkoxide leading to stable colloidal solutions of monodispersed zirconia nanoparticles. In contrast to basic medium as discussed above at acidic pH, the protonated alkoxide species $(RO)_3Zr–OH_2^+$ predominates. The electrostatic repulsion reduces the rate of condensation relative to that of hydrolysis. This allows branching to occur, producing a strongly cross-linked gel, which during calcination transforms to zirconia with comparatively more stable structure. However, with high acid concentration, condensation is so severely hindered that only a weakly branched network can form. This gel shows poor stability and collapses to a low surface area material upon calcination. Thus sighting above advantages of controlled hydrolysis and condensation sample ZV prepared under optimal acidic condition is more stable and contains higher proportion of tetragonal zirconia as compared to sample ZI and ZII prepared under basic conditions when calcined at 600 ^oC. However further calcination at 700 ^oC leads to monoclinic phase demonstrating collapse of the structural integrity. Non-siliceous mesostructures are usually more sensitive to thermal treatments and calcination at higher temperatures result in loss of mesoporosity, structural orderness and stability, confirmed by low angle XRD and SAXS, shown in Fig. 3.16.

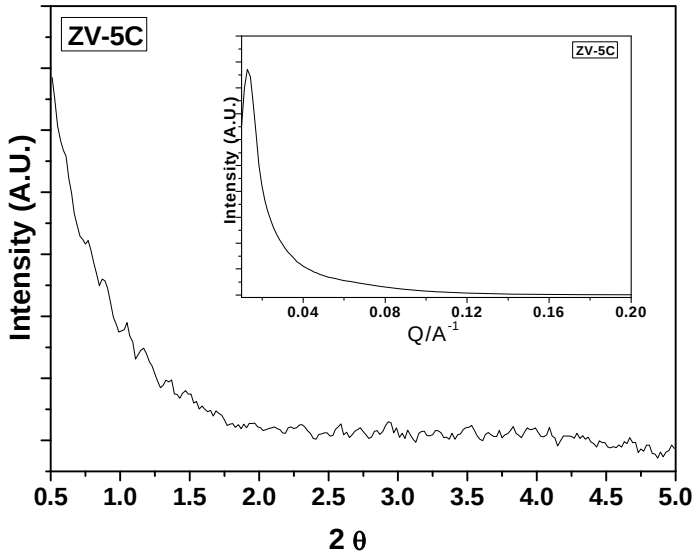

Fig. 3.16: Low angle XRD and SAXS (Inset) pattern of ZV sample prepared by modified sol-gel method and calcined at 500^oC

Hydrolysis, redox reactions or phase transformations account for this lower thermal stability. But further optimization of gel parameters for sample ZV can greatly improve

its thermal stability and porous structure. Typical low angle XRD and SAXS (inset) patterns are shown in Fig. 3.16. The relative position of the SAXS diffraction peaks on the scattering vector (q) axis can be applied to determine the structure of the mesophases [178,179]. The patterns exhibited a continuous decay without any peak, indicating the existence of a size controlled porosity. The decay of the curves clearly demonstrates that the mesoporosity of these samples differs from that of MCM or SBA type mesoporous materials having long range ordering. Although the pore size distribution corresponding to these samples exhibited very narrow shapes, several other causes, such as the tortuosity of the pores or the random position with respect to each other, could contribute to this behavior.

3.8.6. FT-Infrared Spectroscopy Studies

Vibrational spectroscopies are very useful techniques for the determination of the crystal phase for zirconia. During the studies the band observed at 470-501 cm^{-1} is attributed to Zr-O-Zr [137]. A broad absorption band at 3000–3600 cm^{-1}, is assigned to the stretching modes of OH bands related to free water (capillary pore water and surface absorbed water). A peak at 1630 cm^{-1} is due to the bending vibration of H-O-H bond, which is assigned to the chemisorbed water. In addition, all of the samples have the band at around 2360 cm^{-1} that can be attributed to the absorption of CO_2. The water loss is confirmed by FTIR for all samples as the bands related to the presence of hydroxyl group showed a decrease in the intensity with the increase of annealing temperatures, and at 700 °C they almost disappeared for all samples prepared without digestion. The first crystalline phase formed after calcination of zirconium hydroxide precipitate is usually metastable tetragonal phase, unless some carbon is present, in such case the metastable cubic phase may form. The formation of the cubic phase has been strongly associated with the presence of residual carbon [180,181]. Therefore in order to confirm the presence of tetragonal form and absence of cubic form IR spectra of samples calcined at 700^oC were compared as shown in Fig. 3.17. As seen previously the XRD peaks of cubic ZrO_2 overlap with those of tetragonal ZrO_2, resulting in the difficulty identifying the presence of cubic ZrO_2. IR spectra might be more sensitive than X-ray diffraction patterns to small changes in the crystal lattice of the phases of ZrO_2. The spectra for the

cubic phase are expected to be very simple, with broad main maximum at 530 cm^{-1}, with a pronounced shoulder near 620 cm^{-1}, while the IR spectra of tetragonal zirconia shows one broad dominant maximum around 500 cm^{-1} , the spectrum is similar to that of the cubic phase, but without the component near 620 cm^{-1} [182]. Owing to the different spectra, vibrational spectroscopy (IR and RAMAN) was used widely in the past to characterize zirconia for distinguishing cubic, tetragonal and monoclinic phases [183-188].

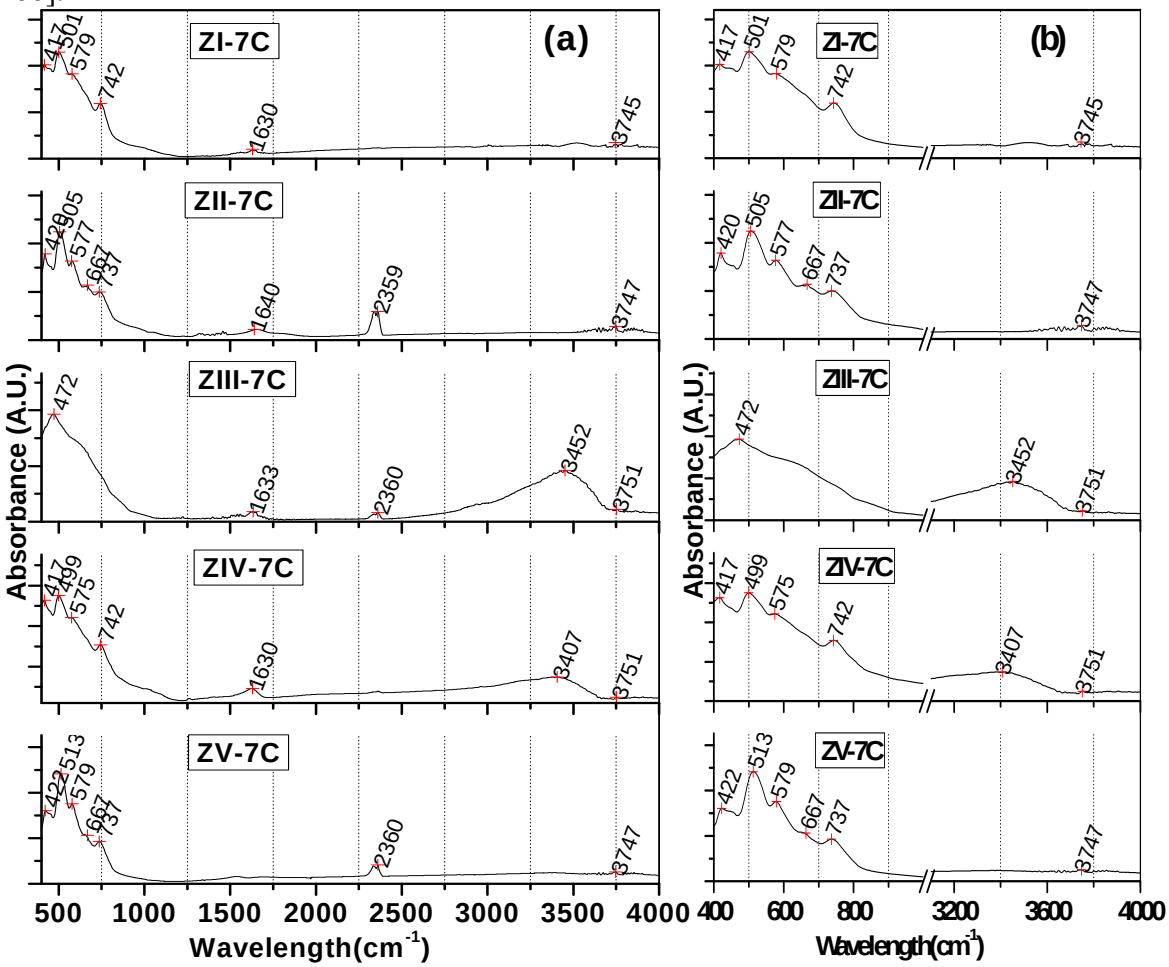

Fig. 3.17: FT-IR spectra of **(a)** zirconia samples calcined at 700°C **(b)** expanded view of the region 400-800 cm^{-1} and 3000-3800 cm^{-1}.

Actually, Raman spectra are generally well defined and very useful for characterization, while IR spectra are more difficult to apply. The IR spectrum of sample ZIII-7C shows a broad main maximum at 471 cm^{-1} and absence of peaks around 530 cm^{-1} with shoulder near 620 cm^{-1} confirms tetragonal zirconia. For the samples ZI, ZII, ZIV and ZV calcined at 700°C the OH groups were driven off as water and simultaneously the formation of the

monoclinic phase was noted by the new bands occurring around 417, 575 and 740 cm^{-1} [133,189,190,191]. The details of the band assignments of various phases and groups are tabulated in below Table 3.3.

Table 3.3: Infrared characteristic bands observed in ZrO_2 samples

Band Position (cm^{-1})	**Tentative Band Assigments**
3000-3600	O-H stretching in $ZrO(OH)_2.xH_2O$ or adsorbed water
1630	O-H bending in H_2O
1400-1418	O-H bending in $ZrO(OH)_2$
1348	asymmetric O-H stretching
417-422, 499-515, 577-579, 664-667, 737-742	Monoclinic Zr-O stretching vibration
471-501	Tetragonal Zr-O stretching vibration

FTIR spectra of as-synthesized and unwashed ZV sample had strong absorption bands associated with residual surfactant, water and solvent present after sample preparation. The absorption intensity of the methyl groups (2854 cm^{-1} and 2924 cm^{-1}) of the block copolymer surfactant (PEO-block-PPO), P123 becomes rather weak after washing, indicating that there is still some surfactant remaining in the pores. This also shows that the interaction between the Zr–O–Zr framework and surfactant is weak.

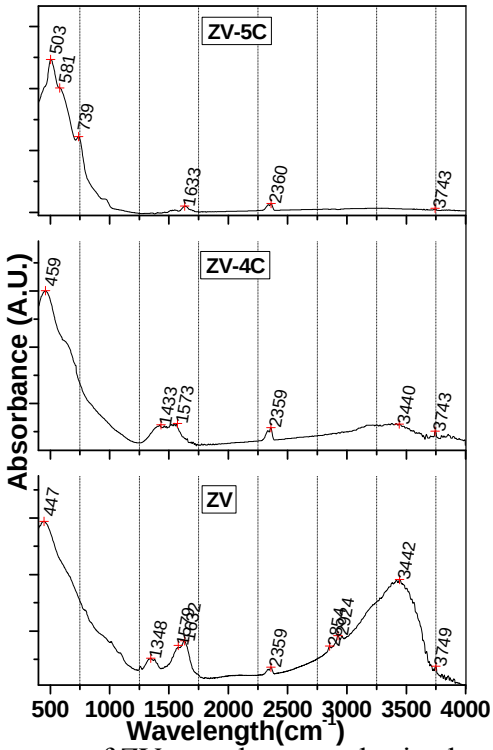

Fig. 3.18: FT-IR spectra of ZV sample as-synthesized and calcined at 500°C.

However, the peaks arising from the surfactant completely disappear after the calcinations at 500 ^oC as seen in Fig. 3.18. For samples ZII and ZV where in zirconium tert-butoxide is used as starting precursor bands at 1573 cm^{-1} and 1433 cm^{-1} attributed to C-H (-CH_3 and -CH_2–) vibrations are observed when calcined at 400^oC, these bands disappear when the temperature is above 500 ^oC. It means that to completely remove the surfactant and residual carbon species from the pores, calcination at 500 ^oC and above temperature is required which is in agreement with TG/DTA curves of the sample ZII and ZV indicating almost no weight loss after 500 ^oC. Whereas zirconia prepared via precipitation route using zirconium oxy-nitrate calcined at 400 ^oC is sufficient to convert into tetragonal phase without impurities.

3.8.7. Scanning Electron Microscopic Studies

SEM images of the ZrO_2 samples calcined at 700 ^oC are shown in Fig. 3.19. The particles of all the samples prepared are found to be agglomerated and of irregular shape and size.

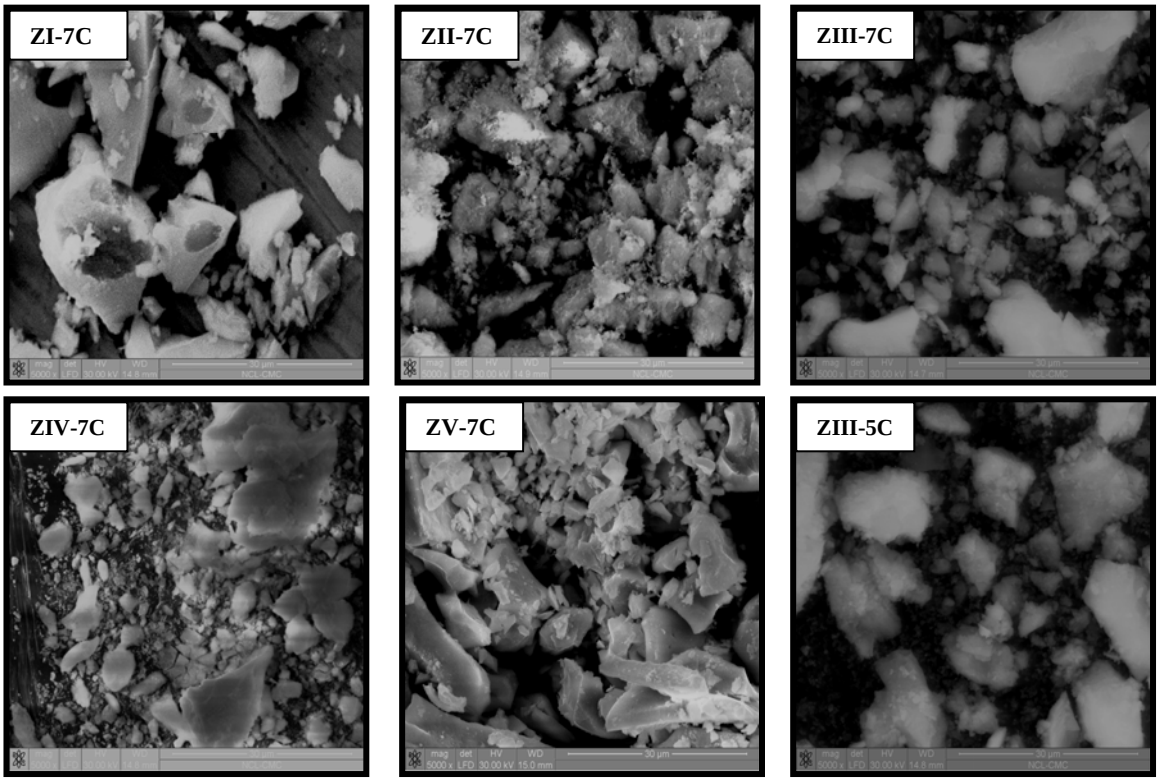

Fig.3.19: SEM images of samples ZI to ZV calcined at 700^oC and ZIII calcined at 500^oC.

The average particle size for ZI-7C and ZV-7C samples is found to be between 10 to 20 μm, while rests of the materials have particles with sizes ranging from 5 to 15 μm. Some uniformity in particle size and shape is seen for ZIII-5C sample due to lower calcination temperature. The particles of sample ZII-7C prepared via precipitation technique using ZrBt appear spongy in nature. SEM micrographs do not show any fractures in the particles although calcined at 700 °C, due to the tetragonal– monoclinic transformation of zirconium oxide which is usually seen in zirconia samples calcined at higher temperatures. In general, shape and surface properties of samples ZI-7C, ZIV-7C and ZV-7C seem to be identical, which is quite surprising even though these 3 samples are prepared in completely different manner and with different precursors. Similarly sample ZIII-7C and ZII-7C shows some identical features in their images; here also ZIII sample is prepared using ZrONit followed by digestion-d2 while sample ZII is prepared from ZrBt without digestion. Therefore in the present studies, it implies that particle morphology is neither dependent on synthesis procedure nor on starting precursor which may be due to substantial agglomeration of small crystallites.

3.9. CONSLUSIONS

In conclusion, a large number of preparation routes have been developed earlier to obtain high surface area zirconia. The role of the principal preparation variables controlling the phase composition and thermal stability, such as pH, concentration and temperature of the solution, the nature of parent zirconium salt as well as aging of the precipitate is studied. Precipitation from zirconium salts using optimized synthesis offers the most economical route, as compared to use of zirconium alkoxides or surfactants to form mesoporous zirconia. Digestion of the hydrous oxide can increase the thermal stability of the resulting zirconia considerably. It was shown that extended digestion of the precipitated gel at 80 °C for 24 h is beneficial for preparing t-ZrO_2 with a specific surface area of 90 m^2/g, which is stable up to 700 °C. Surface areas ~200 m^2/g can be obtained as long as the calcination temperature is kept below 500 ^oC. Heating to higher temperatures led inevitably to a loss in surface area. Phase transformation and stabilization was observed to be related to OH^- ions and Zr vacancies in the crystalline structure, while satisfactory explanation of the stabilization based of the critical crystallite

size is not found. Modified sol-gel synthesis shows the stabilization of tetragonal phase whereas complete phase transformation was observed in the samples prepared by precipitation method at same temperature. Irrespective of preparation method and precursor used the morphology of the particles remained same.

3.10. REFERENCES:

[1] L. Milgrom, Chemistry World, Feb 2007

[2] Ceram Research http://www.ceram.co.uk/

[3] T. Takahashi, N.Q. Minh, Science and Technology of Ceramic Fuel Cells; Elsevier: New York, 1995.

[4] J.B. Miller, E.I. Ko, Catal. Today,1997, 35, 269.

[5] M. Chidambaram, D. Curulla-Ferre, A.P. Singh, B.G. Anderson, J. Catal. 2003,220,442.

[6] W. Stichert, F. Schuth, Chemistry of Materials, 1998, 10, 2020.

[7] M. H. Bocanegra-Bernal, S. D´iaz de la Torre, J. of Material Science 2002, 37, 4947

[8] E.H. Kisi and C.J. Howard, Key Engineering Materials 1998, 153-154, 1-36.

[9] M. Yashima, M. Kakihana, K. Ishii, Y. Ikuma and M. Yoshimura, Mater. Res.1996, 11, 1410-1420.

[10] R. Srinivasan, S.F. Simpson, J.M. Harris and B.H. Davis, J. Mater. Sci. Lett.1991, 10, 352-354.

[11] D.K. Smith and H.W. Newkirk, Act Cryst. 1965, 18, 989-991.

[12] G. Skandan, C.M. Foster, H. Frase, M.N. Ali, J.C. Parker and H. Hahn,, Nanostruct. Mater. 1992, 1, 313-318.

[13] O. Ruff and F. Elbert, Z. Anorg. Allg. Chem. 1929, 180, 19-41 (In German).

[14] G.L. Clark and D.H. Reynolds Ind. Eng. Chem. 1937, 29 [6], 711-715.

[15] R. Cyprès, R. Wollast and J. Raucq, Ber. Dtsch. Keram. Ges. 1963, 40, 529-532,

[16] R.C. Garvie, J. Phys.Chem. 1965, 69, 1238-1243.

[17] S. Shukla and S. Seal, Rev. Adv. Mat. Sci. 2003, 5, 117.

[18] T. Birkby and H Hodgun, Eur. Ceram. Proc. Symp.,1989, (pub 1991), 167.

[19] D.A. Ward and E.I. Ko, Chem. Mater.,1993, 5, 956-969.

[20] R. Srinivasan, C.R. Hubbard, O.B. Cavin and B.H. Davis, Chem. Mater.,1993, 5, 27.

[21] X. Turrillas, P. Barnes, D. Häusermann, S.L. Jones and C.J. Norman, J. Mater. Res. ,1993, 8, 163-168.

[22] X. Turrillas, P. Barnes, D. Gascoigne, J.Z. Turner, S.L. Jones, C.J. Norman, C.F. Pygall and A.J. Dent, Radiat. Phys. Chem.,1995, 45, 491-508.

[23] M.A. Villa Garcia, M.C. Trobajo Fernandez and C. Otero Arean," Thermochimica Acta .,1988, 126, 33-41.

[24] T. Kosmač, V. Kraševec, R. Gopalakrishnan and M. Komac, Advances in Ceramics , 1988, 24 (Science and Technology of Zirconia III), 167-172.

[25] M. Li and Z. Chi, Advances in Ceramics.,1988, 24 (Science and Technology of Zirconia III), 243-250.

[26] R. Srini vasan, B.H. Davis, O.B. Cavin and C.R. Hubbard, J. Am. Ceram. Soc., 1992, 75, 1217-1222.

[27] M. Inoue, K. Sato, T. Nakamura, T. Inui, Catal. Lett., 2000, 65, 79–83.

[28] J. Hu, Y. Cao, J. Deng, Chem. Lett., 2001, 30, 398–400.

[29] D.J. Suh, T.J. Park, H.Y. Han, J.C. Lim, , Chem. Mater., 2002, 14, 1452–1454.

[30] J.A.Wang, M.A. Valenzuela, J. Salmones, A. Vázquez, A. Garcia-Ruiz, X. Bokhimi, Catal. Today., 2001, 68, 21–30.

[31] D.H. Aguilar, L.C. Torres-Gonzalez, L.M. Torres-Martinez, T. Lopez, P. Quintana, J. Solid State Chem., 2001, 158, 349–357.

[32] C. Su, J. Li, D. He, Z. Cheng, Q. Zhu, Appl. Catal., A Gen., 2000, 202, 81–89.

[33] P.D.L. Mercera , J.G. Van Ommen , EBM Doesburg , A.J. Burggraaf , JRH Ross, Appl Catal, 1990, 57, 127.

[34] T Yamaguchi , K Tanabe , Mater Chem Phys., 1986, 16, 67.

[35] R. Srinivasan , MB Harris , SF Simpson , De Angelis RJ, BH Davis , J Mater

Res.,1988, 3, 787 – 797.

[36] F.G.R Gimblett , A Rahman , K.S.W Sing , J Colloid Interface Sci., 1984, 102, 483

[37] A. Benedetti , G. Fagherazzi , F Pinna , S Polizzi , J Mater Sci., 1990, 25, 1473 .

[38] A Benedetti , G. Fagherazzi , F Pinna , J Am Ceram Soc.,1989.

[39] G.K. Chuah , S Jaenicke , S.A. Cheong , K.S. Chan , Appl. Catal., A 1996, 145, 267–284.

[40] G.K. Chuah , S. Jaenicke , B.K. Pong , J. Catal. 1998, 175, 80–92.

[41] K.T. Jung , A. Bell , T. J. Mol. Catal. A 2000, 163, 27–42.

[42] H.C. Wang , K.L. Lin , J Mater Sci. 1991, 26, 2501.

[43] M. Inoue, H .Kominami , T. Inui , Appl Catal A1983, 97, L25.

[44] M.L. Rojas-Cervantes , R.M. Martin-Aranda , A.J. Lopez-Peinado , J.D. de Lopez-Gonzalez , J Mater Sci, 1994, 29, 3743.

[45] E. Djurado , E. Meunier , J. Solid. State. Chem. 1998, 141, 191–198.

[46] S. Shukla , S. Seal , R. Vanfleet , J. Sol-Gel Sci. Technol. 2003, 27, 119–136.

[47] S. Shukla , S. Seal , R. Vij , S. Bandyopadhyay , J. Nanopart. Res. 2002, 4, 553–559

[48] S. Shukla , S. Seal , S. Int. Mater. ReV. 2005, 50, 45–64.

[49] S. Shukla , S. Seal , J. Phys. Chem. B 2004, 108, 3395–3399.

[50] S. Shukla , S. Seal , R. Vij , S. Bandyopadhyay , Z. Rahman , Nano Lett. 2002, 2, 989–993.

[51] S. Shukla , S. Seal , ReV. AdV. Mater. Sci. 2003, 4, 123–126.

[52] J. Joo, T. Yu , Y.W. Kim , H.M. Park , F. Wu ,J.Z. Zhang , T.J. Hyeon , Am. Chem. Soc. 2003, 125, 6553–6557.

[53] Q. Sun , Y. Zhang , J. Deng , S. Chen , D. Wu , Appl. Catal., A 1997, 152, L165-L171.

[54] S.G. Liu, H. Wang, J.P. Li, N. Zhao, W. Wei, Y.H. Sun, Materials Research Bulletin, 2007, 42, 171–176.

[55] J.Y. Zheng, J.B. Pang, K.Y. Qiu, Y. Wei, Microporous Mesoporous Mater., 2001,

49, 189–195.

[56] J.L. Blin, R. Flamant, B.L. Su, Int. J. Inorg. Mater., 2001, 3, 959–97.

[57] M. Q. B. Takmeel, S. K. Mohanty, A. Mondal and B. B. Nayak, PS- 44, International Conference on Advanced Functional Materials, December 2009, 9-10, (Trivandrum, India).

[58] L.L. Hench , J.K. West , Chem. Rev. 1990, 90,35-40.

[59] O. Lev , et al. Analytical Chemistry. 1995, 67, 22A-30A.

[60] C.J. Brinker and G.W. Scherer, Sol-Gel Science: The Physics and Chemistry of Sol-Gel Processing (Academic Press, Inc.: New York, 1990).

[61] C.N. Satterfield, Mass Transfer in Heterogeneous Catalysis, MIT Press, Cambridge, MA, 1970.

[62] T. Yamaguchi , Catal. Today, 1994, 20, 199.

[63] K. Tanabe. M. Misono, Y. Ono and H. Hattori, New Solid Acids and Bases, Kodansha-Elsevier, Tokyo-Amsterdam, 1989, 4.

[64] C.J. Brinker, G.W. Xcherer, Sol-gel Science, academic Press, New York, 1990

[65] C.T. Kresge, M.E. Leonowicz, W.J. Roth, J.C. Vartulli, J.S. Beck, Nature, 1992, 359, 710.

[66] J.S. Beck, J.C. Vartulli, W.J. Roth, M.E. Leonowicz, C.T. Kresge, K.D. Schmitt, C.T.W. Chu, D.H. Olson, E.W. Sheppard, S.B. McCullen, J.B. Higgins, J.L. Schlenker, J. Am. Chem. Soc., 1992, 114, 10834.

[67] D.M. Antonelli, J.Y. Ying, Angew. Chem., Int. Ed. Engl., 1995, 34, 2014.

[68] H. Yoshitake, T. Sugihara, T. Tatsumi, Chem. Mater., 2002, 14, 1023.

[69] J.A. Knowles, M.J. Hudson, J.Chem. Soc., Chem. Commun. 1995, 2083.

[70] U. Ciesla, S. Schacht, G.D. Stucky, K.K. Unger, F. Schuth, Angew. Chem. Int. Ed. Engl., 1996, 35, 541.

[71] U. Ciesla, M. Froba, G.D. Stucky, K.K. Unger, F. Schuth, Chem. Matet., 1999, 11, 227.

[72] J.L. Blin, R. Flamant, B.L. Su, Inter. J. Inorg. Mater., 2001, 3, 959.

[73] N. Ulagappan, V.N. Raju, C.N.R. Rao, Chem. Commun., 1996, 2243.

[74] D.M. Antonelli, Adv. Mater., 1999, 11, 487.

[75] J. S. Reddy, A. Sayari, Catal. Lett., 1996, 38, 219.

[76] E. Zhao, S.E. Hardcastle, G. Pacheco, A. Garcia, A.L. Blumenfeld, J.J. Fripiat, Micropor. Mesopor. Mater., 1999, 31, 9.

[77] G. Pacheco, E. Zhao, A. Garcia, A. Sklyarov, J. Fripiat, Chem. Commun., 1997, 491

[78] M.S. Wong, J.Y. Ying, Chem. Mater., 10, 1998, 2067.

[79] Y.Y. Huang, T.J. McCarthy, W.M.H. Sachtlet, Appl. Catal. A: Gen., 1996, 148, 135

[80] H.R. Chen, J.L. Shi, W.H. Zhang, M.L. Ruan, D.S. Yan, Micropor. Mesopor. Mater., 2001, 47, 173.

[81] D.J. Mcntosh, R.A. Kydd, Micropor. Mesopor. Mater., 2000, 37, 281.

[82] G. Larsen, E. Lotero, M. Nabity, L.M. Petkovic, D.S. Shobe, J. Catal.,1996, 164, 246, 134-147.

[83] B. Lee, D.L. Lu, J.N. Kondo, K. Domen, J. Am. Chem. Soc., 2002, 124,11256.

[84] D.M. Antonelli, J.Y. Ying, Chem. Mater., 1996, 8, 874.

[85] S.A. Bagshaw, T.J. Pinnavaia, Angew. Chem. Int. Ed. Engl., 1996, 35, 1102.

[86] P. Liu, J. Liu, A. Sayari, Chem. Commun., 1997, 577.

[87] K.G. Servin, T.M. AbdeFattah, T.J. Pinnavaia, Chem. Commun., 1998, 1471.

[88] Z. Tian, W. Tong, J. Wang, N. Duan, V.V. Krishnan, S.L. Suib, Science, 1997, 276, 926.

[89] P. Yang, D. Zhao, D.I. Margolese, B.F. Chmelka, G.D.Stucky, Nature, 12, 1998, 396

[90] G. Pacheco, E. Zhao, A. Garcia, A. Sklyaro, JJ. Fripiat, J Mater Chem.,1998, 8, 219.

[91] Ne´ F, F. Testard, T. Zemb, I. Grillo, Langmuir, 2003, 19, 8503-8510.

[92] D.M. Antonelli, Adv. Mater., 1999, 11, 487.

[93] E. Zhao, S.E. Hardcastle, G. Pacheco, A. Garcia, A.L. Blumenfeld, J.J. Fripiat, Micropor. Mesopor. Mater., 1999, 31, 9.

[94] I. Parvulescu, H. Bonnemann, V. Parvulescu, B. Endruschar, A.Ch.W. Rufinska, B. Tesche, G. Poncelet, Appl. Catal. A: Gen., 2001, 214, 273.

[95] R. Srinivasan and B.H. Davis, Catal. Lett., 1992, 14, 165.

[96] M. Henry, J.P. Jolivet and J. Livage, in: Ultrastructure Processing of Advanced Materials, eds. D.R. Uhlmann and D.R. Ulrich, (Wiley, New York), 1992, 23.

[97] J.P. Jolivet, De la Solution `a l'Oxyde (CNRS, Paris), 1994, 174.

[98] T.C.W. Mak, Can. J. Chem., 1968, 46, 3491.

[99] A. Singhal, L.M. Toth, J.S. Lin and K. Affholter, J. Am. Chem. Soc., 1996, 118, 11529.

[100] A. Clearfield, Rev. Pure & Appl. Chem., 1964, 14, 91.

[101] P. Afanasiev , A. Thiollier , M. Breysse and J.L. Dubois, Topics in Catalysis, 1999, 8, 147–160.

[102] M. Rezaei, S. M. Alavi , S. Sahebdelfar, Zi-Feng Yan, J Porous Mater, 2008, 15, 171 –179.

[103] M. Rezaei, S.M. Alavi, S. Sahebdelfar, Zi-Feng Yan, Powder Technology, 2006, 168, 59–63

[104] K.L. Lin and H.C. Wang, J. Mater. Sci. Lett., 1989, 8, 49.

[105] M.J. Hudson and J.A. Knowles, J. Mater. Chem., 1996, 6, 89-95.

[106] G. Larsen, E. Lotero, M. Nabity, L.M. Petkovic and D.S. Shobe, J. Catal., 1996, 164, 246.

[107] U. Ciesla, M. Fro¨ba, G. Stucky, F. Schu¨th, Chem Mater, 1999, 11, 227.

[108] V.I. Parvulescu, V. Parvulescu, U. Endruschat, Ch. W. Lehmann, P.Grange, G. Poncelet, H. Bonnemann, Meso. And Micro. Mat. , 2001, 44-45, 221-226.

[109] B.Tian, H.ang, X.Liu, S.Xie, C.Yu, J. Fan, Bo Tu and Dongyuan Zhao, Chem. Commun. , 2002, 1824–1825.

[110] D. Zhao, Q. Huo, J. Feng, B. F. Chmelka, and G. D. Stucky J. Am. Chem. Soc. 1998, 120, 6024-6036

[111] J. Sun, J. A. Moulijn, K. C. Jansen, Th. Maschmeyer, and M. O. Coppens Adv. Mater., 2 March 2001, 13, 5.

[112] P. Fulvio , S. Pikus, M. Jaroniec Journal of Colloid and Interface Science, 2005, 287, 717–720.

[113] S.S. Jada and N.S. Peletis, J. Mater. Sci. Lett.,1989, 8, 243-246.

[114] J. Livage, K. Doi, C. Mezieres, J Am Ceram Soc., 1968, 51, 349.

[115] G.T. Mamott, P. Barnes, S.E. Tarling, S.L. Jones, C.J. Norman, J Mater Sci., 1991, 26,4054.

[116] G.M. Pajonk, Catal Today, 1997, 35, 319.

[117] T.Y. Tseng, C.C. Lin and J.T. Liaw, J. Mater. Sci., 1987, 22, 965.

[118] J.P. Jolivet, Metal oxide chemistry and synthesis. Wiley, Chichester, 2000.

[119] S. Jaenicke, G. K. Chuah, V. Raju, Y. T. Nie, Catal Surv Asia, 2008, 12, 153–169.

[120] Jr.R.P. Denkewicz, K.S. TenHuisen, and J.H. Adair, J. Mater. Res., 1990, 5, 2698.

[121] P.D.L. Mercera, J.G.Van Ommen, E.B.M. Doesburg, A.J. Burggraaf, and J.R.H. Ross, Appl. Catal., 1991, 78, 79.

[122] G. Aguila, S. Guerrero, F. Gracia, P. Araya, Appl Catal A, 2006, 305, 219.

[123] G.A. Carter, R.D. Hart, M.R. Rowles, C.,E. Buckley, M.I. Ogden Powder Technol., 2009, 191, 218.

[124] Y. Murase, E. Kato, J. Am. Ceram. Soc., 1979, 62, 527.

[125] Y. Murase, E. Kato, J. Am. Ceram. Soc., 1983, 66, 196.

[126] J.C. Duchet, M.J. Tilliette, D.Cornet, Catal Today, 1991, 10, 507.

[127] H.H. Kung, E.I. Ko, Chem Eng J, 1996, 64, 203.

[128] B.E. Yoldas, J Am Ceram Soc., 1982, 65, 387.

[129] B.E. Yoldas, J Mater Sci., 1986, 21, 1080.

[130] J. Mrowiec-Białon, L. Pajak, A.B Jarzebski, A.I. Lachowski, J.J. Malinowski, J Non-Cryst Solids, 1998, 225, 115.

[131] D.J. Suh, T.J. Park, Chem Mater, 1996, 8, 509.

[132] C. Sto¨cker, A. Baiker, J Non-Cryst Solids, 1998, 223, 165.

[133] A. Srivastava And M.K. Dongare , Materials Letters 1981, 5, 3.

[134] R. Ramamoorthy, D. Sundararaman, S. Ramasamy, Journal of European Ceramic Soc., 1999, 19, 1827- 1833

[135] G. K. Chuah, S. Jaenicke and T. H. Xu, Surface and Interface Analysis, 1999, 28, 131-134.

[136] B. Ksapabutr, Erdogan Gulari, Sujitra Wongkasemjit, Powder Technology, 2004, 148, 11-14.

[137] Beena Tyagi, Kalpesh Sidhpuria, Basha Shaik, and Raksh Vir Jasra Ind. Eng. Chem. Res., 2006, 45, 8643-8650.

[138] M. Tahmasebpour, A.A. Babaluo, M.K. Razavi Aghjeh, Journal of the European Ceramic Society, 2008, 28, 773–778.

[139] M.M. Rashad, H.M. BaioumyJournal of materials processing technology, 2008, 195, 178– 185.

[140] AIP Conf. Proc., 2008, 1063, 206.

[141] Y. Cao, J. Hu, Z. Hong, J. Deng, and K. Fan. Catal. Lett., 2002, 81, 107-112.

[142] K. Cassiers, T. Linssen, K. Aerts, P. Cool, O. Lebedev, G. Van Tendeloo, R. Van Grieken, and E. F. Vansant. J. Mater. Chem., 2003, 13, 3033-3039.

[143] N. L. Wu and T. F. Wu, J. Am. Ceramic. Soc., 2000, 83, 3225.

[144] J. Liang, X. Jiang, G. Liu, Z. Deng, J. Zhuang, F. Li, Y. Li, Mater. Res. Bull., 2003, 38, 161.

[145] H .Zhu, D. Yang, L. Zhu, J. Amer. Ceram. Soc., 2007, 90, 1334.

[146] R. Srinivasan, L. Rice, B. H. Davis, J. Am. Ceram. Soc., 1990, 73, 3528.

[147] F. J Berry, S. J. Skinner, I. M. Bell , R. J. H. Clark, C. B. Ponton, J. Sol. State Chem., 1999, 145, 394.

[148] S.D.Ramamurthi, Z. Xu, D.A. Payne, J. Am. Ceram. Soc., 1990, 73 [9], 2760-2763.

[149] C.J. Norman, P.A. Goulding, I. McAlpine, Catal Today, 1994, 20, 313−322.

[150] P. Jakubus, A. Adamski, M, Kurzawa, Z. Sojka , J Therm Anal Calorim , 2003, 72, 299−310.

[151] A. Adamski, P.Jakubus, Z. S. Nukleonika. 2006, 51(Supplement 1), S27−S33

[152] K. S. Chan, G. K. Chuah, S. Jaenicke, Journal Of Materials Science Letters, 1994, 13, 1579-I581

[153] Lu Daling, T Katou, K. Domen, Chem. Mater., 2005, 17, 632–637.

[154] M. Niederberger, G. Garnweitner, Chem. Eur. J. 2006,

[155] L. R. S. Rice and B. H. Davis, J. Am. Ceram. Soc., 1990, 14, 3528.

[156] D. Yapryntseva, A. E. Baranchikovb, N. N. Gubanovac, V. K. Ivanovb, and Yu. D. Tret'yakova, Inorganic Materials, 2012, 48, 5, 494–499.

[157] D Zhao, JFeng, Q Huo, N Melosh, G H.Fredrickson, BF. Chmelka,G D. Stucky, Science , 1998, 279, 548.

[158] P. Yang, D. Zhao, D.I. Margolese, B. F. Chmelka, and G D. Stucky , Chem. Mater. 1999, 11, 2813-2826.

[159] K. Matsui, M. Ohgai, J Am Ceram Soc., 1997, 80, 1949−1956.

[160] S.J. Gregg, K.S. Sing, W. Adsorption, Surface Area and Porosity, 2nd ed.; Academic Press: New York, 1982.

[161] M. M. Dubinin. In: Cadenhead DA, editor, Progress in surface and membrane science, New York: Academic Press, 1975, 9, 1.

[162] J. L. Shi, C. W. Lu, C. L. Kuo, Z. X. Lin & T. S. Yen, Ceramics International, 1992, 18, 155-159.

[163] J.R. Sohn, M.Y. Park, Langmuir, 1998, 14, 6140.

[164] A. Clearfiled, G.P.D. Serrette, A.H. Khazi-Syed, Catal Today, 1994, 20, 195−312.

[165] S.G. Chen, Y.S.Yin, D.P. Wang, J Mol Struct, 2004, 690, 181−187.

[166] A. Clearfield, P.A. Vaughan, Acta Crystallogr, 1956, 9, 555−558.

[167] P. Southon, Ph.D Thesis,University of Technology, Sydney, November 2000

[168] K. Matsui and M. Ohgai, J. Am. Ceram. Soc.,2001, 84, 2303–12.

[169] V. Luca, E. Drabarek, C.. S. Griffith, and T. L. Hanley, Chem. Mater. 2010, 22, 3832−3842

[170] Li. Weizhen, H. Huang, Li. Hongjia, W. Zhang, and H. Liu, Langmuir, 2008, 24, 8358-8366.

[171] S. Gutzov, J. Ponahlo, C.L. Lengauer and A. Beran, J. Am. Ceram. Soc.,1994, 77 ,1649-1652.

[172] F.C. Wu and S.C. Yu, J. Mater. Sci., 1990, 25, 970-976.

[173] M.C. Silva, G. Trolliard, O. Masson, R. Guinebretiere, A. Dauger, A. Lecomte and B. Frit, J. Sol-Gel Sic. Tech., 1997, 8, 419-424.

[174] H. Saricimen, Powder Technol. 27, 23 (1980). // P. E. D. Morgan, J. Am. Ceram. Soc.,1984, 67, C-204.

[175] X. Bokhimi, A. Morales, O. Novaro, M. Portilla, T. Lo« pez,à F. Tzompantzi,à and R. Go«mez, Journal Of Solid State Chemistry, 1998, 135, 28.

[176] P.J Moles, M. Ikeda, C.J. Norman,Stud Surf Sci., 1995, 92, 419.

[177] E. Bernstein, M.G. Blanchin, R. Ravelle-Chapiu, J. Rodriguez- Carvajal, J Mater Sci., 1992, 27, 6519.

[178] P. Holmqvist, P. Alexandridis, B. Lindman, J. Phys. Chem.,1998, B 102, 1149.

[179] T. Hahn (ed.), International tables for crystallography, vol. A, D. Reidel Publishing Company: Dortrecht, 1983.

[180] H. Preiss, L.M. Berger and K. Szulzewski, Carbon, 1996, 34,109-119.

[181] A. C. Geiculescu and H.G. Spencer, J. Sol-Gel Sci. Tech., 1999, 14, 1-16.

[182] E. F. Lo´pez, V. S. Escribano, M. Panizza, M. M. Carnascialic, and G. Busca, J. Mater. Chem., 2001, 11, 1891–1897 .

[183] C. M. Phillippi and K. S. Mazdiyasni, J. Am. Ceram. Soc., 1971, 54, 254.

[184] D. P. C. Thackeray, Spectrochim. Acta, Part A, 1974, 30, 549.

[185] C. H. Perry, D. W. Liu and R. P. Ingel, J. Am. Ceram. Soc., 1985, 68, C184.

[186] T. Hirata, H. Zhu, T. Furubayashi and I. Nakatani, J. Am. Ceram. Soc., 1993, 76, 1361.

[187] T. Hirata, E. Asari and M. Kitajima, J. Solid State Chem., 1994, 110, 201.

[188] C. G. Kontoyannis and G. Carountsos, J. Am. Ceram. Soc., 1994, 77, 2191

[189] N.T. McDevitt and W.L. Baun, Spectrochim. Acta, 1964, 20, 799.

[190] D. Mao, G. Lu, Q. Chen, Applied Catalysis A: General, 263, 83-89.

[191] It. Cypres, R. Wollast. and J. Raucq, Ber. Deut. Keram. Ges..1963, 40, 527.

CHAPTER – 4

MOLYBDENUM OXIDE SUPPORTED ZIRCONIA

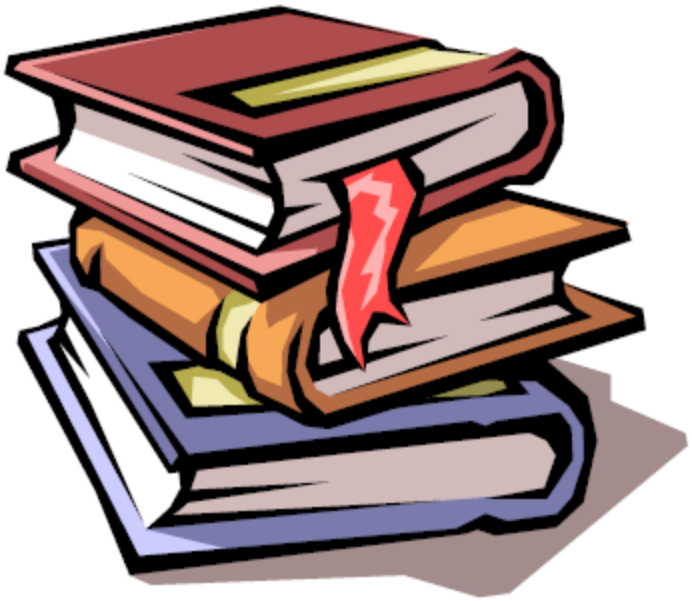

4.1. INTRODUCTION

The development of environmentally friendly solid catalysts for the synthesis of fine chemicals and pharmaceuticals is becoming an area of growing interest because the use of heterogeneous catalytic processes allows easier separation, recovery and recycling of the catalysts from the reaction mixtures [1,2,3]. To maintain economic viability, a suitable heterogeneous system should also display activities and selectivity's comparable or superior to the existing homogeneous route [4]. However, most of them require rather complicated preparation of the catalysts or the use of expensive toxic solvents to facilitate heat and mass transfer in liquid-phase reaction systems. As a clean route for organic synthesis, the ultimate goal of many heterogeneous catalytic processes is to eliminate the use of solvents. Among heterogeneous catalysts employed, heteropoly acids, zeolites, sulfated metal oxides, clays and composite oxides are the most widely investigated catalysts. Metal oxides based solid acid catalysts offer several advantages over microporous and mesoporous based catalysts. These are active over a wide range of temperatures and more resistant to thermal excursions. During the past decade there has been an increasing interest to study the effect of various elements upon the textural, structural and catalytic properties of composite oxide catalysts. Among them, WO_3 and MoO_3 based oxides are the most extensively investigated catalysts. These oxides show strong surface acidic and redox properties and varied surface molecular structures [5]. Among different supported MoO_3 materials, supported MoO_3-/ZrO_2 catalyst is the most promising heterogeneous catalyst used in extremely important industrial reactions. The MoO_3-/ZrO_2 catalyst have also been investigated for several industrial applications such as cumene dealkylation, ethanol conversion, ammoxidation of picoline and toluene, synthesis of methoxymethyl benzene, methylcyclopentane conversion, methanol oxidation reactions and methane combustion reaction [6-11]. Recently, it was observed that MoO_3-/ZrO_2 materials exhibit good catalytic properties in some vital organic reactions [5,12,13,14,15]. The high flexibility of supported Mo-catalysts is related to the different molecular structures that molybdenum species can simultaneously posses when supported and to the ability of Mo atoms to assume various oxidation states, depending on the synthesis procedure and post-treatment. Molybdenum species supported on a variety of oxide supports such as SiO_2, Al_2O_3, and TiO_2 etc have been extensively

investigated in the recent past [16-21]. The dispersion of molybdenum oxide, its oxidation state, and structure strongly depend on the support. In turn, all these factors are likely to affect the catalytic properties. In the recent past, zirconia has attracted considerable interest because of its potential use as a catalyst support as well as a catalyst. [22-34]. Porous ZrO_2 is attracting increasing interest as a useful catalytic support partly due to its reducing and oxidizing surface properties, mechanical properties, acid-base nature [22,35], and also because it is chemically more stable than the classic materials such as γ-alumina and silica [36]. Different methods have been used to synthesize such catalysts based on zirconia modified by molybdenum oxides, aimed at optimized materials, especially those characterized by high surface area, low contents of impurities, and a significant proportion of tetragonal zirconia [8,37]. These aspects are of considerable importance due to their effects on the crystalline structure, which determines the properties of the oxides. The crystal phase of ZrO_2 (monoclinic and/or tetragonal) strongly influences the catalyst activities and selectivitys [38-41]. These marked differences in catalytic performance clearly necessitate high surface area and the existence of pure t-ZrO_2 phase in the catalyst, for which a variety of synthesis approaches have been accordingly employed to date. Unlike m-ZrO_2, at room temperature t-ZrO_2 is meta-stable and tends to transform to m-ZrO_2 upon thermal treatment or contact with water vapor [42,43]. Stabilization of the surface area and meta-stable tetragonal phase can be accomplished by manipulating the preparation variables. In this regard pH, starting precursor, temperature and time of digestion of the precursor etc seem to be the key parameters to obtain high surface samples which are stable after calcination at temperatures above 600 ^oC [44,45]. Stabilization of the tetragonal phase of ZrO_2 has also be achieved by doping a second oxide on the zirconia grain surface [46,47,48], which is often accomplished with the co-precipitation, wet-impregnation and thermal-dispersion methods [49]. Zhao et al. have found that the surface areas of several ZrO_2-supported catalyst systems such as MoO_3, WO_3, CuO, Fe_2O_3 and NiO etc, are much larger that that of pure ZrO_2 treated at the same temperature [46]. Similar results have been obtained by Arata et al. for similar catalyst systems [47,48]. Deposition of MoO_3 and WO_3 on ZrO_2 increases acidic character of zirconia, and there are even claims that it can lead to super-acidity [50,51]. These facts seem to indicate that t-ZrO_2 supported catalysts with high

surface area could be obtained at different preparation conditions. However, most of these synthesis routes to prepare high surface area t-ZrO_2 are complicated and require tedious procedures, close control of reaction parameters such as temperature, pressure, and pH, or the use of relatively expensive and zirconium alkoxides. In this context, simple, easy synthesis routes are highly desired, especially for the practical applications of t-ZrO_2 with high surface area. Inexpensive and nontoxic inorganic zirconium salts (e.g., zirconyl nitrate) with facile synthesis procedures were used for initial ZrO_2 support preparation, and these pure zirconium hydroxide precursors are then used to prepare ZrO_2 supported MoO_3 catalysts. The majority of MoO_3/ZrO_2 catalysts described in the literature were conventionally synthesized by wet impregnation of the zirconia support with an aqueous solution of ammonium hepta molybdate $(NH_4)_6Mo_7O_{24}$ (AHM), [7,52,53,54], but to the best of our knowledge, none of them have optimized the synthesis parameters in order to have high surface area with t-ZrO_2. We are therefore particularly interested in the preparation conditions of MoO_3/ZrO_2 catalysts obtained by the impregnation method, as some detailed studies for co-precipitation method have already been reported [8]. The purpose of this work is to investigate the thermal stability, structural and physico-chemical properties of molybdenum oxide on zirconia surface as a function of molybdenum loading, digestion time, surfactant addition, calcination temperature, synthesis method etc. Although there are investigations on the catalytic applications of MoO_3–$/ZrO_2$ for industrially important reactions, the applicability of this important material to organic synthesis involving biologically important molecules is yet to be explored.

For the last 50 years, the synthesis of chalcones and their derivatives have been a research topic of great interest. Every year, several thousands of chalcones and chalcones derivatives have been synthesized in the research laboratories. The sustained interest in chalcones is due to their wide range of biological activity. The Claisen-Schmidt condensation (CSC) reaction is extremely useful and important method for the synthesis of vide variety of biologically active chalcone-structure compounds for over a century due to its simplicity and efficiency. Chalcones constitute an important group of natural products and some of them possess anticancer, anti-malarial, anti-microbial, anti-tuberculosis, anti-hyperglycemic and anti-inflammatory activities [55-62]. Chalcones also

serve as precursors for the synthesis of different classes of flavonoids [63,64]. The name "Chalcones" was given by Kostanecki and Tambor [65]. These compounds are also known as benzalacetophenone or benzylidene acetophenone. In chalcone, two aromatic rings are linked by an aliphatic three carbon chain. The Claisen-Schmidt condensation (CSC) is an important C-C bond forming reaction for the synthesis of chalcones [66]. Chalcones are α,β-unsaturated ketone containing the reactive ketoethylenic group "-CO-CH=CH-". These are colored compounds because of the presence of the chromophore "-CO-CH=CH-", which depends in the presence of other auxochromes. Traditionally, synthesis of these chalcones was carried out in basic (NaOH, KOH) or acidic ($AlCl_3$, HCl) media under homogeneous conditions [67-71]. The formation of chalcone by the acid catalyzed condensation of acetophenone and benzaldehyde has been studied earlier [72,73]. The acid catalyzed methodologies also include the use of $Zn(bpy)(OAc)_2$, $TiCl_4$, $Cp_2ZrH_2/NiCl_2$, and $RuCl_3$. Recently $BF_3{\cdot}Et_2O$, $SOCl_2/EtOH$, and Brønsted acidic ionic liquid catalysts have been used to effect this reaction [74-81]. The above reported procedures have several disadvantages such as poor selectivity, long reaction times, generation of wastes, difficulty in the catalyst preparation, use of special apparatus, costly reagents/solvents and laborious separation techniques make these catalysts practically inconvenient. Heterogeneous solid basic catalysts like magnesium oxide, potassium carbonate, hydrotalcites, barium hydroxide, aminopropyl-functionalized SBA-15 mesoporous silica, alumina and natural phosphates modified with $NaNO_3$ or KF and alkali exchanged zeolites have been used as alternatives for the conventional homogeneous alkaline hydroxides [4,82,83]. Even though, the solid basic catalysts provide advantages due to its heterogeneous nature, the major drawback is associated with the poor selectivity to chalcone due to the competitive Cannizzaro reaction of the aldehyde and other undesired side reactions like Michael addition at the strong basic sites [84]. To improve the selectivity in synthesis of chalcones, solid acid catalysis has been tried, but only few have been reported [85,86,87]. It is also known [88] that acid zeolites can catalyze crossed Aldol reactions of an aliphatic aldehyde with formaldehyde. Although zeolites are quite reliable, activities of these materials are much lower than the conventional homogeneous acids due to pore blocking and hydration. In the present work we report the use of MoO_3-/ZrO_2 catalysts for CSC of benzaldehyde (BA) with

acetophenone (AP) under solvent-free conditions to give Chalcone. We feel that our results will extend the scope of molybdenum oxide supported zirconia solid acid catalyst in organic synthesis involving biologically important molecules.

4.2. RESULT AND DISCUSSION

4.2.1. Synthesis of Catalysts

A series of MoO_3-ZrO_2 catalysts with different MoO_3 loadings (1–40 wt%) were prepared by modified co-precipitation method. Although we studied samples containing molybdenum oxide up to about 40 wt.%, we focused our attention on catalysts with loading in the range 15-30 wt%, because they are reported to show highest activity, stability, surface area and acidity [7,53,54,87]. Further we have narrowed down to 15 wt% MoO_3 for the preparation and optimization of the impregnation catalyst, from the initial characterization data. Three impregnation MoO_3/ZrO_2 catalysts were prepared by varying the synthesis parameters, the details of the preparation procedures and sample designation is given in Chapter-2, Section 2.3.2. Where ever possible in this chapter for simplicity we have denoted "MoO_3/ZrO_2" for impregnation and "MoO_3-ZrO_2" for co-precipitation. Please note the difference "/" for impregnation and "–" for co-precipitation, while the denotation "MoO_3-/ZrO_2" in general means catalyst, prepared via impregnation and co-precipitation. The particulars such as samples designation, digestion time, temperature, synthesis method of the MoO_3-/ZrO_2 samples studied in this chapter is given in Table 4.1.

Table 4.1: Details of MoO_3-/ZrO_2 catalyst prepared with different MoO_3 loadings (10–30 wt%) via co-precipitation method and 15 wt% MoO_3 via impregnation method.

Sr. No.	Sample Designation	Synthesis Method	Surfactant used	Digestion pH/Time/Temp	% Weight Loss [TG]
1	10MZcp-I	Co-Precipitation	Nil	12/12 h/80 ^oC	ND*
2	15MZcp-I	Co-Precipitation	Nil	12/12 h/80 ^oC	25.69
3	20MZcp-I	Co-Precipitation	Nil	12/12 h/80 ^oC	ND*
4	30MZcp-I	Co-Precipitation	Nil	12/12 h/80 ^oC	28.89
5	15MZim-I	Impregnation	Nil	12/12 h/80 ^oC	27.59
6	15MZim-II	Impregnation	Nil	12/24 h/80 ^oC	23.99
7	15MZim-III	Impregnation	P123	12/12 h/80 ^oC	26.51

ND*-Not Determined

The catalysts used in the study were characterized by a number of techniques, and these results are presented and discussed in this following section.

4.2.2. TG-DTA Analysis

The thermal behavior of un-calcined MoO_3-/ZrO_2 samples is represented in Fig. 4.1.

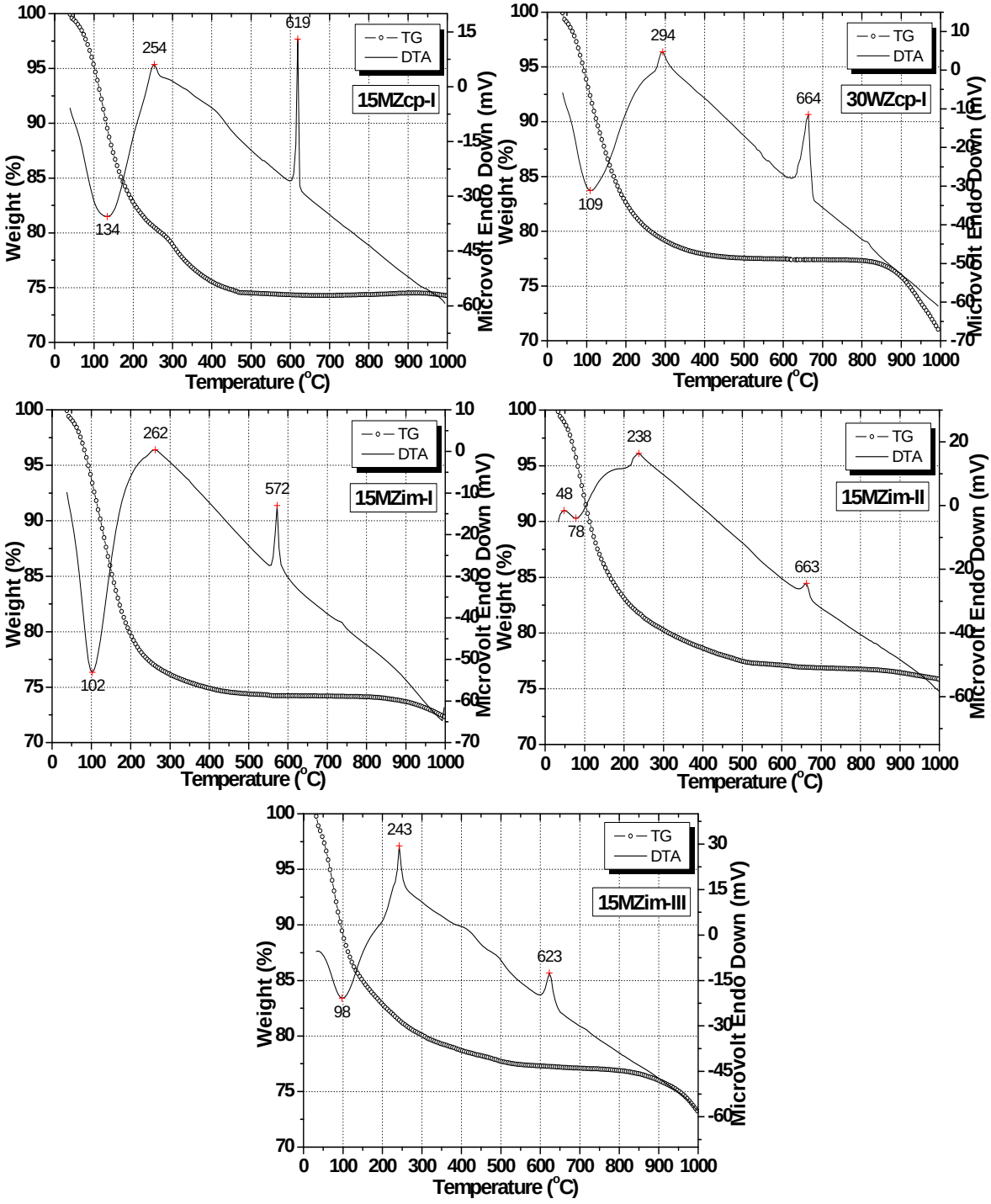

Fig. 4.1: TG-DTA curves of various as-synthesized MoO_3-/ZrO_2 samples (Analysis carried out in air atmosphere with heating rate 10 °C/min.)

Irrespective of the preparation method the weight loss for MoO_3-/ZrO_2 samples was found to be between 25 to 30 wt% according to TG curves, actual values are given in Table 4.1. Astoundingly sample 15MZim-III prepared using impregnation technique with the use of surfactant shows a weight loss of only 26.5 %, which is very low for the materials, prepared using surfactant. The reason for the lower weight loss, is due to washing given to zirconium hydroxide precursor used for sample 15MZim-III, before impregnation was done, thereby loosely bound surfactant could not been retained in the structure. In DTA profiles positive peaks indicate exothermic processes whereas negative peaks represent endothermic processes. One broad endothermic peak was detected between 50-200 ^oC which was likely due to removal of adsorbed water. In fact, when samples were dried at 110 ^oC for few hours prior to DTA measurements, the intensity of the peak reduced drastically. There is continuous step by step elimination of water from these types of materials. After the initial loss of physically absorbed water, terminal water and hydroxy groups are lost approximately between 100 and 200 °C along with limited oxolation of hydroxy bonds in the first stage. The second stage was thought to involve loss of 'inner water' and non-bridging hydroxy groups between 200 and 400 °C. The third stage is final oxolation of all remaining hydroxy bridges immediately before crystallization of tetragonal from amorphous hydroxide. For samples of low MoO_3 loading, namely less then 20 wt.%, minute weight loss was observed above 450 ^oC corresponding to the decomposition of $Zr(MoO_4)_2$, while the samples containing high MoO_3 loading equal or exceeds 25 wt.% exhibits a sharp weight loss at 900 ^oC in TG curve associated with the decomposition of $Zr(MoO_4)_2$. It was reported that, this is may be due to melting of molybdenum oxide, after which, a progressive decrease in weight loss is observed due to the evaporation of this phase [88,89]. A separate exothermic peak assigned for the formation of $Zr(MoO_4)_2$ around 500 ^oC and above temperatures could not seen in the DTA curves but this phase was observed in XRD, IR and RAMAN data, this peak might have got merged with crystallization peak of tetragonal zirconia [53]. Two exothermic peaks are also present in all samples. The first peak occurs around 200-400 ^oC for all samples is probably the decomposition of organics residues, trace amounts ammonium nitrate and nitrate containing zirconium hydroxy compounds through high temperature hydrolysis [90]. This process occurs in parallel with oxolation of hydroxy

bridges as explained above. Complete removal of nitrates through pyrolysis occurs above 400 °C. Second exothermic peak was observed in the temperature zone 570-670 ºC. This exothermic peak was not accompanied by any weight loss. This peak was due to a change in phase, conversion of the amorphous zirconia phase to the meta-stable tetragonal zirconia, confirmed by XRD and TEM results. DTA measurements clearly reveal the influence of the MoO_3 loading on the zirconia crystallization process. Pure ZrO_2 sample ZIV (Please refer to Chapter-3, Fig. 3.5) had showed exothermic peak of crystallization at 493 ^oC, but as soon as MoO_3 is loaded on zirconia using the same synthesis condition the peak has shifted to higher value. Analogous results can be seen for pure ZrO_2 sample ZIII and 15MZim-II. It is also observed that this temperature of conversion increases as the digestion time increases or synthesis method changes from impregnation to co-precipitation. Sample 15MZim-II prepared utilizing digestion-d2 exhibits exothermic peak at 663 ^oC, while sample 15MZim-I prepared utilizing digestion-d1 show the same peak at lower temperature (572 ^oC). Also when the synthesis method is changed this peak maxima also changes, for eg sample 15MZim-I which showed exothermic peak at 572 ^oC is prepared using impregnation method with digestion-d1, while sample 15MZcp-I is prepared using co-precipitation method with same digestion-d1 shows the peak at 619 ^oC. The position and exothermity of such peak is also affected by amount of MoO_3 loading. DTA results indicate that the exothermic crystallization peak shifted to higher temperatures when the amount of MoO_3 was increased. Samples prepared via co-precipitation method with varying amount of MoO_3, the crystallization peak is shifted to higher temperature, the exothermic peak for 15MZcp-I occurred at 619 ^oC, while that of 30MZcp-I occurred at 664 ^oC. These differences are definitely due to difference in the synthesis methodologies adapted which in turn modifies the structure and thermal stability properties.

4.2.3. Powder X-Ray Diffraction Analysis

The peak position 2θ, full width at half maximum (FWHM) and intensity was calculated using commercially available soft ware (Origin 8.0) for each peak of the XRD data. The indexing of the peaks was carried out using 2θ and intensity value of each peak using standard computer software supplied with the instrument (Rigaku Miniflex). The

XRD lines have been examined with the help of JCPDS (PCPDFWIN v.2.02) data to identify the species present in the samples. ZrO_2 exhibits three well-established polymorphs: the monoclinic, tetragonal and cubic phase of ZrO_2. The diffraction lines at $2\theta = 24.0^o$, 24.4^o, 28.1^o, 31.4^o, 34.1^o, 34.3^o, 35.3^o, 40.7^o, 44.8^o, 45.5^o, 49.2^o, 50.1^o, 54.1^o , 55.4^o, 55.8^o, 60.0^o, 62.8^o and 65.7^o correspond to the monoclinic phase of ZrO_2, peaks at $2\theta = 30.2^o$, 34.60^o, 35.2^o, 43.0^o, 50.2^o, 50.8^o, 59.3^o, 60.3^o, 62.9^o, 73.0^o and 74.7^o correspond to the tetragonal phase of ZrO_2, while the peaks at $2\theta = 30.1^o$, 34.9^o , 50.2^o, 59.7^o, 63.7^o and 74.0^o correspond to cubic phase of ZrO_2 and $2\theta = 23.1^o$, 30.5^o , 35.4^o, 38.6^o, 47.2^o, 50.0^o, 54.2^o, 56.7^o, 57.5^o, 63.5^o, 68.6^o and 74.9^o correspond to $Zr(MoO_4)_2$ spinel phase. Molybdenum trioxide (MoO_3) can exist in two crystalline polymorphs, the thermodynamically stable orthorhombic MoO_3 and meta-stable monoclinic β-phase. Pure MoO_3 shows well defined diffraction peaks at 2θ values of 12.7°, 23.3°, 25.7°, 27.3°, 33.7°, 38.9°, 46.2°, and 49.2° corresponding to orthorhombic phase ((JCPDS file No. 05-0508). From above 2θ values it can be seen that the diffraction peaks of cubic zirconia appear at same 2θ as that of tetragonal zirconia with similar relative intensities, thus making it very difficult to differentiate cubic and tetragonal zirconia phase just with the help of XRD spectrum. Also some of the 2θ values of monoclinic phase either overlap or fall adjacent to the 2θ values of pure MoO_3 and/or $Zr(MoO_4)_2$ phase. Therefore additional spectroscopy and microscopy techniques were used to confirm the meta-stable tetragonal phase and the formation $Zr(MoO_4)_2$, which will seen later in this chapter. MoO_3-/ZrO_2 catalyst prepared in this study clearly confirmed the beneficial effect of molybdenum on zirconia, with respect to surface area and tetragonal phase stability (Table 4.2). The size of the t-ZrO_2 crystallites, estimated from X-ray line broadening were found to be between 10 to 22 nm. The t-ZrO_2 crystallites of the impregnated samples were smaller as compared to the crystallites of the sample prepared via co-precipitation method, with same MoO_3 loading. Fig. 4.2 shows the XRD patterns of 15MZcp-I catalyst calcined at temperatures from 400 ^oC to 800 ^oC. Initially at 400 ^oC 15MZcp-I sample is totally amorphous, when calcined at 500 ^oC poorly crystalline with majority of the phase still amorphous is obtained. However, formation of pure tetragonal zirconia is observed at 600 ^oC. This phase is stable up to 800 ^oC. The characteristics peak reflections from the monoclinic phase are absent in the XRD profile of 15MZcp-I sample calcined at all

temperatures. The selective formation of the tetragonal phase can be ascribed to the reduction in the grain boundary area which prevents the mobility of the ions during phase transformation. It has also been reported that there is a critical crystallite size of zirconia below which the tetragonal phase is stabilized [6].

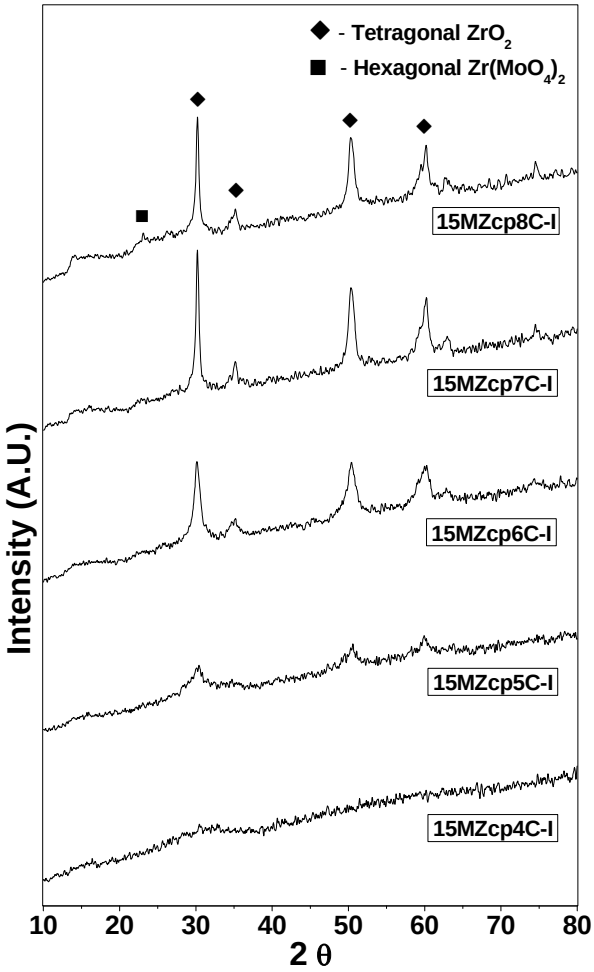

Fig. 4.2: XRD patterns of 15MZcp-I catalyst calcined at various temperatures from 400 ^{o}C to 800 ^{o}C.

In the present study, it is believed that, crystallites lower then 30nm and well dispersed mono-layer formation of MoO_3 on the surface and grain boundary region helps in the stabilization of the tetragonal phase. As no XRD lines were observed due to crystalline MoO_3 phase, it can be inferred that the molybdenum oxide is in a highly dispersed state or the formed crystallites if any are less than the detection capacity of the XRD technique. This observation also back up the possibility that 15 wt % loading of molybdenum oxide chosen in the present investigation corresponds to the monolayer

capacity of the support. Calafat et al. [8] reported X-ray diffraction patterns of MoO_3-ZrO_2 catalysts and the formation of $Zr(MoO_4)_2$ at equivalent contents of MoO_3 for catalysts obtained by co-precipitation and calcined at 700 ^oC. Such a product of the solid-state reaction between the deposited MoO_3 and ZrO_2 matrix is often formed at higher molybdena (>10wt%) loadings and upon calcination temperatures exceeding 500 ^oC [8,91,92]. However in our studies, XRD patterns of the 15MZcp7C-I shows no detectable crystalline phase by XRD corresponding to $Zr(MoO_4)_2$, even though the sample contains more then 10 wt% of MoO_3 and has been calcined at 700 ^oC. Non observation of this phase at the particular temperature may be attributed to the modified synthesis procedure and optimized calcination programme, due to which the MoO_3 is in amorphous phase or in molecular-type species without well defined crystallinty and/or due to limitations of XRD. But when calcination temperature is increased to 800 ^oC, along with pure tetragonal zirconia small ratio of $Zr(MoO_4)_2$ is also formed, which could be detected by XRD. When catalyst is calcined at 800 ^oC, slight decrease in the intensity of ZrO_2 line was found, this clearly suggests the formation of $Zr(MoO_4)_2$ compound is at the expense ZrO_2 species. To assess the formation of bulk $Zr(MoO_4)_2$ as a function of MoO_3 loading at fixed calcination temperature (700 ^oC), MoO_3-ZrO_2 catalyst prepared via co-precipitation method with different loading of MoO_3 were analyzed by XRD (Fig 4.3). In addition to tetragonal peaks, a peak at 2θ value 23$\pm$0.1 was observed for samples 20MZcp7C-I and 30MZcp7C-I, which has been assigned to $Zr(MoO_4)_2$, whose XRD reflections were indexed as a hexagonal cell (JCPDS file No. 38-1466). Assignment of this peak to $Zr(MoO_4)_2$ was done only after studying Raman and FT-IR data because of their ability to discriminate various oxide species. The stable structure of $Zr(MoO_4)_2$ at 700 ^oC is hexagonal with two-dimensional networks of MoO_4 tetrahedra and ZrO_6 octahedra [93]. The intensity of the $Zr(MoO_4)_2$ peak was found to increase with the increase of MoO_3 loading which is in accordance with earlier reports [54]. For comparison purpose XRD pattern of orthorhombic MoO_3 is also given in Fig. 4.3. From 2θ values mentioned at beginning and the XRD patterns given in Fig. 4.3, it can judged that it is pretty difficult to identify and differentiate various phases formed in the MoO_3-ZrO_2 catalyst using XRD technique alone.

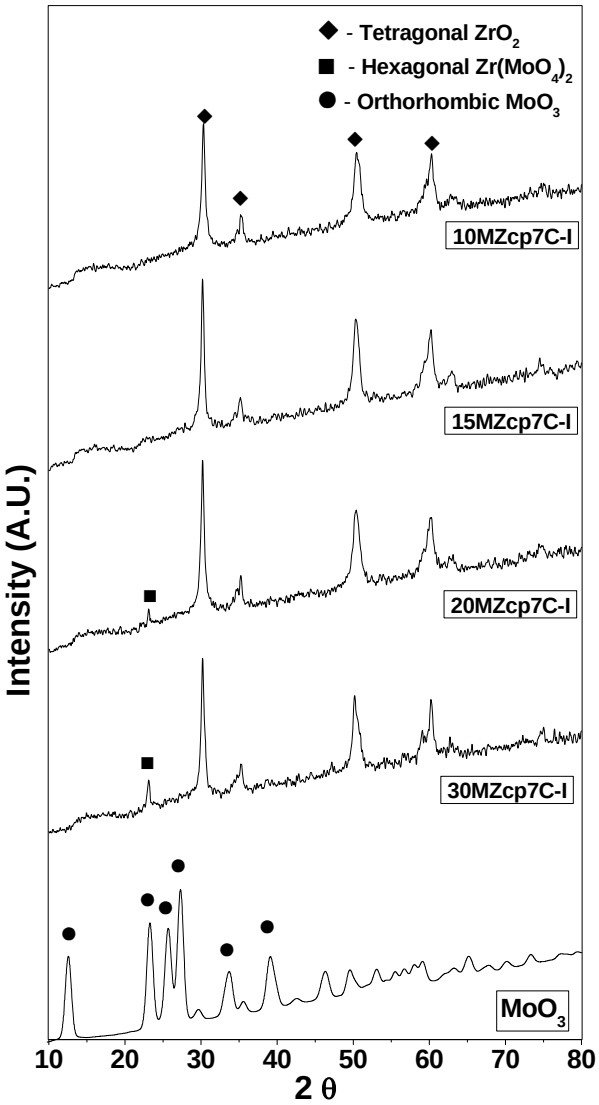

Fig. 4.3: XRD patterns of MoO_3-ZrO_2 catalyst prepared via co-precipitation method with varying MoO_3 content and calcined at temperature 700 ^oC. Orthorhombic α-MoO_3 is also shown at the bottom.

Influence of various process parameters for impregnation catalyst as well influence of synthesis method adopted on the phase formation was analyzed by XRD. Fig. 4.4 shows XRD profiles of MoO_3-/ZrO_2 catalyst having 15wt% MoO_3, calcined at 700 and 800 ^oC. The selective stabilization of the tetragonal phase was also noted for impregnated samples, however, $Zr(MoO_4)_2$ phase transformation is more pronounced, which may be due to impregnation of MoO_3 on ZrO_2 rather then co-precipitation. Formation of the $Zr(MoO_4)_2$ compound is been attributed to the resemblance in the sizes of ZrO_2 and Mo^{6+} as suggested in literature [94]. Meanwhile, the increase of peak intensity at 2θ value of

23±0.1 when calcination temperature is increased from 700 to 800 ^{o}C indicates elevated formation of $Zr(MoO_4)_2$ [6]. From the above results it can be concluded that different materials are obtained by different methods of preparations which leads to the formation of different phases when calcined at higher temperatures

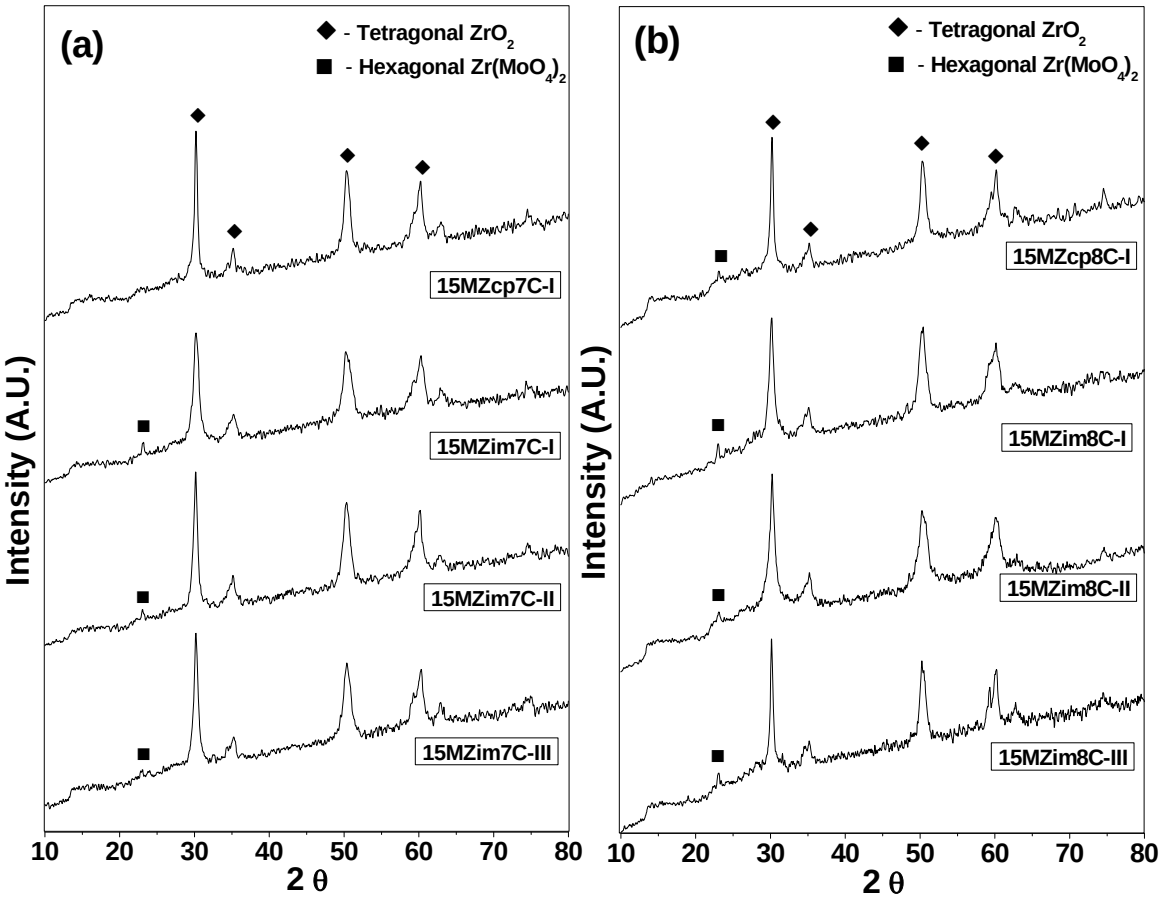

Fig. 4.4: XRD patterns of 15wt%MoO_3-/ZrO_2 catalyst prepared by different synthesis parameters and methods **(a)** calcined at 700 ^{o}C, **(b)** calcined at 800 ^{o}C.

4.2.4. N_2 Adsorption Analysis

It is necessary to examine the effect of molybdenum oxide on the surface properties of catalysts, that is, specific surface area, pore volume/diameter, acidity, and acid strength. The specific surface areas, pore volume, pore diameter etc of samples calcined at 700 ^{o}C for 3 hr are listed in Table 4.2. The presence of molybdenum oxide strongly influences the surface area in comparison with the pure ZrO_2. Specific surface areas of MoO_3-/ZrO_2 samples are larger than that of pure ZrO_2 calcined at the same temperature, showing a gradual increase in surface area with increasing loading of molybdenum oxide content up to 20 wt%. The observed increase in the specific surface

areas may be due to the formation of Mo−O−Zr linkages, resulting in mesoporosity [95]. Please refer to Chapter-3 wherein pure ZrO_2 sample ZIV-7C shows surface area of 73 m^2/g with some monoclinic phase, this sample is prepared and calcined under identical conditions as that of sample 15MZcp7C-I.

Table 4.2: Volume % tetragonal phase of zirconia, particle size, BET surface area, pore volume, pore diameter and acidity of MoO_3-/ZrO_2 catalysts calcined at 700 ^oC.

Sr. No.	Sample Designation	Volume % t-ZrO_2 [XRD]	Particle Size (nm) [XRD]	S_{BET} (m^2/g)	Pore Dia. (nm)	Pore Vol. (cc/g)	NH_3 desorbed (mmol/g)
1	10MZcp7C-I	100	15.2	79	7.8	0.15	0.35
2	15MZcp7C-I	100	15.3	81	6.0	0.13	0.38
3	20MZcp7C-I	100	14.7	93	6.0	0.12	0.40
4	30MZcp7C-I	100	22.0	64	5.6	0.10	0.40
5	15MZim7C-I	100	11.7	84	5.9	0.12	0.38
6	15MZim7C-II	100	10.3	96	7.7	0.18	0.45
7	15MZim7C-III	100	14.9	90	7.2	0.17	0.41

Comparing the surface area of sample ZIV-7C with MoO_3-/ZrO_2 catalyst with varying MoO_3 loading, indicates that difference in their surface areas is not noticeably higher when compared with 10MZcp7C-I (79 m^2/g), but as the MoO_3 loading increases the surface area gradually increases, providing extra MoO_3 for stabilization of ZrO_2. It seems likely that the interaction between molybdenum oxide and ZrO_2 protects catalysts from sintering. A loss in surface area is observed on increasing MoO_3 loading beyond 20wt% which is accordance with the earlier reports [53,96]. The pore volumes of the samples also decrease with Mo loading at same calcination temperatures. The loss in pore volume noticed is probably due to the blocking of some of the pores by large MoO_3 deposits or solid state reaction between Mo and Zr forming bulkier $Zr(MoO_4)_2$ reducing the pore volume without much affecting the diameter of the residual pores. These species are also less effective in improving the thermal stability of ZrO_2. In general, the average pore diameters of samples loaded with 15wt% MoO_3 and calcined at 700 ^oC is between 5.9 - 7.7 nm. Sample 15MZim7C-III prepared in the presence of surfactant under identical synthesis condition as that 15MZim7C-I show very marginal increase in surface area, while a substantial increase in pore size and volume was observed [50,97]. Although the results are not exciting since the increase in surface area is not high enough even after the addition of surfactant, but indicates, addition of surfactant helps in increasing the mesoporosity of the samples. One apparent possible reason for under achieved surface

area could be due to higher calcination temperatures, pore collapse and various other reasons as discussed in detail under the section 3.6 (Mesoporous Zirconia) in Chapter-3. Further more optimization of the synthesis parameters was not done for the preparation of 15MZim-III, with respect to surfactant to zirconia ratio etc., if done can lead better quality of materials with improved surface area. Highest surface area is obtained for sample 15MZim7C-I (96 m^2/g), which is prepared using digestion-d2 method, is also higher when compared to pure ZrO_2 sample ZIII-7C (90 m^2/g) prepared under identical conditions in the absence of Mo. From these observations it can concluded that using optimized synthesis parameters for obtaining high surface zirconia, loading them with foreign ion will definitely increase its stability to a great level, but not the surface area, to a higher extent. However MoO_3-/ZrO_2 samples prepared in this study showed higher surface area than found by other works in the literature [7,8]. This suggests that the precursors and synthesis method used are appropriate for production of catalysts with high surface area and single tetragonal phase. A comparison between synthesis procedure used and the surface area obtained for 15wt% MoO_3-/ZrO_2 catalyst, calcined at 700 ^oC (Fig. 4.5) gives an idea about the changes in the properties of the sample upon altering the synthesis procedure.

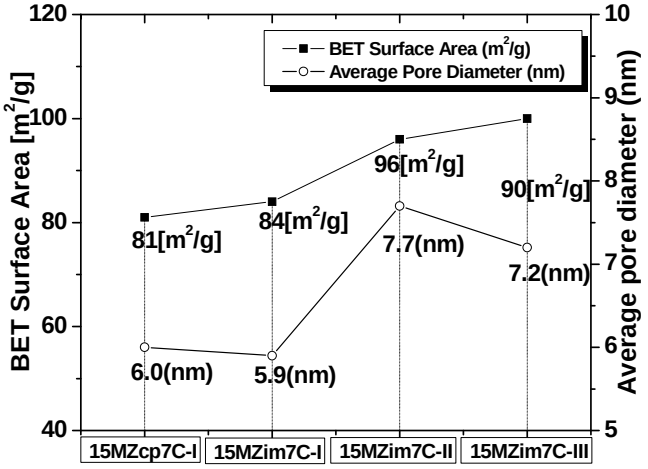

Fig. 4.5: Surface area and pore diameter of 15 wt%, MoO_3-/ZrO_2 catalyst prepared under varying synthesis conditions and calcined at 700 ^oC.

The nitrogen adsorption–desorption isotherms in Fig. 4.6 are of mix type, primarily III and IV type, with the presence of both H2 and H3 hysteresis indicating the combined presence of ink-bottle, wedge and slit-shaped pores. Samples 15MZcp7C-I and

15MZim7C-I show isotherms closer to Type IV, with H2 type of hysteresis while samples 15MZim7C-II and 15MZim7C-III display Type III isotherm, with H3 hysteresis. Typically H2 hysteresis loop has a strong steep desorption branch and a more or less sloping adsorption branch. It may arise from the same types of open capillaries as are responsible for H1 hysteresis. H2 type hysteresis loop is typical for wormhole structured mesoporous materials such MSU, disordered MCM-41 etc [98].

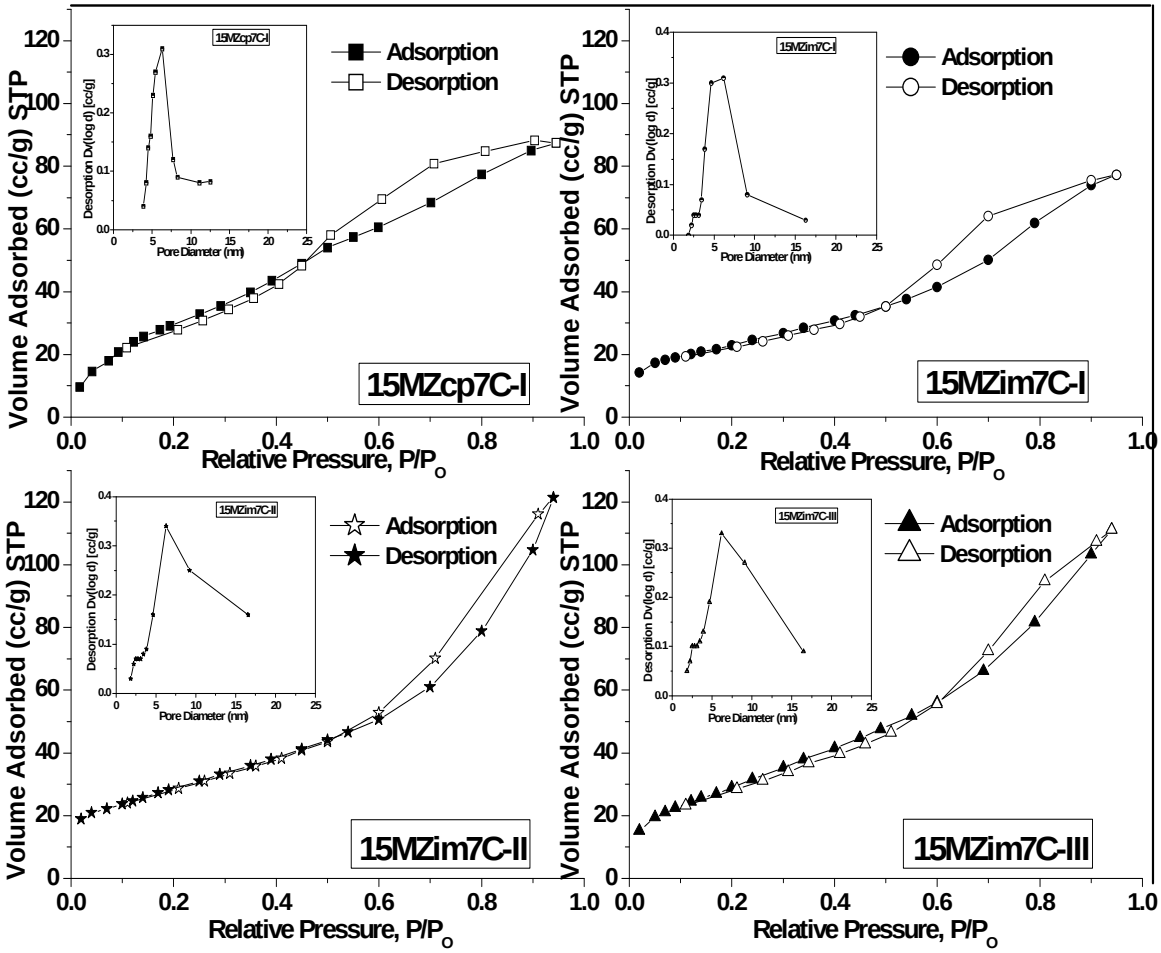

Fig. 4.6: N_2 adsorption/desorption isotherms and corresponding BJH pore size distribution (Inset) of 15 wt%, MoO_3-/ZrO_2 catalyst prepared under varying synthesis conditions and calcined at 700 ^oC

A change of hysterisis loop shape towards H3 type indicates changes in the mesopore size and shape towards micro-porosity level. While Type H3 is usually found on solids consisting of aggregates or agglomerates of particles forming slit shaped pores (plates or edged particles like cubes), with non-uniform size and/or shape. Although there is variation in the hysteresis loops, all of them have appeared in the relative pressure range

of 0.50-0.90, and also these samples showed narrow BJH pore size distributions, which is probably cased by the oxygen escape from the metal oxide surface under high calcined temperature [99]. These indicated that the samples were of mesoporous type rather then microporous. Sample 15MZim7C-II is digested for longer period of time while 15MZim7C-III is prepared in the presence of surfactant, therefore both these samples are expected to have pores larger in size as compared to samples 15MZim7C-I and 15MZcp7C-I. This was evident from pore volume and pore diameter data given Table 4.2. Surprisingly isotherms of the sample 15MZim7C-I and 15MZcp7C-I are some what identical even though they have been prepared by different methods, impregnation and co-precipitation respectively. On the other hand isotherms of the samples 15MZim7C-I and 15MZim7C-II are different even though they have been prepared by impregnation method. The relative changes in the synthesis parameters have led to formation different isotherms. Dependence of the type and shape of isotherms and hysteresis loop for similar type of materials was also observed earlier [100].

4.2.5. Temperature Programmed Desorption of NH_3

Temperature-programmed desorption (TPD) using probe molecules like ammonia and pyridine is a popular method for the determination of acidity of solid catalysts as well as acid strength. In the present investigation the acidity measurements have been carried out by the ammonia TPD method. The temperature-programmed desorption profiles of 15 wt % MoO_3-/ZrO_2 catalysts are presented in Fig. 4.7.

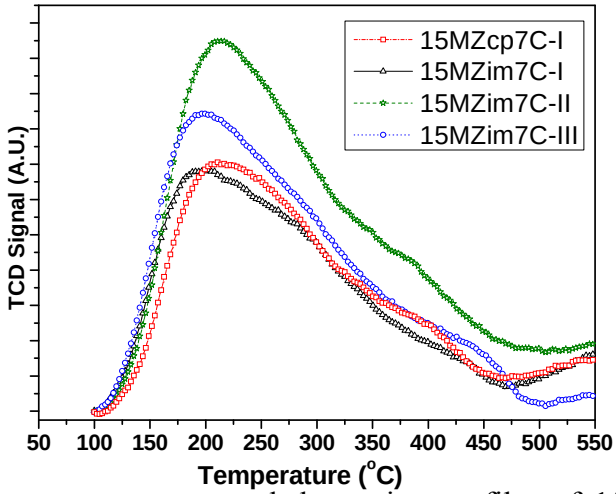

Fig. 4.7: NH_3-Temperature programmed desorption profiles of 15 wt % MoO_3-/ZrO_2 catalysts prepared via different synthesis method and parameters.

The temperature programmed desorption-curves were integrated and the total amount of NH_3 desorbed was calculated from the curves by injection of known volumes of a standard mixture of NH_3/He. In order to understand the acidity characteristics of the samples better, it was decided to remove the contribution from physical adsorption (if any) and from very weak acid sites. Therefore, the acidities of the samples were calculated from the amount of NH_3 desorbing in the temperature range of 100-500 ^oC. The acidity values of MoO_3-ZrO_2 catalyst with varying MoO_3 loading prepared by co-precipitation method and 15 wt % MoO_3/ZrO_2 catalyst prepared by impregnation method by changing the synthesis parameters are given in Table 4.2. The area of the NH_3 TPD profile in the temperature regions, < 250, 250–450, and >450 ^oC, are defined here, respectively, as "weak", "medium", and "strong" acid sites to understand the distribution of acid site concentration. A broad desorption peak, with a peak top at 200 ^oC was obtained for sample 15MZcp7C-I, which indicates the equal contribution of weak and medium acid sites in to the total acid amount of catalyst. Similar distributions of weak and medium acid sites are observed for 10 and 30 wt.% MoO_3 loaded catalysts, whereas 20wt% MoO_3-ZrO_2 has slightly higher concentrations of both. It is evident from the data that there is an initial increase in the acidity up to 20wt% loading, and thereafter no major changes in the acidity could be seen. ZrO_2 is an almost neutral metal oxide, the acid site (Zr^{4+}) and the base site (O^{2-}) being very weak [101]. As proposed earlier by Zaho et al. [22,91,102], MoO_3 at monolayer coverage on ZrO_2 support leads to the formation of Mo-O-Zr surface species. This Mo-Zr interaction was found responsible for the higher acidity in the respective catalyst. The generation of acid sites attributed to polymolybdate species was greatly improved upon increasing the molybdenum content up to 20wt%. However, formation of MoO_3 or $Zr(MoO_4)_2$ phases at higher calcination temperature (700°C) and MoO_3 loading may lead to drastic decrease of both Lewis surface acidity and surface area of the samples. However from Table 4.2 sample 30MZcp7C-I show decrease in surface area but acidity remains same. Such differences are probably due to the basicity of ammonia, pore blocking or due to the different extent with which ammonia and N_2 diffuse into the interior of MoO_3-/ZrO_2 micro-pores, respectively. It was found that the sample 15MZim7C-II calcined at 700 ^oC posses' highest acidity (0.45 mmol/g) as compared with all other samples. A broad desorption peak similar to the TPD profile of

sample 15MZcp7C-I, with a peak top at 220 ^{o}C is observed for sample 15MZim7C-II. It can therefore be concluded that all MoO_3-/ZrO_2 catalyst irrespective of preparation method or MoO_3 loading contains contribution of weak and medium acid sites only in the total acid amount of catalyst. Form various spectroscopy and X-ray results, 15wt% MoO_3/ZrO_2 catalysts prepared by impregnation method, MoO_3 is present in highly dispersed state below temperatures 600 ^{o}C and are transformed to $Zr(MoO_4)_2$ crystallites when temperature is increased above 600 ^{o}C, these crystallites are comparatively higher in impregnated samples when compared with sample 15MZcp7C-I which shows very less presence $Zr(MoO_4)_2$. Inexplicably catalysts prepared by impregnation method shows higher acidity as compared to catalyst prepared using co-precipitation method with same loading of MoO_3. There could various possible reasons for this kind of behavior; such as difference in surface area, pore size etc and also due to some un-certainty of ammonia TPD, few of which are mentioned in chapter-1.

4.2.6. Surface Density – EDX/AAS

The Mo surface densities per unit surface area were calculated from the MoO_3 concentration and the BET surface area measured using EDX/AAS and N_2 physisorption respectively. The molybdenum surface densities, expressed as the number of Mo atoms per nanometer square area (Mo-atoms/ nm^2), were calculated using the following equation: Surface density of Mo = {[MoO_3 loading (wt.%)/100] × 6.023×10^{23}} / {[144 (F.W. of MoO_3) × BET surface area (m^2/g) × 10^{18}]} and are given in Table 4.3.

Table 4.3: MoO_3 concentration (wt%) measured and surface density (Mo-atoms/nm^2), estimated by EDX and AAS, averaged values of both the techniques are also given.

Sr. No	Sample Designation	Wt.% MoO_3 Concentration			Mo-atoms /nm^2		Average Wt.% MoO_3 Conc.	Average Mo-atoms/nm^2
		Input	**EDX**	**AAS**	**EDX**	**AAS**		
1	10MZcp7C-I	10	7.9	9.9	4.19	5.27	8.94	4.73
2	15MZcp7C-I	15	11.6	14.4	6.03	7.46	13.07	6.75
3	20MZcp7C-I	20	14.4	19.0	6.49	8.55	16.73	7.52
4	30MZcp7C-I	30	25.3	28.7	16.53	18.76	27.02	17.66
5	15MZim7C-I	15	12.0	13.8	5.98	6.87	12.91	6.43
6	15MZim7C-II	15	13.9	14.4	6.06	6.27	14.17	6.17
7	15MZim7C-III	15	13.1	14.3	6.09	6.65	13.74	6.39

They show that an increase of the MoO_3 loading results in an increase of the Mo surface density. The Mo surface densities of MoO_3-/ZrO_2 catalysts also depend on the calcination

temperature and surface area. All 15 wt% MoO_3-/ZrO_2 catalysts calcined at 700 ^oC showed surface density ~ 6.4 Mo-atoms/nm^2, well above the reported mono-layer coverage. I. E. Wachs has determined monolayer coverages of several surface metal oxides on different oxide supports by Raman spectroscopy [103]. In his report molybdenum on zirconia formed a monolayer and almost completely covered the surface with ~5 Mo-atoms/nm^2. The polymolybdate saturation capacity on several metal oxide supports has been reported to be ~5 Mo-atoms/nm^2, from equilibrium adsorption measurement from aqueous molybdate solutions [104,105,106] X-ray diffraction, [10,49,107,108,109] and XPS [110,111]. These experimental results are in agreement with the theoretical monolayer coverage of 4.9 Mo-atoms/nm^2 calculated from the effective ionic diameter of MoO_6 octahedra [112]. The surface density of MoO_3 on ZrO_2 is widely utilized to evaluate the activity, MoO_3 cluster size, acid nature, and structure of MoO_3-/ZrO_2 and related materials [6,10,19,54,113]. As we can see that surface density plays a very important role in these type of solid acid catalyst, and therefore its estimation/calculation from measured MoO_3 concentration and surface area is also important. Consequently surface density estimation/calculation depends on how accurately/systematically MoO_3 concentration in the catalyst and surface area is determined. There are barely any reports were in estimation of MoO_3 concentration has been done systematically or given significance. During these studies we have tried to estimate MoO_3 concentration by different analytical techniques with highest possible accuracy and an average value is used for calculation of surface density, thereby achieving closet actual surface density. All the MoO_3-/ZrO_2 sample surfaces were analyzed by SEM-EDX to determine the surface composition and the morphologic features. An illustration, 30MZcp7C-I sample EDX spectrum in given in Fig. 4.8. The elemental wt % given in the inset of Fig. 4.8 is converted to oxide wt% and this value is reported. Similarly MoO_3 wt % for all other MoO_3-/ZrO_2 catalyst is been estimated and its corresponding surface density values are given in Table 4.3. If not otherwise mentioned, all concentration values are given in percent of the element as oxide in its highest stable state of oxidation in the sample. AAS was also employed for the estimation of MoO_3 concentration, as the determination of bulk chemical composition is of paramount importance in monitoring and evaluating the properties and stability of

catalysts. Surface density values were calculated from the MoO_3 concentration obtained from AAS analysis. The results of the investigations by EDX and AAS are summarized in Table 4.3. In general, the surface concentration of MoO_3, determined by EDX, was lower than that determined from AAS analysis. Similar results were observed previously for MoO_3 based oxide materials [19]. Sighting differences in the MoO_3 concentration and its corresponding surface density values from the two analytical methods, an average of EDX and AAS values are composed and tabulated, which throws light on surface and bulk MoO_3 concentration and its surface density values.

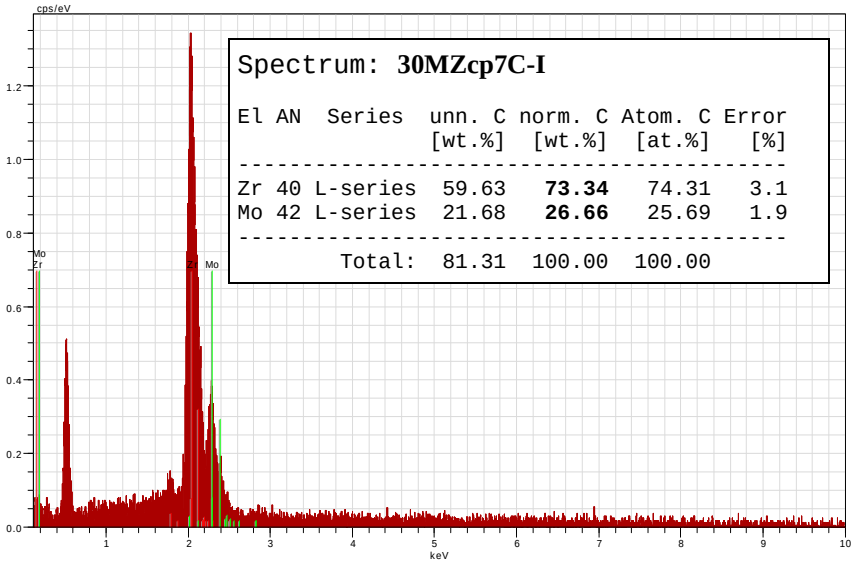

Fig. 4.8: EDX spectrum of 30MZcp7C-I sample. (Inset normalized Wt.% of Mo and Zr).

The strong variation and lower values of the EDX, is the result of a typical behavior of the SEM-EDX, it is surface analysis, and shows therefore only a part of the whole analytical information, this is in total contrast to conventional AAS which shows an averaged analysis for every sample. However dissolution process necessary for conventional atomic spectroscopy is sometimes tedious and requires a good analytical hand, while sample preparation for EDX is fast and easy. AAS has the advantage of lower detection limits with a higher accuracy, even for the light elements, compared to the SEM-EDX. On the other hand SEM-EDX is non-destructive; able to detect elements like S, but it is a standard-less technique (semi-quantitative). The final conclusion of this investigation is that the ideal way is an analysis of the sample with both systems; first

qualitative and semi-quantitative overview by SEM-EDX and then a precise quantification of the results by AAS.

4.2.7. Raman Analysis

Zirconia supports possess strong Raman bands below approximately 700 cm $^{-1}$ because of some covalent bonding character of Zr-O bond. Strong background frequencies below 700 cm^{-1} of tetragonal zirconia can mask the absorption of the MoO_3. If these support bands do not get subtracted off reliably; the region above 700 cm^{-1} is generally used for analysis, this is especially true when MoO_3 loading is below monolayer coverage. As monolayer completes at surface density ~5 Mo-atoms/nm^2, the ZrO_2 bands are hardly seen above this loading, above monolayer loadings only MoO_3 bands are seen [53]. Sighting above reasons Raman spectra for MoO_3-/ZrO_2 catalysts only above 700 cm^{-1} was collected in the present study. This frequency range covers the anti-symmetric Mo-O-Mo and symmetric and anti-symmetric Mo=O terminal stretches of the isopolyanions of molybdenum and oxygen. Raman spectroscopy is a valuable tool for the characterization of dispersed metal oxides and detects vibrational modes of surface and bulk structures. The Raman spectrum of amorphous zirconia is characterized by a 168, 402, and 525 cm^{-1} bands or a very weak and broad band is observed at 550-600 cm^{-1} [53,54]. The Raman spectrum of a pure metastable cubic ZrO_2, showed only a weak broad line at 490 cm^{-1} [114]. Tetragonal zirconia is expected to yield a spectrum consisting of Raman bands with frequencies at about 148, 263, 325, 472, 608, and 640 cm^{-1}, while monoclinic zirconia exhibits the characteristic features at 180, 188, 221, 380, 476, 618 and 637 cm^{-1} [115,116]. Shown in Fig. 4.9 **(a)**(Inset), is our Raman result of pure zirconia (ZIV-7C) scanned below 700 cm^{-1}. In the lower-frequency region, characteristic bands of monoclinic and tetragonal zirconia were observed for the sample ZIV-7C with no band at 490$\pm$10 cm^{-1}, which are consistent with XRD and FT-IR results. The frequency shifts of the tetragonal and monoclinic vibrational modes are slightly modified due to thermal broadening [117]. Confirmation of tetragonal phase for MoO_3-/ZrO_2 samples was confirmed by XRD and FT-IR results which are consistent with TEM (SAED) results. The major vibrational modes of MoO_3 are located at 992, 818, 662, and 280 cm^{-1} (Fig. 4.9 **(a)**), and have been assigned to the Mo=O stretching mode, the Mo-O-

Mo stretching mode, OMo3 vibration mode, and the Mo=O deformation mode, respectively [118].

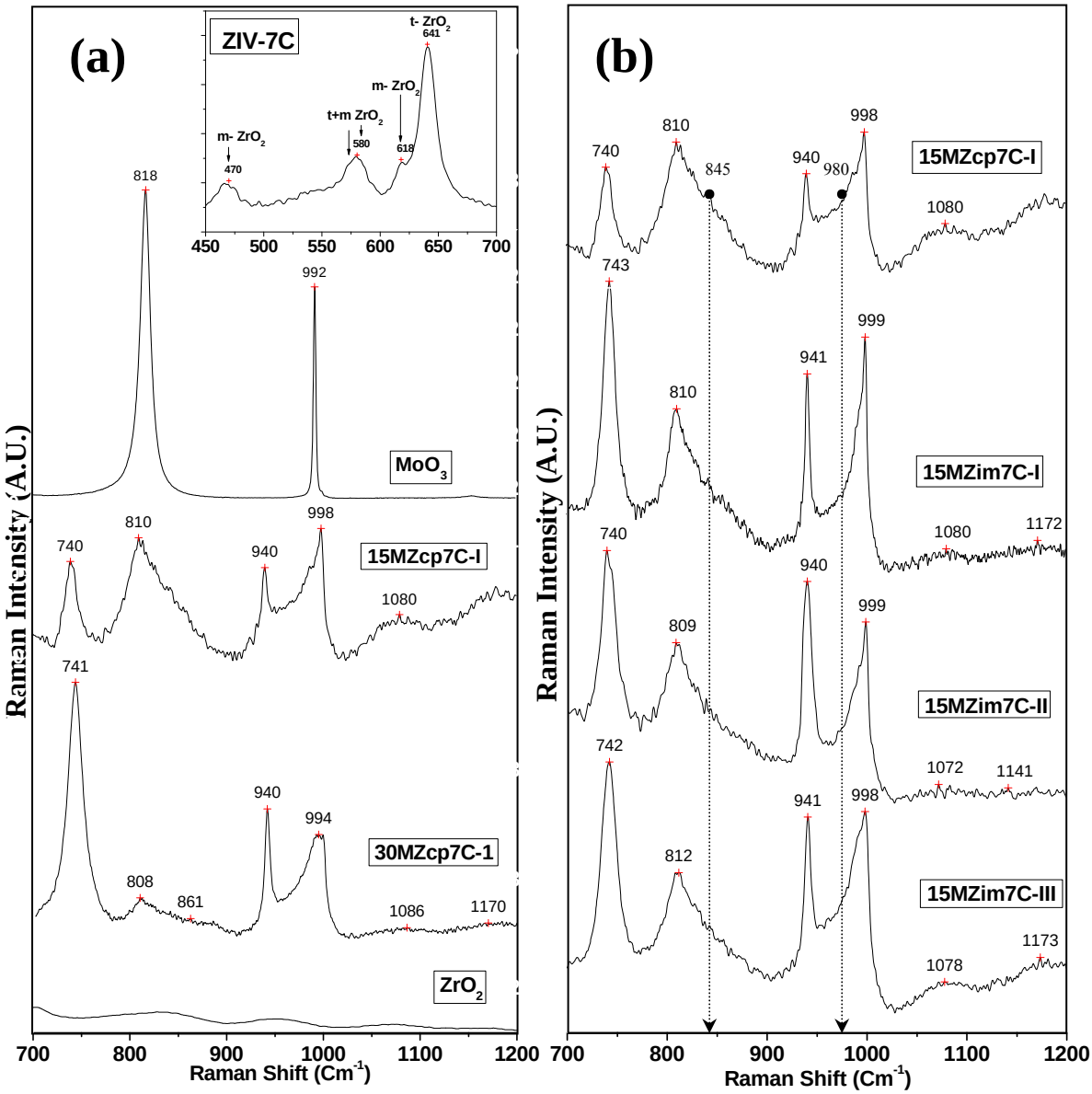

Fig. 4.9: Raman spectra of **(a)** Pure ZrO_2 and MoO_3, 15 and 30 wt% MoO_3-ZrO_2 catalysts prepared by co-precipitation method and calcined at 700 ^oC. (Inset Raman spectra of sample ZIV-7C) **(b)** 15wt%MoO_3-/ZrO_2 catalyst prepared by different synthesis parameters and methods calcined at 700^oC

The Raman bands at 740, 940, and 998 cm^{-1} were assigned to $_{vsym}$(O-Mo-O), $_{vasym}$(O-Mo-O), and $_v$(M=O) vibrational modes of $Zr(MoO_4)_2$. S. Xie et. al. detected MoO_3 and $Zr(MoO_4)_2$ by Raman and for larger crystallites by X-ray diffraction, for MoO_3-/ZrO_2 samples with Mo surface densities greater than 5 Mo/nm^2 [54]. The detection limit of

XRD for MoO_3 crystals lays around 5 nm sized crystallites [119,120]. Raman spectroscopy analysis is delicate in the present case because of the intense fluorescence background of the zirconia support [121]. On the other hand, MoO_3 crystals, even very small crystallites are strong Raman scatterer and are readily detected if present [122,123]. In the present studies all the 15 wt% MoO_3-/ZrO_2 catalyst prepared, completes monolayer coverage with surface densities greater than 5 Mo-atoms/nm^2 and show $Zr(MoO_4)_2$ phase, (Fig. 4.9 **(b)**), identified by its characteristic Raman bands at 740, 940, and 998 cm^{-1}. Also shown in Fig. 4.9 **(a)**, the amount of $Zr(MoO_4)_2$ phase increased with the MoO_3 loading from 15wt% to 30 wt% [10]. $Zr(MoO_4)_2$ bands become more intense with increasing MoO_3 loading at the expense of weaker MoO_3 bands, suggesting that $Zr(MoO_4)_2$ forms via reaction of MoO_3 crystallites with ZrO_2, as discussed earlier in the XRD section. The two bands at 845 and 980 cm^{-1} in the range of 800-1000 cm^{-1} are been masked by the more intense and broad 810 and 998 cm^{-1} bands which may be due to the strong interaction of molybdena with ZrO_2. The distortion and different extent of interaction among surface molybdenum oxygen species should be responsible for the large width and shift of the bands as compared with the bands of lone oxides. The 845 and 980 cm^{-1} bands correspond to Mo-O-Mo and Mo=O stretching vibrations in polymolybdates, respectively [54,124,125]. The band at 980 cm^{-1} arise from Mo=O stretching modes of dispersed two dimensional polymolybdates and the band at 845 cm^{-1} is assigned to isolated tetrahedral MoO_4 species [126]. Generally, tetrahedral MoO_4 species have been assigned for low MoO_3 loading samples, and two-dimensional polymolybdates or octahedral molybdenum–oxygen species with characteristic band around 950–980 cm^{-1}, for high MoO_3 loading samples [110,127]. For samples with, well below the monolayer value of ~5 Mo/nm^2 neither Raman spectroscopy nor X-ray diffraction detected bulk MoO_3 or $Zr(MoO_4)_2$ structures at all treatment temperatures. [54]. However in our case surface density is well above 5 Mo-atoms/nm^2 for all 15wt % MoO_3-/ZrO_2 catalyst, which showed band at 810 cm^{-1} that is characteristic of crystallite MoO_3, which suggests the presence of crystalline MoO_3 structure. The fraction of Mo present as crystalline MoO_3 for this sample was estimated by Raman spectroscopy using a method previously reported, [128] which was less then 5 % for sample 15MZcp7C-I. Thus, we conclude that 15wt% MoO_3-/ZrO_2 catalysts contain predominately

polymolybdates, as also evidenced by the absence of any MoO_3 diffractions in the XRD patterns (Fig. 4.4). In such polymolybdates most Mo sites on the catalysts are very much accessible to the reactants [124]. At such low content of crystalline MoO_3 and its relatively intense Raman peak at 810 cm^{-1} reflects the consensus that Raman scattering cross sections are $10\text{-}0^3$ greater for crystallite MoO_3 than for dispersed MoO_3 species [125,129,130].

4.2.8. DR-UVis Analysis

Among the polymorphic forms of zirconia, the octa-coordinated tetragonal (space group $P4_2/nmc$) and cubic (space group Fm3m) phases shows UV absorption maxima in the range of 200–210nm where as the heptacoordinated monoclinic phase (space group P_21/c) shows maxima around 240nm [131]. It has been observed that as the coordination number of Zr^{4+} ion decreases from 8 to 6, the ligand–metal charge transfer transition (LMCT) absorption maxima progressively shifts to lower energy (higher wavelength) [116,132]. UV and Raman spectroscopy is useful in distinguishing the monoclinic and tetragonal phases of zirconia [133]. The UV–Vis spectra of pure ZrO_2 was also taken (Fig. 4.10) in order to substantiate various phases observed in XRD and other spectroscopy techniques. Even though, diffuse reflectance usually gives broad and overlapping bands leading to a biased spectral analysis, (Chapter-2, DR-UVvis section 2.4.5) ZrO_2 spectrum was primarily used to ascertain any overlapping bands with that of MoO_3-/ZrO_2 catalysts. The prominent absorption band observed for pure zirconia (ZIV-7C, Chapter-3) at peak maxima of 213 nm can be assigned to the $O^{2-} \rightarrow Zr^{4+}$ charge transfer transition arising out of the tetragonal phase of zirconia. This observation is complementary to the XRD and FT-IR result where stabilization of meta-tetragonal phase was observed. Although the band is not sharp with peak maximum at 213 nm, it also shows a broad absorption at around 248nm. These data strongly support the idea that eight-coordinate tetravalent Zr species (like those of tetragonal zirconia) are responsible for the absorption in the range 200 – 215 nm, while seven-coordinate Zr species (like those of monoclinic zirconia) are responsible for a split absorption with an additional component at 248 nm [134]. UV results corroborate with the XRD and IR values thus supporting the evidence of tetragonal phase with small amount monoclinic phase in

sample ZIV-7C (Chapter-3, Fig. 3.14). Addition of MoO_3 to zirconia matrix significantly modifies the spectra of ZrO_2 materials (Fig. 4.10).

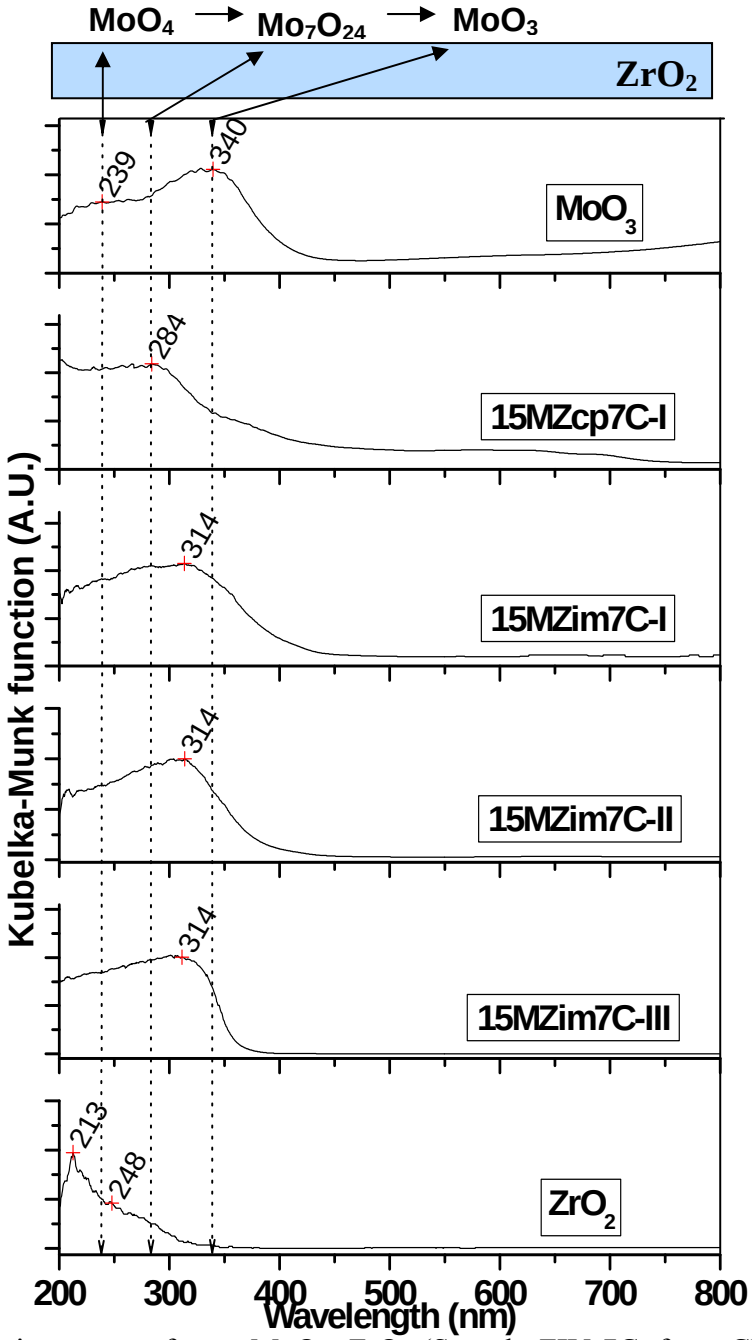

Fig. 4.10: UVvis spectra of pure MoO_3, ZrO_2 (Sample ZIV-7C, from Chapter-3) and 15 wt% MoO_3-/ZrO_2 catalyst calcined at 700 ^oC, prepared under different synthesis conditions.

The MoO_3-/ZrO_2 catalyst shows absorption features which are different from the individual oxide components. Earlier studies on the UV–vis spectra of dispersed MoO_3

system have revealed three absorption regions corresponding to the presence of isolated molybdate species (220–250 nm), polymolybdate clusters (260–290 nm) and bulk type molybdate (>315 nm) [10,135,136,137,138]. Various oxo-molybdenum compounds give absorption bands in UV-vis region due to ligand-metal charge transfer ($O^{2-} \rightarrow Mo^{6+}$). The position of this electronic transition depends on the ligand field symmetry surrounding the Mo centre. For oxygen ligands, a higher energy transition is expected for tetrahedral (Td) Mo^{6+} than for an octahedral (Oh) one [111,139]. The absorption at 285 nm has been assigned by earlier workers to octahedral Mo species, and 230 run to both octahedral and tetrahedral Mo species [140]. As the absorption at 230 nm could arise from both tetrahedral and octahedral Mo^{6+} species, it is not possible to know if Mo is present in tetrahedral coordination in the samples. In any case, more Mo ions are likely to be present as octahedral species. These species are probably associated with defect sites. The UV-visible DR spectra of 15wt% MoO_3-/ZrO_2 catalysts calcined at 700 ^oC, prepared under different synthesis conditions are shown in Fig. 4.10, are helpful in identifying the structures of the molybdenum species dispersed in/on t-ZrO_2. Broad absorption bands in the range of 220–315 nm are observed for all the samples with the different absorption maximum for co-precipitation sample 15MZcp7C-I being at 284 nm, while the absorption maximum for all impregnated samples was at about 314 nm. The UV–Vis spectra of the MoO_3-ZrO_2 materials prepared by impregnation method and calcined at 700 ^oC show a prominent peak at 314 nm corresponding to coexistence of surface poly-molybdate species with $Zr(MoO_4)_2$ compound. The inclination, broadness and the range of the bands suggest the presence of a wide variety of Mo^{6+} species in the samples with both Tetrahedral (Th) and Octahedral (Oh) coordination. Considering the asymmetric nature of the spectra for the MoO_3-/ZrO_2 catalyst it is likely that poly-molybdate species such as hepta-molybdate clusters can exist on the zirconia surface. Liu et al. have assigned the peak at ~300 nm to the presence of hepta-molybdate clusters for MoO_3/ZrO_2 catalyst [10]. In the present study, such clusters can exist in the zirconia matrix in a well dispersed state. However most likely species are of poly-oxo molybdenum with Oh coordination and some dispersed zirconium molybdate with Td coordination. There is a decrease in the band intensity after peak maximum at 284 nm for sample 15MZcp7C-I suggests fewer formation $Zr(MoO_4)_2$, also supported by XRD and RAMAN data. Pure

MoO_3 shows two well defined absorption bands at 240 and 340nm (Fig. 4.10). Since Mo^{6+} has a d^0 electronic configuration, the only absorption feature expected is due to the ligand–metal charge transfer transition (LMCT), $O^{2-} \rightarrow Mo^{6+}$ which occur in the range of 200–400 nm. Depending on the coordination preference and local symmetry, Mo (VI) ions show different absorption bands in the electronic spectrum. The peak at 240nm for pure MoO_3 has been assigned to the isolated MoO_4 species with tetrahedral symmetry where as the peak at 340nm has been assigned to bulk type polymolybdate species [10,135,136]. UV Vis studies also ascertain that the molybdate species exist in a highly dispersed from in the composite oxide and indication of the presence of bulk type molybdate in the differently prepared 15wt% MoO_3-/ZrO_2 catalyst calcined at 700 ^oC. However the band with peak maxima at 340 nm corresponding to the bulk type MoO_3 was absent for all samples, but showed absorption in that region, indicating presence of small amounts of bulk type molybdate, also identified by Raman studies.

4.2.9. FT-Infrared Spectroscopy Analysis

The surface metal oxide species are usually the active catalytic components (chromium oxide, molybdenum oxide, tungsten oxide, vanadium oxide, etc.) on the high surface area oxide support (alumina, titania, zirconia, niobia, silica, etc.), in such supported metal oxide catalysts. Raman and infrared are complementary spectroscopies that are among the unique characterization techniques that provide fundamental molecular level information about the surface properties of supported metal oxide catalysts: molecular structure of the surface metal oxide species (ambient and in situ conditions), location of the surface metal oxide species, surface coverage of the metal oxide over layer, distribution of surface Lewis and Bronsted acid sites as well as the structure of the active surface metal oxide species during catalytic reactions. The intensities of IR absorption bands depend on the change of the dipole moment brought about by variations in the molecular geometry for the vibration concerned, while the intensities of Raman bands depend on the change of polarizability associated with the vibration. Consequently, bonds possessing ionic character tend to give strong IR signals and bonds possessing covalent character tend to give strong Raman signals [141]. The oxide supports generally terminate with -OH bonds which are quite polar and give rise to strong IR bands in the 3000-4000 cm^{-1} region. The superior surface hydroxyl signals

observed with IR spectroscopy has made this characterization technique the method of choice when investigating the surface hydroxyl chemistry of supported metal oxide catalysts. The IR band at the highest frequency has been assigned to the most basic hydroxyl group and the decrease in frequency of the surface hydroxyls has been associated with increasing acidity [103,142]. Deposition of metal oxides on alumina reveals that the alumina surface hydroxyls are being consumed and that the consumption of surface hydroxyls proceeds in a sequential fashion: the bands due to the most basic hydroxyls, located at the higher frequencies, disappear first with bands due to neutral and more acidic ones disappearing at higher loadings [143]. The broad band centered at about 3400 cm^{-1} is characteristic of residual chemisorbed water. The presence of the adsorbed moisture also causes the vibrations of OH groups to shift to lower frequency due to hydrogen bonding [142]. In principle, it should be possible to determine monolayer surface coverage of the surface metal oxide species from IR experiments since complete consumption of surface hydroxyls of the oxide support should correspond to monolayer coverage. However, the IR signal of the surface hydroxyls decreases somewhat more rapidly than the increasing surface metal oxide coverages [143]. This trend may be due to broadening of the surface hydroxyl IR signals at high surface metal oxide coverages, which makes it more difficult to detect their IR signals. CO_2 chemisorption on oxide supports, monitored by IR spectroscopy, also generally provides qualitative information about the surface metal oxide coverage on oxide supports because of its preferential chemisorption on the more basic hydroxyls that are usually titrated at low surface coverages [144]. Thus, only qualitative information about the surface coverage of surface metal oxide species on oxide supports can generally be obtained with IR spectroscopy. Quantitative determination of the surface coverage of the surface metal oxide species on oxide supports can be obtained from Raman spectroscopy measurements precisely because of its ability to discriminate between surface metal oxide species and microcrystalline metal oxides.

The infrared absorption spectra of various MoO_3-/ZrO_2 samples prepared in this study, calcined at 700°C are shown in Fig. 4.11. The IR bands at 987, 879 and 623 cm^{-1} in Fig. 4.11 **(b)** of bulk MoO_3 are assigned to Mo=O stretching mode, asymmetric Mo-O-Mo stretching mode and Mo−O−Mo bending vibration mode, respectively [145]. The first

strong band in the region 470-501 cm^{-1} is attributed to Zr-O-Zr, stretching vibration [146].

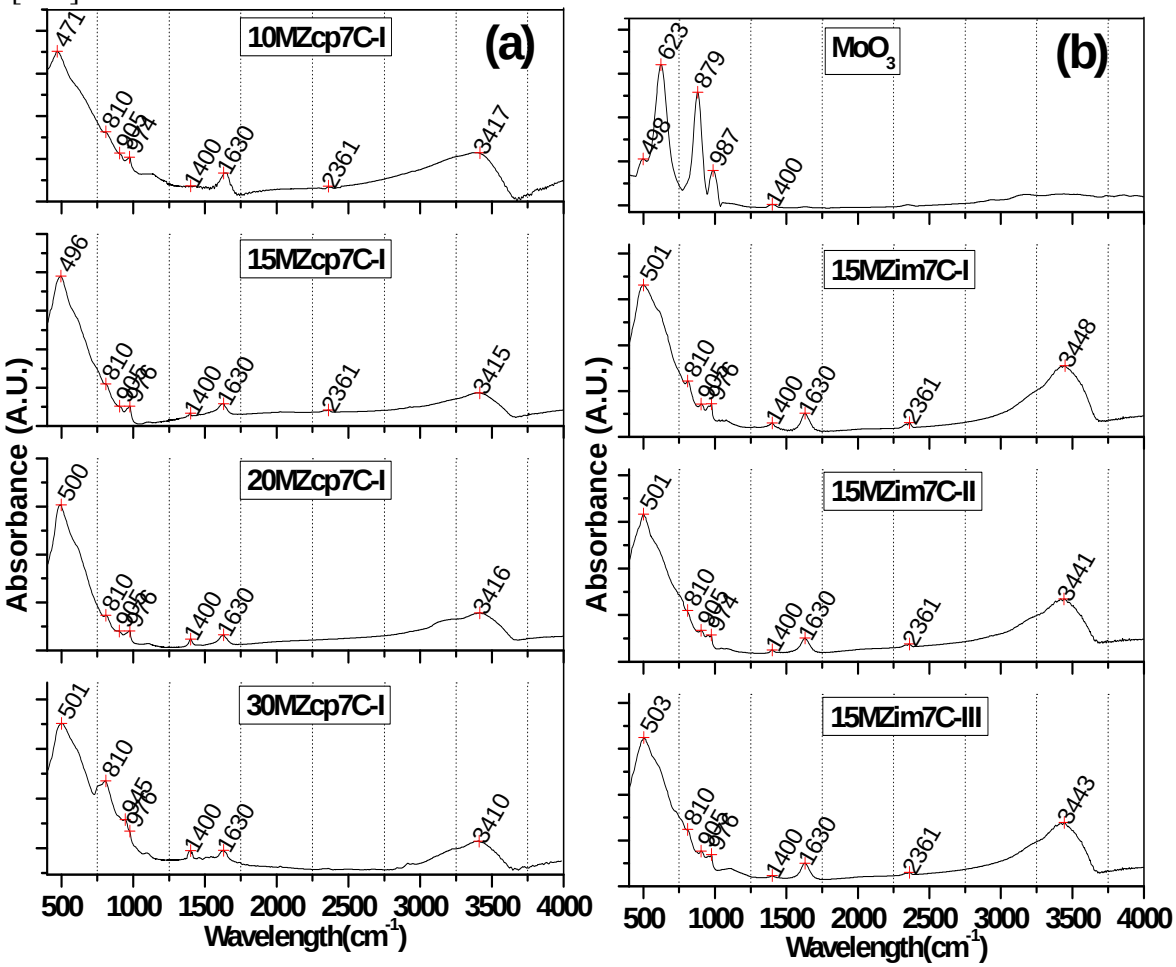

Fig. 4.11: FT-IR spectra of **(a)** MoO_3-ZrO_2 samples with different molybdenum loadings (10, 15, 20 and 30 wt%) prepared by co-precipitation **(b)** Pure MoO_3 and 15wt% MoO_3/ZrO_2 samples prepared by impregnation methods calcined at 700°C.

A strong and wide band was observed amid 3400-3450 cm^{-1} for all spectra expect for bulk MoO_3, this band could be attributed to O–H stretching vibration. The involvement of zirconia surface hydroxyls in the interaction with molybdenum MoO_4^{2-} species, during catalyst preparation, is manifested by [147]; lower intensity of the band due to free isolated OH groups compared with the unloaded sample. IR spectrum of all the MoO_3-$/ZrO_2$ catalyst also exhibits a band at 1630 cm^{-1} (O-H bending vibration) indicating the presence of coordinated chemisorbed water molecules, with the peak at 1400 cm^{-1} (O-H bending vibration) representing surface hydroxyl on the metal oxide surface [148]. In addition, all impregnated 15wt% MoO_3/ZrO_2 samples and 10 and 15wt% MoO_3-ZrO_2

samples have a band at around 2361 cm^{-1} that can be attributed to the absorption of CO_2. Frausen at al. [149,150] reported the formation of $Zr(MoO_4)_2$ by heating ZrO_2 with MoO_3 together which showed the IR bands at 980, 920 and 800 cm^{-1}. By virtue, our IR results can give an evidence for the formation of the latter compound in spite of the expected interference with polymolybdate and octahedral molybdenum species. The bands at 976, 905 and 810 cm^{-1} are matching with those at 980, 920 and 800 cm^{-1} respectively, which confirms formation of $Zr(MoO_4)_2$ in all samples prepared by co-precipitation and impregnation method. The intensity of these peaks was found to increase with increasing MoO_3 loading (Fig. 4.11**(a)**). In 30MZcp7C-I sample, presence of higher quantity of $Zr(MoO_4)_2$ fuses 905 and 950 cm^{-1} bands thus giving a major band at 946 cm^{-1} with a down shoulder at 976 cm^{-1}. Also the intensity of $Zr(MoO_4)_2$ bands is higher for samples by impregnation method as compared to co-precipitation method with same MoO3 loading. Thus, the IR results corroborate well with the Raman and XRD results. The 30MZcp7C-I sample showed a shoulder band at 751 cm^{-1} along with strong band at 810 cm^{-1}, which was related to $Zr(MoO_4)_2$ [96]. This band is usually assigned to monoclinic zirconia [151,152,153], but none of analytical techniques used in this study for the examination of 30MZcp7C-I sample confirmed its formation, therefore the existence of monoclinic phase was ruled out. Generally, in the case of molybdate-promoted samples the region at 900-1050 cm^{-1} represents terminal Mo=O stretching vibration and that at 700-800 cm^{-1} represents the region of anti-symmetric Mo−O−Mo or O−Mo−O stretching vibrations. In the present study a remnant shoulder at 950 cm^{-1}, which has been masked by the presence of more intense band at 976 cm^{-1} under ambient condition (Fig. 4.12) is assigned to the terminal Mo=O stretching vibration of the hydrated form of the surface molybdenyl species [154,155]. This can be rationalized by assuming that the adsorption of water causes a strong perturbation of the corresponding molybdenum oxide species, with a consequent strong broadening and shift down of this band. This isolated molybdenum oxides species is stabilized through multiple Mo-O-Zr bonds between molybdenum and zirconia surface [10,156]. J. R. Sohn et.al. observed IR band at 997 cm^{-1} for 15wt% MoO_3/ZrO_2 sample after evacuation at 500 ^oC, due to Mo=O stretching mode of the molybdenum oxide complex bonded to the ZrO_2 surface, on wet sample this band shifted to 946 cm^{-1}, thus supporting our assignment and assumption [53,154,157].

Absence of any band around 987 cm^{-1} confirms that Mo oxide is in highly dispersed state in to zirconia oxide support, which is inline with the earlier reported results.

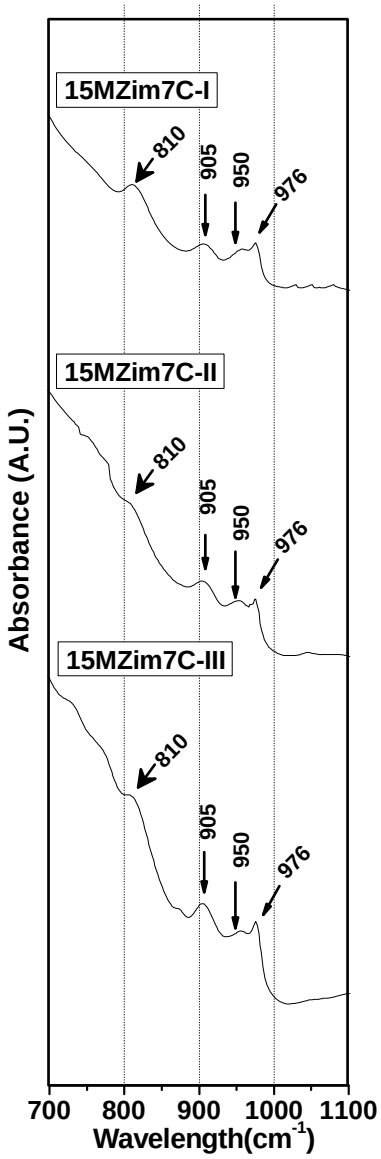

Fig. 4.12: FT-IR spectra in the region 700-1100 cm^{-1} of 15wt% MoO_3/ZrO_2 samples prepared by impregnation method calcined at 700°C.

4.2.10. SEM & TEM Analysis

The scanning electron micrographs (SEM) of MoO_3-ZrO_2 catalysts prepared via co-precipitation method with MoO_3 loading varying from 10 to 30 wt% is shown in Fig. 4.13. Catalysts prepared by impregnation method with 15 wt% MoO_3 are also shown in this figure. From the SEM images it can depicted that MoO_3-ZrO_2 catalysts consists of

irregular shape and size particles with good dispersion of the component oxides. However some visible difference can be spotted in terms of shape of the agglomerates of the sample prepared via different synthesis methods. Samples prepared via impregnation method shows mixture of particles consisting of different size (5-10 μm) and shape (round + irregular) while samples prepared via co-precipitation method consists of only larger irregular agglomerates of size 10-12 μm.

High resolution transmission electron microscopy (HRTEM) analysis was also performed. As an example to compare samples prepared via different methods, TEM images of samples 15MZcp7C-I and 15MZim7C-I are given in Fig. 4.14 which shows particle morphology, pore structure and crystal lattice fringes of MoO_3-/ZrO_2 particles. Interconnected particles with size of 6−12 nm are observed. Mo dispersion on zirconia prepared by co-precipitation method seems to be more uniform comparatively to sample prepared via impregnation method, which may be due to difference in the synthesis procedure which is reasonably expected. The particles of sample 15MZcp7C-I appear to be fused and more agglomerated while sample 15MZim7C-I shows loosely bound particles of primarily round shaped, also supported by SEM images. Selected area electron diffraction (SAED) pattern of the corresponding image is inserted into the TEM micrograph. The corresponding diffraction pattern (Inset of Fig. 4.14) shows the presence of few clear spots along with connecting diffraction rings. The presence of spots along with the streaks shows the presence of crystallite of reasonably sufficient sizes to diffract. It also indicates that, after calcination at 700 ◦C, the particles have been completely crystallized, since only diffraction spots and not amorphous diffraction rings are observed. The connecting streaks indicating the short-range order due to presence of some smaller size particles. Therefore, a well interconnected crystal network has been formed in the MoO_3-/ZrO_2 particles. SAED pattern, Inset of Fig. 4.14 shows (101), (110), (112) and (211) diffraction rings. The d-spacings corresponding to the diffraction rings of the SAED pattern are in agreement with the tetragonal structure (JCPDS 79-1770). Reflections, such as (102), are allowed for tetragonal structures and forbidden for the cubic structures [158]. Thus, electron diffraction confirmed that the MoO_3-/ZrO_2 catalysts consist of tetragonal phase rather than cubic structure.

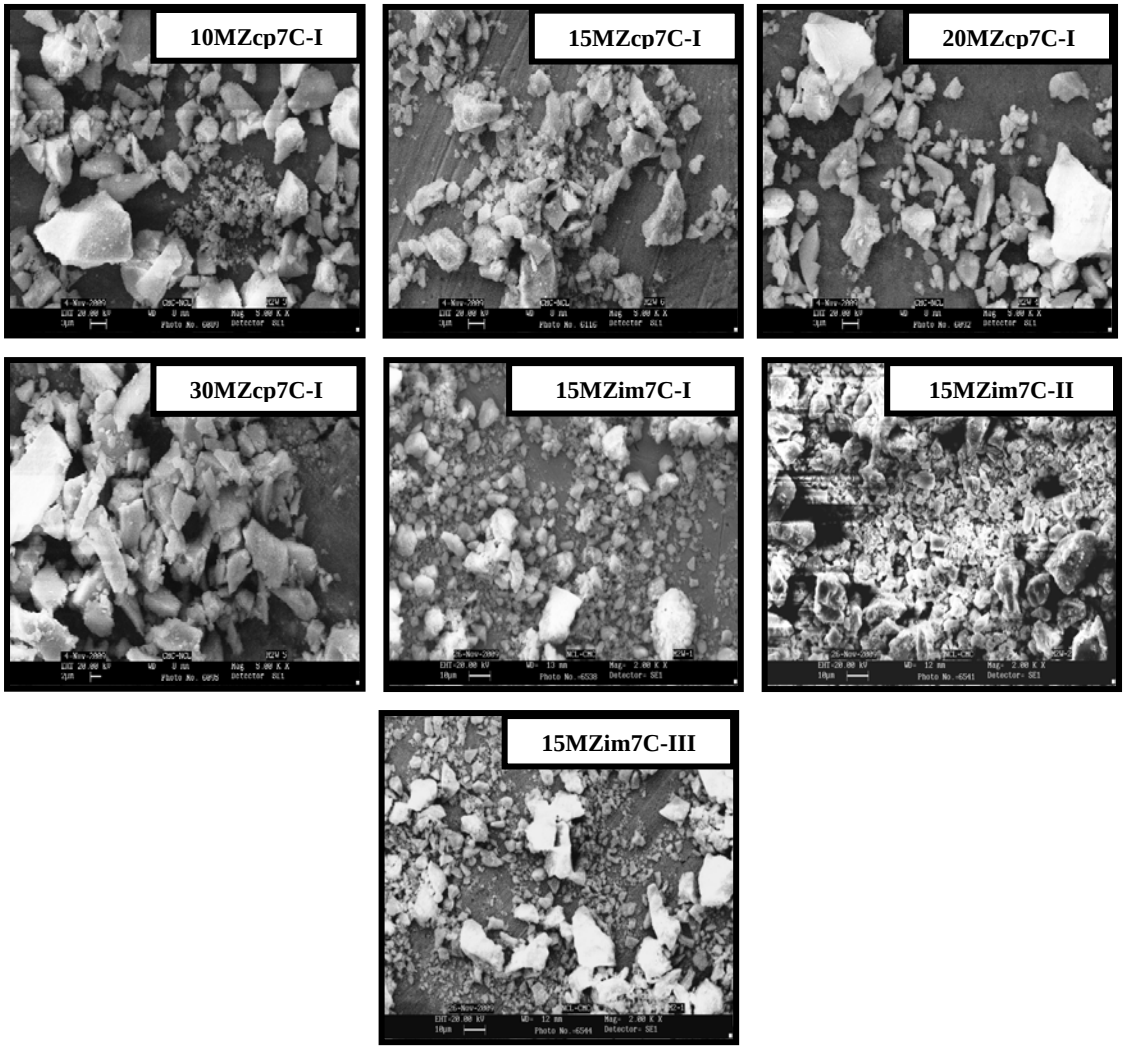

Fig. 4.13: SEM images of various MoO_3-/ZrO_2 catalysts calcined at 700^{o}C.

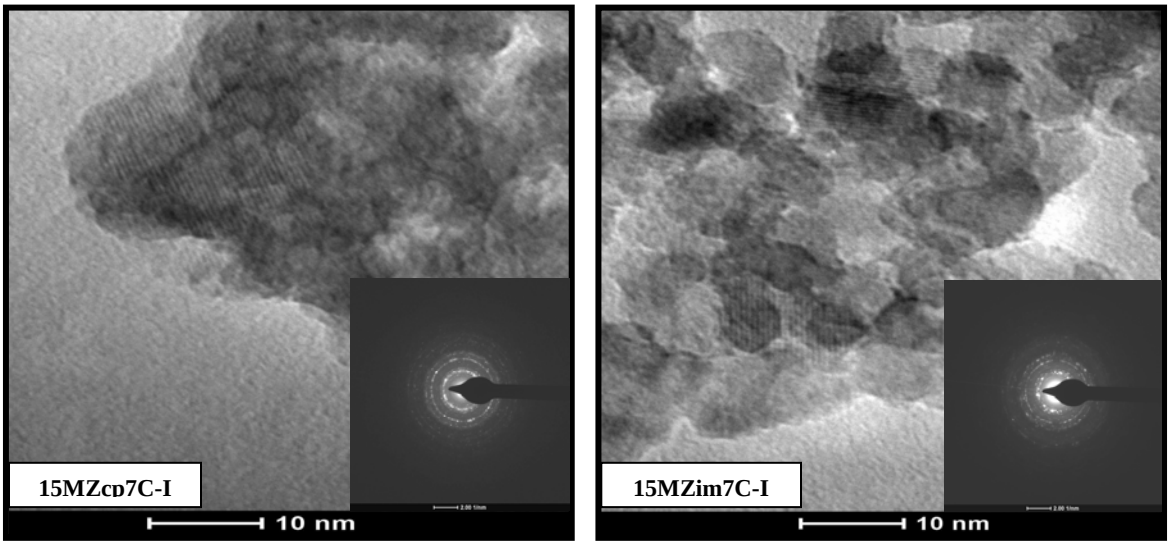

Fig. 4.14: TEM micrographs of 15wt% MoO_3-ZrO_2 catalysts prepared via co-precipitation (15MZcp7C-I) and impregnation (15MZim7C-I) method. (Inset-corresponding SAED patterns).

4.3. CATALYTIC ACTIVITY FOR SYNTHESIS OF CHALCONES

Chalcones have been found numerous applications as pesticides, food additives, solar creams, plastics, pharmaceuticals due to its interesting biological activities. Traditionally, the synthesis of chalcones via Claisen-Schmidt condensation is carried out either in basic or in acidic media under homogenous conditions, but poor selectivity, generation of wastes and laborious separation techniques makes these catalysts practically inconvenient. In the latest decades, heterogeneous catalysis is widely accepted as an environmental friendly alternative for fine chemicals synthesis. Metal oxide catalysts have been used extensively either as such or as supports in conjunction with other active components for many important industrial reactions. Especially, molybdenum oxide loaded on various supports have been applied to a vide variety of catalytic reactions. Molybdenum oxides are the most versatile catalysts which have been used in a wide range of applications. Although MoO_3-/ZrO_2 catalyst is well known for its use in industrially important reactions, the applicability of this important material to organic synthesis involving biologically important molecules is yet to be explored. This motivated us to extend their applications to our reaction. Here we report our recent findings on the efficient synthesis of chalcones by the Claisen-Schmidt condensation reaction under solvent-free conditions catalyzed by molybdenum oxide on zirconia materials. Since elimination of organic solvents is a frequent goal in green chemistry, our catalyst represents a potentially valuable and clean route to prepare a large group of organic compounds useful for pharmaceuticals. A detailed study of the MoO_3 loadings, reaction temperature, influence of solvents, various other reaction conditions and substituting groups in the aromatic rings on the catalytic performance is carried out.

4.3.1. Catalytic testing of various catalysts

The reaction and analytical procedures adopted have been described in Chapter-2, Section 2.5.1. The influences of various catalyst and process parameters on isolated yield and product selectivity were investigated in the studies. The turnover frequency (TOF in $mol/mol_{Mo}.h$) for all the catalysts was calculated from the mol. of product formed after 16 h, the actual Mo present and catalyst weight used during the reaction. These are reported and discussed below. On the basis of some similarities and differences in the

characteristics of various MoO_3-/ZrO_2 samples, some initial optimization studies were carried out using 15MZcp7C-I for evaluating the efficiency in Claisen-Schmidt condensation reaction. 15MZcp7C-I sample was selected on basis of the results obtained from XRD, UV-vis, RAMAN, IR and surface density characterization techniques and the reactions were carried out with equimolar quantities of benzaldehyde and acetophenone. The blank reaction carried with pure zirconia sample (ZIV-7C) without MoO_3 loading, showed a chalcone product yield less than 30%, as expected, with the increase in percentage MoO_3 concentration the yield of chalcone increases (Fig. 4.15).

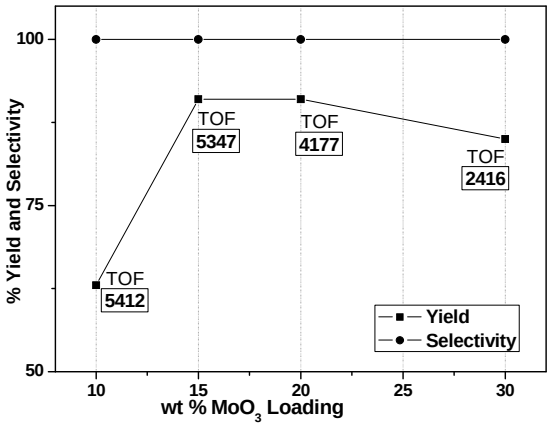

Fig. 4.15: Effect of MoO_3 loading (wt%) on the yield of chalcone when reaction was carried out at 150 ^oC, 16 h in the presence of 1.5 wt% catalyst. TOF values also provided

The inactivity in the condensation reaction on pure zirconia suggests that Mo ions are necessary for the higher activity. In order to confirm whether the reaction is based on pure MoO_3 it was also tested for the reaction, which showed % yield of 65. Invariably, the chalcone selectivity was found to be 100 % for all MoO_3-/ZrO_2 catalyst, irrespective of the conversion levels, except for the pure zirconia and MoO_3 where in selectivity was less then 100 %. The details of reactions conditions and %yield are summarized in Table 4.4. Without column chromatography pure products in good yields are obtained using simple ethanol recrystallization. Moreover, no by products other than chalcone were observed in our reaction products, indicating that Cannizzaro reaction of aldehyde or condensation of ketone does not take place under the present reaction conditions. Increasing the Mo loading increases the product yield, up to 15wt % MoO_3 when calcination is done at 700 ^oC. Even though 20MZcp7C-I showed slightly higher surface area and better acid strength the required active Mo species for the reaction may be

buried/blocked due to formation of $Zr(MoO_4)_2$ around 700 ^oC, due to which no increase in the yield was observed for 20wt % MoO_3 loading. Further increasing the MoO_3 loading decreases the yield.

Table 4.4: Effects of different parameters on MoO_3-/ZrO_2 catalyzed CSC.

Entry No.	Catalyst	BA/AP molar ratio	*Catalyst Wt. (%)	Reaction temp (◦C)	Reaction Time (h)	% Yield	TOF[#]
(A) Comparison with other catalyst			--	--	--	--	--
1	ZIV-7C	1:1	1.5	150	16	26	--
2	MoO_3	1:1	1.5	150	16	65	499
3	15MZim7C-I	1:1	1.5	150	16	88	5235
4	15MZim7C-II	1:1	1.5	150	16	88	4770
5	15MZim7C-III	1:1	1.5	150	16	90	5031
(B) Effect of BA/AP molar ratio			--	--	--	--	--
6	15MZcp7C-1	1:0.5	1.5	150	16	48	--
7	15MZcp7C-1	1:1	1.5	150	16	91	5347
8	15MZcp7C-1	1:2	1.5	150	16	92	--
(C) Effect of Solvent			--	--	--	--	--
9	15MZcp7C-1	1:1[a]	1.5	150	16	50	2938
10	15MZcp7C-1	1:1[b]	1.5	150	16	7	411

*- Catalyst Wt% with respect to the weight of total reaction mixture.
a - Solvent benzonitrile (5ml), b - Solvent Dimethyl sulfoxide (5ml).
[#] -TOF in $mol/mol_{Mo}.h$ [Turn over frequency i.e. the number of molecules formed per mole of Mo (catalytic site) per hour]

Using calcination temperature below 700 ^oC could have reduced the formation of $Zr(MoO_4)_2$ but for complete crystallization of zirconia, higher temperatures were necessary as most of the catalyst prepared showed crystallization exotherm above 600 ^oC (Section 4.2.2. TG-DTA Analysis, Fig. 4.1). The rate of chalcone formation (TOF) decreases continuously due to corresponding increase in the concentration of Mo in the total amount of catalyst used. This suggests that well dispersed active Mo-surface polymeric species expected above monolayer coverage are present, while at higher loadings these species convert into bulk MoO_3 and/or from solid solution of $Zr(MoO_4)_2$ which are less active. Superior activity may be due to higher calcination temperatures which favor formation of more polymeric species. Initial investigations of the various 15 wt% MoO_3-/ZrO_2 catalyst prepared via different method and synthesis parameters on the reaction yielded some interesting results. Although, impregnated samples 15MZim7C-I, 15MZim7C-II and 15MZim7C-III are having more or less identical surface density ~6.3 Mo atom/nm^2, the catalytic performance of co-precipitation sample 15MZcp7C-I whose

surface density is ~6.7 Mo atom/nm^2 was found to be almost identical. Fig. 4.16 shows that the catalyst under solvent-free conditions has much higher yields for chalcone, indicating that solvent can hamper the conversion of the reactants. This may be due to dilution of the concentration of the reactant by the solvent molecules, which would reduce the contact probability between the reactant molecules and the acid active sites on the catalyst. Conversion of the product was also found dependent on the basis of the polarity of the solvents used (Table 4.4). The decrease in activity with increasing polarity of the solvent may be due to stronger interaction of the surface hydroxyl group with the solvent molecules. As a result, the solvent molecules block the active sites and hinder the adsorption of the reactant molecules. In highly polar DMSO (Di-methyl Sulfoxide), the product yield was only 7 % after 16 h. In comparison, when less polar Benzonitrile was used as solvent, product yield was 50 %, with no variation in selectivity.

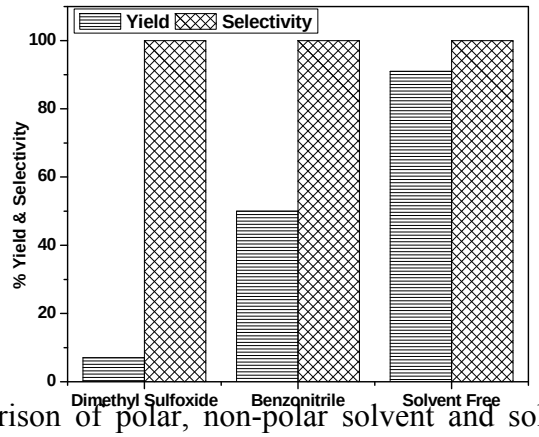

Fig. 4.16: Comparison of polar, non-polar solvent and solvent free conditions on the yield and selectivity of chalcone when condensation was carried out at 150^{o}C in the presence of 15MZcp7C-I catalyst (1.5 wt%). Solvent – 5ml.

4.3.2. Influence of the reaction time

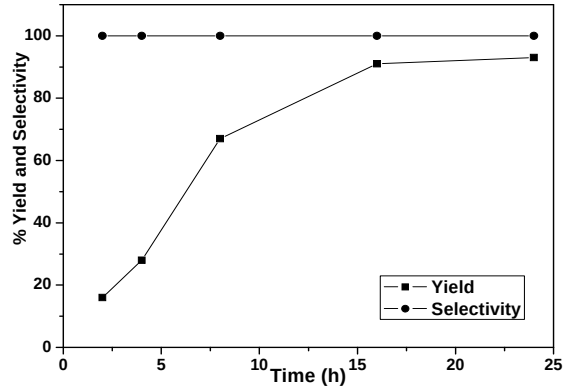

Fig. 4.17: Influence of reaction time on the yield and selectivity of chalcone when condensation was carried out at 150^{o}C in the presence of 15MZcp7C-I catalyst (1.5 wt%)

The influence of run duration on product yield and selectivity during the Claisen-Schmidt condensation reaction under solvent-free conditions catalyzed by 15MZcp7C-I at 150 ^{o}C with 1.5 wt% catalyst is presented in Fig. 4.17. It is noted that the yields increased linearly with the reaction time till 16 h. All the samples have shown the maximum conversion after 16 h, continuing the reaction up to 24 h, only marginal increase in the yield was observed. Therefore, for comparison purpose, the catalytic data after 16 h was considered.

4.3.3. Influence of the catalyst concentration

The effect of catalyst (15MZcp7C-I) amount on the synthesis of chalcone was investigated by varying the catalyst amount from 0.7 to 6.0 wt% with respect to total weight of the reaction mixture (Fig. 4.18).

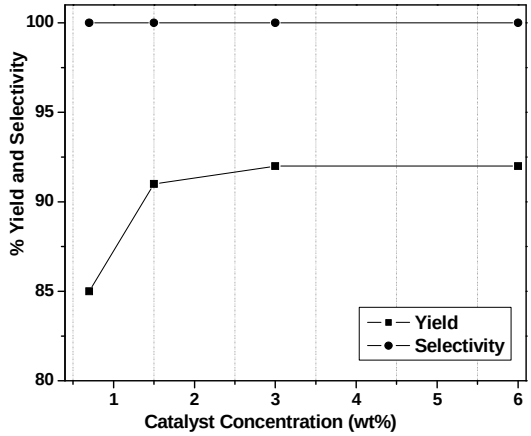

Fig. 4.18: Effect of catalyst weight (%) on the yield of chalcone at 150 ^{o}C, 16 h.

As the amount of catalyst increased from 0.7 to 1.5 wt%, formation of chalcone increases from 85 to 91%. Above 1.5 wt% of the catalyst, no significant change occurred. The optimum catalyst loading was found to be 1.5 wt% for the synthesis of chalcone [benzaldehyde to acetophenone molar ratio (1:1)], indicating only catalytic amount of catalyst is required for the reaction which is far less then usually reported catalyst amount.

4.3.4. Influence of the temperature

The effect of the reaction temperature on the catalytic activity and selectivity was examined between 100 and 175 ^{o}C in the absence of solvent over 15MZcp7C-I catalyst, are illustrated in Fig. 4.19. It was found that the product yield increased gradually with

increasing reaction temperature from 100 to 150 ^{o}C. One of the reasons for the increased yields at higher temperature may be ascribed to an enhancement of the rate of interaction of the reactants on the catalyst surface. As the temperature was further increased, the yield was almost unchanged and kept around 92%. The leveling off is probably due to the blockage of catalytic centers by the high concentration of the products at this high conversion stage. As significant increase in the yield was not noticed beyond 150 ^{o}C, all experiments were done at 150 ^{o}C.

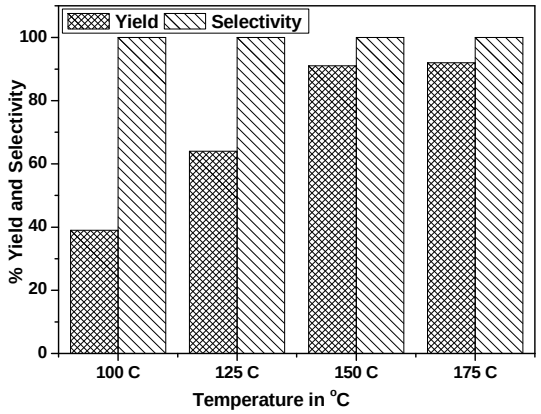

Fig. 4.19: Influence of reaction temperature on the yield of chalcone when condensation was carried out for 16 h in the presence of 15MZcp7C-I catalyst (1.5 wt%)

4.3.5. Influence of molar ratio of the reactants

For stoichiometric conversion 1 mole of benzaldehyde and 1 mole of acetophenone are required. An excess of acetophenone in the reaction mixture can increase the rate of conversion. The molar ratios were changed by keeping the amount of benzaldehyde constant. The influence of molar ratio on the formation of chalcone was investigated and the results are presented in Table 4.4. An increase in the molar ratio from 1 to 2, does not increase the product yield, but the decrease in the molar ratio significantly decreases the yield. The selectivity does not appear to be influenced by the molar ratio of the feeds over this catalyst. Based on the above observation, we found that 1:1 molar ratio of benzaldehyde : acetophenone is optimum for high yields.

4.3.6. Catalyst leaching and recycle studies

These experiments were again carried out over the 15MZcp7C-I catalyst. In order to check the leaching of active species from MoO_3-ZrO_2 catalysts into the reaction medium during CSC reaction, the reaction mixture was filtered while hot after 4h of the

reaction. The reaction was continued with the filtrate for 16 h. The yield remained same even after 16h of reaction, which indicates that no active species is leached into the reaction medium. In order to check the stability and catalytic activity, the catalyst was recycled (fresh + three cycles) in the condensation reaction. The results are presented in Fig. 4.20.

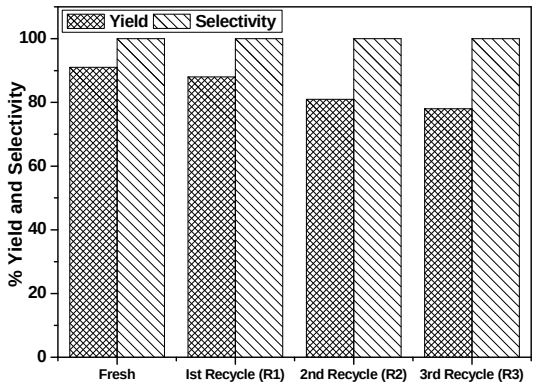

Fig. 4.20: Catalyst recyclibility study

15MZcp7C-I catalyst which gave highest yield, was separated from the reaction mixture by filtration, washed with acetone many times to remove adsorbed reactants and products, dried at 110 ^{o}C for 10 h in air heated oven and reused for the next experiment. After every recycle, same procedure was repeated and used for the next recycle. It is observed that yield decreases to 78 % after third recycle. The decrease in activity is due to the progressive obstruction of the active sites of the catalyst by reaction product or reactants are not completely removed during the washing and drying process. Therefore the catalyst was calcined at 500 ^{o}C for 4 h and reused, giving 90 % product yield. The catalyst recovered after the third recycle was calcined and analyzed by AAS for Mo content, which showed almost no loss of Mo.

4.3.7. Influence of substituting groups

The effect of substituting groups in the para position of benzaldehyde as well as acetophenone was probed to know the role of ring substituents in condensation reactions in the absence of solvent (Scheme. 4.1).

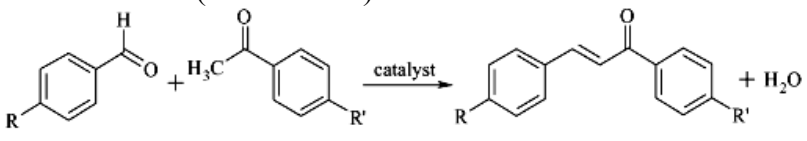

R, R' = H, OCH_3, Cl

Scheme 4.1: Claisen-Schmidt condensation (CSC) of substituted benzaldehyde and acetophenone over 15MZcp7C-1 catalyst.

The substituting groups in the aromatic rings have a great influence on the conversion and selectivity. Results summarized in Table 4.5 showed that the presence of electron donating groups in the para position of benzaldehyde or acetophenone had a positive effect in the conversion while the presence of electron withdrawing groups in the para positions decreased the conversion.

Table 4.5: Reactions of benzaldehyde and Acetophenone with various substituting groups in the absence of solvent over 15MZcp7C-1 catalyst at 150 ^{o}C for 16 h.

Sr. No.	R	R'	% Yield	Selectivity	BA/AP (M.R.)	Catalyst Wt. (%)
1	H	H	91	100	1:1	1.5
2	H	OCH_3	76	100	1:1	1.5
3	H	Cl	97	100	1:1	1.5
4	OCH_3	H	78	100	1:1	1.5
5	Cl	H	96	100	1:1	1.5

These trends in conversion are in line of those observed on other solid base or acid catalysts [84,159,160]. The steric effect of substituting groups such as NO_2, Cl, and OCH_3 are known to decrease catalytic activities over other solid acid/base catalysts [161,162]. However, this seems to be negligible in our system, which may be due to the relatively high surface activity of the MoO_3 based catalyst.

4.3.8. Reaction Mechanism

Acid-base and redox properties are the most important types of surface chemical properties of metal oxide catalysts. When a base catalyst is used, the reaction mechanism generally involves the formation of the anion of acetophenone through the deprotonation of the methyl group, followed by its attack on the carbonyl group on benzaldehyde. Since the catalyst applied is a solid acid catalyst this reaction follows the mechanism of acid-catalyzed condensation reactions. In our case MoO_3-/ZrO_2 catalysts acts as a solid acid catalyst, protonating the aldehyde. This protonated aldehyde is attacked by the enolic form of acetophenone. This catalyst also initiates the dehydration of the condensed product to form chalcone. A similar mechanism has been proposed for this reaction with the acid catalyst [157,163,164]. MoO_3-/ZrO_2 catalysts therefore have proved to be an excellent heterogeneous catalyst for solvent free preparation of chalcone with yield as high as 93 % in the present studies.

4.3.9. Analysis of the Reaction Products

In the present studies the product obtained was confirmed using FT-IR (Fig. 4.21), GC-MS (Shimadzu QP 2000 A) by injecting authentic samples and ^{1}H-NMR and ^{13}C-NMR. The GC-MS spectrum has one strong peak and gave the molecular weight of benzalacetophenone (208).

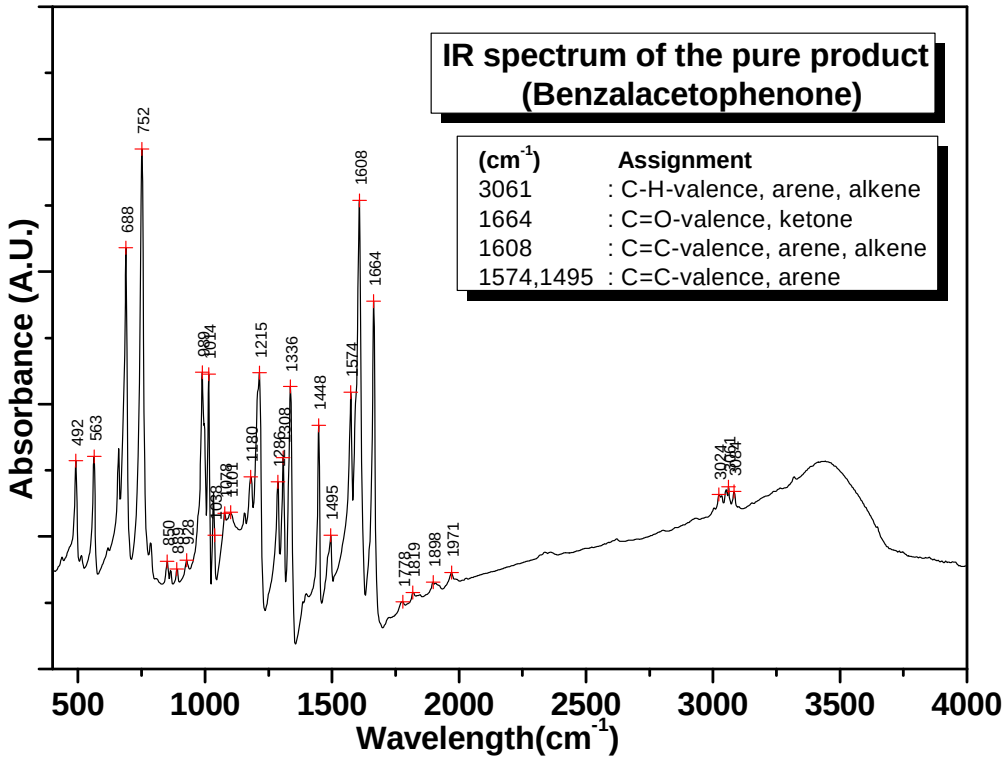

Fig. 4.21: IR spectrum of the Benzalacetophenone (Chalcone) obtained at 150 ^{o}C after 16 h of reaction.

NMR is widely used as one of an armory of instrumental techniques for the identification and confirmation of the product structure. Two important NMR spectroscopy techniques ^{13}C (Carbon-13) NMR and ^{1}H (H-1) proton NMR where utilized for the confirmation of the product. ^{1}H NMR ($CDCl_3$, 200 Mhz): 7.38-7.67 (m, 9H), 7.78 (d, 1H), 7.99-8.05 (m, 2H). ^{13}C NMR ($CDCl_3$, 200 Mhz): 122.11, 128.50, 128.55, 128.67, 129.00, 130.60, 132.64, 144.93, 190.69.

4.4. CONSLUSIONS

This research study, describe the synthesis, characterization and catalytic application of MoO_3-/ZrO_2 catalyst with various composition. Addition of Mo stabilizes ZrO_2 in the meta-stable tetragonal phase instead of turning into the monoclinic phase. Even at higher temperatures of calcination, this phase is preserved by modified synthesis procedure. This modified synthesis procedure has led the formation of catalyst with high surface area and stable tetragonal phase. Keeping identical synthesis conditions an addition of surfactant has shown no significant effect on the structural properties of the MoO_3-/ZrO_2 catalyst. A more complexing initial precursor and/or further optimization of synthesis parameters may be required to obtain higher surface areas in the presence of surfactant (P-123). The digestion at pH=12 for 24 hrs at 80 ^oC lead to a decrease in the crystallite size of the zirconia, resulting in an increase in the specific surface area. The surface area and phase formation of MoO_3-/ZrO_2 catalysts strongly depend upon the preparation procedure. The interaction between molybdenum oxide and zirconia influences the physicochemical properties is be ascertained by a combination of FTIR, Raman spectroscopy, TG-DTA, UV and XRD characterization techniques. Isolated tetrahedral MoO_4, two-dimensional polymolybdates, crystalline MoO_3 and $Zr(MoO_4)_2$ species are detected using Raman, FTIR, UV and X-ray diffraction, in the samples loaded with 15 wt % MoO_3 on ZrO_2, calcined at 700 ^oC. MoO_3-ZrO_2 samples calcined at 700 ^oC, prepared with MoO_3 loading from 10 to 30 wt%, shows presence of $Zr(MoO_4)_2$, whose quantity increased upon increasing MoO_3 loading. Even though 10wt% MoO_3-ZrO_2 catalyst prepared via co-precipitation method exhibited surface density below monolayer value ~5 Mo/nm^2, $Zr(MoO_4)_2$ is detected. Independent of methodology (coprecipitation and impregnation) adopted for 15 wt% MoO_3-/ZrO_2 catalysts prepared via modified preparation techniques prove to be an excellent heterogeneous catalyst for solvent free synthesis of chalcone with yield as high as 93 %, by using only 1.5 wt% of catalyst. The etiquette developed for the solvent free synthesis of chalcone using the MoO_3-/ZrO_2 catalyst was beneficial in terms of simple experimentation, deterrence of toxic solvents, recyclable catalyst, high yield and purity of the products. All these catalyst showed the presence of small amounts of crystalline MoO_3 and $Zr(MoO_4)_2$ species.

4.5. REFERENCES:

[1] R.A. Sheldon, R.S. Downing, Appl. Catal. A, 1999, 189,163.

[2] M. Besson, M.C. Bonnet, P. Gallezot, I. Tkatchenko, A. Tuel, Catal. Today, 1999, 51, 547.

[3] Y. Kubota, Y. Nishizaki, H. Ikeya, M. Saeki, T. Hida, S. Kawazu, M. Yoshida, H. Fujii, Y. Sugi, Micropor. Mesopor. Mater., 2004, 70, 135.

[4] X. Wang, Soofin Cheng, Catalysis Communications, 2006, 7, 689–695.

[5] S. Samantaray, G. Hota, B.G. Mishra, Catalysis Communications, 2011, 12, 1255-59

[6] E.A. El-Sharkawy, A.S. Khder, A.I. Ahmed, Micropor. Mesopor. Mater.,2007, 102, 128–137.

[7] K.V.R. Chary, K.R. Reddy, G. Kishan, J.W. Niemantsverdriet, G. Mestl, J. Catal., 2004, 226, 283–291.

[8] A. Calafat, L. Avilán, J. Aldana, Appl. Catal. A, 2000, 201, 215–223.

[9] D.S. Kim, I.E. Wachs, K. Segawa, J. Catal.,1994, 146, 268–277.

[10] Z. Liu, Y. Chen, J. Catal.,1998, 177, 314–324.

[11] A.S.C. Brown, J.S.J. Hargreaves, Top. Catal., 2009, 52,458–463.

[12] X. Wang, C. Li, Y. Wang, and T.Xi. Cai, Catalysts, Catal. Today, 2004, 93–95, 135–140.

[13] T. Matsuda, H. Sakagami, and N.Takahashi, Appl. Catal., A, 2001, 213, 83–90.

[14] Y. Ono, A, Catal. Today, 2003,81,3–16.

[15] B. M. Reddy and M. K. Patil, Chemical Reviews, 2009,109, 2186.

[16] S.M. Kemdeo, V.S. Sapkal , G.N. Chaudhari, Bulletin of Chemical Reaction Engineering & Catalysis, 2010, 5, 39 – 49.

[17] Abd El-Aziz A Said and Mohamed MM Abd El-Wahab, J Chem Technol Biotechnol , 2006, 81, 329–335.

[18] D. P. Debeckera, M Stoyanovab, URodemerckb, E M. Gaigneaux, Journal of Molecular Catalysis A: Chemical, 2011, 340, 65–76.

[19] A Gervasini, L Wahba, M D Finol, J-F Lamonier , Materials Sciences and Applications, 2012, 3, 195-212.

[20] T.M. Sankaranarayanan, A. Pandurangan, M. Banu, S. Sivasanker, Applied Catalysis A: General, 2011, 409– 410, 239– 247.

[21] L Dall'Acqua, I Nova, L Lietti, GRamis, G Buscac and E. Giamello, Phys. Chem. Chem. Phys., 2000, 2, 4991-4998.

[22] T. Yamaguchi, Catal. Today, 1994, 20, 199.

[23] P.D.L. Mercera, PhD thesis, Twente Institute of Technology, 1991.

[24] H. Miyata, S. Tokuda, T. Ono, T. Ohno, F. Hatayama, J. Chem. Soc., Faraday Trans. ,1990, 86, 2291.

[25] K.V.R. Chary, K. Ramesh, G. Vidya sagar, V. Venkat Rao, J. Mol. Catal., 2003, 198,195.

[26] M. Vrinat, D. Hamon, M. Breysse, B. Durand, T. des Courieres, Catal.Today, 1994, 20, 273.

[27] J.G. van Ommen, P.J. Ceilings, J.R.H. Ross, in: D.M. Bibby, C.D.Chang, R.F. Howe, S. Yurchak (Eds.), Methane Conversion, Elsevier,Amsterdam, 1988, 213.

[28] Y. Amenomiya, Appl. Catal.,1987, 30, 57.

[29] T. Iizuka, M. Kojima, K. Tanabe, J. Chem. Soc., Chem. Commun., 1983, 638.

[30] Y. Cai, Y. Niu, Z. Chen, Fuel Process. Technol.,1997, 50, 163.

[31] M. Gruttadauria, L.F. Liotta, G. Deganello, R. Noto, Tetrahedron Lett., 2003, 59, 4997.

[32] S. Wang, J.A. Guin, Fuel Process. Technol., 2003, 84, 135.

[33] M. Kim, C. DiMaggio, S. Yan, H. Wang, S.O. Salley, K.Y. Simon Ng, Bioresour. Technol., 2011, 102, 2380–2386.

[34] J. G.Weissman, U. S. Patent , 2009, 7569512.

[35] K. Tanabe, Mater. Chem. Phys., 1985, 13, 347.

[36] R. Gopalan, C.H. Chang, Y.S. Lin, J. Mater. Sci., 1995, 30, 3075.

[37] G. Jin, G. Lu, Y. Guo, et al., J. Mol. Catal. A: Chem., 2005, 232, 165.

[38] M.D. Rhodes, A.T. Bell, J. Catal. 2005, 233, 198–209.

[39] W. Stichert, F. Schuth, S. Kuba, H. Knozinger, J. Catal. 2001, 198, 277–285.

[40] W. Li, Y.Q. Yin, R.X. Gao, R.L. Hou, J. Mol. Catal. (China) 1999, 13, 186–192.

[41] D. He, Y. Ding, H. Luo, C. Li, J. Mol. Catal. A 2004, 208, 267–271.

[42] K.T. Jung, A.T. Bell, J. Mol. Catal. A 2000, 163, 27–42.

[43] S. Xie, E. Iglesia, A.T. Bell, Chem. Mater. 2000, 12, 2442–2447.

[44] G.K. Chuah, S. Jaenicke, S.A. Cheong, K.S. Chan, Appl. Catal. A: General, 1996, 145, 267.

[45] A. Calafat, in B. Delmon, P.A. Jacobs, R. Maggi, J.A. Martens, P. Grange, G. Poncelet (Eds.), Preparation of Catalysis VII, Elsevier, Amsterdam, 1998, 837.

[46] B. Zhao, X. Xu, H. Ma, D. Sun, J. Gao, Catal. Lett., 1997, 45, 237.

[47] K. Arata, M. Hino, Mater. Chem. Phys.,1990, 26, 213.

[48] K. Arata, Adv. Catal., 1990, 37, 165.

[49] Y.C. Xie, Y.Q. Tang, Adv. Catal., 1990, 37, 1.

[50] M. Hino, K. Arata , Chem Lett., 1989, 971.

[51] B. Samaranch , P. Ramirez de la Piscina, G. Clet, M. Houalla, N. Homs, Chem Mater, 2006, 18, 1581.

[52] M.A. Banares, H.C. Hu, I.E. Wachs, J Catal, 1994, 150, 407.

[53] J. R. Sohn, E. W. Chun, and Y. I. Pae, Bull. Korean Chem. Soc., 2003, 24, 12, 1785.

[54] S. Xie, K. Chen, A. T. Bell and E. Iglesia, J. Phys. Chem., B 2000, 104, 10059-68

[55] D.M. Tomazela, M.T. Pupo, E.A.P. Passador, M.F.G.F. da Silva, P.C. Vieira, J.B.Fernandes, F.E. Rodrigues, G. Oliva, J.R. Pirani, Pyrano Phytochemistry 2000, 55, 643.,

[56] L.W. Wattenberg, J.B. Coccia, A.R. Galbraith, Cancer Lett. 1994, 83, 165.

[57] A.T. Dinkova-Kostova, C. Abeygunawardana, P. Talalay, J. Med. Chem. 1998, 41, 5287.

[58] V.J. Ram, A.S. Saxena, S. Srivastava, S. Chandra, Bioorg. Med. Chem. Lett., 2000, 10, 2159

[59] M. Kidwai, P. Sapra, P. Misra, R.K. Saxena, Bioorg. Med. Chem. 2001, 9, 217.

[60] J.F. Ballesteros, M.J. Sanz, A. Ubeda, M.A. Miranda, S. Iborra, M. Paya, J. Med. Chem., 1995, 38, 2794.

[61] L.M. Lin, Y. Zhou, M.T. Flavin, L.M. Zhou,W. Nie, F.C. Chen, Bioorg. Med. Chem., 2002, 10, 2795–2798.

[62] M. Satyanarayana, P. Tiwari, B.K. Tripathi, A.K. Srivastava, R. Pratap, Bioorg. Med. Chem., 2004, 12, 883–886.

[63] J.B. Harbone, T.J. Mabry, The Flavonoids: Advances in Research; Chapman & Hall: New York, 1982.

[64] M.T. Drexler, M.D. Amiridis, J. Catal. 2003, 214, 136.

[65] S. V. Kostanecki and Tambor, J. Chem Ber., 1921, 32, 1899.

[66] H.O. House, Modern Synthetic in Organic Synthesis, 2nd ed. (W.A. Benjamin, New York, 1972).

[67] H. Rupe and D. Wasserzug, J. Chem Ber.,1901, 34, 3527.

[68] S. A. Hermes, Chem Ber.,1969, 70, 96422h.

[69] D. S. Breslow and C. R. Houser, Chem Ber., 1940, 62, 2385.

[70] N.O. Calloway, L.D. Green, J. Am. Chem. Soc., 1937, 59, 809–811.

[71] T. Sz'ell, I.Can. Sohalr, J. Chem., 1969, 47, 1254–1258.

[72] D. S. Noyce and W. A. Pryor, J. Am. Chem. Soc, 1955, 11, 1397.

[73] D. S. Noyce, W. A. Pryor and A. H. Bottini, J. Am. Chem. Soc, 1955, 77, 1402.

[74] K. Irie, K. Bull. Watanabe, Chem. Soc. Jpn. 1980, 53, 1366–1371.

[75] L. Mazza, A. Guaram, Synthesis 1980, 41–44.

[76] T. Nakano, S. Irifune, S. Umano, A. Inada, Y. Ishii, M. Ogawa, J. Org. Chem., 1987, 52, 2239–2244.

[77] N. Iranpoor, F. Kazemi, Tetrahedron, 1998, 54, 9475–9480.

[78] T. Narender, K. Papi Reddy, Tetrahedron Lett., 2007, 48, 3177–3180.

[79] D.F. Huang, J.X. Wang, Y.L. Hu, Chin. Chem. Lett., 2003, 14, 333–334.

[80] O. Petrov, Y. Ianova, M. Gerova, Catal. Commun., 2008, 9, 315–316.

[81] J. Shen, H. Wang, H. Lia, Y. Sun, Z. Liu, J. Mol. Catal. A: Chem. 2008, 280, 24–28.

[82] M. L. Kantam, B. V. Prakash, and Ch. V. Reddy, Synthetic Communications, 1978, 35, 14,1971.

[83] Q. Xu, Z. Yang, D. Yin, F. Zhang, Catalysis Communications, 2008, 9, 1579–1582.

[84] S. Shylesh , P. P. Samuel , Ch. Srilakshmi , R. Parischa , A.P. Singh, Journal of Molecular Catalysis A: Chemical, 2007, 274, 153–158.

[85] M.J. Climent , H. Garcia, J. Primo and A Croma Catalysis Letters, 1990, 4, 85-92.

[86] D.N. Dhar, The Chemistry of Chalcones and Related Compounds; Wiley: New York, 1981.

[87] A. Adamski, P. Zapała, P. Jakubus, Z. Sojka, Top Catal, 2009, 52, 993–1000.

[88] W W.M. Shaheen, Mater. Lett., 2002, 52, 272.

[89] M. Shaheen, M.M. Selim, J. Therm. Anal. Calorim., 2000, 59, 961.

[90] J. Michael. Hudson and James A. Knowles , J. Muter. Chem., 1996, 6, 89-95.

[91] B. Zhao, X. Wang, H. Ma, Y. Tang, J Mol Catal A, 1996, 108, 167.

[92] P. Afanasiev, C. Geantet, M. Breysse, J Mater Chem., 1994, 4, 1653.

[93] M. Auray, M. Quarton, P. Tarte, Acta Crystallogr., 1986, C42, 257.

[94] T. Ono, H. Kamisuki, H. Hisashi, H. Miyata, Journal of Catalysis, 1989, 116, 303-07

[95] B.M. Reddy, B. Chowdhary, P.G. Smirniotis, Appl. Catal. A: Gen., 2001, 211, 19.

[96] A. M. Garrido Pedrosa, D. M. A. Melo, M. J. B. Souza, And A. S. Araujo, Inorganic Materials, 2008, 44, 285–290.

[97] P. Afanasiev, Mater. Chem. Phys., 1997, 47, 231.

[98] K.S.W. Sing, D.H. Everett, R.A.W. Haul, L. Moscou, R.A. Pierotti , J. Rouquerol and T. Siemienewska, Pure & Appl. Chem.,1985, 57, 603.

[99] D.Y. Zhao, J.Y. Sun, Q.Z. Li, Chem. Mater., 2000, 12, 275.

[100] P. Afanasiev, A. Thiollier , M. Breysse and J.L. Dubois, Topics in Catalysis, 1999, 8, 147–160.

[101] K. Tanabe, M. Misono, Y. Ono and H. Hattori, New Solid Acids and Bases, Kodansha-Elsevier, Tokyo-Amsterdam, 1989, 4.

[102] J.C. Yori, C.L. Pieck, J.M. Parera, Catalysis Letters, 2000, 64, 141-146.

[103] I. E. Wachs, Catalysis Today, 1996, 27, 437-455.

[104] E, Hillerova, H. Morishige, K. Inamura, M. Zdrazil, M. Appl. Catal. A: Gene., 1997, 156, 1.

[105] F. Prinetto, G. Cerrato, G. Ghiotti, A. Chiorino, M.C. Campa, D. Gazzoli, V. Indovina, J. Phys. Chem., 1995, 98, 5556.

[106] J. Sonnemans, P. Mars, J. Catal. 1973, 31, 209.

[107] X. Wang, B. Zhao, D. Jiang, Y. Xie, Appl. Catal. A: Gene 1999, 188, 201.

[108] Z. Liu, L. Dong, Y. Chen, J. Chem. Soc., Faraday Trans. 1998, 94, 1137.

[109] M. Del Arco, S.R.G. Carraza´n, V. Rives, F.J. Gil-LlambRas, P. Malet, J. Catal., 1993, 141, 48.

[110] P. Dufresne, E. Payne, J. Grimblot, J.P. Bonnelle, J. Phys. Chem, 1981, 85, 5, 2344

[111] D.S. Zingg, L.E. Makovsky, R.E. Tischer, F.R. Brown, D.M. Hercules, J. Phys. Chem., 1980, 84, 2898.

[112] J.C. Edwards, R.D. Adams, P.D. Ellis, J. Am. Chem. Soc.,1990,112, 8349.

[113] Takehiko Ono, Hisashi Miyata and Yutaka Kubokawa, J. Chem. Soc., Faraday Trans. I, 1987, 83, 1761-1770.

[114] C. M. Phillippi And K. S. Mazdiyasni, Journal Of The American Ceramic Society, 1971, 54, 258.

[115] J.R. Sohn, I.J. Doh, Y.I. Pae, Langmuir 2002, 18, 6280. 36.

[116] M. Scheithauer, R.K. Grasselli, H. Knözinger, Langmuir, 1998, 14, 3019.

[117] R.E. Benner, A.S. Nagelberg, Thin Solid Films, 1981, 84, 89.

[118] M.R. Smith, U.S. Ozkan, J. Catal., 1993, 141, 124.

[119] U. Rodemerck, P. Ignaszewski, M. Lucas, P. Claus, Chem. Eng. Technol., 2000, 23, 413–416.

[120] O. Collart, P. Van der Voort, E.F. Vansant, E. Gustin, A. Bouwen, D. Schoemaker, R.R. Rao, B.M.Weckhuysen, R.A. Schoonheydt, Phys. Chem. Chem. Phys.,1999, 1, 4099–4104.

[121] D.P. Debecker, M. Stoyanova, U. Rodemerck, A. Leonard, B.L. Su, E.M. Gaigneaux, Catal. Today, 2010, 07,026.

[122] D.P. Debecker, M. Stoyanova, U. Rodemerck, P. Eloy, A. Lnard, B.L. Su, E.M. Gaigneaux, J. Phys. Chem., 2010, C 114, 18664–18673.

[123] D.P. Debecker, M. Stoyanova, U. Rodemerck, E.M. Gaigneaux, Stud. Surf. Sci. Catal., 2010, 175, 581–585.

[124] W. Li, H. Huang, H. Li, W. Zhang, and H. Liu, Langmuir, 2008, 24, 8358-8366.

[125] H. Liu, P. Cheung, E. Iglesia, J. Catal. 2003, 217, 222–232.

[126] G. Mestl, T. Srinivasan, K. K. Catal. ReV., 1998, 40, 451.

[127] H. Hu, and I.E. Wachs, J. Phys. Chem., 1995, 99, 10897.

[128] J.P. Baltrus, L.E. Makovsky, J.M. Stencel, D.M. Hercules, Anal.Chem., 1985, 57, 2500–2503.

[129] R. Radhakrishnan, C. Reed, S.T. Oyama, M. Seman, J.N. Kondo, K. Domen, Y. Ohminami, K. Asakura, J. Phys. Chem., 2001, B. 105, 8519–8530.

[130] C.C. Williams, J.G. Ekerdt, J.M. Jehng, F.D. Hardcastle, I.E. Wachs, J. Phys. Chem., 1991, 95, 8791–8797.

[131] E.F. Loıpez, V.S. Escribano, M. Panizza, M.M. Carnascialic, G. Busca, J. Mater.Chem., 2001, 11, 1891–1897 .

[132] M. Li, Z. Feng, G. Xiong, P. Ying, Q. Xin, C. Li, J. Phys. Chem., 2001, B.105, 8107–8111.

[133] B.S. Umansky, W.K. Hall, J Catal, 1990, 124, 97–108.

[134] E. F. Lo´pez, V. S. Escribano, M. Panizza, M. M. Carnascialic, and G. Busca, J. Mater. Chem., 2001, 11, 1891–1897.

[135] M. Henker, K.P. Wendlandt, J. Valyon, Appl. Catal., 1991, A. 69, 205–220.

[136] M.M. Mohamed, S.M.A. Katib, Appl. Catal., 2005, A 287, 236–243.

[137] N. Giordano, J.C.J. Bart, A. Vaghi, A. Castellan, and G. Martinotti, J. Catal., 1975, 36, 81.

[138] P. Afanasiev, C. Geantet, and M. Breysse, J. Catal., 1995, 153, 17.

[139] B.M.E. Russbueldt, W.F. Hoelderich, J. Catal., 2010, 271, 290–304.

[140] H. Heziorowski and H. Knozinger, J. Phys. Chem., 1979, 83, 1166.

[141] J. Ryczkowski Catalysis Today, 2001, 68, 263–381.

[142] H.P. Boehnm and H. Knozinger in J.R. Anderson and M. Boudart (Editors), Catalysis, 1983, 4, 2. (Springer, Berlin).

[143] A.M. Turek, I.E. Wachs and E. DeCanio, J. Phys. Chem., 1992, 96, 5000.

[144] F.M. Mulcahy, K.D. Kozminski, J.M. Slike, F. Ciecone, S. J. Scierka, M.A. Eberhardt, M. Houlla and D.M. Hercules, J. Catal., 1993, 139, 688.

[145] T.S. Sian, G.B. Reddy, Appl. Surf. Sci., 2004, 236, 1.

[146] B Tyagi, K Sidhpuria, B. Shaik, and R V Jasra Ind. Eng.Chem. Res., 2006, 45, 8643-508650.

[147] B.A. Marrow and A.J. Mcfarlan, J. Non-Cryst. Solids, 1990, 120, 61.

[148] H. Liu, X. Sun, C. Yin, C. Hu , Journal of Hazardous Materials, 151, 616–622.

[149] B. Delmon, P.A. Jacobs, G. Poncelet, eds. 1976. Preparation of Catalysts.

[150] T. Fransen, P.C. Van-Berge, P. Mars, 23, 405-420, Elsevier, Amstardam.

[151] N.T. McDevitt and W.L. Baun, Spectrochim. Acta, 1964, 20, 799.

[152] A. Srivastava And M.K. Dongare , Materials Letters 1981, 5,3.

[153] D. Mao, G. Lu, Q. Chen, Applied Catalysis A: General, 263, 83-89.

[154] L. Litteti, I. Nova, G. Ramis, L. DallAcqua, G. Busca, E. Giamello, P. Forzatti,

F. Bregani, J. Catal., 1999, 187, 419.

[155] L. Seguin, M. Figlarz, R. Cavagnat, and J.C. Lasseguies, Spectrochim. Acta, 1995, 51, 1323–1344.

[156] K. Chen, S. Xie, E. Tglesia, A. Bell, J. Catal., 2000, 189, 421.

[157] D.C. Rocchiccioli, M. Amirouche, M. Che, J.M. Tatibouet and M. Fournier, J. catal., 1990, 125, 292.

[158] Z. Ji, J.A. Haynes,U, M.K. Ferbe, J.M. Rigsbee, Surface and Coatings Technology, 2001, 135, 109-117.

[159] M.J. Climent, A. Corma, S. Iborra, J. Primo, J. Catal., 1995, 60.

[160] D.J. Macquarrie, R. Nazih, S. Sebti, Green Chem., 2002, 4, 56.

[161] A. Guida, M.H. Lhouty, D. Tichit, F. Figueras, P. Geneste, Appl. Catal., 1997, A 164, 251.

[162] M.J. Climent, A. Corma, S. Iborra, A. Velty, J. Catal., 2004, 221, 474.

[163] J. Shen, H. Wang, H. Liu, Y. Suna, Z. Liu, J. Mol. Catal. A: Chemical 280, 2008, 24–28

[164] A. Aguilera, A.R. Alcantara, J.M. Marinas, J.V. Sinisterra, Can. J. Chem.1987, 65, 1165.

CHAPTER – 5

TUNGSTATED ZIRCONIA SOLID ACID CATALYST

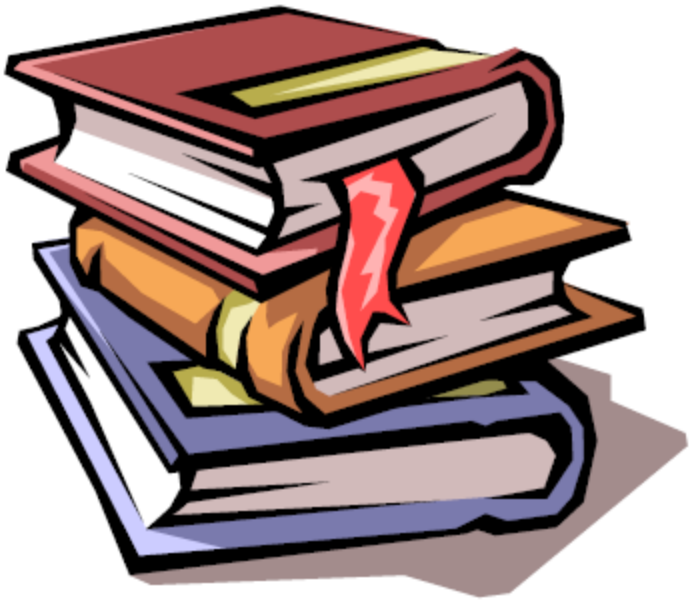

5.1. INTRODUCTION

Growing environmental concerns and corrosion problems caused by the use of liquid acids and halogen-containing solid acids has forced the scientific community to look for highly acidic, environmentally friendly, and more stable solid acids catalysts. In this direction, various solid acid systems were introduced which include hetropolyacids, ion exchange resins (Amberlyst and Nafion-H), zeolites, binary oxides and clays. Among the numerous solid acid catalysts binary oxide based catalysts offer several advantages over the other catalysts since they are active over a wide range of temperatures and more resistant to thermal excursions. Supported solid acid catalysts in which a metal oxide is supported on a different metal oxide (Binary oxide) find tremendous use in commercial chemical production, petroleum refining, and environmental remediation [1]. Amid the solid super acid oxide based catalysts, zirconia-supported sulfated catalysts has attracted much attention because of its ability to catalyze a wide range of reactions such as cracking, alkylation, and isomerization, all needing strong acidity [2]. One of the major drawbacks of sulfate promoted zirconia is the likely sulfate leaching during reaction [3]. Despite this, the catalyst is commercially used [4,5]. On the other hand tungstated zirconia materials are very attractive, environmentally friendly solid acids catalyst firstly primed by Hino and Arata, for light alkane isomerisation over 30 years ago[6]. Since then there has been a continued interest in these materials as a robust alternative to sulphated zirconia and other acid catalysts in industrial acid catalytic processes. Although less active than their sulfate-promoted counterparts, tungstated zirconia catalysts offer inherent advantages over the former from the standpoint of industrial application, such as higher stability under high-temperature treatments, lower deactivation rates during catalysis, superior stability under both reducing and oxidizing conditions, fairly easier regeneration and preparation methods [3,7,8,9,10]. Supported tungsten oxide catalysts are widely used for hydro-desulfurization, alkene metathesis, dehydrogenation of alcohols, and hydro-cracking of heavy fractions in the petroleum industry [11-16]. In addition, WO_3 forms an important component of DeNOx catalysts [17,18,19]. The origin of the catalytic activity and selectivity for these various reactions appears to be related to the WO*x* species present in the acidic catalysts. Depending upon the nature and abundance of these species, a highly active catalyst with strong acidity is developed which is more

efficient and selective [20,21]. However in most of the cases the exact cause for the appearance of strong acidity in tungstate-containing zirconia systems remains unclear and continues to be discussed in the literature [22-28]. In the field of heterogeneous catalysis, the catalytic active species-support interaction has attracted much attention because it plays an important role in controlling the active phase features and in affecting the support properties. Especially in the case of tungstated zirconia solids the interaction between WO_3 and zirconia is of prime importance in order to understand its superior acidic properties. Out of the rich literature available for tungstated zirconia materials, most of them propose and accept the following theory for the formation of highly acidic catalyst. The initial formation of dispersed tungstate species occurs via anion exchange or condensation reactions of hydrated aqueous tungstate anions with surface OH species in zirconium oxy-hydroxide. The resulting high dispersion of WO*x* species inhibits the crystallization and sintering of the zirconia support leading to the formation of WO*x* clusters of varying size and catalytic properties. The catalyst with tungsten loading slightly exceeding the theoretical monolayer coverage was found to be the most active [29,30,31]. Under these conditions tungsten oxide species exist as three-dimensional poly-tungstate clusters on the surface of zirconia. The tungsten atoms in these poly-tungstate clusters are located in a distorted octahedral environment, which are grafted to the support through W-O-Zr bridges. The structure and the size of these clusters, as well as their specific interactions with the zirconia support, largely determine the acidic, redox, and catalytic properties of these catalysts. In tungstated zirconia catalysts, WO_3 poly-tungstate clusters of intermediate size delocalize a net negative charge caused by the slight reduction of W^{6+} centers in reactant environments containing H_2 or hydrocarbons. This temporary charge imbalance leads to the formation of Brönsted acid centers on the zirconia support. A recent publication from W. Zhou et.al in a Nature article [32] has given direct atomic-scale imaging of supported WO*x* species present, including surface mono and poly-tungstate species. It was concluded that the active species in a heterogeneous catalyst system can be positively identified and appropriate modifications to the catalyst preparation route can be devised to increase the number density of these desirable active species, and hence improve the overall activity of the catalyst. Despite several papers devoted to the physical and chemical characterization of tungstated

zirconia materials, the various tungsten dispersion states, their quantification, as well as the features of the interacting species remain controversial [24-46]. The reason underlying this is, the use of different steps and synthesis methods applied during the preparation of tungstated zirconia catalyst which leads to the generation of different WO*x* species, even if catalysts has same tungsten loading, starting precursor, calcination temperature, surface density etc [26,46,47,48,49]. The crystalline structures, acidity and catalytic properties of zirconia-tungsten oxides are greatly dependent on synthesis method. Many synthetic techniques, such as conventional precipitation with different impregnation techniques (evaporation, incipient wetness), micro-emulsion, and sol-gel, have been employed for the preparation of WO_3-/ZrO_2 oxides [22,50,51,52,53]. Tungstated zirconia materials prepared using sol-gel, reverse micelle, hydrothermal synthesis etc processes has also been widely studied [54,55,56,57]. Even-though several techniques have been used for the preparation of tungstated zirconia solid acid catalyst, very few give information regarding the comparison of the properties of materials [22,46,47,51,58]. Santiesteban et al. gives one of such comparison, [51,59] where in the sample prepared by coprecipitation contained twice the amount of strong acid sites and displayed higher activity for n-pentane isomerization compared with another one obtained by impregnation, both with similar W loadings and surface areas and thus similar tungsten surface density. The X-ray diffractograms reported in the work clearly revealed that the intensity of the peaks associated with three-dimensional WO_3 crystallites was much higher for the impregnated catalyst, suggesting that the coprecipitation method favored the dispersion of the WO*x* species on the zirconia surface retarding the formation of WO_3 crystallites. Other authors also emphasized the high degree of dispersion of WO*x* species achieved in tungstated zirconia materials prepared by coprecipitation [60] and sol–gel routes [61]. Most of the tungstated zirconia materials prepared by above methods have relatively small surface area 30-60 m^2/g, the reason for sharp decline in the surface area at high temperatures been the crystalline modifications of zirconia. The influence of Cr, Mo and W species on the surface area and tetragonal phase of supported-zirconia solids is a well known phenomena in the materials science community [30,62,63]. Addition of tungstate retards the growth of zirconia crystals, but the traditional synthesis methods fail to achieve high surface areas along with 100 %

tetragonal phase of zirconia. It has been proposed that the tetragonal phase of zirconia plays an important role in catalytic activity and stability [38,64]. Structure-forming organic templates/surfactants has also been used for gaining mesoporosity with enhanced surface area, nevertheless calcination at temperatures above 500 ^{o}C, the initially formed mesoporous structure collapses during burning down the template/surfactant. In this context, simpler synthesis routes especially for achieving high surface area with tetragonal phase consisting tungstated zirconia materials is highly desired. The objective of our work is to modify the traditional preparation methods to obtain materials with enhanced thermal stability, surface area and study the influence of modified preparation method, process parameters using the same and/or different raw materials on the solid acid catalysts properties (acidity, chemical composition, surface area and percentage of tetragonal phase of zirconia, presence of bulk WO_3 crystals and identification of various WO*x* species). Inclusion of organic surfactant in the modified synthesis procedure in order to obtain still higher surface area is also attempted. The materials prepared with and without surfactant have being compared and studied.

5.2. RESULT AND DISCUSSION

5.2.1. Synthesis of Catalysts

In order to prepare tungstated zirconia (WO_3-/ZrO_2) solid acid catalysts with higher thermal stability, enhanced surface area, acidity and tetragonal phase, the common impregnation, co-precipitation and sol gel methods were modified, the detailed preparation procedures are given in Chapter 2, Section 2.3.3. A series of tungstated zirconia solid acids containing WO_3 content up to 20wt.% covering a wide range of tungsten surface densities (W-atoms/nm^2) were prepared by non-conventional/modified impregnation, sol-gel and co-precipitation routes leading to samples with enhanced surface area with tetragonal phase on annealing at 500-800 ^{o}C. Choosing 20 wt.%, of WO_3 loading was based upon the exhaustive literature done prior to starting this study [17,45,51]. The differentiation in process parameters, sample designation, % weight loss (TG), catalyst color, starting precursor and other details are tabulated in Table 5.1. To examine the relationship between several synthesis variables (viz. precursor effect, pH, gel composition, calcination temperature, digestion time duration, etc.) on the acidity,

physicochemical, morphological properties including its stability the samples were characterized by Powder XRD, N_2 adsorption-desorption, TG/DTG, TEM, SEM, XPS, Ammonia-TPD, XRF, ICP and EDX, the results of which are presented and discussed in this subsequent sections.

Table 5.1: Details of WO_3-/ZrO_2 catalyst prepared with different synthesis methods, starting precursor and process parameters.

Sr. No.	Sample Designation	Synthesis Method	Starting Precursor		Surf-actant Used	Syn pH*	Dig-estion	Catalyst Color Calcination Temp		% Weight Loss (TG)
			Zr	W				700 °C	800 °C	
1	20WZim-I	W-Impg	ZrONit	AMT	Nil	11	Nil	WYT	FYG	26.73
2	20WZim-II	W-Impg	ZrONit	AMT	Nil	11	d1	W	W	23.39
3	20WZim-III	W-Impg	ZrONit	AMT	Nil	11	d2	W	W	20.01
4	20WZim-IV	W-Impg	ZrONit	AMT	P123	11	d1	W	W	23.26
5	20WZim-V	W-Impg	ZrOCl	AMT	Nil	11	d1	W	W	23.59
6	20WZcp-I	Co-Ppt	ZrONit	AMT	Nil	11	d1	W	FYG	23.88
7	20WZcp-II	Co-Ppt	ZrONit	AMT	P123	11	d1	W	FYG	39.89
8	20WZcp-III	Co-Ppt	ZrOCl	AMT	Nil	11	d1	W	W	19.66
9	20WZsg-I	Sol-Gel	ZrBtCl	AMT	P123	2	d1	W	W	38.76
10	20WZsg-II	Sol-Gel	ZrBtCl	AMT	P123	2	Nil	WYT	FYG	46.11

W-Impg = Wet Impregnation, Co-Ppt = Co-Precipitation, * = precipitating pH.
d1 = (12/12 h/80 °C, pH/Time/Temp), d2 = (12/24 h/80 °C, pH/Time/Temp).
W = White, WYT = White with a tinge of yellow green, FYG = Faint yellowish green

5.2.2. TG-DTA Analysis

Thermo Gravimetric (TG) and Differential Thermal Analysis (DTA) of the as synthesized tungstated zirconia samples, prepared using different synthesis methods and process parameters are illustrated in Fig. 5.1 and Fig. 5.2. Thermo-gravimetric analysis of the un-calcined tungstated zirconia samples in air showed a weight loss of 19-46 % (Table. 5.1). Weight loss is high for 20WZsg-I and 20WZsg-II samples since both the samples were prepared using surfactant P-123 and zirconium alkoxide as starting precursors as compared to other samples which were prepared using zirconium salts. A minor modification was done while processing sample 20WZcp-II. After the sample was prepared it was filtered, and without giving any washing it was dried as per standard procedure adapted for other samples. This was done expecting that presence of template during the calcination might increase the mesoporosity and surface area. Due to this modification, the weight loss observed for sample 20WZcp-II was high, indicating that the surfactant is retained in the as-synthesized materials. Such a high weight loss was not

seen in sample 20WZim-IV since the surfactant P-123 used during synthesis, had got sluice down during washing of initial zirconium hydroxide before impregnation of W.

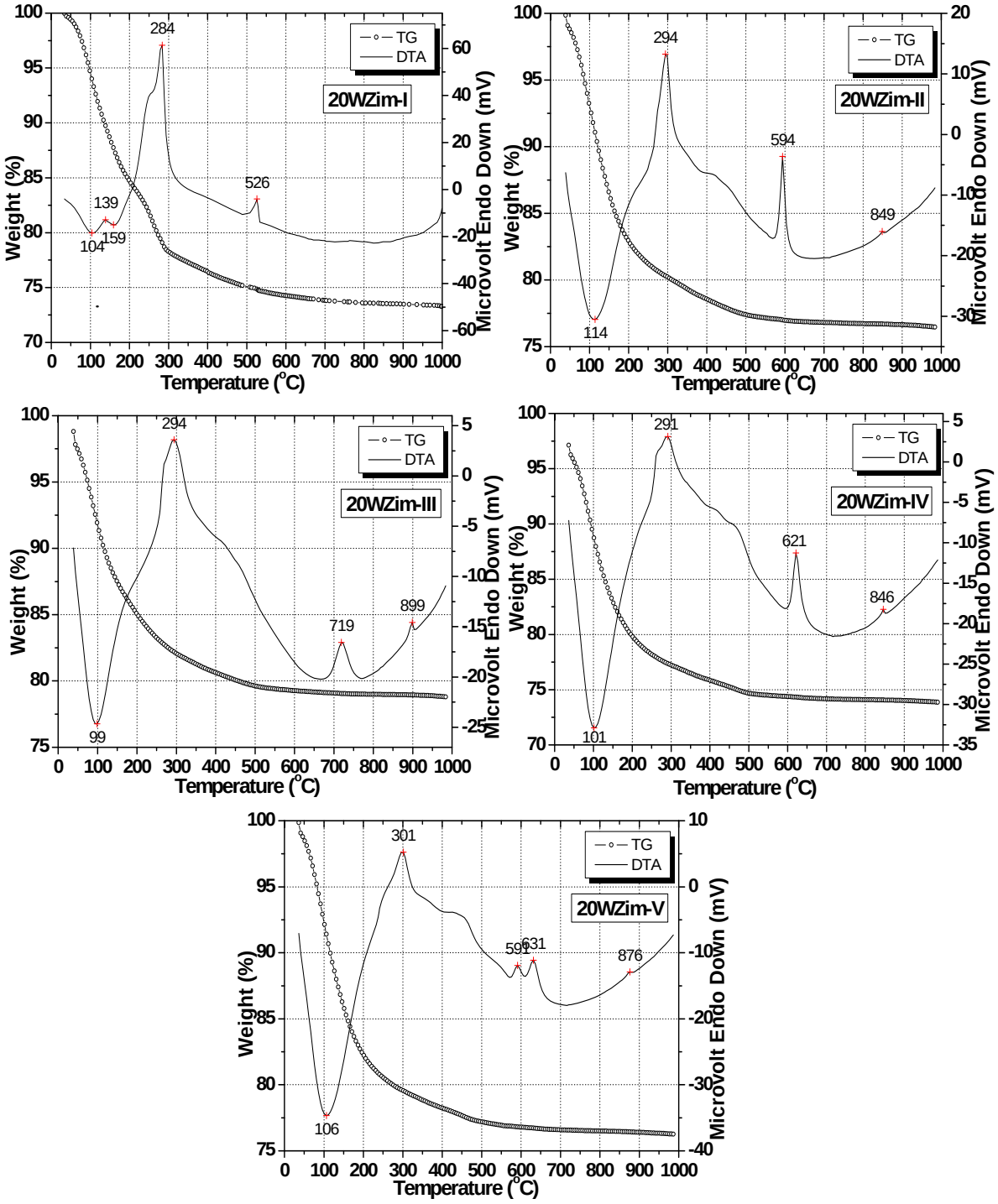

Fig. 5.1: TG-DTA of as-synthesized tungstated zirconia samples prepared using modified impregnation method.

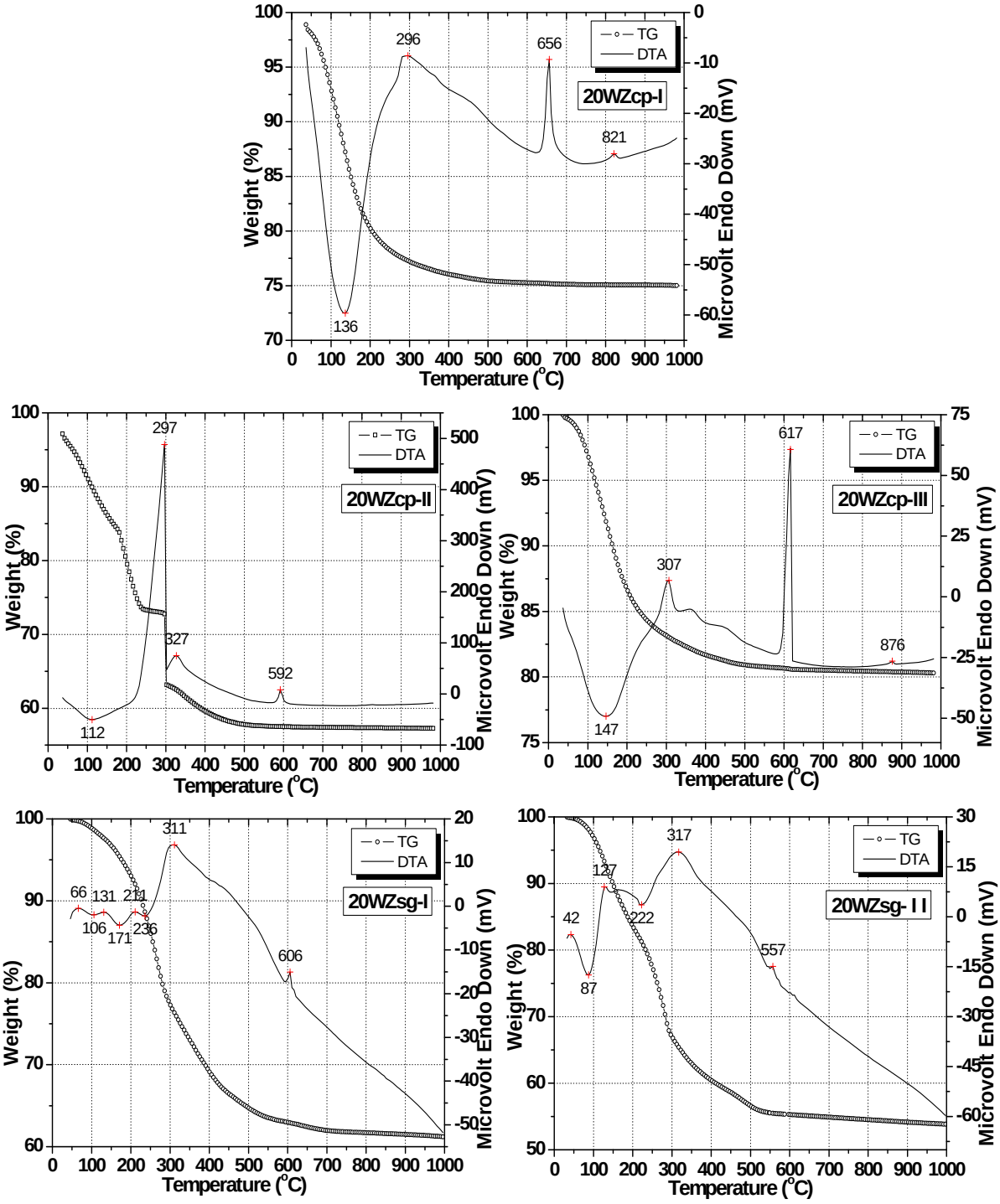

Fig. 5.2: TG-DTA of as-synthesized tungstated zirconia samples prepared using modified co-precipitation and sol-gel methods.

Otherwise all the as-synthesized tungstated zirconia samples prepared by modified impregnation and co-precipitation method showed a weight loss in the range 19 to 26 %. Every sample yielded endothermic peak and exothermic peaks. DTA curves show two

major exothermic peaks and an endothermic peak. The endothermic peaks at temperatures between 50 °C and 200°C are due to the elimination of residual water and solvent species, dehydration of surface hydroxyl groups. 20WZsg-I and 20WZsg-II samples prepared by sol-gel method shows multiple exothermic and endothermic peaks accompanied by weight loss in the temperature range from 50°C to 250°C, as expected due to the formation of various organic/inorganic complexes. Out of the two major exothermic peaks, the first peak at ~300 ^{o}C is due to decomposition of nitrates or organic materials, and the second peak is owing to transformation of amorphous to crystalline phase, which has tetragonal crystal structure. According to XRD, the later exothermic peak between 525 °C to 725 °C observed for various samples, but not followed by any weight loss is attributed to the allotropic transformation of zirconia. The addition of 20 wt% WO_3 to zirconia shifted the phase transition of pure zirconia from amorphous to tetragonal to higher temperature due to the interaction between WO_3 and zirconia. The exothermic peak temperature obtained by DTA is 493 °C for ZIV pure zirconia sample which rises to 594 °C for 20WZim-II sample containing about 20 wt% WO_3 loading. ZIV and 20WZim-II sample are been prepared under identical synthesis conditions, the only difference been the addition of WO_3 in the later. In addition the peak temperature has a tendency to shift towards the higher temperature with modification of various synthesis parameters such as digestion time, synthesis method etc. On the other hand, the first broad exothermic peak appeared for all the samples between 250 and 350 ^{o}C. This peak is attributed to the oxidation of organics residues and the decomposition of surfactants, nitrate group; trace amounts of ammonium nitrate and nitrate containing zirconium hydroxy compounds. The DTA curves of the studied samples differ markedly in shape depending upon the synthesis method and process parameters. Yet another but much broader and less intense exothermic peak between 350 - 500 °C has been seen samples in few samples which could be due to complete removal of nitrates through pyrolysis. The pyrolytic character of the high temperature nitrate decomposition step can only be seen in 20WZim-II, IV V and 20WZcp-III samples. This peak might have got masked in other samples due to presence of nearby peaks. Simultaneously, the TG curve is leveled off at about 500 °C, meaning that no further weight loss occurred from 500 to 1000 ^{o}C, indicating that no W is lost from the surface at higher calcination temperatures. Above

700 °C, the DTA curves of the impregnated and co-precipitated samples showed a shift of base line indicating thermal energy been produced during the calcination, with small random exothermic peaks at high temperatures (between 800 and 900°C) without any weight loss. A further study at higher temperatures above 800 ^{o}C is required to identify its cause. It is to be noted that at present there is no obvious interpretation of these peaks, although it is most likely to correspond to phase transition or changes in the oxidation state of the tungsten oxides [65].

5.2.3. XRD Analysis

The calcination temperature of tungsten oxide promoted zirconia plays a vital role in the properties of WO_3-/ZrO_2 solid acid catalyst [10]. It is also an important factor impacting the final structure, especially with materials prepared with surfactants. Because violent physical and chemical procedures take place during the removal of the surfactant, the temperature has to be raised gently to preserve the porous structure. Normally, the temperature is increased slowly with a ramp of 2 °C/min to obtain mesoporous structure. In addition, the temperature has to be maintained at 250 °C or 300 °C depending upon the type of surfactant used, for 1 or 2 hours during calcination so that the polymer surfactant has sufficient time to start decomposing and the primary particles could rearrange to fit the great change of thermal environment. Keeping these points in view, optimization of calcination programme was done, whose details are elaborated in Chapter-2, Section 2.3.4. Out of the several calcination programmes studied, the details of four calcination programme were mentioned there, and the resultant XRD patterns for sample 20WZim-II are given in Fig. 5.3. Out of the four calcination programs, calcination program “A” in not suitable for materials with surfactant, while program “B” leads to excessive heating which results in the formation of monoclinic phase with decrease in surface area. Appearance of a weak hump near 2θ value 28.2°, observed in the XRD pattern of 20WZim7C-II(B)-Fig. 5.3, implies the presence of small amount of monoclinic zirconia at temperature 700 ^{o}C. Program “C” developed by reducing the time by half of program “B”, is not suitable for low temperature calcinations due to incomplete decomposition of organic species. On the basis of the data obtained from various characterization techniques, calcination program “D” was finalized for calcining samples at various end

temperatures and used further for calcination of other samples studied in this thesis. On the other hand, no diffraction peak due to bulk WO_3 nor to any tungsten-containing compound is observed, indicating that the supported phase is highly dispersed, probably as polytungstates. For comparison purposes, the XRD pattern for pure WO_3 is also included at the bottom of the Fig. 5.3. WO_3 is a complicated material with respect to its crystal structure and thermal stability because of the several known polymorphs such as triclinic, monoclinic, orthorhombic, hexagonal, tetragonal and cubic [66,67,68,69].

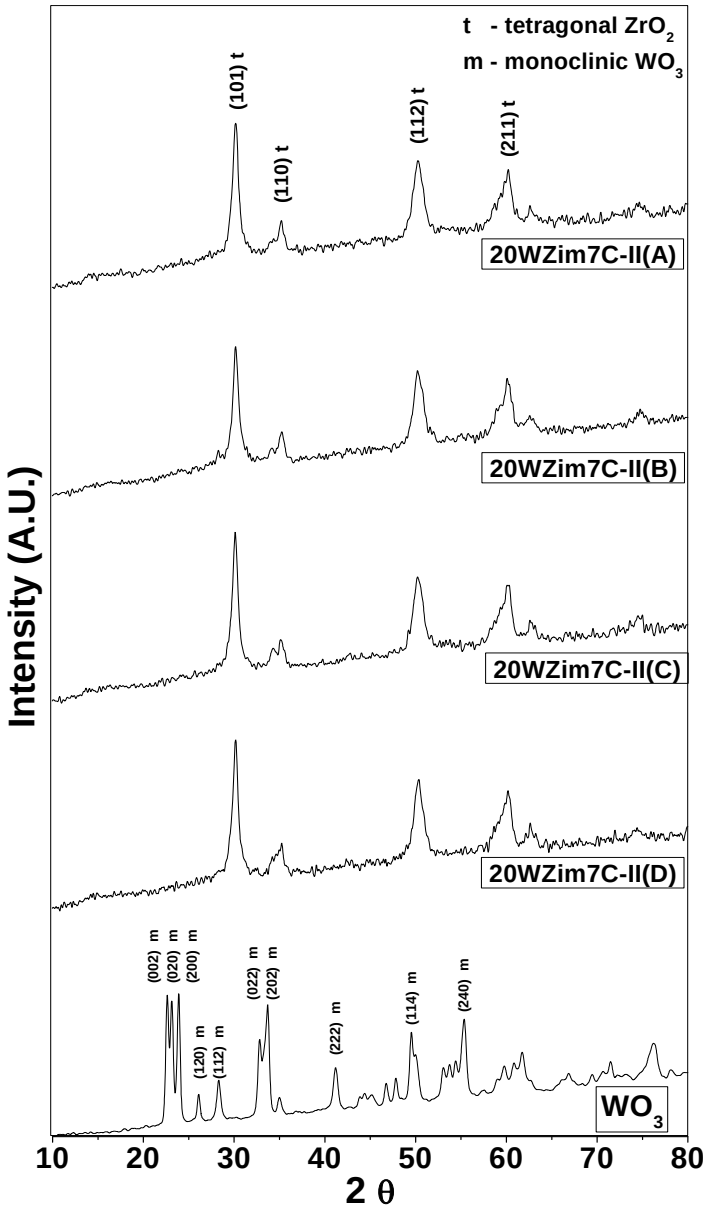

Fig. 5.3: XRD patterns of sample 20WZim-II calcined at 700 ^{o}C using different calcination programme as indicated in the figure. For comparison purpose XRD spectrum of pure WO_3 is given at the bottom.

However the most stable WO_3 phase at room temperature has been reported to be having monoclinic structure when tungsten trioxide powders are calcined at 350 to 600 °C, but this phase transforms to an orthorhombic or hexagonal phase at higher temperatures [70,71]. Nevertheless there are reports where in high temperature orthorhombic structure may reversibly be transformed to monoclinic phase when the temperature was decreased to room temperature [66,72]. It is also hard to distinguish between monoclinic and orthorhombic phases as they are structurally similar. Bearing in mind the above reports and comparing the bulk WO_3 peaks data with JCPDS records, (JCPDS file no. 43-1035 for monoclinic phase and JCPDS file no. 20-1324 for orthorhombic phase), the peaks arsing due to WO_3 in tungstated zirconia samples were amicably assigned to monoclinic phase, which is also in accordance with a recent publication of similar type of materials [73]. The calcined tungstated zirconia samples exhibited major peaks at 2θ values = 30.1°, 34.4°, 35.2°, 42.8°, 50.1°, 50.7°, 59.2°, 60.2°, 62.8° and 74.7° corresponding to only the tetragonal phase, moreover at all stages of calcination there was no indication of monoclinic phase whose major peaks appears at 2θ values = 28.2°, 31.5°, 34.1°, 34.4°, 35.3°, 40.7° and ZrW_2O_8 (Zirconium tungstate, JCPDS file no. 13-0557), whose major peaks appears at 2θ values = 21.5°, 23.6°, 27.4°, 32.3°, 36.6°. The peaks of tetragonal phase at 2θ values = 34.4° and 35.2°, 2θ value = 50.1° and 50.7°, 2θ values = 59.2°, 60.2° are not resolved well in the XRD figures due to small particle size. The tetragonal to monoclinic zirconia transformation was most likely inhibited by small particle size and WO_3 that helped to stabilize the tetragonal phase of zirconia. The effect of calcination temperature on the stability of the tetragonal phase for tungstated zirconia sample 20WZim-II was obtained using powder XRD analysis (Fig. 5.4). It is obvious that no diffraction peaks were detected for sample 20WZim4C-II, as the exothermic peak due to crystallization of zirconia occurred at temperatures higher then 500 ^oC for this sample. This indicates that the 20WZim4C-II sample is amorphous. The 20WZim-II sample calcined at 500 ^oC presented broad peaks of tetragonal phase indicating only partial crystallization. After calcination at 600 ^oC, peaks located at 2θ values 30.2°, 35.2°, 50.2°, 60.2°, 63.0° and 74.6° were detected. From phase analysis, it can concluded that tetragonal crystalline zirconia was formed. When calcined at 700 ^oC, the sample 20WZim-II crystallized well with tetragonal phase which is maintained till 800 ^oC. The

planes ({101}, {110}, {112} and {211}) corresponding to tetragonal zirconia have been assigned to 2θ values 30.2, 35.2, 50.2 and 60.2, and labeled respectively in the Fig. 5.4 for sample 20WZim8C-II.

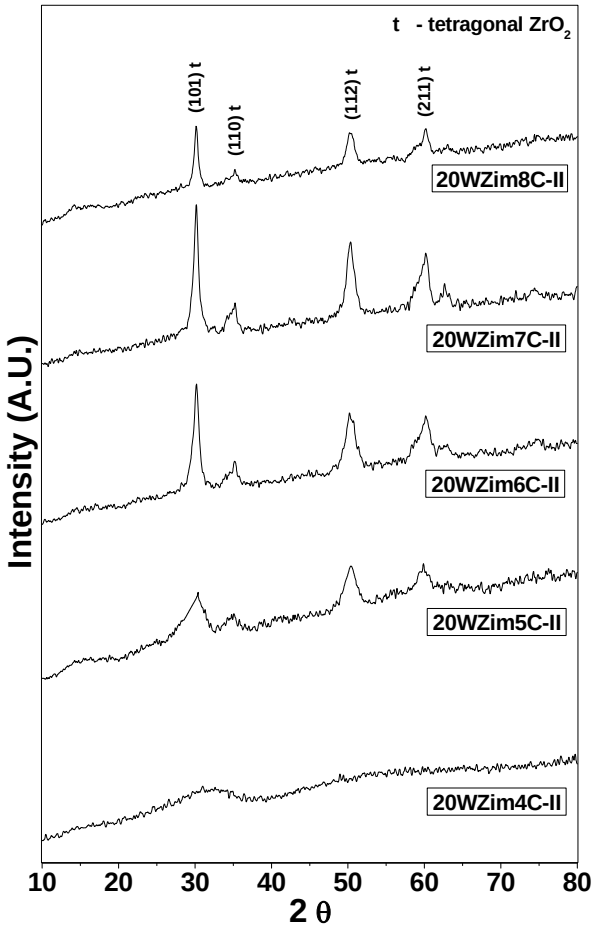

Fig. 5.4: XRD patterns of sample 20WZim-II as a function of calcination temperature.

Thus, tungsten oxide seems to retard the phase transformation from tetragonal to monoclinic zirconia and also inhibits sintering of the zirconia matrix, which is assumed to be due to the interaction of tungstate anions with the hydroxyl groups of zirconia. No indication of crystalline WO_3 was observed, although its concentration was well above the detection limit of about 1% for XRD. This suggests WO_3 must be in the non-crystalline form with high degree of dispersion. In the present studies besides sample 20WZim7C-I (prepared using standard impregnation method) all samples calcined at 700 ^oC, showed non appearance of bulk WO_3. Fig. 5.5 shows XRD patterns of tungstated zirconia samples calcined at 700 ºC.

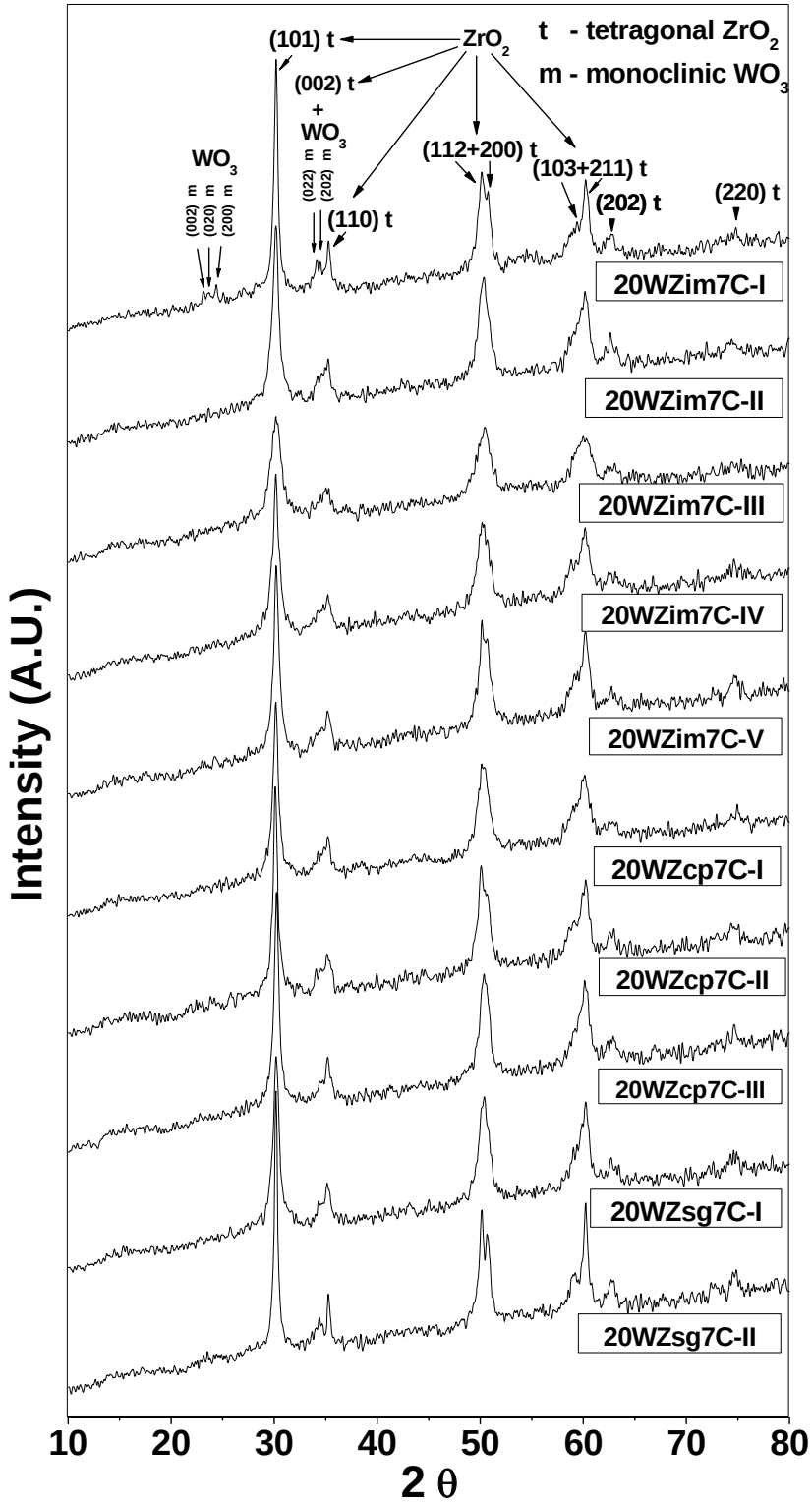

Fig. 5.5: XRD patterns of tungstated zirconia samples prepared via modified impregnation, co-precipitation, sol-gel methods and calcined at 700 ^{o}C.

Typically tungstated zirconia samples having surface density more than 10 W-atoms/nm^2, are known to show XRD peaks related to bulk WO_3. In the present case sample

20WZim7C-I exhibits surface density more then 10 W-atoms/nm^2, thereby displaying bulk WO_3 peaks which is in accord with the literature [31], but to our surprise sample 20WZsg7C-II which also exhibits surface density more then 10 W-atoms/nm^2 does not display bulk WO_3 peaks. Obvious possible reason could be due to difference in synthesis method, starting precursor and/or other process parameters. Usually sol-gel solids consist of homogeneous phase composition; therefore slightly higher temperatures are required for expelling WO_3 from the bulk of zirconia to its surface for the formation of WO_3 crystallites as compared to impregnated solid. To further access the thermal stability of the tungstated zirconia samples they were calcined at 800 ^oC. Additional peaks are observed for few samples calcined at 800 ^oC in the 2θ range of 23-25°, suggesting surface density exceeding monolayer capacity. This 2θ range has been marked (dotted line) for the samples calcined at 800 ^oC, which show the additional peaks due to bulk WO_3 (Fig 5.6). For example sample 20WZcp8C-II shows diffraction peaks at 2θ equal to 23.1°, 23.6° and 24.3° corresponding to d values = 0.385, 0.376 and 0.365 nm have been marked specially with a dashed box. These peaks correspond to the (002), (020), and (200) planes. These three distinct XRD peaks can be assigned to monoclinic WO_3 phase according to JCPDS data (JCPDS 43-1035) having d values = 0.384, 0.376, 0.364 nm. The appearance of crystalline tungsten oxide for the sample calcined at 800 ^oC can be attributed to the reduction of surface area, therefore a high surface concentration of WO_3 species, exceeding monolayer coverage are formed which agglomerate to form WO_3 micro-crystallites on the zirconia surface [74,75]. Only four samples 20WZim8C-I, 20WZcp8C-I, 20WZcp8C-II and 20WZsg8C-II exhibited peaks corresponding to bulk WO_3 when calcined at 800 ^oC, which is a good match with catalyst color comparison given in Table 5.1. Similar observations were reported earlier, wherein tungsten oxide loaded on zirconia powders had light yellow color when calcined at temperatures 800 ^oC and above [24,76]. Since samples 20WZim8C-I and 20WZsg8C-II have not been digested after preparation, a possible cause of displaying bulk WO_3, but samples 20WZcp8C-I and 20WZcp8C-II even though digested show peaks of bulk WO_3 phase. Though we did not find a satisfied interpretation for this, it is suggested related to surface area and actual concentration of WO_3 that results in different phase compositions and crystalline size distributions.

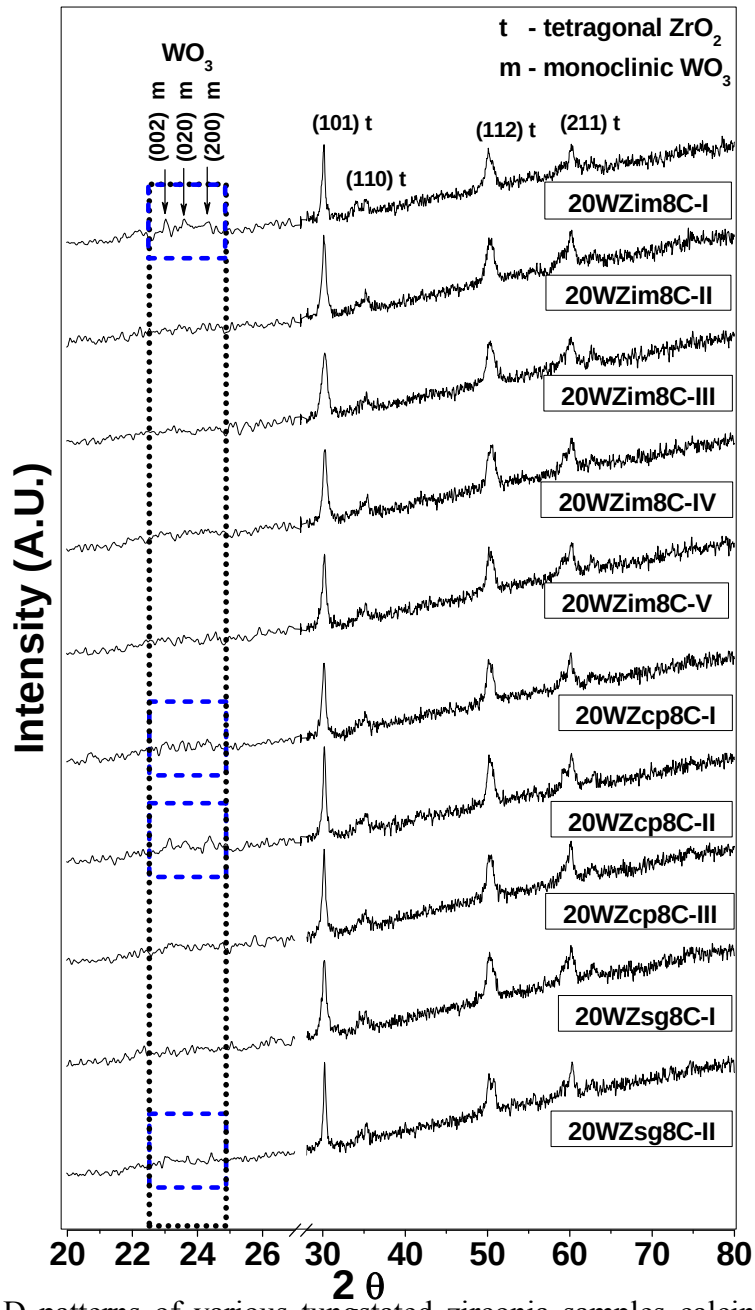

Fig. 5.6: XRD patterns of various tungstated zirconia samples calcined at 800 ^{o}C. 2θ region where bulk WO_3 peaks occur is been highlighted by dotted line. Samples displaying bulk WO_3 peaks are enclaved in dash boxes.

For rest of the samples no diffraction peaks up till calcination temperature 800 ^{o}C, due to WO_3 crystallites are observed. These results suggest that the tungsten oxide species exists mainly in an amorphous, non-crystalline state when calcined at 800 ^{o}C or the particles are too small to be detected by XRD. It should be pointed out that care should be taken while assigning the peaks due to bulk WO_3 crystallites in the presence of monoclinic phase of

zirconia as the peak having 2θ value 24.4° could be due to monoclinic zirconia and not WO_3 crystallites [77].

A less common technique to obtain a particle size is the analysis with nitrogen sorption. The evaluation according to BET theory (Brunauer–Emmet–Teller) allows to obtain information on the size of non-agglomerated and dense particles, the relationship between particle size and surface area is given by the formula: "$d = 6000/(\rho \times S_{BET})$", where d is the average particle size (nm), S_{BET} is the specific surface area expressed in m^2/g^{-1} and ρ = specific density [78,79]. However in the present studies this technique could not applied successfully due to diverse densities of zirconia, tungsten oxide and tungstated zirconia samples. XRD and TEM techniques are well known for their application in finding out particle sizes of various crystalline materials. Major limitation of XRD is that this technique requires samples possessing sufficient long-range order. Amorphous phases and small particles give either broad and weak diffraction lines or no diffraction at all which makes them virtually invisible for XRD. It is also well documented that, as Scherer's equation provides only a measurement of the extension of the coherently diffracting domains, the particle sizes estimated by this method can be significantly under estimated [80,81]. In addition factors such as dislocations, strain, stacking faults, heterogeneities in composition and instrumental broadening can contribute to peak broadening, making it almost unfeasible to extract a reliable particle size solely from XRD [80,82]. Even though TEM provides real images up to atomic resolution, these images are only a representative of the selected number of particles, also poor contrast or overlap of particles sometimes could complicate their analyses. In this connection, a combination between TEM and XRD techniques was employed for particle size measurement. The values obtained from these XRD measurements and TEM figures are presented in Table 5.2. TEM results show lower values as compared to XRD values. Irrespective of synthesis method (impregnation, co-precipitation, sol-gel), the samples undergone digestion have average crystallite size less then 14 nm, while samples obtained without digestion independent of synthesis method have crystallite size more then 20 nm and reduced surface area. These results are valuable because it shows that modifying the preparation method, along with optimized calcination temperature

programme, tungstated zirconia can be obtained with crystallite size as low as 10 nm with good dispersion of WO_3.

Table 5.2: Volume % t-ZrO_2, BET surface area, acidity, particle size of various tungstated zirconia solid acid catalysts calcined at 700 ^oC.

Sr. No.	Sample Designation	% t-ZrO_2 [XRD]	S_{BET} (m^2/g)	NH_3 Desorbed (μmol/g)	NH_3 Desorbed (μmol/m^2)	Average Particle Size (nm)	
						XRD	**TEM**
1	20WZim7C-I	100	43	109.6	0.11	20.9	18
2	20WZim7C-II	100	98	471.2	0.47	13.3	9
3	20WZim7C-III	100	112	516.9	0.52	8.7	8
4	20WZim7C-IV	100	97	499.5	0.50	14.4	10
5	20WZim7C-V	100	94	317.8	0.32	16.3	10
6	20WZcp7C-I	100	81	383.0	0.38	15.5	11
7	20WZcp7C-II	100	88	406.0	0.41	17.5	12
8	20WZcp7C-III	100	91	302.4	0.30	16.4	9
9	20WZsg7C-I	100	80	367.4	0.37	15.2	10
10	20WZsg7C-II	100	40	157.9	0.16	25.5	20

5.2.4. N_2 Adsorption Analysis

In the present studies the samples prepared with optimized synthesis conditions display high surface areas. Surface area as high as 112 m^2/g can be achieved using modified synthesis procedures. The surface area values of various tungstated zirconia samples calcined at 700 ^oC are tabulated in Table 5.2. The higher surface area values found for samples digested at basic pH are related to the larger fraction of hydrous zirconium oxide surface involved in the adsorption. The surface fraction of a zirconia involved in the adsorption of anionic tungsten species is related to the pH of the contacting solution [83]. At high pH values, the small sized WO_4^{2-} anions in solution may diffuse into the support micropores and tungsten species are adsorbed all over the surface. Conversely, at low pH, the large polyoxoanions present in solution cannot diffuse into the support micropores and only a small fraction of the support surface is involved in the adsorption. Therefore the sample 20WZsg-II prepared via sol-gel method at acidic pH bears less surface area, on the other hand when the similar sample 20WZsg-I prepared via sol-gel method at acidic pH, when digested at high pH the initially precipitated hydrous zirconia precursor undergoes dissolution and re-precipitation strengthening the network of primary particles also binding the W species strongly to hydrous zirconia thereby increasing it thermal stability and surface area. Having said this, the sample 20WZim-I prepared under basic pH should posses high surface area, but its actual surface area value

is analogous to the sample 20WZsg-II prepared at acidic pH. This suggests that at high pH values, even though the small sized WO_4^{2-} anions diffused into the support micropores and/or adsorbed all over the surface are not strongly bounded on to zirconia surface which is mainly due to the electrostatic repulsions between negatively charged zirconia surface and $(WO_4)^{2-}$ anions therefore limiting their interaction. This results in the formation of bulk WO_3 crystallites at high temperatures which are not effective in stabilization of zirconia crystallites, the consequence of which is inferior surface area. Strongly bound surface oxides inhibit inter-crystallite sintering by reducing the rate of zirconia surface diffusion. However as the calcination temperature reaches 900 ^oC, surface WO_3 species agglomerate into WO_3 crystallites and become less effective sintering inhibitors. These surface oxides thereby lose their effectiveness at high temperatures because they diffuse into the bulk, desorb and crystallize as separate phase or zirconia particles agglomerate to form poorly interacting clusters. Sulphate species are also known to inhibit the loss of zirconia surface area after high temperature calcination. However, these species decompose and desorb as SO_3 at relatively low calcination temperatures as compared to tungstated zirconia, leading to rapid zirconia sintering. Surface area also depends on WO_3 loading. At a given calcination temperature, surface area increases with WO_3 concentration. Measurements of the surface area with different concentrations of tungsten oxides on the zirconia support done by Sohn and Park [45] proved that the content of tungsten also strongly influences the surface area, giving a much larger surface area with increasing tungsten oxide content, up to a maximum at 20 wt. % which corresponds to sub-monolayer coverages. In addition, the maximum tetragonal content was also detected at this WO_3 concentration. This is one of the reasons why only 20 wt% WO_3 is been selected in our studies. From the above data it can suggested that strong binding sites for meta-tungstate ions exist on zirconia surface which inhibit zirconia sintering, while the loosely bound or excess meta-tungstate ions leads to formation of bulk WO_3 crystallites that are not effective in stabilization of zirconia crystallites. Thus the amount of tungsten directly anchored on the zirconia surface controls the surface area shrinkage and the fraction of tetragonal zirconia. The effect of calcination temperature on the surface area of the tungstated zirconia was studied using nitrogen adsorption and desorption. The resulting specific surface areas were calculated

using the BET method and its values are provided in Fig 5.7. In agreement with the literature [45], an almost linear decrease of surface area with increasing calcination temperature was found in the temperature range studied for sample 20WZim-III. Sample calcined at 800 ^{o}C shows better surface area as compared to other reports [45] possibly due to modified synthesis procedures. In most cases surface area is related to the pore size and the pore volume i.e. the larger the pore volume the larger is the surface area and the smaller the pore size the higher is the surface area. This general trend seems to be applicable in our system as illustrated in Fig. 5.7.

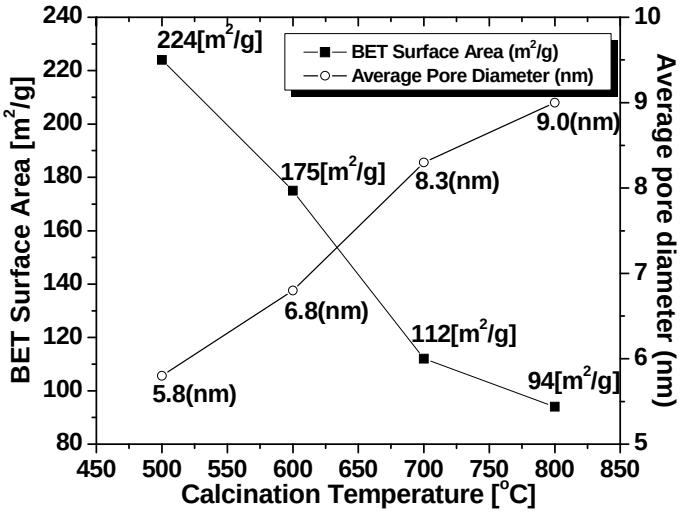

Fig. 5.7: Effect on surface area and pore diameter as a function of calcination temperature studied for sample 20WZim-III.

High surface areas obtained at lower calcination temperatures is due amorphous nature of the materials predicted from TG-DTA and XRD studies for sample 20WZim-III. The influence of calcination temperature for sample 20WZim-III on the N_2 sorption behaviors is manifest in Fig. 5.8. It is obvious that following the calcination at higher temperatures the isotherms determined lower adsorbed volumes. This must indicate that the sample surfaces have been rendered less accessible to the adsorbate molecules as a result of increasing calcination temperature. According to the classification given by Brunauer et al. [84], the isotherms on sample 20WZim-III calcined at various temperatures are of type-III. All of the isotherms exhibit obvious H3 type hysteresis loops. The fact that all of the isotherms determined on the calcined samples exhibit hysteresis loops indicates porous nature of the materials. As discussed elsewhere [85,86], certain types/shapes of hysteresis loops are associated with specific pore structures. A type-H3 loop is attributed

to adsorbate condensation in capillary spaces between parallel plates or open slit-shaped capillaries. Similar type of isotherms and hysteresis were seen for pure zirconia sample (ZIII) prepared under identical synthesis condition. Thus incorporation of WO_3 does not modify the type of porosity to a greater extent. The pore size distribution curves shown in Fig. 5.8 confirm the porosity of all the four samples, the maximum contribution to the surface area is arising from pores with diameters ranging between 5-9 nm.

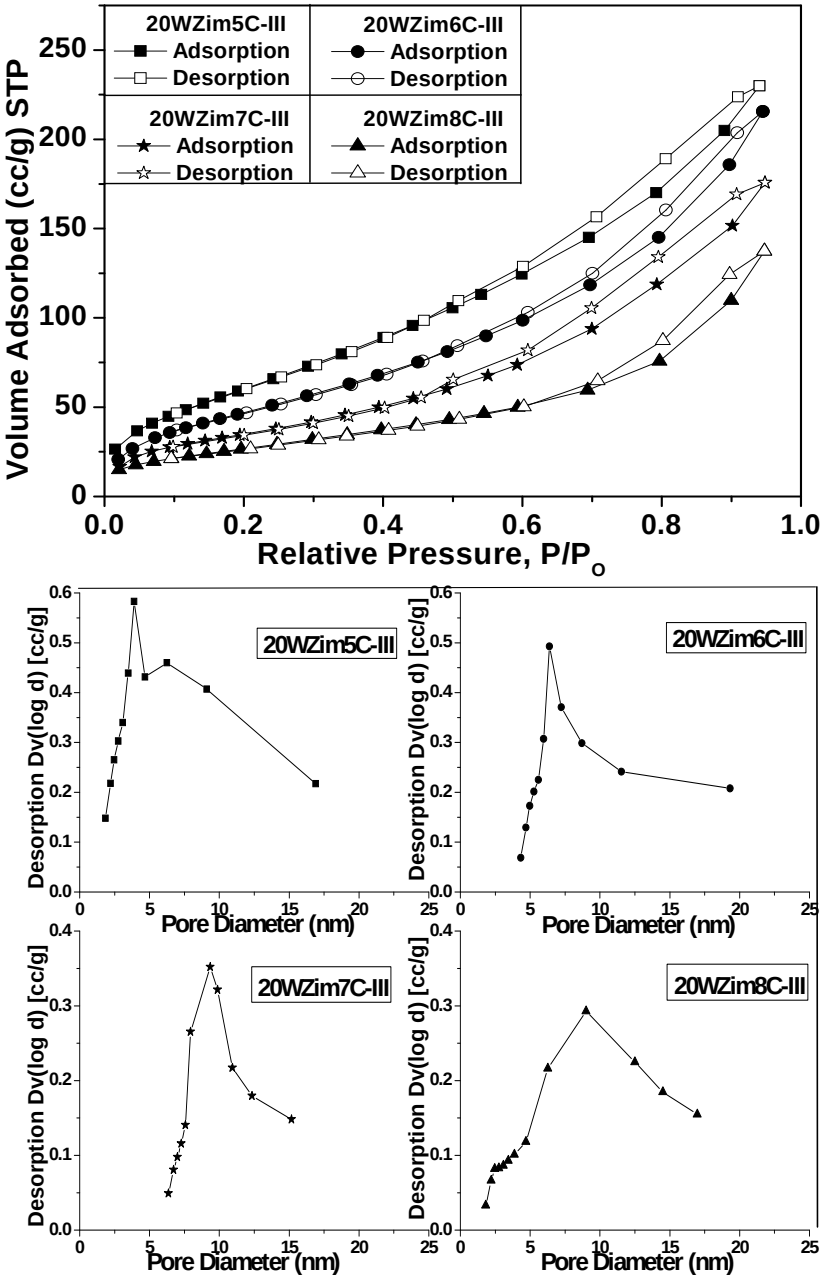

Fig. 5.8: N_2 adsorption-desorption isotherms determined at 196 ^oC and pore size distribution curves of calcined tungstated zirconia 20WZim-III sample as indicated.

5.2.5. Temperature Programmed Desorption of NH_3

The total acidity of solid acid catalyst was measured with NH_3-TPD. In NH_3-TPD measurements, the temperature of the maximum ammonia desorption reflects the relative strength of the acid sites. The total amount of desorbed ammonia corresponds to the total amount of ammonia adsorbed on the Lewis and Brønsted acid sites. Even though the applied technique does not allow distinguishing between these two types of the sites, it still provides valuable information about changes in acidity of the catalysts caused by different modifications of the synthesis procedures, calcination temperatures, WO_3 loading etc. According to the earlier reports Lewis and Brønsted acid sites exists on the surface of tungstated zirconia but the relative concentration and strength of these acid sites increases significantly with the increase of surface WO_3 concentration, which eventually depends on surface density, [26,51] and surface density depends upon WO_3 loading and surface area. Furthermore surface area depends upon synthesis method and calcination temperature. Sighting the significance of calcination temperature, it influence on acidity was investigated. Sample 20WZim-III was calcined at different temperatures and its acidity been measured by NH_3-TPD (Fig. 5.9).

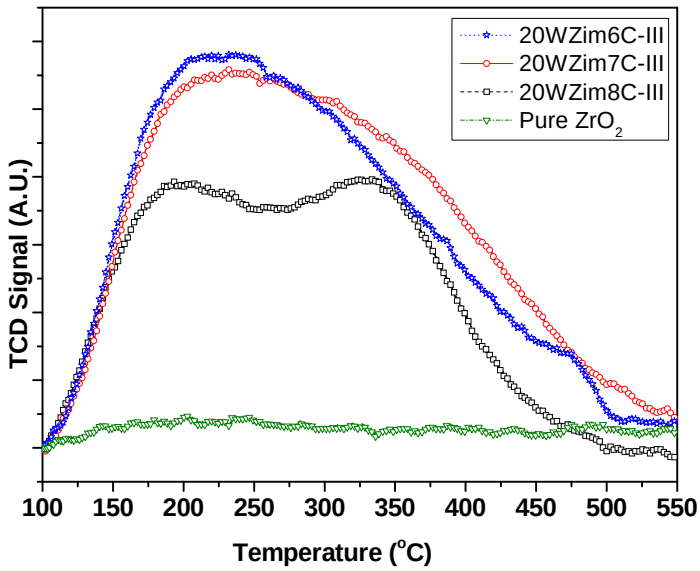

Fig. 5.9: NH_3-TPD profiles of pure ZrO_2 calcined at 700 °C and 20WZim-III catalyst calcined at 600 °C, 700 °C and 800 °C.

The results from these experiments were also utilized to finalize the calcination temperature of all the other catalyst prepared in this study. In our experiments when W

oxide was incorporated into zirconia matrix, the concentration of acid sites increased drastically when compared to that of pure zirconia support. It is apparent from Fig. 5.9, that pure zirconia has practically no surface acidity. The high acid strength and high acidity of the tungstated zirconia samples were responsible for the W=O bond nature of complex formed between WO_3 and zirconia. Further when 20WZim-III catalyst was calcined at different temperatures, going from the amorphous tungstated zirconia to the crystalline zirconia (~600 ^oC) acidity increases slightly showing a maximum at 700 ^oC and then decreases further due to the lower surface areas of the samples calcined at high temperatures. Since the surface area of the tungstated zirconia is decreasing with increasing calcination temperature, the abundance of acid sites also varies significantly. However there is not much difference in the acidity and acid strength of 20WZim-III catalyst calcined at 600 ^oC and 700 ^oC. A broad TPD profile is observed for samples 20WZim6C-III and 20WZim7C-III as shown in Fig. 5.9, revealing that the surface acid strength is widely distributed. But when the calcination temperature reaches 800 ^oC the amount of adsorbed ammonia decreases with the change in the acid strength. The dependence of the amount of adsorbed NH_3 for a given sample calcined at different temperatures, it may be observed that an increase of the surface WO_3 causes an increase of the total number of acid sites, reaches a maximum, further increasing temperature causes loss of surface area which brings a decrease of the total number of acid sites. This phenomenon could be attributed to the relative extent of formation of bulk WO_3 crystallite at the expense of the bonded monolayer dispersed WO_3 on zirconia. The deposition of the WO_3 species causes a shift of the maximum to lower temperature, indicating the creation of relatively weak acid sites [87,88]. To research the acidity of our catalyst prepared via different synthesis methods and process parameters calcined at 700 ^oC, they were subjected to NH_3-TPD analysis. The results are summarized in Table 5.2. The values of concentration of acid sites per/m^2 are also presented in the table which provides good information of the relative surface acidic properties. All tungstated zirconia samples show a broad TPD profile similar to that of the sample 20WZim7C-III, revealing that the surface acid strength is widely distributed. The temperature of maximum ammonia desorption was found to be more or less the same for all tungstated zirconia samples. Highest acidity is exhibited by sample 20WZim7C-III, whilst the

lowest by 20WZim7C-I (Table 5.2). Sample prepared in acidic pH as well basic pH with out the aid of digestion show lowest acidity. In general impregnated samples prepared via modified synthesis procedures have shown higher acidity as compared to samples prepared by modified co-precipitation and sol-gel methods. Due to numerous variable factors like specific surface area, pore diameter, percentage of tetragonal phase of zirconia, actual concentration of WO_3 incorporated on/in the zirconia matrix, presence of WO_3 crystallites etc and complicated nature of NH_3-TPD, it was not possible to associate acidity to any one of the factor or factors.

5.2.6. XPS Analysis

There is an evident need for a surface characterization of tungstated zirconia catalyst prepared using different methods. To investigate the surface properties of the tungstated zirconia powders, and to evaluate the oxidation state of Zr and W, X-ray photoelectron spectroscopy (XPS) studies were carried out. XPS spectra are, for the most part, quantified in terms of peak intensities and peak positions. In principle, the peak positions in terms of binding energy provide information about the chemical state for a material. The peak intensities measure how much of a material is at the surface, while the peak positions indicate the elemental and chemical composition. Other values, such as the full width at half maximum (FWHM) are useful indicators of chemical state changes and physical influences. An experimental problem in XPS is that electrically insulating samples may charge during measurement, as photoelectrons leave the sample. Due to the positive charge on the sample, all XPS peaks in the spectrum shift by the same amount to higher binding energies. Calibration for this effect can be done by using C(1s) binding energy (284.9 eV) from carbon contamination. The B.E. shift of 3-4 eV due to electro statical charging, can also be corrected using $Zr(3d_{5/2})$ level of the ZrO_2 carrier at 182.2 eV [89] as a reference for the binding energies determinations. XPS spectra were recorded in the accumulated and smoothed mode. The experimental peaks were decomposed into individual components using mixed Gaussian-Lorentzian functions, non-linear squares fitting algorithm and Shirley-type background subtraction. The W(4f) lines were analyzed with a curve-fitting procedure according to the Doniach and Sunjic theory [90,91] which takes into account the experimental resolution approximated by a

Gaussian line shape, the photoemission line which has been fitted with an asymmetrical Lorentzian shape line and secondary emissions. The XPS spectrum of the all the calcined tungstated zirconia samples showed significant differences in the shape of W(4f) doublet and Zr(4p) component in the Zr(4p)+W(4f) region. Changes in the Zr(4p)+W(4f) signal shape of the samples prepared using various synthesis methods and calcined at different temperature were analyzed by a curve fitting procedure with variable values for the full widths at half maximum and binding. The W/Zr surface ratios were calculated using the sensitivity factors, as determined by Scofield [27,92]. The de-convolution of the XP-peaks as well as the whole evaluation of the spectra was performed using XPSPEAK (v 4.1) software from RCSMS lab. According to the literature, Zr(4p) region and W(4f) region are superimposed and a part of W is in the valence state of +5 [27,93]. On the basis of XPS analysis, the main part of W in tungstated zirconia samples has a valence of +6 and that a part exists in the valence state of +5 [27,93,94]. Taking these data into consideration, we measured XPS of tungstated zirconia samples and the complex features were de-convoluted into two doublets corresponding to W^{6+} and W^{5+} peaks to obtain the individual W^{6+} and W^{5+} components. The two doublets were fitted to account the whole W(4f) energy region in the range of 35-39 eV, besides a doublet corresponding to the Zr(4p) component as shown in Figures 5.10, 5.11 and 5.12. Independent of the W content, the XPS signals in the W(4f) region can be fitted with two components as expressed above. The larger one, at 35.2 and 37.4 eV [25] for the W4f spin-orbit components, is attributed to W^{6+} surface species and the second one at 34.2 and 36.4 eV [95] is assigned to W^{5+} species. In this study the average binding energies for the doublet W^{6+} was observed at 35.5 and 37.7 eV and for W^{5+} it was at 34.5 and 36.7 eV which is close match to the values reported elsewhere [27,96]. The details of binding energy and its respective assignment to W^{6+} and W^{5+} for various tungstated zirconia samples are presented in Table 5.3. The binding energy values for all catalysts could not be approximated to be same value, which is due to the small differences in the interaction and portion of the highest oxidation state W^{6+} in the differently prepared tungstated zirconia catalysts. This is also evidenced by the full-width at half-maximum (FWHM) values, which are between 1.7 – 2.2 eV.

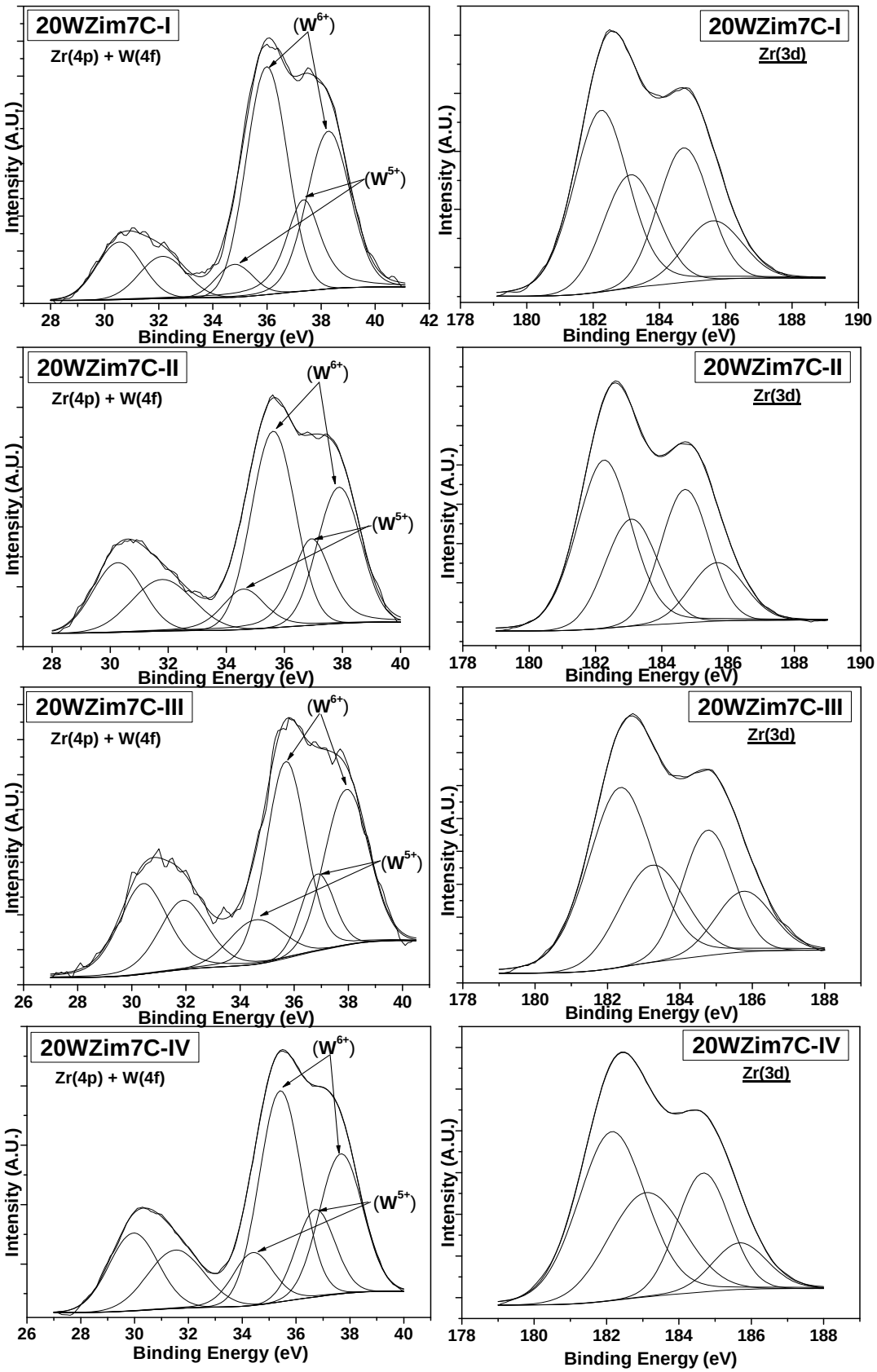

Fig. 5.10: [Zr(4p)+W(4f)] XPS spectra (left) of various tungstated zirconia samples, and the corresponding XPS spectra of Zr(3d) (right) as mentioned in the figures.

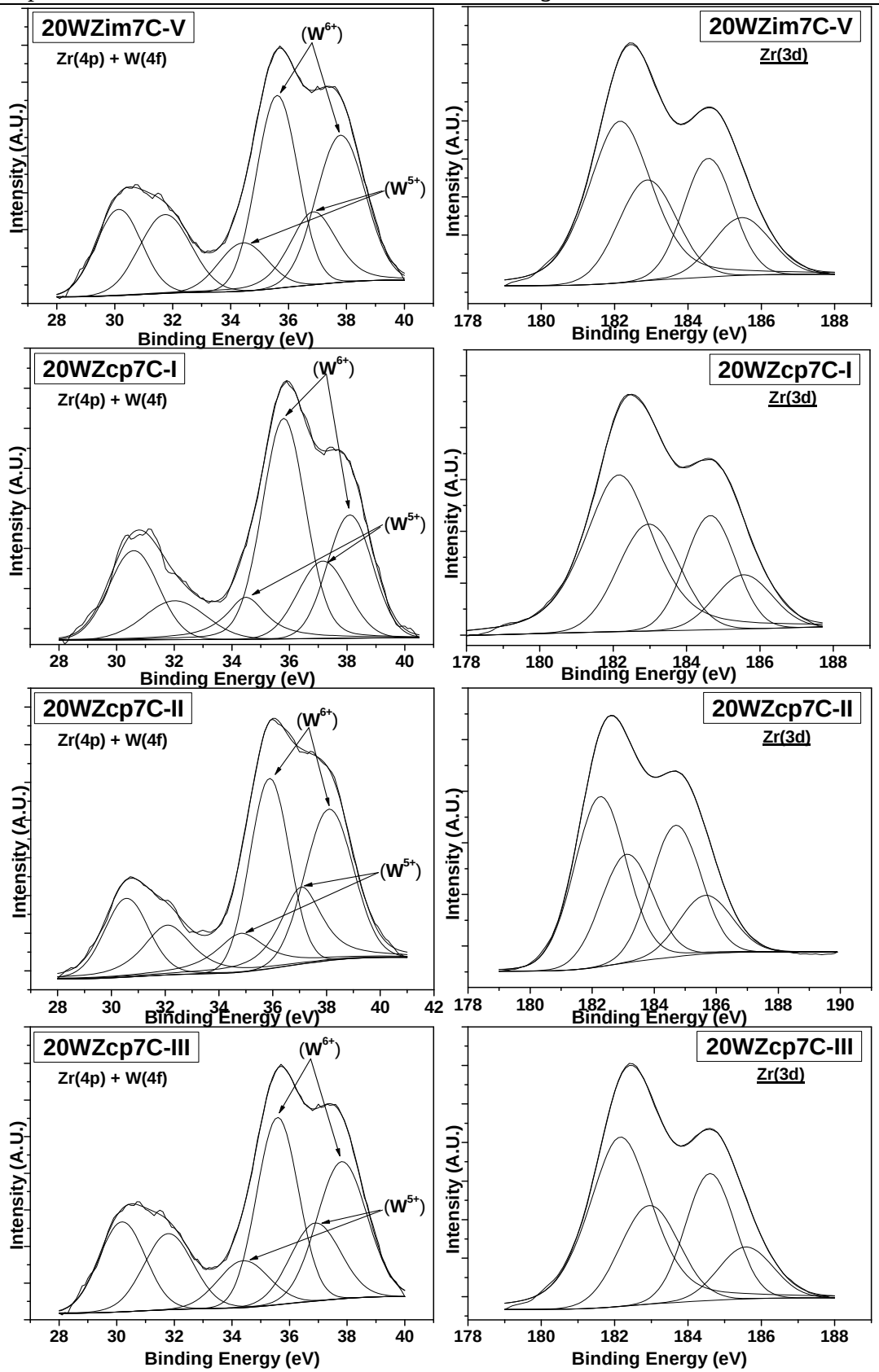

Fig. 5.11: [Zr(4p)+W(4f)] XPS spectra (left) of various tungstated zirconia samples, and the corresponding XPS spectra of Zr(3d) (right) as mentioned in the figures.

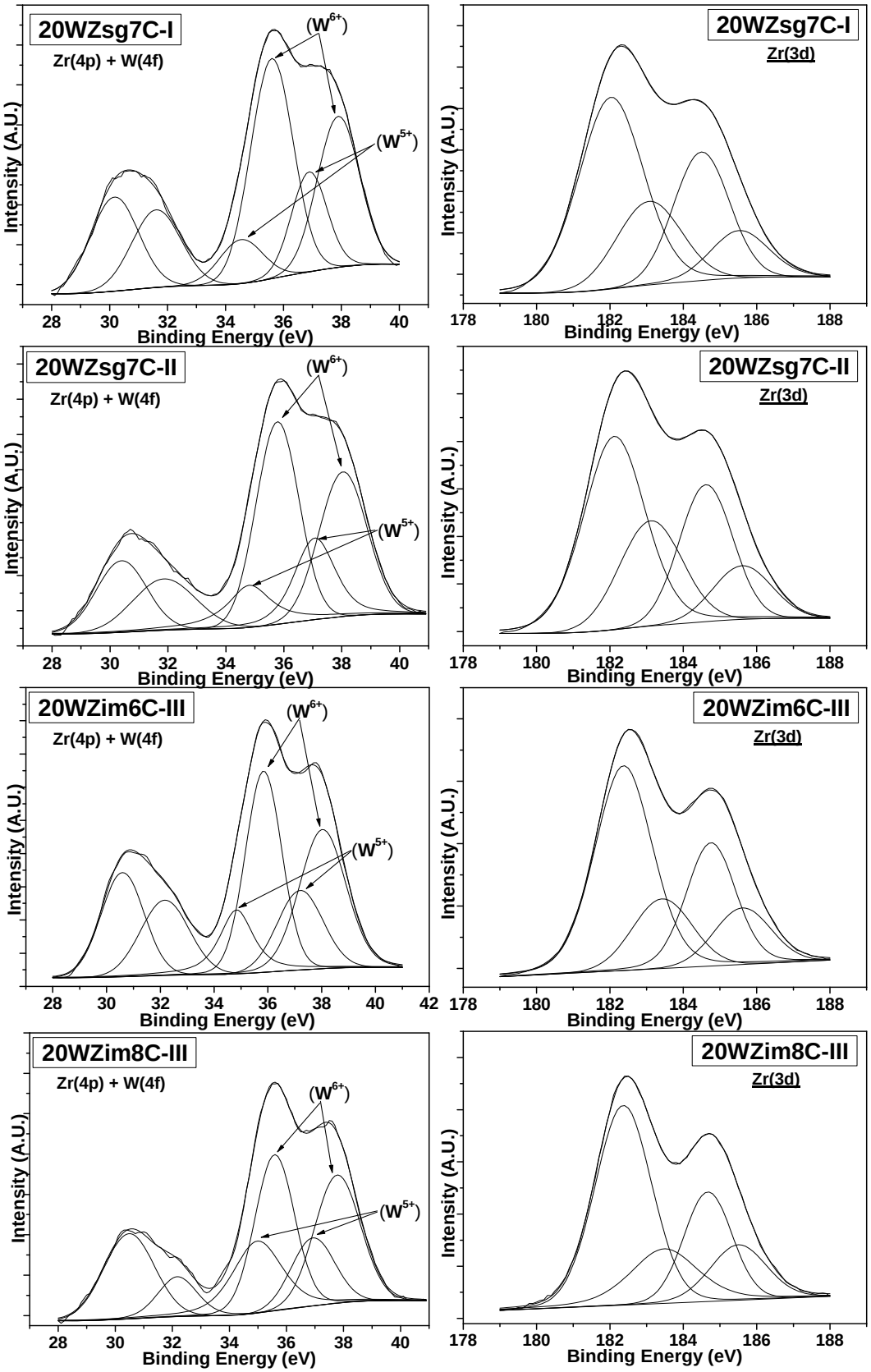

Fig. 5.12: [Zr(4p)+W(4f)] XPS spectra (left) of various tungstated zirconia samples, and the corresponding XPS spectra of Zr(3d) (right) as mentioned in the figures.

Table 5.3: XPS parameters of the W(4f) region and binding energy difference between O(1s) line and Zr($3d_{5/2}$) line of various tungstated zirconia catalyst

Sr. No	Sample Designation	Binding Energy (eV) And Assignment				B.E. diff. between [O(1s)] & [Zr($3d_{5/2}$)]
		W^{6+}	W^{6+}	W^{5+}	W^{5+}	
1	20WZim7C-I	35.89	38.18	34.80	37.25	347.88
2	20WZim7C-II	35.62	37.89	34.60	36.94	347.90
3	20WZim7C-III	35.69	37.93	34.59	36.86	347.96
4	20WZim7C-IV	35.41	37.67	34.40	36.72	347.86
5	20WZim7C-V	35.61	37.80	34.43	36.85	348.25
6	20WZcp7C-I	35.80	38.10	34.50	37.16	347.92
7	20WZcp7C-II	35.88	38.10	34.82	37.07	347.88
8	20WZcp7C-III	35.58	37.82	34.40	36.90	348.24
9	20WZsg7C-I	35.60	37.90	34.54	36.89	347.99
10	20WZsg7C-II	35.78	38.04	34.82	37.07	348.05
11	20WZim6C-III	35.84	38.03	34.83	37.20	347.98
12	20WZim8C-III	35.49	37.73	34.49	36.72	347.98

Quantification and the ratio of the two species W^{6+} and W^{5+} were calculated from the area under the peaks of the respective components achieved after curve fittings and are presented in Fig. 5.13. It can be learnt from the Fig. 5.13 that all catalyst contains a major fraction of W^{6+} species (~70 %) and the rest been W^{5+} in the total W concentration.

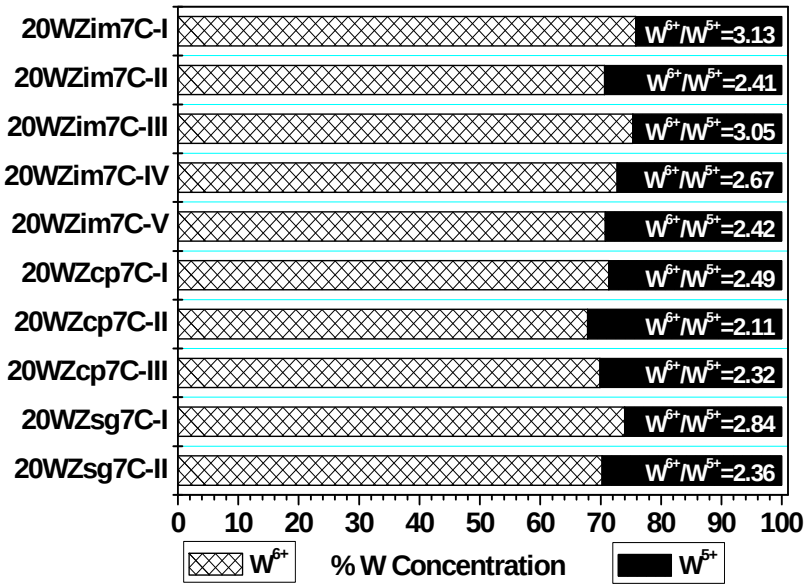

Fig. 5.13: Concentration of W^{6+} and W^{5+} in total W of various tungstated zirconia catalysts calcined at 700 ^{o}C. Ratio of W^{6+} by W^{5+} is shown in bars of W^{5+} concentration.

Minor differences in the amount of W^{6+} and W^{5+} species could be spotted and easily identified from the W^{6+}/W^{5+} ratio, caused by variation in the synthesis parameters. The

XPS spectrum of the sample 20WZim-III calcined at various temperatures did not show any significant differences in the shape of the Zr(4p)+W(4f) region, however the primary W^{6+} binding energy position shifts to lower value as the calcination temperature increases from 600 ^{o}C to 800 ^{o}C. For clarity, only the W(4f) region has been de-convoluted into two components and showed in Fig. 5.14, wherein the shift of binding energy can be seen more distinctively.

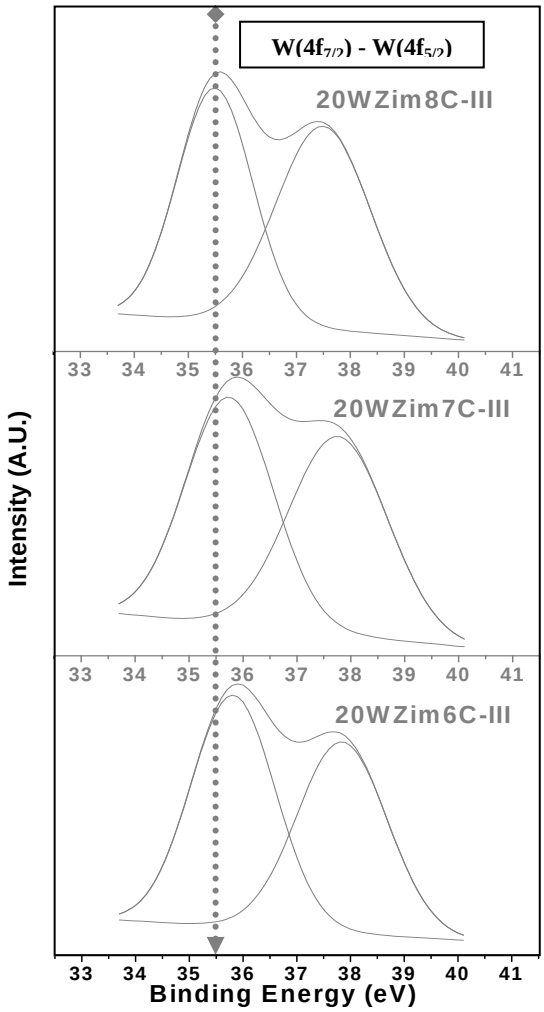

Fig. 5.14: XPS spectra of W(4f) region for sample 20WZim-III calcined at 600 ^{o}C, 700 ^{o}C and 800 ^{o}C, showing binding energy shift of W^{6+}.

The shift is in agreement with previous literature [97], indicating minor change in the oxidation state of the major surface species. Later parameters derived from the XPS curve fitting indicated that tungsten oxidation state also depends on the calcination temperature. The effective concentrations of W^{6+} and W^{5+} present in the sample 20WZim-III calcined at 600 ^{o}C, 700 ^{o}C and 800 ^{o}C were also extracted and it was found that 20WZim8C-III

contains highest amount (75.3%) of W^{6+} in comparison with 20WZim6C-III and 20WZim7C-III. The corresponding XPS spectra at the Zr(3d) region of various samples was fitted by using two doublets for Zr($3d_{5/2}$) and Zr($3d_{3/2}$) photoelectron lines. The first one occurred at nearly same BE for all samples (182.1 $\pm$ 0.1 eV and 184.6 $\pm$ 0.1 eV), with a similar FWHM values of 2.0 and 1.7 eV respectively. The second doublet occurred at high BE values (183.1 $\pm$ 0.1 eV and 185.6 $\pm$ 0.1 eV), with a similar FWHM values of 2.0 and 1.9 eV. This second comparatively broad doublet may correspond to strongly deformed Zr^{4+} cations, which can be caused by a strong interaction with the W atoms, in the formation of Zr–O–W bonds, at least in some surface layers. In fact, the high electron attractor effect of the W atoms deform the electric field around the Zr^{4+} nuclei because the electronic cloud is displaced towards the oxygen atoms bonded to W and Zr atoms. However for current powder samples, relatively narrow and constant FWHM values strongly support the suggestion of the dominance of Zr^{4+} in the studied materials, implying that only one type of doublet may be present, which provides evidence for the presence of one type of zirconium oxide with an oxidation state of 4+. Additionally, the energy difference between the O(1s) and metal 3d lines can be used to gauge an effective average oxidation state of a metal in an oxide compound. This method is often used when the de-convolution appears to be difficult, e.g. when the powder materials are studied, where the differential charging might deform the peaks leading to the appearance of apparent oxidation states. The usefulness of such a criterion was also demonstrated on vanadium-based oxide catalysts [98,99]. In our case, the energy difference between the principal O(1s) line and the Zr($3d_{5/2}$) line, for almost all the tungstated zirconia samples amounts to 347.9 $\pm$ 0.1 eV, which is in a perfect agreement with the known literature data. Please refer to Table 5.3 for actual values. 347.9 eV is been reported for pure zirconia [100], similar values are obtained elsewhere [101,102]. In present studies pure zirconia sample ZIV-7C displayed an energy difference value of 347.91 between O(1s) and Zr($3d_{5/2}$) line. Since this criterion is independent of the charging effects as well as of the calibration of the energy scale, and due to a significant chemical shift of Zr(3d) region of 4.23 eV in respect of the pure Zr-metal [102], one can conclude with a sufficient reliability that no reduction of zirconia is observed and also none of possible UHV-induced [98] or photoreduction (caused by X-rays) [103] effects take place under the

present conditions. Thus XPS studies confirm W^{6+} and Zr^{4+} as main oxidation states of tungsten and zirconium in the studied samples. The ratio of the two species, W and Zr is a good measure of the degree of dispersion of W on the zirconia surface. The surface W/Zr ratios of samples can be determined from the ratio of the integrated area of W(4f) XPS peaks to the integrated area of Zr(3d) XPS peaks with consideration of the atomic sensitivity factors of W and Zr. The results of the XPS are compiled in Table 5.4. W/Zr calculated from other characterization techniques are also given in this table for comparison. By taking into account the average of all the techniques the nearest possible true value can be reached. Constant W concentration per unit area is known to give different surface W/Zr ratios because of different degrees of aggregation of WO_3 on the surface of zirconia [104]. Multilayer structures of WO_3 on zirconia would give a higher value of W/Zr compared to monolayer ones. In order to access the supposition, 20WZim-III catalyst was calcined at 500 ^oC, 600 ^oC, 700 ^oC and 800 ^oC and its surface ratios were measured using EDX and XPS, both being surface techniques.

Table 5.4: WO_3 concentration (wt %) measured and the corresponding W/Zr atomic ratio calculated using EDX, ICP and XPS, averaged values from these three techniques along with averaged surface density (W-atoms/nm^2) is provided.

Sr. No	Sample Designation	Wt. % WO_3 Concentration				W/Zr Atomic Ratio			Avg. Wt % WO_3 Conc.	Avg. W-atoms /nm^2	Avg. W/Zr atomic ratio
		Input	EDX	ICP	XPS	EDX	ICP	XPS			
1	20WZim5C-III	20	10.08	19.03	15.01	0.12	0.25	0.19	14.71	1.71	0.18
2	20WZim6C-III	20	11.15	19.03	19.63	0.13	0.25	0.26	16.60	2.47	0.21
3	20WZim7C-III	20	13.84	19.03	20.89	0.17	0.25	0.28	16.67	3.87	0.21
4	20WZim8C-III	20	15.35	19.03	24.14	0.19	0.25	0.34	19.51	5.39	0.26

EDX and XPS measurements yielded results in harmony to earlier reports of W/Zr ratio with increasing calcination temperatures starting from 500 ^oC to 800 ^oC. From the values present in the Table 5.4 it can be understood that as the calcination temperature increases the surface W/Zr ratio also raises, which means an increase in the concentration of W atoms on the surface of zirconia. As the amount of the W atoms is constant in the sample, the increase of the W/Zr ratio with the annealing temperature must correspond to the migration of W atoms from the bulk to the zirconia surface or diminution of dispersion of WO_3 on the surface of zirconia, however if one compares the W/Zr ratios obtained from the two different surface techniques (EDX & XPS) for a particular temperature it can noticed that there is discrepancy in the W/Zr values. Therefore to avoid huge divergence

from actual values, bulk W/Zr measured using ICP was also considered for calculating the average W/Zr values, which are presented in Table 5.4. From the evolution of the average W/Zr surface atomic ratios, it is clear that the increase of this ratio with the calcination temperature is not linear when combined values of bulk and surface characterization techniques are considered. This suggest that the dispersion of the tungstate surface species is not the same with increasing temperature and that the deviation from linearity is obtained at near-saturation monolayer coverage in the case of 20WZim-III. Another noticeable facet is that, even though WO_3 loading for a particular sample is constant, tungsten densities can vary, as for example 20WZim-III sample calcined at four different temperatures from 500 to 800 ^oC for 3 h in air has tungsten densities 1.7 to 5.4 W-atoms/nm^2 depending upon the calcination temperature. Surface density is a key factor for solid acid catalysts such as tungstated zirconia catalyst in terms of activity and property, consequently will be discussed in the next separate section.

5.2.7. Surface Density – EDX/XRF/ICP

The surface density of WO_3 on zirconia is widely used to evaluate the activity [105], WO_3 cluster size [24], acid nature [26], and structure [25] of tungstated zirconia catalyst. The tungsten surface densities, expressed as the number of W-atoms per nanometer square area (W-atoms/nm^2) and were calculated using the equation: surface density of W = {[WO_3 loading (wt.%) / 100] × 6.023 ×10^{23}} / {[231.8 (formula weight of WO_3) × BET surface area (m^2/g) × 10^{18}]}. The surface density of atomic tungsten of all the catalyst was determined by taking into account the surface area values specified in Table 5.2, and the amount of tungsten actually present in the sample, as determined by various characterization techniques. Even though of prime importance surface density has been occasionally reported, assuming all the input tungsten atoms have been incorporated in/on zirconia and homogeneously distributed. In this context we thought of determining surface density considering the actual amount of WO_3 present in the solid acid tungstated zirconia materials, rather then assuming all inputted tungsten atoms been incorporated in the zirconia. Furthermore the small amount of WO_3 actually present in the solid gets segregated as bulk WO_3 crystallites at higher temperatures, which is also considered for surface density calculation which in fact, does not stabilize the zirconia any more. The

concentration of these bulk WO_3 crystallites can be estimated by the difference between the actual amounts of WO_3 species present in the solid minus the amount of bulk WO_3 crystallites segregated, using Rietveld analysis [44]. However when the amount of bulk WO_3 crystallites formed is negligible this point can be overlooked, as in the present studies. At first WO_3 concentration was measured with SEM-EDX instrument, representative EDX pattern of samples 20WZim6C-III and 20WZim8C-III showing average W and Zr concentration in oxide mode are presented in Fig. 5.15.

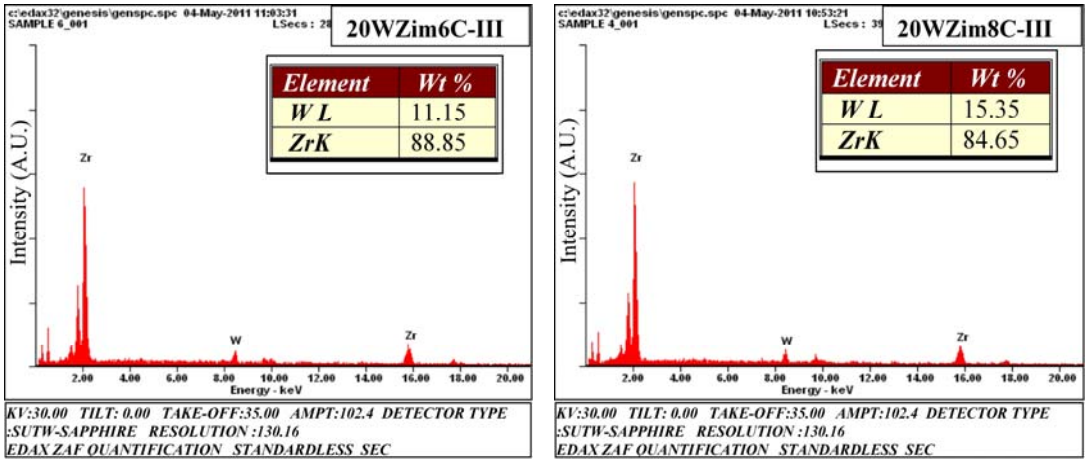

Fig. 5.15: EDX spectrum of samples 20WZim6C-III and 20WZim8C-III (Inset: average wt.% of W and Zr in oxide mode).

EDX is capable of detecting most metals and non-metals, only the lack of detection power for light elements is a limitation of this technique. Nevertheless oxygen is detected indirectly, thereby postulating, that the elements in the sample were present as their metal oxides. Furthermore, for small concentrations this system is not very precise and the detection limit is dependent on the matrix and its surface homogeneity. EDX in conjunction with an SEM is a surface analysis method, and it needs mathematical correction programmes, ZAF corrections, to compensate the background of a not ideal sample matrix [106]. The analytical measurements are performed standard-less, and all the collected data is correlated to the internal calibration which is performed prior to analysis with two pure element standards. Before each quantitative analysis a manual background correction and automated ZAF-corrections are carried out. The optical potential of a SEM-EDX is of great benefit which gives the opportunity to pick different areas for investigation, depending upon the contrast of the image. At-least three different visibly homogenous regions were selected where maximum possible homogeneity on the

surface of the particles in the sample was seen and average values have been considered. Despite the best efforts the WO_3 concentration received from SEM-EDX was invariable as well as displayed lower values, as depicted in Fig. 5.16.

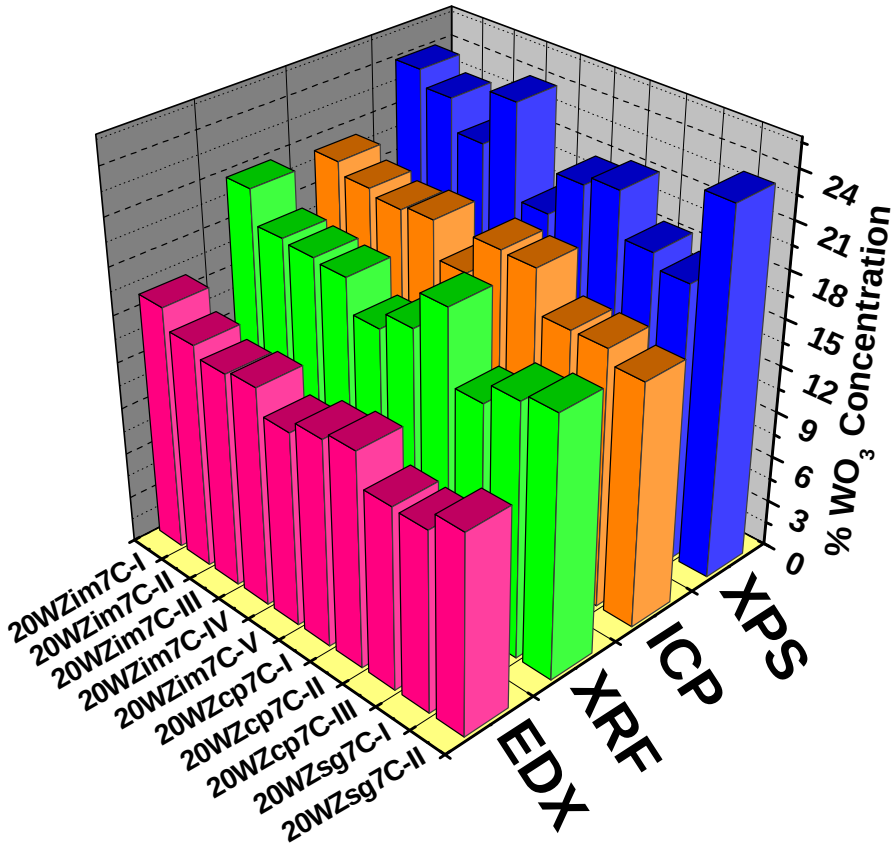

Fig. 5.16: % Wt. WO_3 concentration of various tungstated zirconia samples measured via different characterization techniques

The strong variation of the EDX results in different sample areas is the result of a typical behavior of the SEM-EDX, it is surface analysis, and shows therefore only a part of the whole analytical information. In order to obtain better insight of WO_3 concentration, energy dispersive XRF was employed. Similar to EDX, XRF is predominantly a surface analysis technique, rapid, non-destructive and multi-element analytical technique for the qualitative and quantitative analysis of elements in a variety of materials. X-ray fluorescence makes use of the ability of high energy X-rays to excite electrons in an atom to a higher energy state, while EDX makes use focused beam of electrons to obtain the same. Thereby in XRF, X-rays penetrate much deeper into sample than electrons: possibility of layer thickness determination, however X-ray penetration of the sample is

limited to the top 0.01 - 0.1 mm layer. Comparing EDX vs. XRF measurements, XRF with greater depth of field will measure a much larger volume of sample, resulting in a more consistent and accurate measurement. XRF is a true multi-element analysis, all elements of the periodic table from Beryllium to Uranium can be measured qualitatively, semi quantitatively and quantitatively over a wide range of concentrations in powders, solids and liquids as well which is an additional advantage. To get more accurate results, one must homogenize the samples, especially the powder materials. In case of powders, spinners are can be utilized during measurements or the powder is fused with lithium tetraborate and bromide to obtain fused glass type discs for maximum homogeneity. In the present study all XRF measurements were carried out using spinners containing maximum amount of finely grounded powders and an average of three readings was considered to before reporting the final value of WO_3 concentration. It can clearly seen from the Fig. 5.16 that XRF acquiesce better results then EDX for the tungstated zirconia samples, primarily due to difference in the sampling technique and the source of excitation. Earlier in this section usefulness of XPS to get direct insight into the chemical composition, qualitatively and quantitatively of the surface species has been already elaborated. The peak intensities occurring at different positions for different elements in the XPS spectra can be used to measure the concentration of a specific element with the help of relative sensitivity factors (RSF) of photoelectric peaks which are widely available and tabulated [107]. These RSF have been routinely used to scale the measured intensities as part of the atomic concentration calculation, but RSF can only be accurate for homogenous type materials. If the sample varies in composition with depth, then the kinetic energy of the photoelectric line alters the depth from which electrons are sampled. Therefore measurements were carefully performed for specific elements to attain better accuracy. Using RSF, surface WO_3 concentration was determined taking into account the integrated area of W(4f), Zr(3d) and O(1s) XPS peaks. The WO_3 concentration values in wt% obtained from this exercise are shown Fig 5.16. Comparing the XPS vs. XRF it can observed that XPS values are quite higher then expected along with deviation from the true value, which is due to direct comparison of XPS peak areas which is not a recommended means of comparing samples for the following reasons. An XPS spectrum is a combination of the number of electrons leaving the sample surface and the ability of

the instrumentation to record these electrons; not all the electrons emitted from the sample are recorded by the instrument. Further, the efficiency with which emitted electrons are recorded depends on the kinetic energy of the electrons, which in turn depends on the operating mode of the instrument. As a result, the best way to compare XPS intensities is via, so called, percentage atomic concentrations. The key feature of these percentage atomic concentrations is the representation of the intensities as a percentage, that is, the ratio of the intensity to the total intensity of electrons in the measurement. Should the experimental conditions change in any way between measurements, for example the x-ray gun power output, then peak intensities would change in an absolute sense, but all else being equal, would remain constant in relative terms. Thus in XPS quantification based on standard relative sensitivity factors, precision is achieved not accuracy. Keeping in view the above facts the ratio of W/Zr was calculated from peak areas of W(4f) and Zr(3d) for all the tungstated zirconia samples, besides calculating surface WO_3 concentration using relative sensitivity factors. In XPS measurements the W/Zr ratio is more reliable then % WO_3 concentration, therefore W/Zr ratios were also calculated for EDX and XRF since the WO_3 concentration obtained from earlier EDX and XRF measurements from cannot be directly compared with XPS W/Zr ratio. Total chemical composition, besides surface composition is the one of the most important component in the characterization part as it is the controlling parameter that can decide the performance of the catalyst. The determination and accurate control of bulk chemical composition is of paramount importance in monitoring and evaluating the properties and stability of catalysts. The methodology for certain analysis depends on the nature and concentration of the constituents. In the present activity, initially atomic absorption spectrometry (AAS) technique was used for estimation of W content. The details regarding the equipment and operating conditions employed are mentioned in Chapter 2, Section 2.4.12. The application of AAS in the analysis of tungsten is limited, due to poor sensitivity. The element forms refractory oxides in the flame, which is undesirable in AAS analysis. The use of nitrous oxide-acetylene flame or graphite furnace with the application of pre-concentration techniques, have improved the situation to quite an extent. Nevertheless the temperature of the flame is low to completely atomize highly refractory elements and can thus severely under-read the true concentration of

analyte present if the elements are not in the same chemical state in the sample as in the standard [108]. Another major disadvantage of this AAS technique is that it is extremely slow when compared to multi-element detection methods like ICP-AES. This is due to the inherent limitation that only one element can be detected at a time because of the use of element specific cathode lamps. With the advent of plasma as an excitation source, there has been a marked improvement in the analysis of W by ICP-AES. Plasma emission spectroscopy has been applied in tungsten analysis with higher sensitivity, and can be determined up to 1 ppm accurately [109]. The greatest advantages of the ICP-AES technique are the spectacular linear dynamic range, high sensitivity, low detection limits (ppb range) and multi-element detection capacity [110]. The greatest disadvantage for both the spectroscopic techniques AAS & ICP-AES, lies in the fact that the sample must be in solution, preferably aqueous solution, before it can be analyzed. An advantage gained from the conversion of solid to a liquid is the elimination of heterogeneity, physical form and physical transport problems associated with the solid materials. However, the conversion of solids to liquids presents the analyst with a new and different set of problems. Many, if not most, sample types start out as solids in part or total where a great deal of time and effort is invested into converting them into a liquid form. The chemistry of the elements in aqueous media is of interest as well as the chemistry required to bring them into solution. It is not only concerned with the destruction of the solid, but also the preparation of a solution that is stable and compatible with the chemical components of the standard solution and the physical components of the introduction system. In view of this, initial trials were conducted to establish the suitable method of converting the solid into a liquid form prior to AAS/ICP analysis. Several spectrometric and digestion methods were investigated for the analysis of Zr, Mo and W elements in the presently studied solid acid catalyst. The zirconia matrix of the analyte limited the number of digestion options available. The advantages and disadvantages of each method were weighed in relation to each other before a specific method or instrument was chosen to perform the analysis. These optimization runs were conducted using a representative MoO_3/ZrO_2 and WO_3/ZrO_2 catalyst and liquid form was subjected to the analysis. After completing the analyses, the results were compared. For the compositional analysis using AAS/ICP-AES, three measurements were made and an

average value was considered within the limits of the error. The ICP-AES analysis showed better results for W as compared to AAS analysis. Therefore the concentration of W and Zr was measured using ICP-AES for all the WO_3-/ZrO_2 catalyst, while AAS was employed for measuring Mo and Zr in MoO_3-/ZrO_2 catalyst. Outmost care has been taken to remove all possible errors during the analysis. However all measurements are accompanied by a certain small amount of error, and an estimate of its magnitude is necessary to validate results. The error cannot be eliminated completely, although its magnitude and nature can be characterized and reduced with improved techniques. In general, errors can be classified as random and systematic. If the same experiment is repeated several times, the individual measurements cluster around the mean value. The differences are due to unknown factors that are stochastic in nature and are termed random errors. They have a Gaussian distribution and equal probability of being above or below the mean. On the other hand, systematic errors tend to bias the measurements in one direction. Systematic error is measured as the deviation from the true value which is difficult to detect even for experienced research workers, but can be identified and eliminated. Systematic errors are caused by imperfect calibration of measurement instruments or imperfect methods of observation, or interference of the environment with the measurement process, and always affect the results of an experiment in a predictable direction. All atomic spectroscopy analysis was done on wet basis, and the measured WO_3 concentration can be viewed from Fig. 5.16. W/Zr ratios of various tungstated zirconia samples were also calculated from ICP-AES results and are revealed in Table 5.5. A number of conclusions can be drawn from above characterization studies and are given as follows. The results of ICP and XRF appear much more comparable than the EDX results. This data gives an indication that the SEM-EDX method may not be the most accurate method. However SEM-EDX analytical results showed more details of the sample than an ICP-AES analysis does, and no element specific calibration before the analysis is necessary for quantitative determinations. Sample preparation for SEM-EDX and XRF is fast and easy compared to the dissolution process necessary for conventional atomic spectroscopy, XRF being the technique where in minimum or no sample preparation is required.

Table 5.5: W/Zr atomic ratio and corresponding surface density values calculated using EDX, XRF, ICP and XPS for various tungstated zirconia catalysts.

Sr. No.	Sample Designation	W/Zr Atomic Ratio				Surface Density, W-atoms/nm^2			
		EDX	XRF	ICP	XPS	EDX	XRF	ICP	XPS
1	20WZim7C-I	0.20	0.28	0.27	0.34	9.58	12.51	12.21	14.46
2	20WZim7C-II	0.18	0.24	0.26	0.32	3.84	4.92	5.15	6.06
3	20WZim7C-III	0.17	0.24	0.25	0.28	3.21	4.26	4.42	4.85
4	20WZim7C-IV	0.18	0.24	0.26	0.34	3.76	4.87	5.16	6.51
5	20WZim7C-V	0.15	0.21	0.22	0.24	3.47	4.45	4.69	5.07
6	20WZcp7C-I	0.16	0.22	0.26	0.28	4.25	5.52	6.23	6.72
7	20WZcp7C-II	0.17	0.26	0.26	0.30	4.06	5.77	5.70	6.39
8	20WZcp7C-III	0.14	0.19	0.21	0.25	3.35	4.26	4.74	5.36
9	20WZsg7C-I	0.14	0.21	0.21	0.23	3.77	5.28	5.40	5.81
10	20WZsg7C-II	0.16	0.22	0.20	0.33	8.29	10.86	10.22	15.35

For obtaining consistent average total composition of the catalyst, ICP-AES seems to be the more suitable source, while XRF is appropriate for surface analysis and compatible with total composition of solid materials. ICP-AES has the advantage of lower detection limits with a higher accuracy, even for the light elements, compared to XRF and SEM-EDX. But it should be understood that to get meaningful results, where solution techniques are involved all solid samples containing heavy metals like tungsten and zirconium samples have to be brought in solution, which is still an art of the experienced analytical chemist. XPS results are more informative about the chemical states of the elements present long with surface composition, yet individual % element concentration cannot be explicitly compared using this technique. However ratio of elements can be successfully obtained and used for comparison with better accuracy, rather then comparing individual % elements concentration. Estimation of total compositional WO_3 is rather straight forward, as compared to surface due to un-homogeneity of the heterogeneous tungstated zirconia catalyst. In Table 5.6, an average of WO_3 concentration and W/Zr ratio calculated from four different characterization techniques of various tungstated zirconia samples are given. The first significant difference which can be spotted from Table 5.6 is the highest W/Zr ratio and concentration of WO_3 in sample 20WZim7C-I prepared under basic pH without digestion using ZrONit, while all other samples prepared under basic pH using ZrONit with digestion show WO_3 in the range 17-18 wt%, with W/Zr ratio ~0.24. Unexpectedly lower values of W/Zr ratio and WO_3 concentration were obtained in the samples prepared using ZrOCl under basic pH. The

reason for these unpredictable lower values could not be ascertained as of now. The sample prepared under acidic pH with and without digestion showed identical W/Zr ratios with minor difference in WO_3 concentration. The WO_3 concentration obtained from various characterization techniques for each sample was used for surface density calculation and the averaged surface density evolved from these surface densities was believed to be ideal and true value (Table 5.6).

Table 5.6: Averaged values of WO_3 (Wt. %) concentration, W/Zr atomic ratio and surface density calculated from the four characterization techniques (EDX, XRF, ICP and XPS).

Sr. No.	Sample Designation	Input WO_3	Average WO_3 (Wt. %) Concentration.	Average W/Zr Atomic Ratio	Average Surface Density W-atom/nm^2
1	20WZim7C-I	20	20.66	0.28	12.49
2	20WZim7C-II	20	18.84	0.25	4.99
3	20WZim7C-III	20	18.03	0.24	4.18
4	20WZim7C-IV	20	18.96	0.25	5.08
5	20WZim7C-V	20	15.99	0.20	4.42
6	20WZcp7C-I	20	17.71	0.23	5.68
7	20WZcp7C-II	20	18.55	0.24	5.48
8	20WZcp7C-III	20	15.51	0.20	4.43
9	20WZsg7C-I	20	16.71	0.22	5.43
10	20WZsg7C-II	20	17.21	0.22	11.18

From this table it is understood that an increase of WO_3 concentration with comparable surface area results in an increase of W surface density. Also samples with quite similar WO_3 concentration but having relatively lower surface area leads to higher surface density. Besides sample 20WZim7C-I and 20WZsg7C-II, rest all the samples have surface density in the range 4.1 to 5.6 W-atoms/nm^2. If the average of the surface densities is considered, leaving the recently mentioned two samples a number close to 5 W-atoms/nm^2 is attained. In contrast to the theoretical monolayer models that assume a specific structure for a surface tungsten oxide species, experimental XPS, ISS, and Raman spectroscopic measurements have demonstrated that monolayer coverage actually corresponds to 4-5 W-atoms/nm^2 [111,112,113]. This theoretical surface density value is a close match to that obtained in this study indicating monolayer coverage. The maximum amount of surface polytungstate species should occur at this monolayer surface tungsten oxide coverage, while at lower surface densities mono-meric species would be dominating the zirconia surface [43]. This means that WO_3 is loaded selectively on the surface of zirconia support up till mono-layer coverage, having surface density 4-5

W-atoms/nm^2, and multiple layer of WO_3 is formed on further loading [114]. A pictorial representation of the WO_3 species on zirconia depending upon the surface density is shown in Fig. 5.17 to have a better understanding [24].

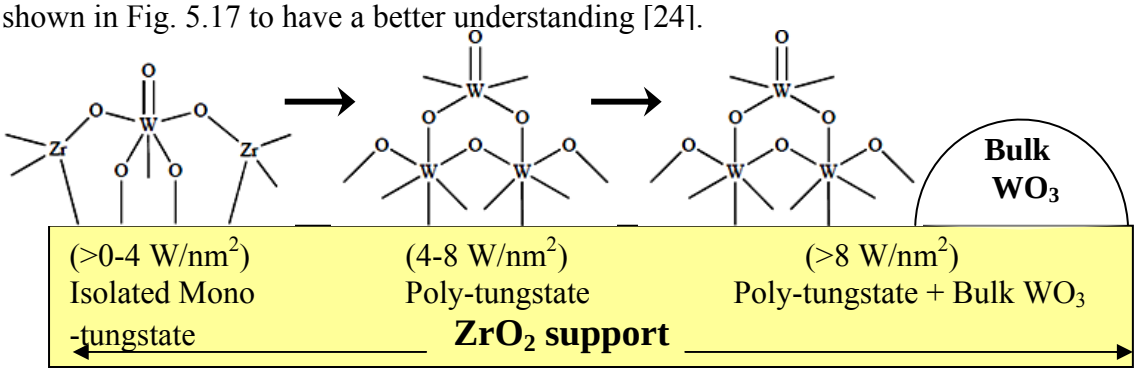

Fig. 5.17: Evolution of various W species on the zirconia support with increasing surface density

Finally, from Fig. 5.17 and combined analysis of experimental and theoretical results three main W species, associated with the surface density can be distinguished: (i) at very low loadings of W (>0-4 W-atoms/nm^2), essentially isolated WO_4 or WO_6 monomers are formed (ii) between 4 and 8 W-atoms/nm^2, polymeric domains of WO_3 anchored to the zirconia surface are expected to be the most abundant ones (iii) at higher values (>8 W-atoms/nm^2), presumably the octahedral polymeric species plus bulk WO_3 crystallites become more abundant [115]. The usefulness of combining results from different analytical methods is thus demonstrated in the characterization of tungstated zirconia catalysts. Data from surface characterization techniques such as EDX, XPS and XRF together with information from ICP-AES were compared and utilized for achieving actual analytical WO_3 concentration, W/Zr ratio and surface density.

5.2.8. FT-IR Analysis

The FT-IR spectrum of various tungstated zirconia catalysts calcined at 700 ^oC are shown in Fig. 5.18. This figure also shows an expanded view of the region 780-1180 cm^{-1} for better visibility. According to the literature the bond, metal and hydroxide (Zr–OH) is noted at 1400 cm^{-1}, the bond metal and oxygen (Zr–O) is situated at 585 cm^{-1} and bonds metal, oxygen and metal (Zr–O–Zr) with high intensity can be detected at ~ 500 cm^{-1} [116]. The band at around 1400-1450 cm^{-1} is also assigned to the stretching vibration of the bonds nitrogen and oxygen (N–H) in the NH^{4+} ions. [117,118].

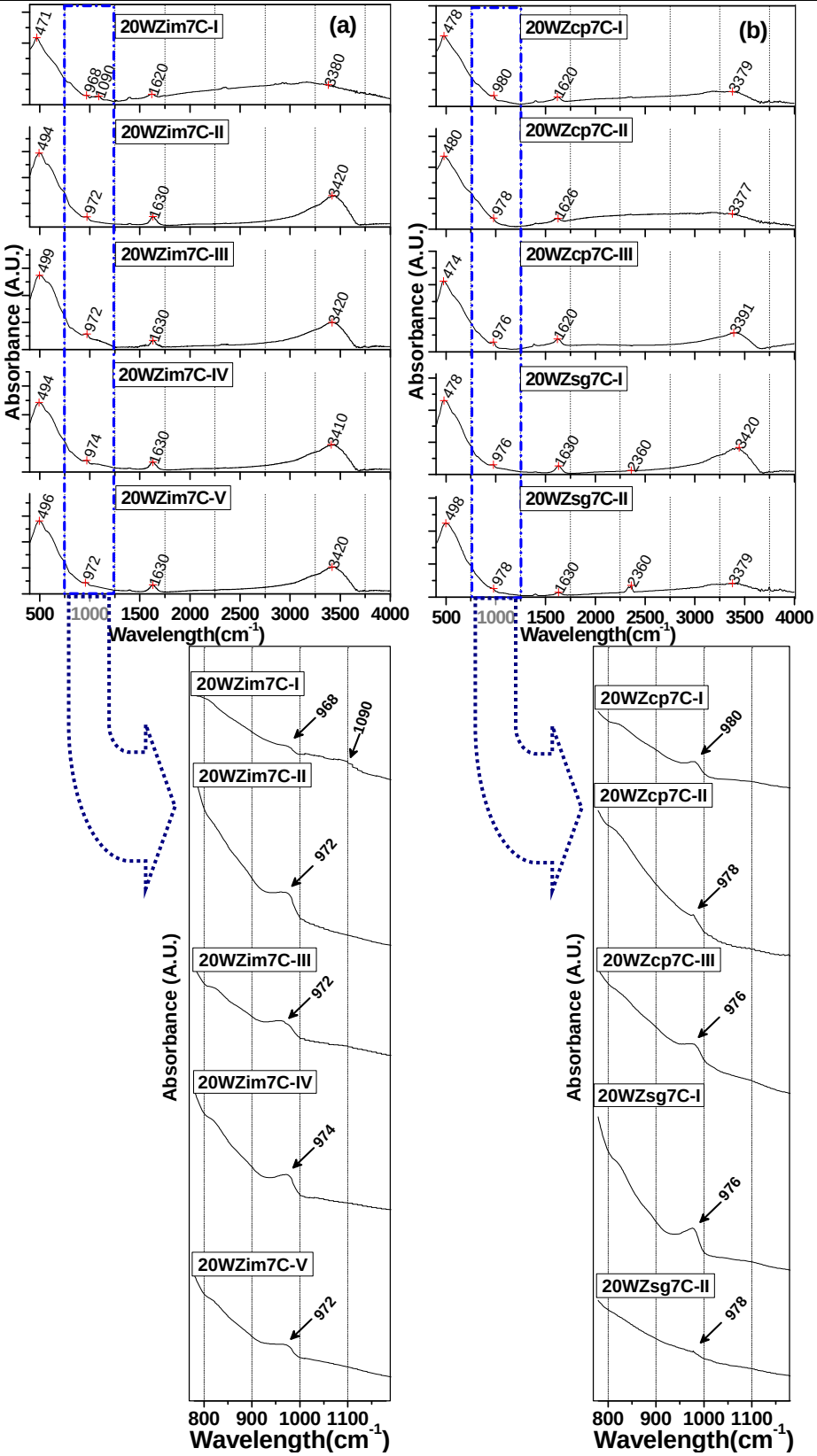

Fig. 5.18: FT-IR spectrum of **(a)** WO_3/ZrO_2 samples prepared by impregnation method. **(b)** WO_3-ZrO_2 samples prepared by co-precipitation and sol-gel method. Zoomed in wavelength region, 780-1180 cm^{-1} revealed below for both the figures, **(a)** and **(b)**.

The bands in the region 1620-1630 cm^{-1} and 3000-3400 cm^{-1} corresponds to the bending and stretching modes of the OH groups of water molecules present in the sample. Normally crystalline WO_3 shows peaks around 805 cm^{-1} and 1100 cm^{-1} [50,119]. The IR spectrum of all the tungstated zirconia samples calcined at 700 ^oC shows a broad main maximum in the region 471-500 cm^{-1} confirming tetragonal zirconia phases, while the absence of distinct bands at 417, 575 and 740 cm^{-1}, rule out the presence of monoclinic zirconium phase, [120,121,122]. Under ambient conditions, the supported metal oxide catalysts contain a thin film of water which hydrates the surface metal oxide species [123]. The W=O and W-O vibrations of the hydrated surface metal oxide species generally occur below 1100 cm^{-1} [22,28,29] which usually makes it difficult to detect these vibrations with IR spectroscopy because of the strong IR absorption of the oxide supports in this region. Even so it was possible in our system to at least detect the terminal W=O vibration in the 900-1100 cm^{-1} region for almost all the samples calcined at 700 ^oC. Regardless of the preparation methods, all the samples showed a band at around ~ 972 cm^{-1}, which was assigned to polytungstate structure with tungsten in octahedral coordination homogeneously distributed on the surface of zirconia [26]. Absorption between 970-980 cm^{-1} is characteristic of polytungstate anions $W_6O_{20}(OH)^{5-}$ $W_{12}O_{41}^{10-}$, or $W_{12}O_{39}^{6-}$ [22], which confirms the formation of the polytungstate structures on the surface of the zirconia. This band has appeared at lower wave numbers than those reported in other works, which are between 1000 and 1020 cm^{-1} [22,45,124,125]. The shift of the band position towards lower wave numbers (~ 972 cm^{-1}) in our samples could be attributed to a strong tungsten-zirconia interaction [50,126,127]. The formation of Zr–O–W bonds can be confirmed by the decrease in the intensity and change in the contour of the bands in the region 2800-3800 for the terminal and bridging OH groups in the IR spectra of most WO_3-/ZrO_2 samples, however it was not possible to correlate the shape/shift in peak position, amount of decreased intensity with surface density, synthesis method, zirconium precursor and other process parameters [26,27,28]. The emergence of a band at 1090 cm^{-1} for sample 20WZim7C-I is related to the formation of crystalline WO_3. The XRD spectrum of this sample also showed the monoclinic WO_3 crystallites, this unambiguously indicates the connection between the 1090 cm^{-1} band and the bulk WO_3 phase. These results are in accord with the earlier reports [22,24]. By comparing the

IR spectrum of sample 20WZim7C-I with other samples, no IR band similar to 1090 cm^{-1} band could be spotted for rest of the samples in the matching wavelength region. This finding is analogous with the XRD results were in no bulk WO_3 phase was detected by XRD besides in sample 20WZim7C-I. Therefore one can assign the band at 1090 cm^{-1} to the presence of some fraction of well-crystallized bulk WO_3 phase, and the band at ~ 972 cm^{-1} to a polytungstate structure. Absence of the high wave number (1090 cm^{-1}) band corresponding to bulk WO_3 phase in almost all the samples calcined at 700 ^oC suggests that the tungsten oxide is in a highly dispersed state on the surface of the zirconia. The high wave number of this band indicates a high bond order of the structure associated to it.

5.2.9. SEM Analysis

To observe the surface morphologies and tungsten distribution the samples, annealed at 700 ^oC were analyzed by SEM/EDX using backscattering electron images. An electron microprobe was used in the energy dispersive mode (EDX) to attain quantitative information on the distribution of the tungsten in the specimens. Fig. 5.19 and 5.20 shows compositional images of various tungstated zirconia samples. At first instance a noticeable feature can be spotted in all tungstated zirconia SEM images. Tiny white particles on the surface of the big gray particles are seen. However, smaller gray particles but bigger then white particles are also present. The SEM images suggest that the gray particles are mainly constituted by zirconia, while the white particles are rich in W. This is because the image formation process is based on the backscatter electrons of the atoms present in the sample: W atoms scatter more electrons than Zr atoms, due to greater atomic number of W as compared to Zr. This condition must produce white contrast images where high W concentration is present. In order to confirm this hypothesis sample 20WZim-II was selected randomly and its images at different calcination temperature including the un-calcined sample were taken, and are produced in Fig. 5.19 and 5.20. Commencing from the un-calcined sample picture (20WZim-II) to the highest calcination temperature (800 ^oC) sample picture 20WZim8C-II, it can be observed that the fractions of white particles are higher in number and size.

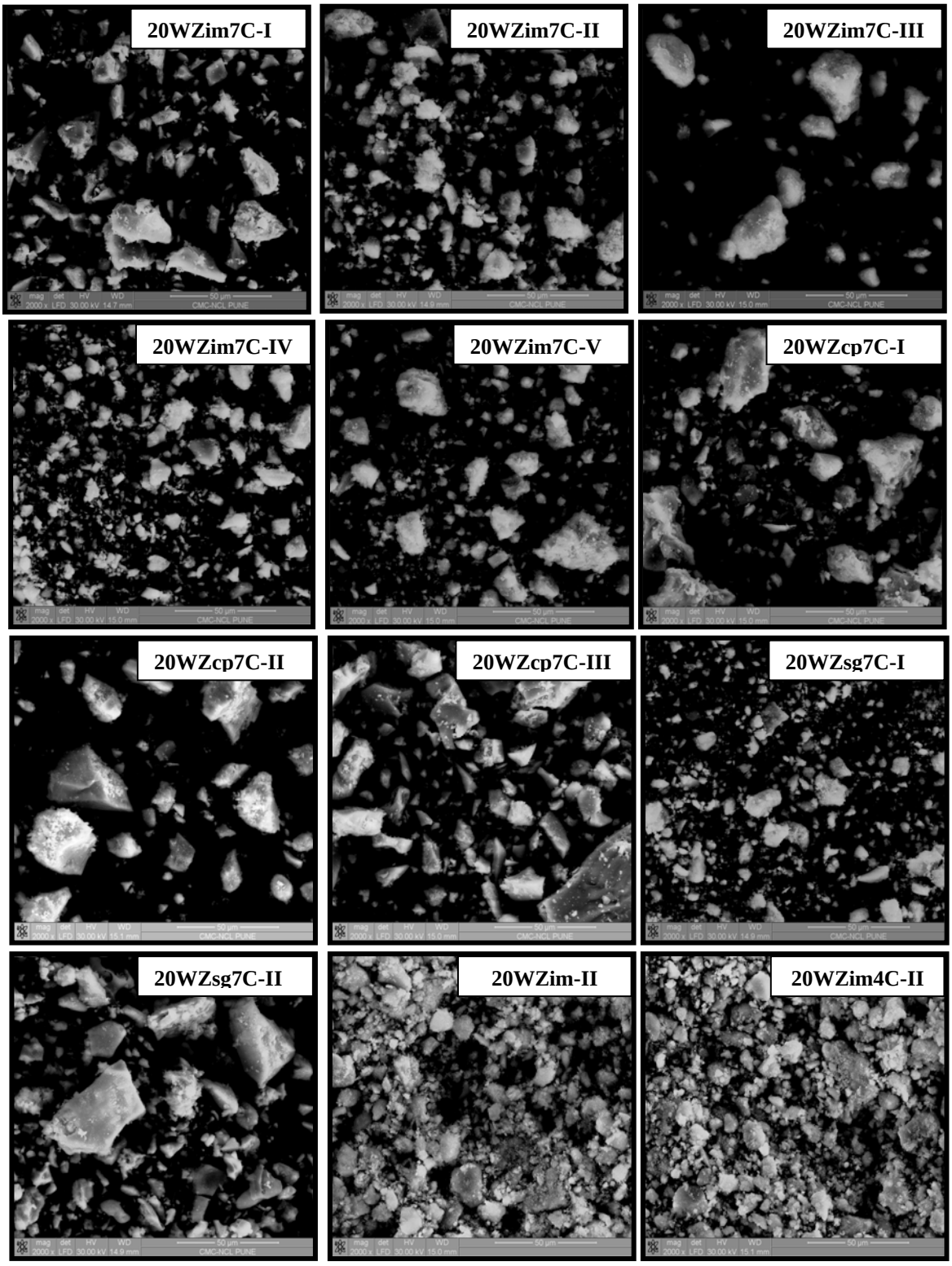

Fig. 5.19: Backscattering SEM micrographs of the various tungstated zirconia samples.

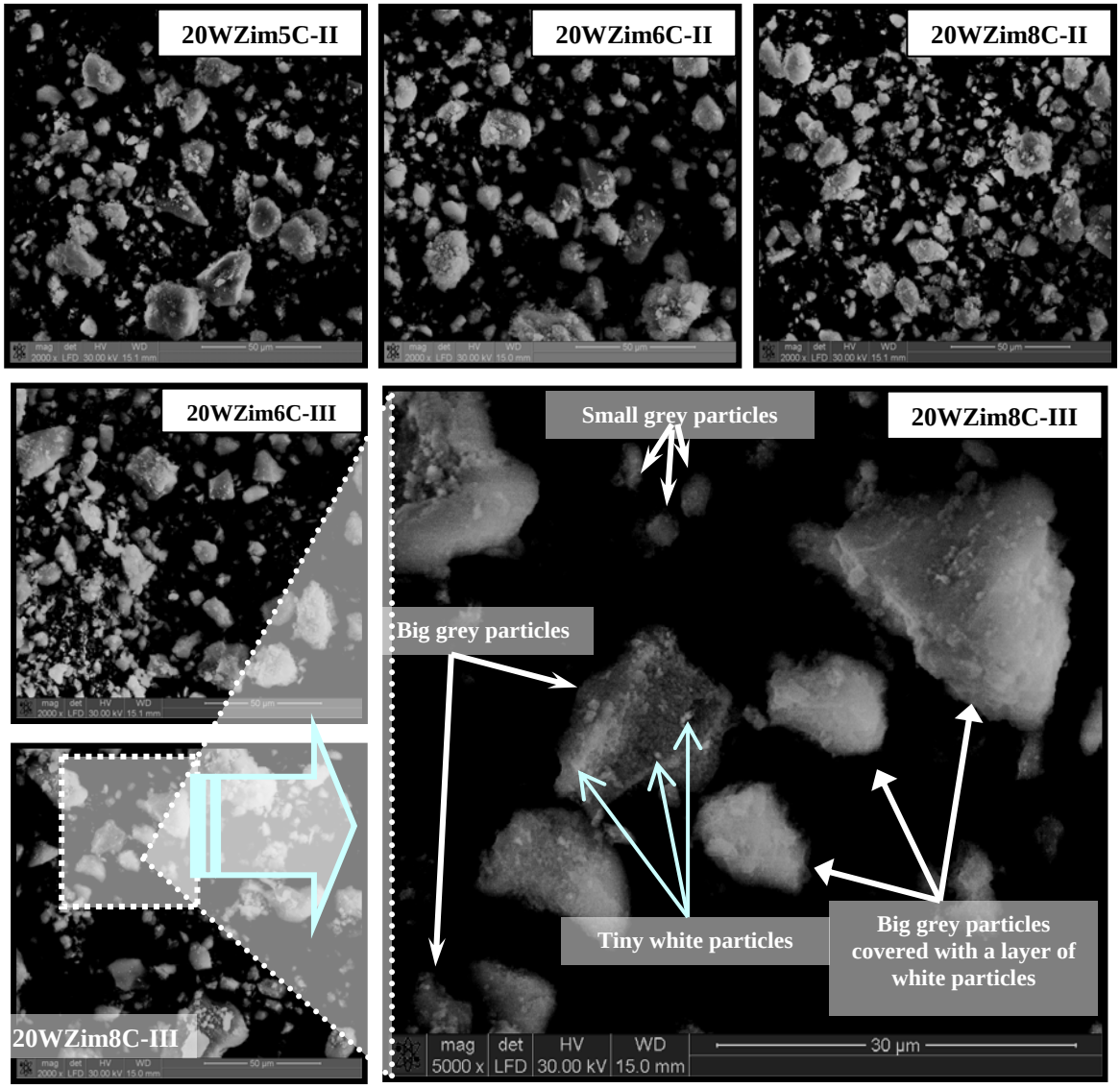

Fig. 5.20: Backscattering SEM micrographs of sample 20WZim-II calcined at 500 ^{o}C, 600 ^{o}C, 800 ^{o}C and 20WZim-III calcined at 600 ^{o}C and 800 ^{o}C. The area under the marked white box of sample 20WZim8C-III is presented with higher magnification.

Also the grey particles appear brighter as the calcination temperature increases, indicating good dispersion of WO_3 on the zirconia surface. Similar results were gained from the images of samples 20WZim6C-III, 20WZim7C-III and 20WZim8C-III calcined at 600, 700 and 800 ^{o}C respectively, thus confirming the earlier interpretation. Fig. 5.20 shows SEM image of sample 20WZim8C-III at higher magnification, in which different particles were identified and tagged only after confirmation by EDX. From this figure it is apparent that WO_3 dispersion is pretty good on zirconia particles. Also as the temperature changes from 400 ^{o}C to 800 ^{o}C, the amount of amorphous type particles

seems to be reduced and particles looks more refined due to thermal treatment. Two types of grey irregular agglomerates are observed in all the samples, smaller been in the range of 3-5 μm, while larger agglomerates are 15-20 μm in size. No definite change in morphology could be seen for the samples prepared with different synthesis method and process parameters. The irregular morphology remains almost same at all calcination stages, with minor increase in the shape and size of the agglomerates with increasing calcination temperature.

5.2.10. TEM Analysis

Transmission electron microscopy is a powerful tool for the investigation of the microstructure of materials, providing crystallographic information and composition at the nanometer scale. Lattice fringe images represent the simplest case and record an intense modulation that gives the spacing of the atomic planes lying parallel to the incident beam, enabling catalyst particles to be identified. In the case of heavy metals, the crystal structure of the particles can also be studied. In the current study representative bright field TEM and HRTEM images with higher magnification of the tungstated zirconia catalysts are shown in Fig's. 5.21-5.24. From HRTEM images all the samples exhibit particles which are uniformly distributed, and have mono-modal distribution and almost spherical in shape. Sol-gel samples were observed to have spherical shaped particle with globular agglomerates, whereas co-precipitation and impregnation samples showed irregular rectangular-shaped agglomerates with round and/or egg shapes particles of varied size. The smaller particles present in tungstated zirconia samples prepared with modified synthesis parameters, especially the digested ones, is a direct consequence of the strong interaction between the WO_3 species with the zirconia support during its crystallization. While samples prepared without the aid of digestion showed larger particle size (Samples 20WZim7C-I and 20WZsg7C-II). All samples also occasionally exhibited highly condensed ZrO_2 particles of around ~20 nm in diameter, which constituted a very small volume fraction of the total support material. These larger particles were presumably formed due to local in-homogeneities during calcinations. HRTEM images with higher magnification revealed atomic lattice fringes and hence supports again the crystalline nature of the particles, thus complimenting XRD results.

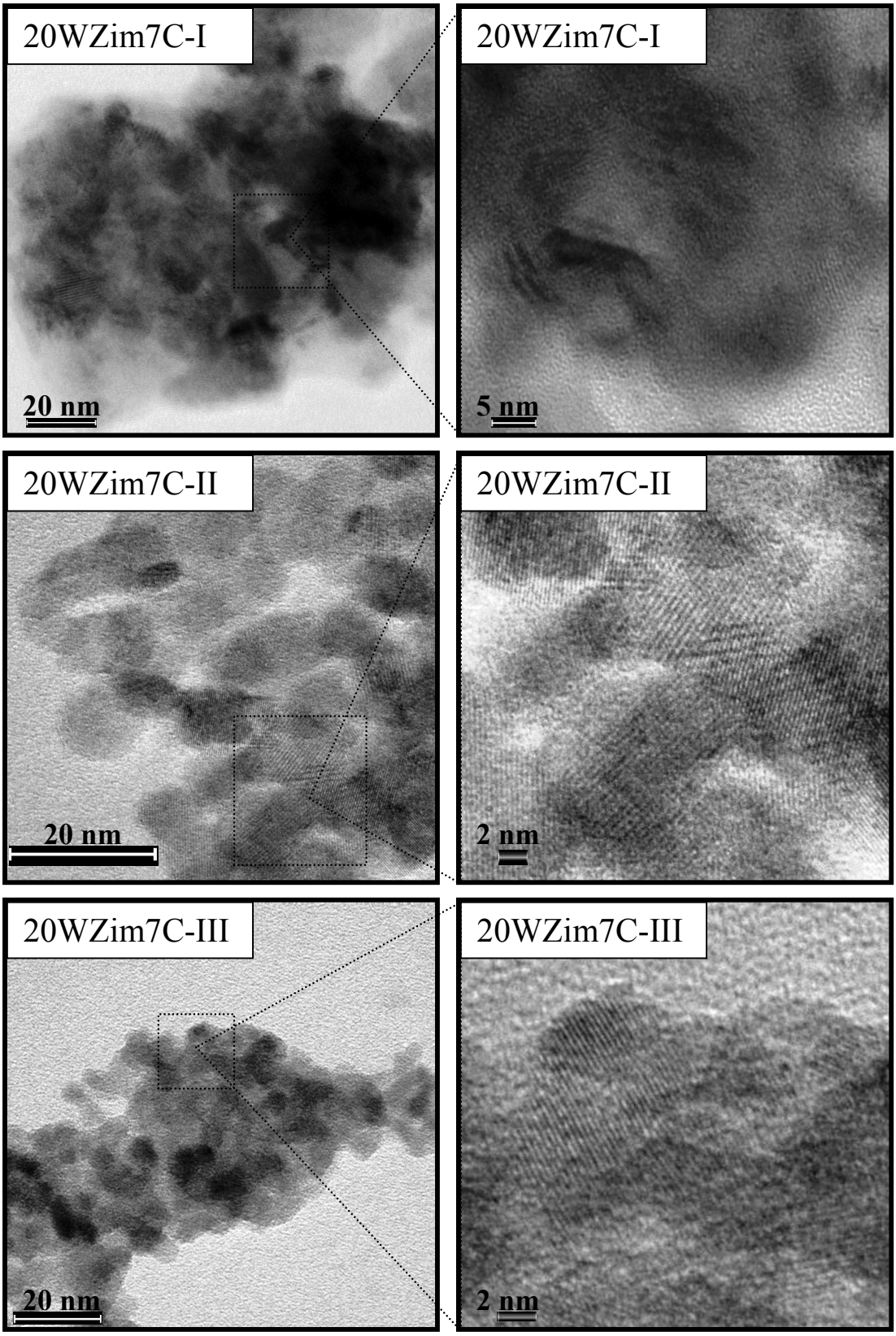

Fig. 5.21: Representative TEM (bright field) and HR-TEM images of various tungstated zirconia samples as indicated with different magnifications.

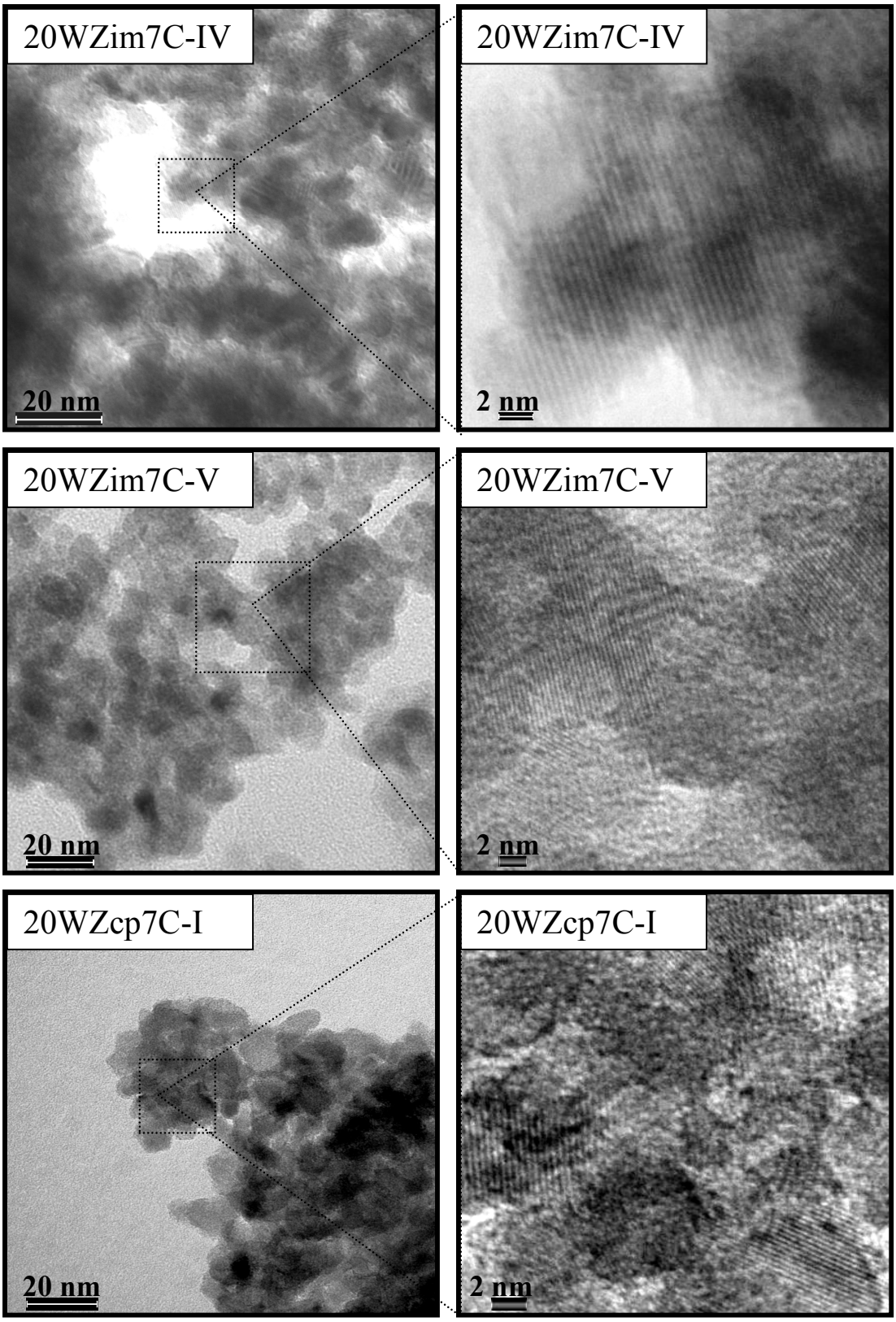

Fig. 5.22: Representative TEM (bright field) and HR-TEM images of various tungstated zirconia samples as indicated with different magnifications.

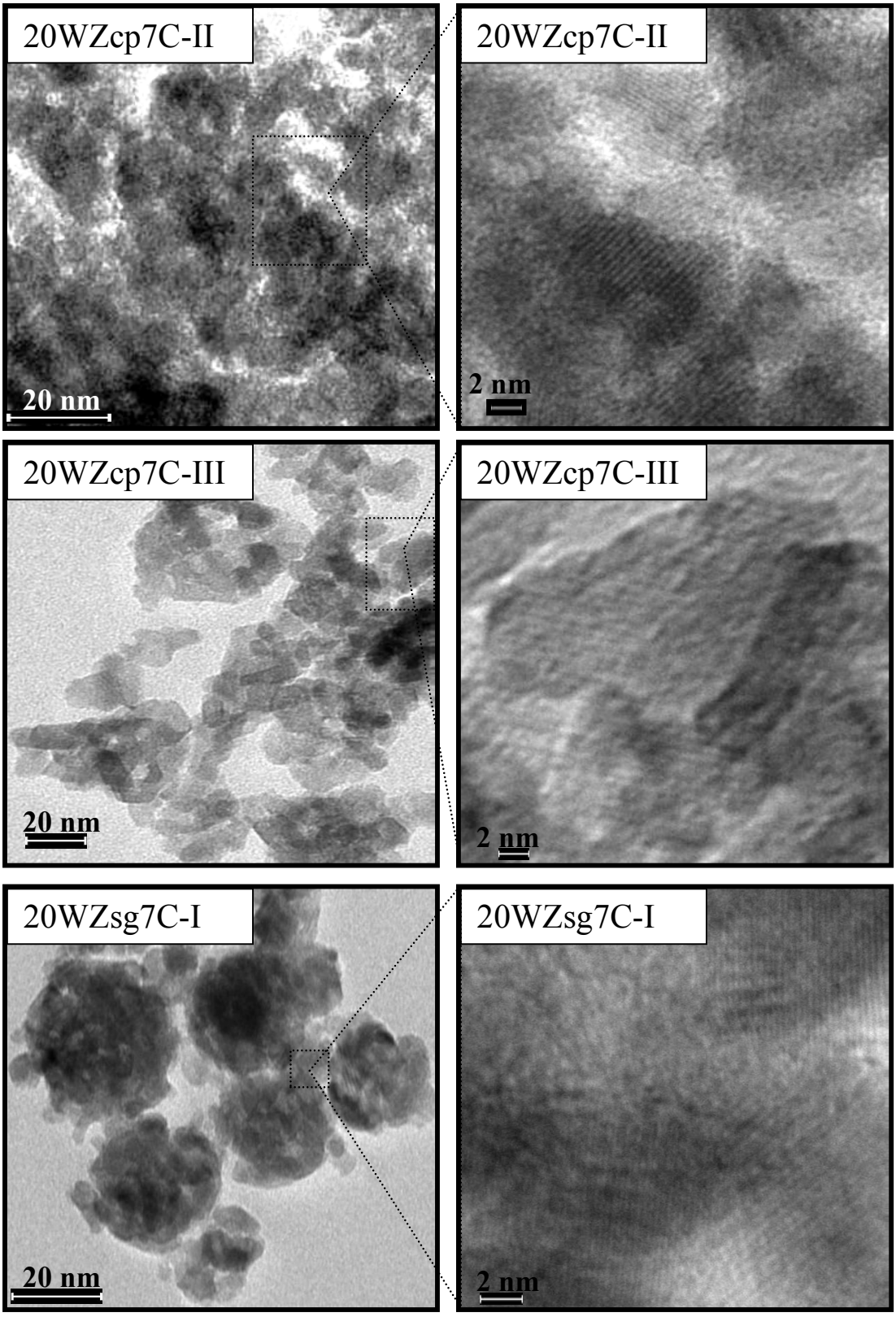

Fig. 5.23: Representative TEM (bright field) and HR-TEM images of various tungstated zirconia samples as indicated with different magnifications.

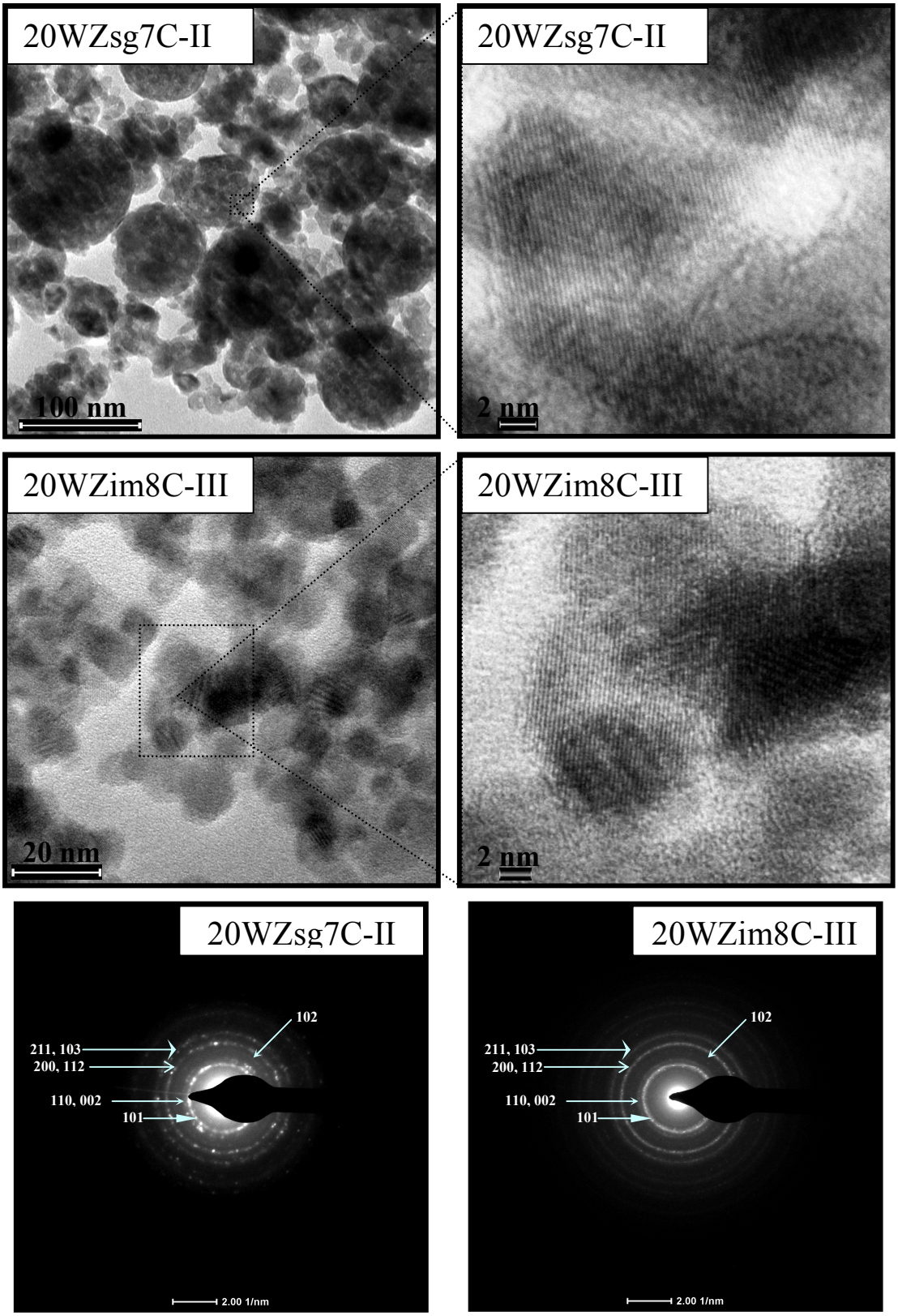

Fig. 5.24: Representative TEM and HR-TEM images of various tungstated zirconia samples. SAED patterns of selected samples 20WZsg7C-II and 20WZim8C-III.

Nanometer scale dark flecks can just be discerned in these images, indicative of WO_3 clusters. These darker flecks (WO_3 clusters) exhibit higher contrast than zirconia support due to their higher mass contrast. However, if one examines images carefully, a clearer picture emerges in which surface mono and poly-tungstate species co-exist. A general trend of increasing concreteness of the dark WO_3 rich specks with increasing W-atoms/nm^2 can be seen for samples 20WZim7C-I and 20WZsg7C-II. In particular, dispersion of the latter sample is better. 20WZcp7C-II and 20WZim7C-IV powders show a more uniform dispersion but the particles do not posses any specific shape, when compared with samples prepared with similar conditions in the absence of surfactant. Also due to fuzzy network of these samples it difficult to predict the average particle size. The comparison of particle size between TEM and XRD has been presented in Table 5.2. The values obtained by XRD are slightly larger than the particle size deduced from TEM images. Selected area electron diffraction (SAED) pattern of samples 20WZsg7C-II and 20WZim8C-III are presented at the end of TEM micrographs. The presence of few clear spots along with connecting diffraction rings shows the presence of crystallite of reasonably sufficient sizes to diffract. SAED patterns of other samples are not shown for brevity.

5.3. CONSLUSIONS

Binary WO_3-/ZrO_2 solids with tetragonal phase are synthesized by using modified impregnation, coprecipitation and sol-gel method under a variety of different process conditions. Influence of the various improved preparation methods on the structure, chemical composition and physicochemical properties of tungstated zirconia (WO_3-/ZrO_2) solid acid catalyst are laid down using a variety of characterization techniques. The addition of tungstate ions to zirconia under identical synthesis condition raises the crystallization temperature of zirconia from 410 °C to 580 °C. All the materials prepared using modified procedure showed mesoporous textures with surface area almost touching 100 m^2/g, with average particle size between 10 to 15 nm. Stronger heat treatment of WO_3-/ZrO_2 above 700 °C leads to a reduction of surface area and formation of bulk WO_3 crystallites. Usually [51] two preparation methods (impregnation and co-precipitation) are used for the synthesis of tungstated zirconia materials, of which the latter yields better

acidity and BET surface area. Dramatically in these studies exactly opposite has happened, the samples calcined at 800 °C prepared using modified impregnation method have shown better surface areas, acidity and no evidence of zirconium monoclinic phase as well as bulk WO_3 crystals, while using co-precipitation method it showed traces of it. Postulated reason may be, the actual amount of tungsten strongly and directly anchored on the zirconia surface which controls the surface area shrinkage and the fraction of tetragonal zirconia. Addition of Pluronic P-123 block copolymer surfactant to the modified synthesis procedure has shown materials with somewhat better surface areas. The traditional procedure for the production of mesoporous oxides using organic template/surfactant is not suitable for the production of mesoporous tungstated zirconia materials since the burning of the template/surfactant above 500 °C leads to the destruction of its porous structure. This work provides new experimental information on how to use various elemental characterization techniques to accurately determine and obtain WO_3-/ZrO_2 binary oxides with different surface density/acidity by treating the precipitated materials under controlled conditions and with identical surface density/acidity by varying synthesis methods and process parameters.

5.4. REFERENCES:

[1] B.M. Reddy, Pavani M. Sreekanth, Y. Yamad, T. Kobayashi, Journal of Mol. Catalysis A: Chemical, 2005, 227, 81–89.

[2] B. M. Reddy and M. K. Patil, Chemical Reviews, 2009, 109, 2186.

[3] F.T.T. Ng, N. Horvat, Appl. Catal., 1995, 123, 197.

[4] Ch. Gosling, R. Rosin, P. Bullen, T. Shimidzu, I. Imai, Petrol. Technol. Q (winter) 1997-1998, 55.

[5] P.G. Blommel, Ch.D. Gosling, S.A. Wilcher, US Patent 5, 1998, 763,713.

[6] H. Hino, K. Arata, J. Chem. Soc. Commun., 1980, 851.

[7] G. Larsen, E. Lotero, R.D. Parra, L.M. Petkovic, H.S. Silva, S. Raghavan, Appl. Catal: A, 1995, 130, 213.

[8] G. Larsen, E. Lotero, R.D. Parra, in: Proc. 11th Intl. Congr. Catal., Baltimore, 1996, 543

[9] E. Iglesia, D.G. Barton, S.L. Soled, S. Miseo, J.E. Baumgartner, W.E. Gates, G.A. Fuentes, G.D. Meitzner, Stud. Surf. Sci. Catal., 1996, 101.

[10] S.R. Vaudagna, S.A. Canavese, R.A. Comelli, N.S. Fı´goli, Appl. Catal., 1998, A 168, 93.

[11] W. Grünert, R. Feldhaus, K.Anders, E.S. Shpiro, J Catal., 1989, 120, 444–456.

[12] B. Ogata, Y. Kamiya, N. Ohta, J Catal., 1973, 29, 296–307.

[13] H. Hattori, N. Asada, K. Tanabe, Bull Chem Soc Jpn., 1978, 51, 1704–1707.

[14] T. Yamaguchi, Y. Tanaka, K. Tanabe, J Catal, 1980, 65, 442–447.

[15] R. Thomas, E.M.van Oers, V.H.J.de Beer, J.A. Moulijn, J Catal., 1982, 76, 241–253.

[16] J.C. Mol, J.A. Moulijn, In: Anderson JR, Boudart M (eds) Catalysis-science and technology. Springer, Berlin, 1987, 8, 69.

[17] J Due-Hansen, A L. Kustov, S Birk Rasmussen, R. Fehrmann, C. H. Christensen Applied Catalysis B: Environmental, 2006,161.

[18] D Yang, Junhua Li , Mingfen Wen, Chongli Song, Cat. Comm. 2007, 8, 2243–2247.

[19] M. Imanari, Y. Watanabe, S. Matsuda, F. Nakajima, Proceedings of the 7th International congress on catalysis. Seiyama T, Tanabe K (eds) Elsevier, Amsterdam, 1981, 841–852.

[20] W.K. Hall, In: Vanselow R, Howe R (eds) Chemistry and physics of solid surfaces IV, 1986, 73.

[21] R.B. Quincy, M. Houalla, D.M. Hercules, J Catal., 1987, 106, 85–92.

[22] R. A. Boyse and E. I. Ko, J. Catal., 1997, 171, 191-207.

[23] D. G. Barton, S. L. Soled, and E. Iglesia, Top. Catal., 1998, 6, 87-99.

[24] D. G. Barton, M. Shtein, R. D. Wilson, S. T. Soled and E. Iglesia, J. Phys. Chem. B, 1999, 103, 630 .

[25] M. Valigi, D. Gazzoli, I. Pettiti, G. Mattei, S. Colonna, S. De Rossi, G. Ferraris, Appl. Catal., 2002, 231, 159.

[26] C. D. Baertsch, S. L. Soled, and E. Iglesia, J. Phys. Chem., 2001, B.105, 1320-1330

[27] F. Di Gregorio and V. Keller, J. Catal., 2004, 225, 45-55.

[28] V. V. Brei, O. V. Melezhyk, S. V. Prudius, et al., Ads. Sci. Techn., 2005, 23, 909-914.

[29] M. Scheithauer, T.K. Cheung, R.E. Jentoft, R.K. Grasselli, B.C. Gates, H. Knözinger, J. Catal., 1998, 180.

[30] M. Scheithauer, R.K. Grasselli, H. Knözinger, Langmuir, 1998, 14, 3019.

[31] D.G. Barton, S.L. Soled, G.D. Meitzner, G.A. Fuentes, E. Iglesia, J. Catal., 1999, 181, 57.

[32] Wu Zhou, E.I. Ross-Medgaarden, W.V. Knowles, M.S. Wong, I.E. Wachs and C.J. Kiely, Nature Chemistry, Dec.2009, 1, 722.

[33] J.G. Santiestaban, J.C. Vartuli, S. Han, R.D. Bastian, C.D. Chang, J. Catal., 1997, 168, 431.

[34] R.A. Boise, E.I. Ko, J. Catal., 1997, 171, 191.

[35] S. Soled, N.C. Despensiere, R. Saleh, in: H. Attori, M. Misono, Y. Ono (Eds.), Studies in Surface Science Catalysis, Elsevier, Amsterdam, 1994, 90, 573.

[36] M. Kudo, Y. Yoshinaga, S. Hasenagawa, in: H. Attori, M. Misono, Y. Ono (Eds.),

Studies in Surface Science Catalysis, Elsevier, Amsterdam, 1994, 90, 549.

[37] D.S. Kim, M. Ostromercki, J.E. Wachs, J. Mol. Catal., 1996, 93, 106.

[38] P. Afanasiev, C. Geantet, M. Breysse, G. Coundurier, J.C. Vedrine, J. Chem. Soc., Faraday Trans., 1994, 90, 193.

[39] G. Larsen, E. Lotero, S. Geghavan, E.R. Parra, C.A. Querini, Appl. Catal: A, 1996, 139, 201m.

[40] G. Larsen, E. Lotero, L.M. Petkovic, L.M. Shobe, J. Catal., 1997, 169, 67.

[41] G. Larsen, S. Reghavan, M. Marquez, E. Lotero, Chem. Lett., 1996, 37, 57.

[42] S. Kuba, P.C. Heydorn, R.K. Grasselli, B.C. Gates, M. Che, H. Knözinger, Phys. Chem. Chem. Phys., 2001, 3, 146.

[43] E I. Ross-Medgaarden, W. V. Knowles, T. Kim, M.S. Wong, Wu Zhou, C J. Kiely, I E. Wachs, J. of Catal., 2008, 256, 108–125.

[44] M. A. Corte´s-Ja´come, J. A. Toledo, and C. Angeles-Chavez, J. Phys. Chem.: B , 2005, 109, 22730-22739.

[45] J.R. Sohn, M.Y. Park, Langmuir, 1998, 14, 6140.

[46] A. Martínez, G.Prieto, M. A. Arribas, P. Concepción, J. F. Sánchez-Royo, Journal of Catalysis, 2007, 248, 288–302.

[47] M.G. Falco, S.A. Canavese, N.S. Fı´goli, Catalysis Today, 2005, 107–108, 778–784

[48] K. Chen, A.T. Bell, E. Iglesia, J. Catal., 2002, 209, 35.

[49] E. Iglesia, Plenary Conference XIX Iberoam, Symposium on Catalysis, Megoli, Appl. Catal. Arida, Me11 September 2004, M4.

[50] H. Armenda´riz, M.A. Corte´s-Ja´come, I. Herna´ndez, J. Navarrete, A.J. Va´zquez, Mater. Chem. 2003, 13, 143.

[51] J.G. Santiesteban, J.C. Vartuli, S. Han, R.D. Bastian, C.D. Chang, J. Catal., 1997, 168, 431.

[52] G.H. Chuah, Catal Today, 1999, 49, 131.

[53] W. Stichert and F. SchÄuth. J. Catal., 1998, 174, 242-245.

[54] O.V. Melezhyk, S.V. Prudius, V.V. Brei, Micro and Meso. Mater., 2001, 49, 39-44

[55] D.A. Ward and E. I Ko. J. Catal., 1995, 157, 321-333.

[56] W. Sun, L. Xu, Y. Chu, and W. Shi. J. Colloid Interface Sci., 2003, 266, 99,106.

[57] E. Tani, M. Yoshimura, and S. Somiya. J. Am. Ceram. Soc., 1983, 66, 11.

[58] K. Arata, M. Hino, J. Chem. Soc., Chem. Commun., 1987, 1259.

[59] D.C. Calabro, J.C. Vartuli, J.G. Santiesteban, Topics Catal., 2002, 18, 231.

[60] M.A. Cortés-Jácome, J.A. Toledo, C. Angeles-Chavez, M. Aguilar, J.A.Wang, J. Phys. Chem.:B, 2005,109, 22730.

[61] A. Barrera, J.A. Montoya, M. Viniegra, J. Navarrete, G. Espinosa, A. Vargas, P. del Angel, G. Pérez, Appl. Catal.:A, 2005, A 290, 97.

[62] A. Cimino, D. Cordischi, S. De Rossi, G. Ferraris, D. Gazzoli, V. Indovina, G. Minelli, M. Occhiuzzi, M. Valigi, J. Catal., 1991, 127, 744.

[63] M. Valigi, A. Cimino, D. Cordischi, S. De Rossi, C. Ferrari, G. Ferraris, D. Gazzoli, V. Indovina, M. Occhiuzzi, Solid State Ionics., 1993, 63-64, 136.

[64] C. Rueca, J.C. Yori, C.L. Pieck, S. Hirusta, J.M. Parera, Appl. Catal: A , 2003, 240, 161.

[65] M. Rezaei, S. M. Alavi, S. Sahebdelfar and Z. Yan, J. Por. Mat., 2008, 15, 171.

[66] C. V. Ramana, S. Utsunomiya, R. C. Ewing, C. M. Julien, and U. Becker, J. Phys. Chem:B, 2006, 110, 10430-10435.

[67] O. Berger, W.J. Fischer, V. Melev, Journal Of Materials Science: Materials In Electronics, 2004, 15, 25-29.

[68] M. Gillet, C. Lemire, E. Gillet, K. Aguir, 2003, 532, 519.

[69] I. Turyan , B. Orel, R. Reisfeld, D. Mandler, Phys. Chem. Chem. Phys., 2003, 5, 33.

[70] E. Salje, K. Viswanathan, Acta Cryst. A , 1975, 31, 356.

[71] T.D. Senguttuvana, Vibha Srivastava, Jai S. Tawal, M. Mishra, S. Srivastava, K. Jain, Sensors and Actuators B: Chemical, 2010, 50, 384–388.

[72] B. Gerand, G. Nowogrocki, J. Guenot, M.J. Figlarz, J. Solid State Chem., 1979, 29, 429.

[73] N. R. Shiju, M. Anil Kumar, W. F. Hoelderich, and D. R. Brown, J. Phys. Chem. C 2009, 113, 7735-7742.

[74] A. Martı´nez, G. Prieto, M.A. Arribas, P. Concepcio´n, J.F. Sa´nchez- Royo, J. Catal., 2007, 248, 288.

[75] A. Martı´nez, G. Prieto, M.A. Arribas, P. Concepcio´n, Appl. Catal: A, 2006, 309, 224.

[76] D. E. López, K. Suwannakarn, D. A. Bruce, J. G. Goodwin Jr, Journal of Catalysis, 2007, 247, 43–50.

[77] V.V. Srdic, M. Winterer, Chem. Mater., 2003, 15, 2668.

[78] G. Beaucage, H.K. Kammler, S.E. Pratsinis, J. Appl. Cryst., 2004, 37, 523.

[79] H.K. Kammler, G. Beaucage, R. Mueller, S.E. Pratsinis, Langmuir, 2004, 20, 1915.

[80] H. Klug, L. Alexander, X-Ray diffraction procedures for polycrystalline and amorphous materials, 2nd edn. Wiley, New York, 1974.

[81] R. Wongmaneerung, R. Yimnirun, S. Ananta, Mater Letters, 2006, 60, 2666.

[82] J.S. Reed, Principles of ceramic processing, 2nd ed. Wiley, New York, 1995.

[83] M. Valigi, D. Gazzoli, A. Cimino, E. Proverbio, J. Phys. Chem: B, 1999, 103, 11318.

[84] S. Brunauer, L.S. Deming, W.S. Deming, E. Teller, J. Am. Chem. Soc., 1940, 62, 1723.

[85] J.H. de Boer, The Structure and Properties of Porous Materials, Butterworths, London, 1958, 68.

[86] S.J. Gregg, K.S.W. Sing, Adsorption, Surface Area and Porosity, seconded., Academic Press, London, 1974, 285–287.

[87] S.L. Soled, G.B. Mcvicker, L.L. Murrel, J. Catal., 1998, 111, 286.

[88] L. Karakonelantis, H. Matralis, Ch Kordulis, Lycourgluotis, J. Catal., 1996, 162, 306

[89] N. Vaydyanathan, D.M. Hercules, M. Houalla, Anal. Bioanal. Chem., 2002, 373, 547.

[90] S. Doniach, M. Sunjic, J. Phys. C, 1970, 3, 285.

[91] F. Le Normand, J. El Fallah, L. Hilaire, P. Légaré, A. Kotani, J.C. Parlebas, Solid State Commun., 1989, 71, 885.

[92] J.H. Scofield, J. Electr. Spectrosc. Relat. Phenom., 1976, 8, 129.

[93] M. Occhiuzzi, D. Cordischi, D. Gazzoli, M. Valigi, P.C. Heydorn, Appl. Catal. A, 2004, 269, 169.

[94] T. Nishiguchi, K.Oka, T. Matsumoto, H. Kanai, K. Utani, S. Imamura, Applied Catalysis A: General, 2006, 301, 66–74.

[95] E. Salje, A.F. Carley, M.W. Roberts, J. Solid. State Chem., 1979, 29, 237.

[96] Farook Adam Anwar Iqbal, Chemical Engineering Journal, 2011, 171, 1379–1386.

[97] M.A. Corte´s-Ja´come, Carlos Angeles-Chavez, Xim Bokhimi, J.A. Toledo-Antonio, Journal of Solid State Chemistry, 2006, 179, 2663–2673.

[98] Y. Suchorski, L. Rihko-Struckmann, F. Klose, Y. Ye, M. Alandjiyska, K. Sundmacher, H. Weiss, Appl. Surf. Sci., 2005, M 249, 231.

[99] G.W. Coulston, E.A. Thompson, N. Herron, J. Catal., 1996, 163, 122.

[100] D.D. Sarma, C.N.R. Rao, J. Electron. Spectrosc., 1980, 20, 25.

[101] R. Kaufmann, H. Klewe-Nebenius, H. Moers, G. Pfennig, H. Jenett, H.J. Ache, Surf. Interface Anal., 1988, 11, 502.

[102] C. Morant, J.M. Sanz, L. Galan, L. Soriano, Surf. Sci., 1989, 218, 331.

[103] Y. Suchorski, J. Gottfriedsen, R. Wrobel, B. Strzelczyk, H. Weiss, Solid State Phenom., 2007, 128, 115.

[104] C.C. Hwang, X.R. Chen, S.T. Wong, C.L. Chen, C.Y. Mou, Applied Catalysis A: General., 2007, 323, 9–17.

[105] C.D. Baertsch, K.T. Komala, Y. Chua, E. Iglesia, J. Catal., 2002, 205, 44.

[106] Ph. Quevauviller, J. L. Imbert, M. Olle, Mikrochim. Acta, 1993, 111, 1.

[107] http://srdata.nist.gov/xps/Default.aspx.

[108] D.A. Skoog, F.J. Holler, T.A. Nieman, Principles of Instrumental Analysis 5th Edition, 1998, 206-225.

[109] S. C. Srivastava, S. R. Bhaisare, D. N. Wagh and C P S Iyer, Bulletin of Materials

Science, 1996, 19, 331-343.

[110] C.B. Boss, K.J. Fredeen, Concepts, Instrumentation and Techniques in Inductively Coupled Plasma Optical Emission Spectrometry, 2004.

[111] N. Vaidyanathan, M. Houalla, D. Hercules, Surf. Interface Anal., 1998, 26, 415.

[112] I.E. Wachs, T. Kim, E.I. Ross, Catal. Today, 2006, 116, 162.

[113] T. Kim, A. Burrows, C.J. Kiely, I.E. Wachs, J. Catal., 2007, 246, 370.

[114] M. Niwa, Y. Habuta, K. Okumura, N. Katada, Catalysis Today, 2003, 87, 213–218.

[115] G. Rodriguez-Gattorno, A. Galano, E. Torres-Garc, Applied Catalysis B: Environmental, 2009, 92, 1–8.

[116] J.Ch. Valmalette, M. Isa, Chem. Mater., 2002, 14, 5098.

[117] Kno¨zinger, H. In Handbook of Heterogeneous Catalysis; Ertl, G., Kno¨zinger, H., Weitkamp, J., Eds.; Wiley-VCH: Weinheim, 1997, 707.

[118] N. Naito, N. Katada, and M. Niwa, J. Phys. Chem. B 1999, 103, 7206-7213.

[119] M.A. Corte´s-Ja´come, C. Angeles-Chavez, E. Lo´pez-Salinas, J. Navarrete, P. Toribio, J.A. Toledo, Applied Catalysis A: General, 2007, 318, 178–189.

[120] Y. Hao, J. Li, Xujie Yang, X. Wang, Lude Lu, Materials Science and Engineering A., 2004, 367, 243–247.

[121] N. Agoudjil, S. Kermadi, A. Larbot, desalination, 2008, 223, 417–424.

[122] D. Gazzoli, A. Marucci, G. Mattei, M. Valigi, R. Dragone, J. Phys. Chem: B, 1997, 101, 11129.

[123] I. E. Wachs, Catalysis Today, 1996, 27, 437-455.

[124] T. Yamagushi, K. Tanabe, Mater. Chem. Phys., 1986, 16, 67.

[125] T.N. Vu, J.U. Gestel, J.P. Glison, C. Collet, J.P. Dath, J.C. Duchet, J. Catal., 2005, 231, 453.

[126] S. Loridant, C. Feche, N. Essayem, F. Figueras, J. Phys. Chem: B, 2005, 109, 5631.

[127] M.K. Dongare, V. Ramaswamy, C.S. Gopinath, A.V. Ramaswamy, S. Scheurell, M. Brueckner, E. Kemnitz, J. Catal., 2001, 199, 209.

CHAPTER – 6

SUMMARY AND CONCLUSIONS

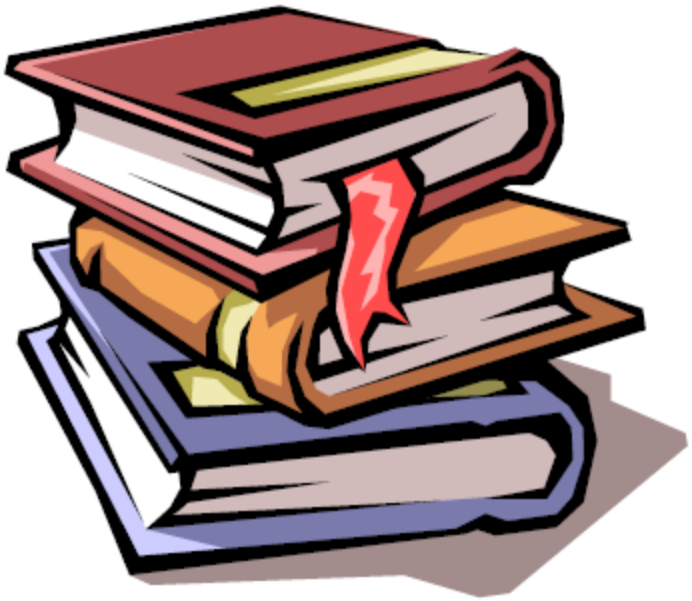

6. SUMMARY AND CONCLUSIONS

- The role of the principal preparation variables controlling the phase composition and thermal stability of pure zirconia, such as pH, concentration and temperature of the solution, the nature of parent zirconium salt as well as aging of the precipitate is studied.
- High surface zirconia can be obtained through optimized synthesis conditions via precipitation method using zirconium salts much economically as compared to zirconium alkoxides. Surface areas ~ 200 m^2/g can be obtained as long as the calcination temperature is kept below 500 ^oC.
- Digestion of the zirconium hydrous oxide increases the thermal stability and volume % of tetragonal phase of the resulting zirconia considerably.
- Addition of Mo and W also stabilizes zirconia in the meta-stable tetragonal phase, which is stable up to 800 ^oC temperature under optimized synthesis conditions.
- Influence of the various improved preparation methods on the structure, chemical composition and physicochemical properties of tungstated and molybdena zirconia solid acid catalyst are laid down by using a combination of analytical and spectroscopic characterization techniques. The interaction between Mo and W oxide with zirconia strongly influences the physicochemical properties.
- In the Mo and W oxide incorporated catalysts, the concentration of acid sites increased drastically when compared to that of pure ZrO_2 support. In particular, the percentage of acid sites on WO_3-/ZrO_2 is higher than on the MoO_3-/ZrO_2.
- Under identical synthesis conditions, addition of Pluronic P-123 surfactant has shown no significant effect on the structural properties of the MoO_3-/ZrO_2 and WO_3-/ZrO_2 catalyst, besides marginal increase in the surface area.
- 15 wt% MoO_3-/ZrO_2 catalysts prepared via modified preparation techniques prove to be an excellent heterogeneous catalyst for solvent free synthesis of chalcone with yield as high as 93 %, by using only 1.5 wt% of catalyst.
- Various elemental characterization techniques such as EDX, AAS, ICP and XRF are used to accurately determine Mo and W in MoO_3-/ZrO_2 and WO_3-/ZrO_2 catalyst respectively, and their results have been compared.

Thank You


1950 - 2010
ncl
Celebrating Sixty Years of Science
CSIR-INDIA
National Chemical Laboratory